CHEMOSENSORY MECHANISMS OF BITTER TASTE RECEPTORS (T2RS) IN MEDIATING HOST-PATHOGEN INTERACTIONS IN AIRWAYS

By

Appalaraju Jaggupilli

A Thesis submitted to the Faculty of Graduate Studies of
The University of Manitoba
In partial fulfillment of the requirements of the degree of

Doctor of Philosophy

Department of Oral Biology
Dr. Gerald Niznick College of Dentistry
University of Manitoba
Winnipeg, Manitoba, Canada

DISCLAIMER

This modified sandwich thesis comprises five multi-authored manuscripts, all of which contain a majority of original work contributed by the author of this thesis, but which also contain varying portions of work contributed by collaborating lab members. The author of this thesis was listed as second author in the fifth manuscript, for contributing the Schild regression analysis of ABA in the manuscript. The introduction of this thesis was published in the international journal of biochemistry and cell biology respectively; expression of T2Rs in different tissues study was published in molecular and cellular biochemistry; characterization of binding sites for antibiotics study was accepted for publication in FASEB journal; characterization of binding sites for acyl homoserine lactones study was published in American chemical society infectious diseases, and abscisic acid as T2R4 blocker study was published in the biochemistry journal. Individual author contributions are given below.

1. Bitter taste receptors: Novel insights into the biochemistry and pharmacology Int J Biochem Cell Biol. 2016 Aug;77(Pt B):184-96. Appalaraju Jaggupilli is the first author of this review article and alogn with Dr. Prashen Chelikani, was primarily responsible for the construction and writing manuscript. Ryan Howard and Jasbir Upadhyaya gave the inputs for the betterment of the manuscript.

2. Analysis of the expression of human bitter taste receptors in extraoral tissues. Mol Cell Biochem. 2017 Feb;426(1-2):137-147. Appalaraju Jaggupilli is the first author of this study toward the study design along with Dr. Prashen Chelikani, and performed the experimentation and data analysis. Appalaraju Jaggupilli worked on the bronchial epithelial cells, worked on breast cancer cells and Jasbir Upadhyaya worked on airway smooth muscle and pulmonary cells. Appalaraju Jaggupilli and Nisha Singh did the nanostring data analysis. Anurag Sikarwar and Mokoto Arakawa provided the inputs for the betterment of the final manuscript.

3. Characterization of the binding sites of bacterial acyl homoserine lactones (AHLs) on human bitter taste receptors (T2Rs). ACS Infect Dis. 2018 Jun;4(7):1041-1157. Appalaraju Jaggupilli is the first author of this study toward the study design along with Dr. Prashen Chelikani. Appalaraju Jaggupilli and Nisha Singh performed all the experiments and analyzed the experimental data. Vivianne Jesus contributed for the plasmids preparation of T2R mutants. Appalaraju Jaggupilli performed molecular modeling and docking analysis. Appalaraju Jaggupilli and Dr. Prashen Chelikani performed subsequent data

analysis and wrote the manuscript.

4. Chemosensory bitter taste receptors (T2Rs) are activated by multiple antibiotics. FASEB J, 2018, July. Appalaraju Jaggupilli is the first author of this study and responsible for the study design along with Dr. Prashen Chelikani; Appalaraju Jaggupilli and Nisha Singh conducted all the experiments and analyzed the data. Appalaraju Jaggupilli generated T2R1 and T2R4 stable cells, Nisha Singh generated T2R20 stable cells and Feroz Ahmed provided T2R14 stable cells. Vivianne C.Jesus and Mohammed S.Gounni contributed to plasmid preparation. Appalaraju Jaggupilli and Premnath Dhanaraj performed the homology modelling and ligand docking. Appalaraju Jaggupilli and Dr. Prashen Chelikani wrote the paper.

5. Abscisic Acid Acts as a Blocker of the Bitter Taste G Protein-Coupled Receptor T2R4, Biochemistry, 2015 April;54(16)**,** 2622-31. Appalaraju Jaggupilli is the second author of this study. Performed Schild regression analysis on abscisicacid at T2R4 and contributed to the writeup of the manuscript.

ABSTRACT

Bitter taste receptors (T2Rs) belong to G protein-coupled receptor superfamily. In humans, 25 T2Rs perform a chemosensory function with little information on their extraoral role. Recent studies suggest the expression of T2Rs in different tissues and their interaction with quorum-sensing molecules (QSMs). In addition, thousands of compounds are known to activate the 25 T2Rs while very few characterized bitter blockers exist. This thesis has two independent hypotheses involving T2Rs: First hypothesis, human airways show differential expression of T2Rs in pathophysiological conditions such as cystic fibrosis (CF). The second hypothesis, bacterial QSMs and bitter compounds mediate host-pathogen interactions through T2Rs in airways. To test these hypotheses, I analyzed the expression patterns of T2Rs at transcript and protein level in normal and CF airway cells. The results suggest a specific pattern of T2Rs with no differential expression in the samples analyzed. Next to assess T2R functionality, I pursued calcium mobilization assays after stimulation of cells with various bitter compounds. The inhibition of Gβγ-subunit and phospholipase-C (PLC) showed the calcium mobilized in these cells predominantly takes place through T2R-Gαβγ-PLC pathway. To test the second hypothesis, combination of molecular and pharmacological approaches were used to study the amino acid interactions in selected T2Rs. In these experiments, commonly used antibiotics in CF treatment, and major QSMs secreted by CF bacteria were tested. The results suggest that antibiotics and QSMs activate multiple T2Rs with different potencies. Extracellular loop-2 in T2Rs performs a key function in binding to the tested compounds. To address the lack of properly characterized bitter blockers, I pursued the characterization of novel T2R4 blockers derived from plant and meat products. A Schild regression analysis on the plant hormone abscisic acid determined

its T2R4 antagonism as surmountable. Further testing with the naturally occuring (+)-ABA isomer indicated that individual isomers do not induce calcium mobilization. Subsequently, I identified and characterized advanced glycation end-products as T2R4 antagonists. Glyoxal-derived lysine dimer inhibited the quinine response while carboxy methyl lysate showed subtle inhibition. In conclusion, these structure-function and mechanistic studies on T2Rs identify as new targets for antibiotics and QSMs. This work provides new insights into the host-pathogen interactions in CF and may lead to novel therapeutic approaches for CF that target T2Rs.

ACKNOWLEDGEMENTS

Completion of this doctoral thesis was possible with the support of various people at different stages of my journey. I would like to take this opportunity to consider and express my sincere gratitude to all of them.

First and foremost, I would like to express my immense gratitude to my advisor Dr. Prashen Chelikani. I am deeply indebted to him for his fundamental role in my doctoral work. It was his excellent guidance, enormous support, profound patience and positive inputs, provided to do research have made my Ph.D experience productive and stimulating. The joy and enthusiasm he has for research was contagious and motivational for me, even during tough times in the Ph.D. pursuit. I thank him for his amicability, freedom and encouragement to accomplish this thesis work.

I would like to extend my gratitude to my thesis committee who have guided me through all these years. A big thanks to Dr. Abdel Soussi Gounni, Dr. Rajinder Bhullar and Dr. Kangmin Duan for their insightful comments and valuable inputs. I am thankful to the Faculty of Dentistry, Faculty of Graduate Studies, University of Manitoba and MITACS accelerate program for their financial support. I thank Linda Delmage, Lisa and Tammy for their wonderful support in administrative related work. Special thanks to Dr. Birek for her joyful conversations in sharing her experiences.

I owe my deepest gratitude to my best friend and colleague Dr. Sai Prasad Pydi for believing in me, to Dr. Nisha Singh and Dr. Raja Chakraborthy who motivated me throughout my PhD and played a key role in completing this thesis. I have also been blessed with an ambience of cheerful people with whom I bagged some wonderful memories and experiences in my daily work. For that, I thank Manoj, Crystal, Feroz, Dr. Anurag Sikarwar, Vivianne, Kun, Ryan, Mohammed and Vikram.

Special thanks to Dr. Anurag Sikarwar for his valuable feedback, support and inputs during the preparation of manuscripts and this thesis.

It is also my pleasure to mention Kiran and Deepak, Amarnath Pisipati and family, for their cordial and moral support during my stay in Winnipeg.

I want to thank my mentors and well-wishers Mr. Nani Babu and Dr. Subba Tata, academic professors Dr. K. Uma Devi, Dr. Arundhati Atluri and Dr. M. V. Subbarao in Andhra University, Dr. Lokesh Battula for their motivation and inspiration to reach the pinnacle.

I shall always be indebted to my best buddies Mukesh, Jaya, Shyamala, Vasu, Uma Mahesh, Swetha, Sarvani, Prathima, Parveen, Bhagya who represent a great bondage of friendship at different stages of my life right from kindergarten to date and stood by me all the time.

I cannot imagine my current position without the love and support from my family. Words cannot express how grateful I am to my loving brother, Dinakar, my sister Ramani, brother-in-law Anand Babu and wonderful nephews Yogi and Haneesh. It is their caring and responsibility in the family gave me emotional strength to cope up with the distance away from home. I am deeply thankful to my parents-in-law, Sanyasi Rao and Nagaveni, brothers-in-law Kishore and Harish for keeping their trust in me.

Finally, but my no means least, I express my immense love and gratitude to my parents, Apparao and Laxmi, for raising me and supporting me in all my pursuits. And most of all to my wife, Aruna, for her love, support, encouragement and patience during the final stages of this Ph.D. This thesis would have never been written without their sacrifices, faith and perseverance towards my comfort during this valuable journey of my life.

TABLE OF CONTENTS **Page Number**

CHAPTER 3

LIST OF FIGURES

LIST OF TABLES

LIST OF COPYRIGHTED MATERIAL FOR WHICH PERMISSION WAS OBTAINED

Chapter 1: Introduction
Bitter taste receptors: Novel insights into the biochemistry and pharmacology. Reprinted with permission from the *The International Journal of Biochemistry & Cell Biology,* 77(Pt B):184-96. © by Elsevier Ltd.

Chapter 4.1:
Figure 4.1.2, figure 4.1.5 and figure 4.1.6 reprinted with permission from the "Analysis of the expression of human bitter taste receptors in extraoral tissues", *Molecular and Cellular Biochemistry*, 426**,** 137-147. *License number*-4305500259375, © by Springer Nature.

Chapter 4.2: Chemosensory bitter taste receptors (T2Rs) are activated by multiple antibiotics.
Reprinted with permission from the *FASEB Journal; License number*-4392091309538 doi.org/10.1096/fj.201800521RR, © by Federation of American Societies For Experimental Biology.

Chapter 4.3: Characterization of the binding sites for bacterial acyl homoserine lactones (AHLs) on human bitter taste receptors (T2Rs).
Reprinted with permission from the *ACS Infectious Diseases*, 2018;4(7):1041-1157, © by ACS Publications.

Chapter 4.4:
Figure 4.4.1 reprinted with permission from the "Abscisic Acid Acts as a Blocker of the Bitter Taste G Protein-Coupled Receptor T2R4", *Biochemistry*, 54(16)**,** 2622-31, © by ACS Publications.

LIST OF ABBREVIATIONS

3DHC	3β-hydroxydihydrocostinolide
3HP	3β-hydroxypelenolide
3-oxo-C_{12}-AHL	*N*-(3-oxododecanoyl)–AHL
ABA	Abscisic acid
AHL	Acyl homoserine lactone
BCML	Nα, Nα-Bis carboxy methy-L-lysine
BEGM	Bronchial epithelial growth medium
C4-AHL	N-Butyryl-DL-homoserine lactone
C8-AHL	N-Octanoyl-DL-homoserine lactone
Ca^{2+}	Calcium
CAMs	Constitutively active mutants
cAMP	Cyclic adenosine monophosphate
CF	Cystic fibrosis
CFTR	Cystic fibrosis transmembrane conductance regulator
CML	ε-N-carboxy methyl-L-lysine
CRS	Chronic rhinosinusitis
C-terminus	Carboxy terminus
CuFi-1	Cystic fibrosis lung bronchial epithelial cells
DAG	Diacyl glycerol
DMEM	Dulbecco's modified Eagle's medium
DPH	Diphenydramine
DXM	Dextromethorphan
EC_{50}	Half maximal effective concentration
ECLs	Extracellular loops

EDTA	Ethylenediaminetetraacetic acid
ENac	Amiloride sensitive epithelial sodium channel
ER	Endoplasmic reticulum
E-tongue	Electronic tongue
FACS	Flow cytometry
FBS	Fetal bovine serum
FFA	Flufenamic acid
GABA	γ-Aminobutyric acid
GOLD	Glyoxal-derived lysine dimer
G-proteins	Guanine nucleotide-binding proteins
GLP-1	Glucagon-like peptide-1
GPCRs	G protein-coupled receptors
H-bond	Hydrogen bond
HCl	hydrogen chloride
HEK cells	Human Embryonic Kidney cells
HGNC	HUGO Gene Nomenclature Committee
HHQ	2-Heptyl-3-hydroxy-4(1H)-quinolone
IC_{50}	Half maximal inhibitory concentration
ICLs	Intercellular loops
IP_3	Inositol triphosphate
IP_3R	Inositol triphosphate receptor
LB	Luria-Bertain
MD	Molecular dynamics
MFI	Mean fluorescence intensities
NHQ	2-nonyl-3-hydroxy-4-quinolone

N-terminus	Amino terminus
NuLi-1	Normal lung bronchial epithelial cells
nsSNPs	non-synonymous single nucleotide polymorphisms
PBS	Phosphate buffer solution
PIP_2	Phosphatidylinositol-4,5-diphosphate
PLC	Phospholipase C
PTC	Phenylthiocarbamide
qPCR	Quantitative PCR
QSMs	Quorum sensing molecules
RFU	Relative fluorescence units
RT-PCR	Reverse transcriptase PCR
SCCs	Solitary chemosensory cells
SEM	Standard error mean
TAE	Tris acetate-EDTA
TAS1R	Sweet/umami taste receptor gene
T1R	Sweet/umami taste receptor
TAS2R/T2R	Bitter taste receptors gene
T2R	Bitter taste receptor
TM	Transmembrane
TRCs	Taste receptor-expressing cells
TRPM5	Transient receptor potential channel M5
WT	Wild type

CHAPTER 1

1.0 INTRODUCTION

1.1 Taste perception

Taste perception is an important chemosensory function of the gustatory system that evaluates the quality of food, and avoids ingestion of poisonous substances (Wu et al., 2002, Herness and Gilbertson, 1999). Humans can recognize five basic tastes namely sweet, umami, bitter, salt and sour. The taste sensation of sweet, umami and bitter is mediated by specific G protein-coupled receptors (GPCRs), while salt and sour taste is perceived by ion channels expressed in taste receptor expressing cells (Hoon et al., 1999, Lagerstrom and Schioth, 2008, Chandrashekar et al., 2006) (**Figure 1.1.1**). The transduction of salt taste happens through the sodium selective channel and amiloride sensitive epithelial sodium channel (ENaC) where the sour taste is transduced by different acid sensitive membrane channels (Hoon et al., 1999, Lagerstrom and Schioth, 2008). The standard symbols for human taste receptor genes have been assigned following HUGO Gene Nomenclature Committee (HGNC) (Gray et al., 2015). TAS1R for type 1taste receptors and TAS2R for type 2 taste receptors. Their corresponding proteins are designated as T1Rs and T2Rs respectively. There are 3 subtypes of T1Rs (T1R1, T1R2 and T1R3) that form heterodimeric receptors to mediate sweet (T1R2/T1R3) and umami (T1R1/T1R3) taste (Zhao et al., 2003). T1Rs belong to Class C GPCR family while T2Rs form a separate group within the GPCR superfamily (Sharman et al., 2013).

Among these tastes, bitter perception is believed to play a critical role in defense mechanisms against numerous toxic substances acting as a central warning signal (Wu et al., 2002). In humans, bitter perception is mediated by 25 T2Rs that are

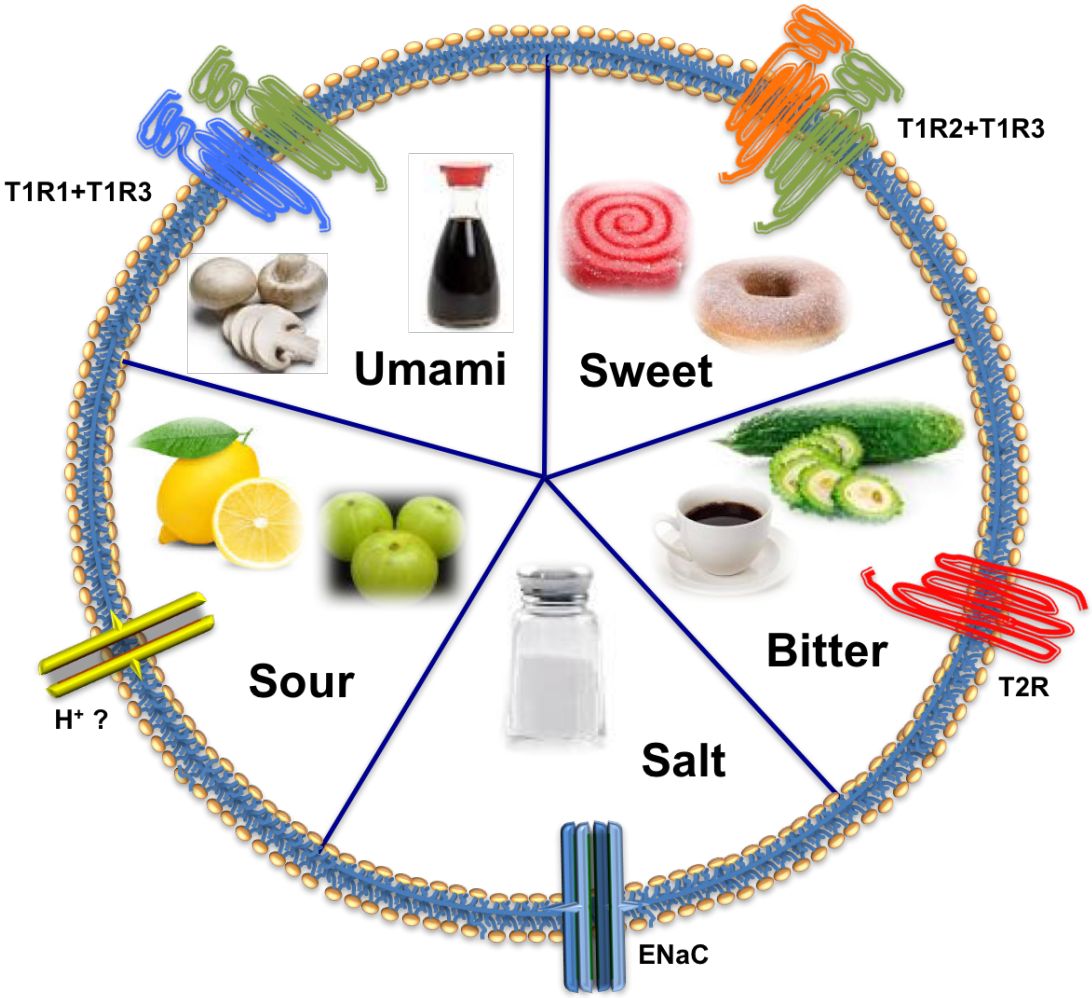

Figure 1.1.1 Schematic representation of the five basic taste perceptions in mammals. Umami and sweet taste perceptions are sensed by heterodimer complex of GPCRs as T1R1-T1R3 and T1R2-T1R3 respectively. These receptors possess a long N-terminal domain and interact with the ligands. Bitter taste is perceived by T2Rs that also belong to GPCR family with short N-terminal and ligands interact with the extracellular portion of the receptor involving extracellular loops and transmembrane domains. Sour and salt are perceived by the specific ion channel proteins present in the cell membrane.

expressed in the oral cavity (Chandrashekar et al., 2000). They are present in 4 chromosomal loci located on 3 chromosomes. Only one T2R is expressed on chromosome 5p (T2R1); 9 T2Rs on chromosome 7q (T2R3, 4, 5, 16, 38, 39, 40, 41 and 60) and the rest 15 T2Rs are expressed on chromosome 12p (Gray et al., 2015). However, T2Rs share low sequence similarity with other GPCRs and their classification is still ambiguous although they are considered as a separate group of receptors (Sharman et al., 2013, Di Pizio and Niv, 2015). In this chapter, I will review recent developments in the structure-function analysis and the pharmacology of bitter taste receptors (T2Rs). A review on the extra-oral functions of T2Rs and their pathophysiological roles are discussed previously (Shaik et al., 2016).

1.2 Bitter Taste Signal Transduction

Bitter taste signaling is initiated by a bitter agonist's interaction with its cognate T2R. This induce a conformational change in the receptor and subsequent activation of intracellular heterotrimeric G-protein complex (Chaudhari and Roper, 2010). In gustatory tissues, it was reported that the heterotrimeric complex comprises of a $G\alpha_{gustducin}$ and $\beta_3\gamma_{13}$ subunits (Wong et al., 1996, Caicedo et al., 2003). Once activated, $G\alpha_{gustducin}$ separates from the complex and activates a phosphodiesterase to reduce cAMP levels while the $\beta_3\gamma_{13}$ dimer activates phospholipase $C\beta_2$ ($PLC\beta_2$) (Caicedo et al., 2003). $PLC\beta_2$ acts on membrane bound phosphatidylinositol-4,5-diphosphate (PIP_2) to generate inositol-1,4,5-triphosphate (IP_3) and diacylglycerol (DAG). The generated IP_3 activates IP_3 specific receptors (IP_3R) present on endoplasmic reticulum to release calcium (Ca^{2+}) (Chaudhari and Roper, 2010). The elevated Ca^{2+} opens transient receptor potential cation channel member 5 (TRPM5) that leads to membrane depolarization and subsequent release of

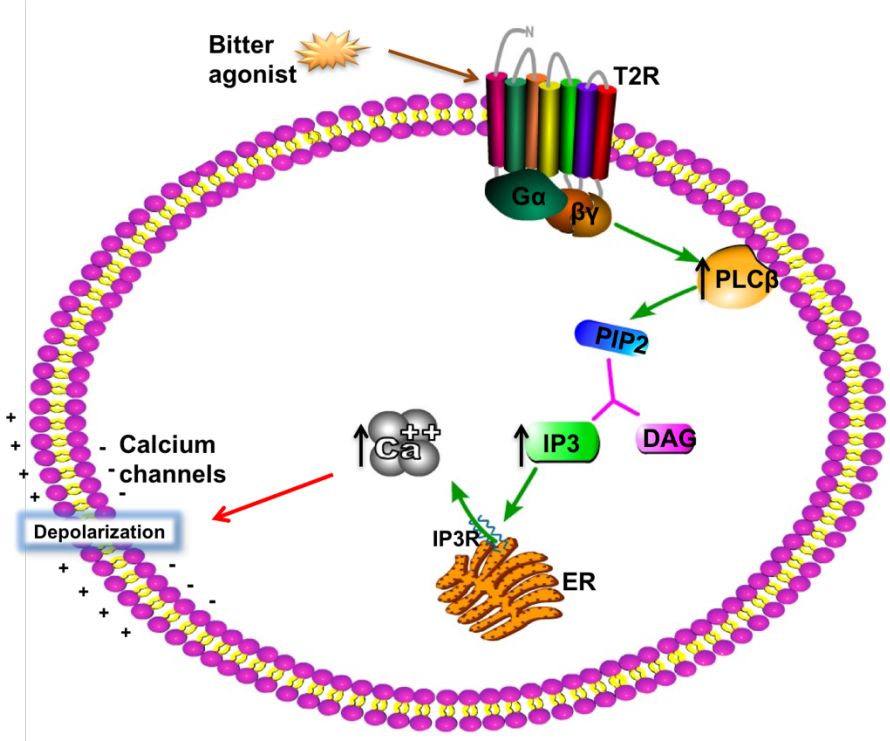

Figure 1.2.1 Schematic representation of the bitter taste signaling pathway. Bitter agonist activating bitter taste receptor (T2R) in turn activate phospholipase C β_2 ($PLC\beta_2$) that hydrolyze phospatidyl-inositol-biphosphate (PIP_2) to generate diacylglycerol (DAG) and inositol triphosphate (IP3). IP3 activate endoplasmic reticulum (ER) to release calcium(Ca^{2+}); The figure was generated using Pathway Builder Tool version 2

ATP as a neurotransmitter to activate gustatory afferents and send signal to the brain (Hofmann et al., 2003) (**Figure 1.2.1**).

1.3 Pharmacology of Bitter Ligands

1.3.1 Bitter agonists

The extra-oral expression of T2Rs strongly suggests for the existence of endogenous ligands, which remains to be elucidated. However, a wide range of structurally diverse compounds can activate T2Rs. More than 700 compounds were suggested to taste bitter while the efficacy of most of these compounds for the different T2Rs remains to be determined, pharmacologically (Wiener et al., 2012, Devillier et al., 2015). These bitter agonists include plant-derived and synthetic compounds such as amides, peptides, heterocyclic compounds, glycosides, alkaloids, terpenoids, phenols and flavonoids (Meyerhof et al., 2010, Pronin et al., 2004). Many pharmaceutical compounds like quinine, chloroquine, erythromycin and ofloxacin, and bacterial stimulants like acyl homoserine lactones are also known to activate T2Rs (Tizzano et al., 2010). Many T2Rs can be activated by multiple bitter molecules, while few T2Rs can only recognize a single compound (Brockhoff et al., 2007, Sakurai et al., 2010b, Behrens et al., 2009). This was extensively studied using activation profile for each T2R in HEK293T cells (Meyerhof et al., 2010). Although the bitter agonists are structurally diverse, some T2Rs exhibit selectivity towards the compounds with conserved moieties and position of reactive groups. For example, compounds with β-d-glucopyranoside moiety activate T2R16 and isothiocyanates activate T2R38 (Sanematsu et al., 2014). A more recent study analyzed the promiscuity and selectivity of both bitter ligands and human T2Rs (Di Pizio and Niv, 2015).

Table 1.3.1. List of T2R agonists (Jaggupilli et al., 2016)

T2R	Agonist	Concentration (μM)	Ref.
T2R1	Alanine	1280±78 (EC50)	(Ji et al., 2014)
	Amarogentin	30 (TC)	(Meyerhof et al., 2010)
	Arborescin	100 (TC)	
	Cascarillin	100 (TC)	
	Chloramphenicol	100 (TC)	
	Dextromethorphan	97±21 (EC50)	(Singh et al., 2011a)
	Diphenidol	100 (TC)	(Meyerhof et al., 2010)
	Gly-Phe dipeptide	7300±1100 (EC50)	(Upadhyaya et al., 2010)
	Gly-Leu-Leu tripeptide	4700±700 (EC50)	
	Histidine	1240±9 (EC50)	(Ji et al., 2014)
	Humulone isomers	1 (TC)	(Meyerhof et al., 2010)
	Ile-Phe dipeptide	7400±900 (EC50)	(Upadhyaya et al., 2010)
	Ile-Gln-Trp tripeptide	6100±2000 (EC50)	
	Leu-Lys-Pro tripeptide	7600±1200	
	Opianyl	230±1.2 (EC50)	(Ji et al., 2014)
	Parthenolide	100 (TC)	(Meyerhof et al., 2010)
	Phenyl alanine	930±270 (EC50)	(Ji et al., 2014)
	Phe-Leu dipeptide	7200±700 (EC50)	(Upadhyaya et al., 2010)
	Phe-Phe-Phe tripeptide	370±110 (EC50)	
	Picrotoxinin	1000 (TC)	(Meyerhof et al., 2010)
	Sodium cyclamate	30000 (TC)	
	Sodium thiocynate	3000 (TC)	
	Thiamine	1000 (TC)	
	2-Thiouracil	2272±260 (EC50)	(Ji et al., 2014)
	Yohimbine	300 (TC)	(Meyerhof et al., 2010)
T2R3	Chloroquine	172±29 (EC50)	
	Glutaronitrile	540±80 (EC50)	(Ji et al., 2014)
T2R4	Allylisothiocynate	300 (TC)	(Meyerhof et al., 2010)
	2-Amino-5-nitro thiazole	1329±60 (EC50)	(Ji et al., 2014)
	Arborescin	30 (TC)	(Meyerhof et al., 2010)
	Artemorin	100 (TC)	
	Azathioprine	300 (TC)	
	Brucine	100 (TC)	
	Campher	300 (TC)	
	Chloropheniramine	30 (TC)	
	Colchicine	1025±121 (EC50)	
	Dapsone	100 (TC)	
	Denatonium benzoate	300 (TC)	
	Diphenidol	100 (TC)	
	(-)-Epicatechin (EC)	30151 (EC50)	(Soares et al., 2013)
	3-(2-hydroxyethyl)-indole	300 (EC50)	(Kohl et al., 2013)
	Parthenolide	30 (TC)	(Meyerhof et al., 2010)
	Quassin	300 (TC)	
	Quinine	1000±380 (EC50)	(Pydi et al., 2012a)
	2-Thiouracil	840±20 (EC50)	(Ji et al., 2014)
	Trp-Trp dipeptide	1000 (EC50)	(Kohl et al., 2013)
	Trp-Trp-Trp tripeptide	10 (EC50)	
	Yohimbine	300 (TC)	(Meyerhof et al., 2010)

T2R5	(-)-Epicatechin (EC)	3210.0 ± 42.0 (EC50)	(Soares et al., 2013)
	Pentagalloylglucose (PGG)	8.5 (EC50)	
	1,10-Phenanthroline	100 (TC)	(Meyerhof et al., 2010)
	Procyanidin trimer	35.6 ± 0.7 (EC50)	(Soares et al., 2013)
T2R7	Caffeine	300 (TC)	(Meyerhof et al., 2010)
	Chloral hydrate	1460 (TC)	(Ji et al., 2014)
	Chloroquine	nd	(Sainz et al., 2007)
	Chloropheniramine	10 (TC)	(Meyerhof et al., 2010)
	Cromolyn	4500±1600 (EC50)	
	Diphenidol	10 (TC)	
	Malvidin-3-glucoside	12.6 ± 0.7	(Soares et al., 2013)
	Papaverine	10 (TC)	(Meyerhof et al., 2010)
	Quinacrine	nd	(Sainz et al., 2007)
	Quinine	10 (TC)	(Meyerhof et al., 2010)
	Strychnine	nd	(Sainz et al., 2007)
T2R8	4,4-Bipyridine	540±570 (EC50)	(Ji et al., 2014)
	Chloramphenicol	30 (TC)	(Meyerhof et al., 2010)
	Denatonium benzoate	1000 (TC)	
	3, 4-Dinitrobenzoic acid	310±210 (EC50)	(Ji et al., 2014)
	Histidine	520±14 (EC50)	
	Parthenolide	100 (TC)	(Meyerhof et al., 2010)
T2R9	Ofloxacin	200 (EC50)	(Dotson et al., 2008)
	Pirenzapine	1800 (EC50)	
	Procainamide	2800 (EC50)	
T2R10	Absinthin	100 (TC)	(Meyerhof et al., 2010)
	Arborescin	100 (TC)	
	Arglabin	100 (TC)	
	Artemorin	3 (TC)	
	Azathioprine	300 (TC)	
	Benzoin	30 (TC)	
	4, 4-Bipyridine	3680±60 (EC50)	(Ji et al., 2014)
	Caffeine	300 (TC)	(Meyerhof et al., 2010)
	Campher	300 (TC)	
	Cascarillin	100 (TC)	
	Chloramphenicol	100 (TC)	
	Chloropheniramine	10 (TC)	
	Chloroquine	10000 (TC)	
	Coumarin	300 (TC)	
	Cucurbitacin B	0.01 (TC)	
	Cucurbitacin E	0.01 (TC)	
	Cycloheximid	100 (TC)	
	Dapsone	100 (TC)	
	Denatonium benzoate	3 (TC)	
	Dextromethorphan*	10 (TC)	
	Diethyl phthalate	5820±330 (EC50)	(Ji et al., 2014)
	Diphenidol	30 (TC)	(Meyerhof et al., 2010)
	Erythromycin	300 (TC)	
	Femotidine	300 (TC)	
	Glutaronitrile	1210±320 (EC50)	(Ji et al., 2014)
	Haloperidol	30 (TC)	(Meyerhof et al., 2010)
	Papaverine	10000 (TC)	

	Parthenolide	30 (TC)	
	Picrotoxinin	1000 (TC)	
	Quassin	300 (TC)	
	Quinine	10 (TC)	
	Strychnine	21.8±7.5 (EC50)	
	Thujon, (-)-α-	100 (TC)	
	Yohimbine	300 (TC)	
T2R13	Diphenidol	30 (TC)	(Meyerhof et al., 2010)
	Denatonium benzoate	30 (TC)	
	Glutaronitrile	7410 (TC)	(Ji et al., 2014)
T2R14	Absinthin	100 (TC)	(Meyerhof et al., 2010)
	o-(p-Anisoyl)benzoic acid sodium salt	1000 (TC)	(Levit et al., 2014)
	2-Amino-5-nitro thiazole	204±20 (EC50)	(Ji et al., 2014)
	Arborescin	100 (TC)	(Meyerhof et al., 2010)
	Arglabin	100 (TC)	
	Aristolochic acid	1.9 (EC50)	(Yamazaki et al., 2014)
	Artemorin	3 (TC)	(Meyerhof et al., 2010)
	Azathioprine	100 (TC)	
	Benzamide	300 (TC)	
	Benzoin	10 (TC)	
	4,4-Bipyridine	1174±40 (EC50)	(Ji et al., 2014)
	Caffeine	300 (TC)	(Meyerhof et al., 2010)
	Campher	3 (TC)	
	Carisoprodol	100 (TC)	
	Cascarillin	100 (TC)	
	Chlonixin	2 (TC)	(Levit et al., 2014)
	Chlorhexidine	0.1 (TC)	(Meyerhof et al., 2010)
	Chloropheniramine	100 (TC)	
	Coumarin	300 (TC)	
	Cucurbitacin B	100 (TC)	
	Datiscetin	10 (EC50)	(Roland et al., 2013)
	Diethylphthalate	696±150 (EC50)	(Ji et al., 2014)
	3,2′-Dihydroxychalcone	24.5 (EC50)	(Roland et al., 2013)
	3,5-Diiodosalicyclic acid	0.5 (TC)	(Levit et al., 2014)
	Diphenhydramine	30 (TC)	(Meyerhof et al., 2010)
	Diphenidol	10 (TC)	
	Divinylsulfoxid	3000 (TC)	
	(-)-Epicatechin gallate (ECg)	70 (EC50)	(Yamazaki et al., 2013)
	(-)-Epigallocatechin gallate (EGCg)	34 (EC50)	
	Equol	47.2 (EC50)	(Roland et al., 2013)
	Eriodictyol	61.4 (EC50)	
	Eriodictyolchalcone	40.7 (EC50)	
	6-Ethoxy-4,4-dimethyl-2-thiouracil	850±570 (EC50)	(Ji et al., 2014)
	Ethylhydrocupreine	10 (TC)	(Levit et al., 2014)
	Falcarindiol	100 (TC)	(Meyerhof et al., 2010)
	Flavone	20.5 (EC50)	(Roland et al., 2013)
	Flufenamic acid	0.137±0.017 (EC50)	(Meyerhof et al., 2010)
	Genistein	28.9 (EC50)	(Roland et al.,

			2013)
	Haloperidol	30 (TC)	(Meyerhof et al., 2010)
	Homoeriodictyol	63.9 (EC50)	(Roland et al., 2013)
	Humulone isomers	0.01 (TC)	(Meyerhof et al., 2010)
	4-Hydroxyanisol	300 (TC)	
	Liquiritigenin	59.2 (EC50)	(Roland et al., 2013)
	Luteolin	6 (EC50)	
	6-Methoxyluteolin	11 (EC50)	
	Naringenin	36.2 (EC50)	
	Noscapine	10 (TC)	(Meyerhof et al., 2010)
	Opianyl	360±20 (EC50)	(Ji et al., 2014)
	Papaverine	10 (TC)	(Meyerhof et al., 2010)
	Parthenolide	3 (TC)	
	Phloretin	30.2 (EC50)	(Roland et al., 2013)
	Picrotoxinin	18 (EC50)	(Meyerhof et al., 2010)
	Pinocembrin	39.1 (EC50)	(Roland et al., 2013)
	Quassin	300 (TC)	(Meyerhof et al., 2010)
	Quercetin	1 (TC)	(Levit et al., 2014)
	Quinine	10 (TC)	(Meyerhof et al., 2010)
	Resveratrol	30.3 (EC50)	(Roland et al., 2013)
	Scutellarein	35 (EC50)	
	Secobarbital sodium	51.12±6.22 (EC50)	(Levit et al., 2014)
	Silibinin	56.1 (EC50)	(Roland et al., 2013)
	Sodium benzoate	300 (TC)	[2]
	Sulfuretin	21.5 (EC50)	(Roland et al., 2013)
	Theaflavin-3-*O*-gallate (TF2A)	14 (EC50)	(Yamazaki et al., 2014)
	Theaflavin-3'-*O*-gallate (TF2B)	5.97 (EC50)	
	2-Thiouracil	100±10 (EC50)	(Ji et al., 2014)
	Thujon, (-)-α-	15 (EC50)	(Meyerhof et al., 2010)
	Tributyrin	32±3.25 (EC50)	(Levit et al., 2014)
	Triethyl citrate	720±90 (EC50)	
	5,7,2′-Trihydroxyflavone	21.1 (EC50)	(Roland et al., 2013)
	7,3′,4′-Trihydroxyflavone	67.3 (EC50)	
	7,8,4′-Trihydroxyisoflavone	124 (EC50)	
T2R16	D-Amygdalin	20000±3400 (EC50)	(Meyerhof et al., 2010)
	Arbutin	5800 ± 900 (EC50)	
	4,4-Bipyridine	810±10 (EC50)	(Ji et al., 2014)
	Diethyl phthalate	499±320 (EC50)	
	Diphenidol	100 (TC)	(Meyerhof et al., 2010)
	Gentiobiose	3840 (EC50)	(Sakurai et al., 2010b)
	Helicin	2300±400 (EC50)	(Meyerhof et al., 2010)
	D-salicin	1400±200 (EC50)	
	Sinigrin	100 (TC)	

	Sodium benzoate	3000 (TC)	
T2R19	na		
T2R20	Cromolyn	45±25 (EC50)	(Meyerhof et al., 2010)
	Diphenidol	100 (TC)	
T2R30/T2R47	Absinthin	0.4±0.06 (EC50)	(Meyerhof et al., 2010)
	Amarogentin	3 (TC)	
	Andrographolide	30 (TC)	
	Artemorin	30 (TC)	
	Campher	300 (TC)	
	Cascarillin	100 (TC)	
	Chloral hydrate	950±40 (EC50)	(Ji et al., 2014)
	Denatonium benzoate	0.27±0.06 (EC50)	(Meyerhof et al., 2010)
	Diphenidol	100 (TC)	
	Picrotoxinin	1000 (TC)	
	Quassin	300 (TC)	
T2R31/T2R44	Acesulfame K	2500±10 (EC50)	(Meyerhof et al., 2010)
	Aloin	30 (TC)	
	Aristolochic acid	0.455±0.0053 (EC50)	
	Chloral hydrate	650 (TC)	(Ji et al., 2014)
	Diphenidol	3 (TC)	(Meyerhof et al., 2010)
	Femotidine	300 (TC)	
	Parthenolide	100 (TC)	
	Qinine	10 (TC)	
	Saccharin	1100 ±10 (EC50)	
T2R38	Acetylthiourea	26± 16 (EC50)	(Meyerhof et al., 2010)
	Allylisothiocynate	10 (TC)	
	Caprolactam	1000 (TC)	
	Chloral hydrate	1070±1070 (EC50)	(Ji et al., 2014)
	Chloropheniramine	100 (TC)	(Meyerhof et al., 2010)
	Dimethylthioformamide	59± 17 (EC50)	
	Diphenidol	100 (TC)	
	diphenylthiourea	1.7± 0.8 (EC50)	
	Ethylpyrazine	783± 185 (EC50)	
	N-Ethylthiourea	30 (TC)	
	N,N'-Ethylenethiourea	10 (TC)	
	Limonin	100 (TC)	
	Methimazole	30 (TC)	
	4(6)-methyl-2 thiouracil	30 (TC)	
	Methylthiourea	58± 38 (EC50)	
	Phenylethylisothiocynate	30 (TC)	
	PTC	1.1± 0.5 (EC50)	
	PROP	2.1±0.9 (EC50)	
	Sinigrin	100 (TC)	
	Sodium cyclamate	30000 (TC)	
	Sodium thiocynate	1000 (TC)	
	Yohimbine	300 (TC)	
T2R39	Acetaminophen	3000 (TC)	(Meyerhof et al., 2010)
	Alanine	580±10 (EC50)	(Ji et al., 2014)
	Amarogentin	300 (TC)	(Meyerhof et al., 2010)
	Chloramphenicol	1000 (TC)	
	Chloropheniramine	100 (TC)	
	Chloroquine	100 (TC)	
	Colchicine	3000 (TC)	
	Cyanidin chloride	187 (EC50)	(Roland et al.,

	Datiscetin	41.6 (EC50)	2013)
	Denatonium benzoate	100 (TC)	(Meyerhof et al., 2010)
	3,2′-Dihydroxychalcone	53.6 (EC50)	(Roland et al., 2013)
	Diphenidol	100 (TC)	(Meyerhof et al., 2010)
	(-)-Epicatechin (EC)	417.7 (EC50)	(Narukawa et al., 2011)
	(-)-Epicatechin gallate (ECg)	88.2 (EC50)	
	(-)-Epigallocatechin (EGC)	395.5 (EC50)	
	(-)-Epigallocatechin gallate (EGCg)	181.6 (EC50)	
	Equol	55.8 (EC50)	(Roland et al., 2013)
	Eriodictyol	62 (EC50)	
	Eriodictyolchalcone	55.5 (EC50)	
	Flavone	45.9 (EC50)	
	Genistein	49.4 (EC50)	
	Gossypetin	388 (EC50)	
	Histidine	430 (TC)	(Ji et al., 2014)
	Homoeriodictyol	84.9 (EC50)	(Roland et al., 2013)
	7-Hydroxyisoflavone	315 (EC50)	
	Liquiritigenin	64.5 (EC50)	
	Luteolin	7.3 (EC50)	
	6-Methoxyluteolin	22.9 (EC50)	
	Naringenin	32.9 (EC50)	
	Opianyl	1100 (TC)	(Ji et al., 2014)
	Pentagalloylglucose (PGG)	6.6 (EC50)	(Soares et al., 2013)
	Phloretin	41.3 (EC50)	(Roland et al., 2013)
	Pinocembrin	48.9 (EC50)	
	Quinine	10 (TC)	(Meyerhof et al., 2010)
	Resveratrol	109 (EC50)	(Roland et al., 2013)
	Scutellarein	40.3 (EC50)	
	Silibinin	99.2 (EC50)	
	Sulfuretin	48 (EC50)	
	Theaflavin (TF1)	2.79 (EC50)	(Yamazaki et al., 2014)
	Theaflavin-3'-*O*-gallate (TF2B)	0.67 (EC50)	
	Theaflavin-3,3'-*O*-digallate (TF3)	1.55 (EC50)	
	Thiamine	1000 (TC)	(Meyerhof et al., 2010)
	5,7,2′-Trihydroxyflavone	35.3 (EC50)	(Roland et al., 2013)
	7,3′,4′-Trihydroxyflavone	141 (EC50)	
	7,8,4′-Trihydroxyisoflavone	184 (EC50)	
T2R40	Chloropheniramine	100 (TC)	(Meyerhof et al., 2010)
	Dapsone	30 (TC)	
	Diphenidol	30 (TC)	
	Humulone isomers	0.01 (TC)	
	Quinine	10 (TC)	
T2R41	Chloramphenicol	300 (TC)	(Thalmann et al., 2013)
	4-Flurophenyl Biguanide	1370±20 (EC50)	(Ji et al., 2014)
T2R42	na		
T2R43	Acesulfame K	10000 (EC50)	(Meyerhof et al., 2010)
	Aloin	28± 0.4 (EC50)	
	Amarogentin	75± 7 (EC50)	
	Arborescin	100 (TC)	
	Arglabin	3 (TC)	

	Aristolochic acid	0.081±0.0008 (EC50)	
	Caffeine	300 (TC)	
	Chloramphenicol	100 (TC)	
	Cromolyn	3000 (TC)	
	Denatonium benzoate	300 (TC)	
	Diphenidol	30 (TC)	
	Falcarindiol	100 (TC)	
	Grossheimin	100 (TC)	
	Helicin	1000 (TC)	
	Quinine	10 (TC)	
	Saccharin	1700±20 (EC50)	
T2R45	na		
T2R46	Absinthin	9.9±0.3 (EC50)	(Meyerhof et al., 2010)
	Amarogentin	65±16 (EC50)	
	2-Amino-5-nitro thiazole	270±6 (EC50)	(Ji et al., 2014)
	Andrographolide	13±2.17 (EC50)	(Meyerhof et al., 2010)
	Arborescin	3 (TC)	
	Arglabin	3 (TC)	
	Artemorin	10 (TC)	
	Azathioprine	300 (TC)	
	Brucine	10 (TC)	
	Caffeine	300 (TC)	
	Cascarillin	10 (TC)	
	Chloramphenicol	10 (TC)	
	Chloropheniramine	100 (TC)	
	cnicin	3 (TC)	
	Colchicine	1580±170 (EC50)	
	Crispolide	10 (TC)	
	Denatonium benzoate	240±192 (EC50)	
	Diphenidol	30 (TC)	
	Grossheimin	1 (TC)	
	Hydrocortisone	3 (TC)	
	Orphenadrine	30 (TC)	
	Parthenolide	1 (TC)	
	Penten-3-ol	740±210 (EC50)	(Ji et al., 2014)
	Picrotoxinin	10 (TC)	(Meyerhof et al., 2010)
	Quassin	300 (TC)	
	Quinine	10 (TC)	
	Strychnine	0.43±0.02 (EC50)	
	Tatridin B	100 (TC)	
	2-Thiouracil	450±50 (EC50)	(Ji et al., 2014)
	Yohimbine	300 (TC)	(Meyerhof et al., 2010)
T2R50	Allylthiourea	720±150 (EC50)	(Ji et al., 2014)
	Amarogentin	100 (TC)	(Meyerhof et al., 2010)
	Andrographolide	22.9±4.9 (EC50)	
	Diethyl phthalate	430 (TC)	(Ji et al., 2014)
T2R60	na		

TC: Threshold concentration; EC50: Half maximal concentration; na: not available; nd: not determined; * Not mentioned as agonist in the subsequent studies

In their study, the authors proposed that promiscuous bitter compounds activate all the selective T2Rs while both selective and promiscuous compounds can activate promiscuous T2Rs. However, no compound is known to activate all 25 T2Rs or no unique compound towards a selective T2R (Meyerhof et al., 2010, Di Pizio and Niv, 2015).

Here, I will review the known bitter agonists to date as well as their activation or threshold concentrations (TC) with respect to the T2Rs (**Table 1.3.1**). Among the 21 deorphanized T2Rs, T2R10, T2R14 and T2R46 are broadly tuned and exhibit a wide receptive range in recognizing structurally different molecules (Brockhoff et al., 2011). Additional ligands were recently discovered for T2R14 (Levit et al., 2014). TAS2R gene expression studies in different tissues showed that these receptors are expressed from moderate to high levels. Thus, consideration of the relatively high expression of these receptors in conjunction with their wide receptive range may suggest an important role for these three receptors in non-gustatory tissues.

Until recently, T2R41 was considered as one of the orphan receptors. Recent investigations showed that chloramphenicol can activate T2R41-P127 and L127 variants with a TC of 300 μM and 600 μM respectively (Thalmann et al., 2013). Another study identified 4-fluorophenyl biguanide as T2R41 agonist with EC_{50} value of 1.37±0.02 mM (Ji et al., 2014). A more extensive study on 97 compounds comprising flavonoids and isoflavonoids have identified 68 compounds activating T2R14, and 70 compounds activating T2R39 with an overlap of 58 compounds activating both the T2Rs between the threshold values ranging from 0.12 to 500 μM (Roland et al., 2013). This study also determined EC_{50} values for some of the identified compounds. However, until now, endogenous agonists for T2Rs are not

known and all the known agonists are exogenous compounds prepared synthetically or derived from plants and bacteria.

1.3.2 Bitter antagonists and inverse agonists (bitter taste blockers)

In simple pharmacological terms an antagonist is considered as a ligand that does not induce any biological response from a GPCR, while a ligand that reduces the basal level activity of a GPCR is called an inverse agonist. These compounds act as competitive or allosteric inhibitors to block the receptor activity. For T2Rs these compounds are referred to as bitter taste blockers or bitter blockers. Until now, only 13 bitter blockers have been identified (Slack et al., 2010, Brockhoff et al., 2011, Greene et al., 2011, Fletcher et al., 2011, Roland et al., 2014, Pydi et al., 2014c, Pydi et al., 2015). However, likewise with agonists, none of these blockers can block all the 25 T2Rs. They interact with only 10 T2R subtypes (**Table 1.3.2**). A recent analysis suggested that agonist-to-antagonist ratio in T2Rs is larger than in Class A GPCRs and thus a need for the characterization of more antagonists (Di Pizio et al., 2016).

The use of bitter taste maskers is a common practice in food and beverage industries to reduce the bitterness and increase palatability (Ley, 2008). Some of the bitter maskers used in food and pharmaceutical industries are summarized in **Table 1.3.3**. Although these compounds are known to mask the bitterness, the T2Rs they interact with and their biochemical pharmacology has not been elucidated. With the recent characterization of extra-oral expression of T2Rs, it is essential to study the interaction of these maskers with T2Rs and identify novel bitter blockers. These bitter blockers have been proposed to have at least three main advantages. First, bitter blockers will increase the palatability of bitter tasting food and beverages; second, they increase the compliance of bitter tasting drugs, especially children's

formulations; and finally reduce or prevent off-target drug effects in the extra-oral tissues (Clark et al., 2012). Thus, the discovery of more potent and selective antagonists is required to overcome these challenges.

GIV3727 (4-(2,2,3-trimethylcyclopentyl) butanoic acid) was the first T2R antagonist discovered by high-throughput screening of 17,854 compounds (Slack et al., 2010). It acts as an orthosteric insurmountable antagonist for T2R31 with an IC_{50} value of 6.4 ± 2.4 μM against acesulfame K. This study was followed by the discovery of sesquiterpene lactones and probenecid as bitter taste blockers (Brockhoff et al., 2011, Greene et al., 2011). Probenecid is originally known as an inhibitor of organic anion transporter channels which is mainly used as a uricosuric drug for treating gout and hyperuricemia (Stamp et al., 2007). It is also commonly used along with the calcium binding dyes to prevent the dye leakage in the calcium mobilization assays while studying the functionality of T2Rs. However, its antagonistic effect on T2R16, 38 and 43 limits its use in the calcium mobilization assays involving these T2Rs. Thus, an alternate channel blocker must be considered while characterizing these receptors. Later study discovered sakuranetin, 6-methoxysakuranetin and jaceosidin as potent inhibitors of T2R31 against saccharin activity (Fletcher et al., 2011). Another study showed the inhibition of T2R39 by 3 flavanones against epicatachin gallate (Roland et al., 2014). More recent studies have identified γ-Aminobutyric acid (GABA), Nα, Nα-bis(carboxymethyl)-L-lysine (BCML) and (±) Abscisic acid (ABA) as competitive inhibitors of quinine-activated T2R4. BCML acts as a potent antagonist of T2R4 with an IC_{50} value of 59 ± 18 nM against quinine. This is the most potent antagonist reported for any T2R till date, followed by GABA with IC_{50} value of 3.2 ± 0.3 μM (Pydi et al., 2014c). ABA inhibits the quinine-activated T2R4 with IC_{50} value of 34.4 ± 1.1μM (Pydi et al., 2015). A summary of the available

Table 1.3.2 Pharmacological properties of bitter taste receptor blockers
(Jaggupilli et al., 2016)

Antagonist/ Compound	Mode of Action	Tested agonist/solution	T2Rs	IC50 (μM)	Ref.
GIV3727 or 4-(2,2,3-trimethylcyclopentyl)butanoic acid	Orthosteric Inhibitor (Biochemically characterized)	Acesulfame K, Saccharin & Aristolochic acid	31	6.4 ± 2.4, 7.9 ± 6.1 & 34.78 ± 5.1	(Slack et al., 2010)
	ND	Aristolochic acid	43	11.33 ± 2.1	
		Colchicine	4	108	
		Cohumulone	40	6.24 ± 1.25	
		Cromolyn	20	ND	
		Cromolyn	7	ND	
3β-Hydroxydihydrocostunolide (3HDC)	ND	Absintin	46	14.1 ± 1.4	(Brockhoff et al., 2011)
		Andrographolide		4.9 ± 0.5	
		Denatonium		6.8 ± 2.3	
		Picrotoxinin		4.7 ± 1.2	
	Surmountable antagonist (Schild analysis)	Strychnine		15.3 ± 5.9	
	ND	Brucine	30	ND	
		Cohumulone	40		
		Aristolochic acids	43		
3β-hydroxypelenolide (3HP)	ND	Absinthin	46	57.8 ± 24.9	(Brockhoff et al., 2011)
		Andrographolide		44.5 ± 34.5	
		Denatonium		51.4 ± 28.8	
		Picrotoxinin		22.9 ± 3.4	
		Strychnine		84.9 ± 50.2	
		Brucine	30	ND	
		Aristolochic acids	31		
		Aristolochic acids	43		
		Cohumulone	40		
Probenecid or p-(dipropylsulfamyl)benzoic acid	Allosteric inhibitor (Biochemically characterized)	Salicin	16	292	(Greene et al., 2011)
	ND	PTC & PROP	38	211	
		Aloin	43	ND	
Sakuranetin	ND	Saccharin	31	5.5 ± 2.5	(Fletcher et al., 2011)

6-methoxy sakuranetin	ND	Saccharin	31	10.2 ± 5.4	(Fletcher et al., 2011)
Jaceosidin	ND	Saccharin	31	11.7 ± 6.0	(Fletcher et al., 2011)
4'-fluoro-6-methoxy flavonone	ND	Epicatechin gallate (ECG), Denatonium benzoate	39	102 ± 9, 55 ± 3	(Roland et al., 2014)
		Epicatechin gallate (ECG) & Genistein	14	79 ± 25, ~500	
6,3'-dimethoxy flavanone	ND	Epicatechin gallate (ECG) & Denatonium benzoate	39	4075± 55, 240 ± 8	(Roland et al., 2014)
		Epicatechin gallate (ECG)	14	~250	
6-methoxy flavanone	ND	Epicatechin gallate (ECG)	39	479 ± 199	(Roland et al., 2014)
		Epicatechin gallate (ECG) & Genistein	14	447 ± 123, 741 ± 143	
γ-Aminobutyric acid (GABA)	Orthosteric Inhibitor (Biochemically characterized)	Quinine	4	3.2 ± 0.3	(Pydi et al., 2014c)
Nα,Nα-bis(carboxymethyl)-L-lysine (BCML)	ND	Quinine	4	0.059 ± 0.018	(Pydi et al., 2014c)
(±) Abscisic acid (ABA)	ND	Quinine	4	34.4±1.1	(Pydi et al., 2015)

ND: Not determined

bitter blockers with their properties, tested agonist, corresponding T2Rs and their respective IC_{50} values are presented in **Table 1.3.2**. Most of the bitter blockers discussed above are moderately selective. A selective receptor antagonist serves as one of the most powerful tools in pharmacological studies. Such compounds have been used in identifying receptor subtypes and elucidate their role in both normal and abnormal conditions. However, inappropriate measurement of antagonist activity or inaccurate interpretations of such measurements would result in erroneous characterization of antagonists and their antagonism (Wyllie and Chen, 2007). It is essential to adopt standard methodologies used in GPCR pharmacology for the identification and characterization of bitter blockers as discussed below.

1.3.3 Pharmacological characterization of antagonism using Schild analysis

Apart from the detection of an antagonist, studying the nature of antagonism is equally as important in GPCR pharmacology. Schild analysis is a quantitative method used in the measurement of antagonist properties (Hill, 2006). It is an efficient tool in the GPCR pharmacology to characterize the nature of antagonism of an inhibitor depending on the functional responses (Hill, 2006). Schild analysis is a combination of the application of law of mass action to the concentration-dependent responses and monitoring the antagonist-receptor interactions. This provides information on the competitive nature (surmountable or insurmountable) and the quantitative estimation (K_B) of an antagonist affinity for its receptor (Hill, 2006). The method incorporates the Gaddum analysis that estimates the concentration of agonist required to obtain the same response of a receptor in the absence and presence of a fixed antagonist concentration. If the antagonist binds competitively and reversibly to the receptor at the same binding site as agonist, then the dose response curve of an agonist will show

Table 1.3.3. Bitter taste maskers used in food and pharmaceutical industries (Jaggupilli et al., 2016)

Antagonist/Compound	**Tested agonist/solution**	**T2Rs**	**Ref.**
Sodium gluconate (NaG)	Quinine, Denatonium, Caffiene & Urea	ND	(Mennella et al., 2014)
Monosodium glutamate (MSG)	Quinine, Denatonium &Urea	ND	(Mennella et al., 2014)
Aspartame	Caffeine solution	ND	(Sharafi et al., 2013)
Sodium acetate (NaAc)	Caffeine solution	ND	(Sharafi et al., 2013)
Homoeriodictyol	Caffeine solution	ND	(Ley et al., 2005)
Homoerdiodictyol sodium salt	Caffeine solution	ND	(Ley et al., 2005)
Sterubin	Caffeine solution	ND	(Ley et al., 2005)
Eriodictyol	Caffeine solution	ND	(Ley et al., 2005)
2,4-Dihydroxybenzoic acid *N*-vanillyl amides	Caffeine solution	ND	(Ley et al., 2006)
Neodiosmin	Citrus juice	ND	(Guadagni et al., 1977)
1-carboxymethyl-5-hydroxy-2-hydroxymethylpyridinium inner salt	Bitter peptides and Caffeine solution	ND	(Soldo and Hofmann, 2005)
Flavan-3-ol−spiro-C-glycosides reaction product (Compound 2)	Caffeine solution	ND	(Zhang et al., 2014)
Poly-γ-glutamic acid	ND	ND	(Ley, 2008)
α,α-trehalose	ND	ND	
Taurine	ND	ND	
[2]-Gingerdione	ND	ND	
2,4-Dihydroxybenzoic acid	ND	ND	
L-Theanine	ND	ND	(Juneja et al., 1999)
Enterodiol	Caffeine solution	10	(Ley et al., 2012)

ND: Not determined

a parallel rightward shift in the presence of antagonist without affecting the maximum response (Wyllie and Chen, 2007). This phenomenon is termed surmountable antagonism or reversible competitive antagonism (Neubig et al., 2003). In the Schild analysis, this relation was derived as

$$\text{Dose ratio (DR)} = 1 + [B]/K_B,$$

where DR is the ratio between EC_{50} values of agonist in the absence and presence of antagonist from Gaddum analysis, B is the concentration of antagonist and K_B is the dissociation constant of the antagonist (Hill, 2006). In logarithmic form, the above Schild equation can be written as

$$\log(DR-1) = \log[B] - \log K_B.$$

When the antagonist shows competitive antagonism, a regression analysis between log(DR-1) against the log[B] should generate a straight line with slope equal to unity and this plot is termed as Schild plot (Wyllie and Chen, 2007). The Schild regression analysis estimates the experimental value of equilibrium dissociation constant (K_B) of a competitive antagonist (Kenakin, 1982). According to the Schild plot, pA_2 (*p* for logarithm) is the concentration of an antagonist required for a 2-fold increase in the agonist concentration (Poch et al., 1992). Therefore, when DR is equal to 2,

$$pA_2 = -\log K_B.$$

Thus, the point of interception of slope with the abscissa gives the K_B value. However, when the slope is not equal to unity, K_B value cannot be determined (Wyllie and Chen, 2007). This would infer that the antagonism is not competitive (Poch et al., 1992). When the slope is < 1, it would be because of the reduced potency of an antagonist with its increasing concentration. When the slope is >1, it would indicate the activity

of an agonist or antagonist on other receptors at their high concentrations (Kenakin, 1982).

Schild analysis has been widely used in GPCR pharmacology to study the antagonism and classification of various blockers (Chu et al., 2010, Casarosa et al., 2010, Yang et al., 1997, Baker and Hill, 2007). For instance, recent discoveries of inhibitors of GABA receptor (2-guanidine-4-methylquinazoline), dopamine receptor (OSU6162), NMDA receptor (TK40) and chemokine receptors (CCL18) were based on Schild regression analysis for their characterization (Kara et al., 2010, Xiao et al., 2013, Krohn et al., 2013, Kvist et al., 2013). This method is also useful in classifying the nature of antagonism. For example, PAR2 receptor antagonist GB88, shows a specific antagonist activity with respect to the agonist and receptor. GB88 is a competitive inhibitor of 2f-LIGRLO-NH_2 and non-competitive inhibitor of trypsin even though they act on the same receptor, PAR2 (Suen et al., 2012). At this stage, the binding site of these ligands should be considered for the classification of antagonists as orthosteric or allosteric.

Despite its acceptance in GPCR pharmacology, the theory of Schild analysis was not fully adopted to study the antagonism of bitter taste blockers. Although there are 13 bitter blockers reported to date, only studies on two blockers used Schild analysis to investigate their antagonism. The discovery of 3HDC as T2R46 inhibitor by Brockhoff et al. was the first to use Schild analysis in T2R pharmacology. Based on the consistency of maximal response and the rightward shift of response curves, this study reported a surmountable inhibition (competitive reversible inhibition) of strychnine-induced T2R46 activity by 3HDC (Brockhoff et al., 2011).

In order to do a proper characterization of an antagonist and understand the nature of antagonism, the data must be carefully considered to confirm that it is

meeting the defined criteria for Schild regression analysis. First the different antagonist concentrations against the response curves of agonist must give clear dose ratios. Then these dose ratios must generate a linear slope equal to unity (Kenakin, 1982). Using this approach, it is safe to conclude that the antagonism is simple competitive. Since it is not always easy to attain true experimental equilibrium conditions, this limits the interpretations using Schild analysis (Kenakin, 1982). Non-equilibrium conditions can make a non-competitive antagonist to appear as a competitive antagonist and vice versa. This could lead to the distortion of the nature of antagonism when using high concentrations of antagonist and different cell models (Kenakin, 1982). In a previous report, similar conditions were observed where the agouti-signaling protein (ASIP) was considered a surmountable antagonist towards human melanocortin receptors showing complex mechanisms with slopes significantly less than unity (Yang et al., 1997). A deviation of slope from unity could be the result of a number of possibilities like multimolecular interactions, non-equilibrium experimental conditions and non-specific responses (Kenakin, 1982).

1.3.4 Pharmacological characterization of T2R antagonists and inverse agonists using T2R constitutively active mutants

Constitutively active GPCRs attain an agonist-independent active state sometimes caused by a mutation that results in a change of receptor conformation. These are termed as constitutively active mutants (CAMs) (Chalmers and Behan, 2002). In GPCRs, the CAMs were first identified for δ opiod receptor and β_2-adrenergic receptors (Koski et al., 1982, Cerione et al., 1984). There are several naturally occurring CAMs in GPCR families A, B and C, where most of them result in causing diseases (Seifert and Wenzel-Seifert, 2002). Mutations in the highly

conserved motifs of GPCRs are the hot spots for majority of the CAMs (Pydi et al., 2014a). CAMs tend to exhibit higher basal level activity than the wild type receptors (Seifert and Wenzel-Seifert, 2002). Thus, these CAMs were used as ligand-free models of active form of GPCRs to study their structural and physiological roles in normal and abnormal conditions (Parnot et al., 2002). Inverse agonists will have a greater binding affinity than an antagonist (Chalmers and Behan, 2002). This property allows inverse agonists to show a larger inhibitory effect on the CAM and decrease their constitutive activity. Therefore, inverse agonists can inhibit both agonist-dependent and agonist-independent activity of the receptor while antagonists can inhibit only agonist-dependent activity (Chalmers and Behan, 2002). As such, inverse agonists are very useful in analyzing the constitutive activity of GPCRs and treatment of diseases caused due to CAMs (Seifert and Wenzel-Seifert, 2002). GPCR CAMs have been used in the detection of inverse agonists like propranolol, cimetidine, and ranitidine (Hill, 2006).

Lack of robust assay technologies has been a limiting factor in the identification of inverse agonists. CAMs have been used as one of the most efficient pharmacological tools to characterize receptor blockers as either an antagonist or an inverse agonist (Chalmers and Behan, 2002, Pydi et al., 2014a). Given the low number of blockers reported for T2Rs (Table 1), T2R CAMs can provide a novel tool for the detection and characterization of bitter taste blockers and identification of T2R inverse agonists. The assays using CAMs are economical and provide reliable information on the given ligand. However, until now there are no reports available about naturally occurring CAMs for T2Rs.

In order to identify possible CAMs in T2Rs, a study has screened more than 100 mutants in TM regions, intracellular regions and C-terminus of T2R4. These studies

led to the identification of the first CAMs in T2Rs (Pydi et al., 2014a, Pydi et al., 2012a, Upadhyaya et al., 2015). The study identified S285A in TM7, H123A and N132A in ICL2 (unpublished data), H214A, Q216A, V234A and M237A in ICL3 region and K296A in C-terminus of T2R4 exhibiting CAM activity (Pydi et al., 2012a, Pydi et al., 2014b, Upadhyaya et al., 2015). Among these, H214A showed the greatest constitutive activity and interestingly H214 is highly conserved (96%) in 24 of the 25 T2Rs (Pydi et al., 2014b). With the aid of H214A, they characterized the T2R4 blockers GABA and ABA as neutral antagonists and BCML as an inverse agonist (Pydi et al., 2014c, Pydi et al., 2015). GABA and ABA failed to reduce the basal intracellular IP_3 production whereas BCML significantly reduced the basal intracellular IP_3 production in H214A expressing cells (Pydi et al., 2014c, Pydi et al., 2015). Considering the high conservation (96%) of H214 (corresponding to the residue number in T2R4), it can be hypothesized that generating a similar mutation at the corresponding position in other T2Rs can lead to CAMs in these T2Rs. More studies (*in vivo*) are required to understand the physiological or pathological features of these CAMs. It is vital to note that the presence of endogenous agonist could make it difficult to determine the true constitutive activity of GPCRs in complex systems like neurons that constitutes neurotransmitter vesicles. The actual concentrations of endogenous agonists need to be determined to analyze the accurate constitutive activity of GPCRs. T2Rs also exhibit basal or constitutive activity and this need to be verified further as there are no identified endogenous agonists yet for T2Rs (Devillier et al., 2015, Seifert and Wenzel-Seifert, 2002).

1.4 Biochemistry of Bitter Taste Receptors

1.4.1 Generic residue numbering for T2Rs

Each class of GPCRs has its own set of highly conserved signature residues that play major role in the structure and function of the receptor. These conserved residues are indexed by a generic numbering system to facilitate the comparison of ligand interactions and structural features within and across the GPCR classes (Isberg et al., 2015). Although different numbering schemes from Olivera (Oliveira et al., 1993), Baldwin (Baldwin et al., 1997) and Schwartz (Schwartz, 1994) exist, the highly accepted scheme for GPCR residue numbering is the Ballesteros-Weinstein numbering scheme (Ballesteros and Weinstein, 1995, Isberg et al., 2015). Based on the updated information available from GPCR database, the generic numbers for the conserved residues among GPCR classes were aligned in Table 3 (Isberg et al., 2015). Despite this information, the generic residue numbering still remains ambiguous for T2Rs, with lack of complete structural and functional information.

Previous studies on activation mechanisms and ligand interactions in T2R10 and T2R46 showed novel insights into the residues involved in structure-function relationship (Born et al., 2013, Brockhoff et al., 2010, Sandal et al., 2015). In these studies, the residue numbering for T2R10 was based on sequence alignment with β2AR (PDB ID: 3SN6), and for T2R46 the residue numbering was derived from alignment between only 3 T2R sequences (T2R31, 43 and 46) that have >85% identity (Brockhoff et al., 2010). By contrast, in a recent study, the residue numbering for T2R46 was given based on the alignment with human dopamine D3 receptor sequence (PDB ID: 3PBL) and the generic number positions available in GPCRDB for this receptor (Sandal et al., 2015). Furthermore, the residue number positions for all 25T2Rs presented in bitterDB shows conserved residues at 1.50 (Asn 92%), 2.50 (Arg 96%), 3.50 (Lys 92%) and 5.50 (Pro 92%) while the positions 4.50, 6.50 and 7.50 are

not conserved (Wiener et al., 2012). However, the positioning in their protein sequence alignment is different from those appearing in other reports. It should be noted that the alignment between 25 T2Rs in bitterDB was generated based on the 3D structural information of 11 distinct-sequence receptors of Class A GPCRs (Wiener et al., 2012). More recently an attempt was made to compare the conserved motifs present in Class A GPCRs and T2Rs where the generic numbering was based on information available in bitterDB and a previous study (Di Pizio et al., 2016, Born et al., 2013). This study showed that 4.50 and 6.50 are not conserved while serine residue at 7.50 is conserved.

While such numbering systems are useful in the context of specific studies as described above, their general applicability to all the 25 T2Rs remains ambiguous. These discrepancies in generic number positions for a single T2R or among the T2Rs from different studies might lead to confusion. When a residue is assigned with a generic residue number (X.50), it indicates that the residue is highly conserved across the subtypes of its family (Isberg et al., 2015). Thus, it is essential to analyze and validate those residues for their vital role in structure and function of the receptor. Although there exist some uncertainty in using a universal generic residue numbering for T2Rs, it is more reliable to use a nomenclature derived from a large-scale analysis of T2Rs from different species rather than one derived from an analysis performed with very few receptors, such as the 25 T2Rs in humans. A previous study performed multiple amino acid sequence analysis of 188 T2Rs from different species (human, rat, mouse, chimpanzee, macaque, baboon, orangutan, and zebrafish), followed by computational and mutational studies on human T2R1 (Singh et al., 2011a). Based on these findings, the study presented the generic residue numbers for the highly conserved residues as follows: Asn (1.50), Leu (2.50), Trp (3.50), Leu or Val (4.50),

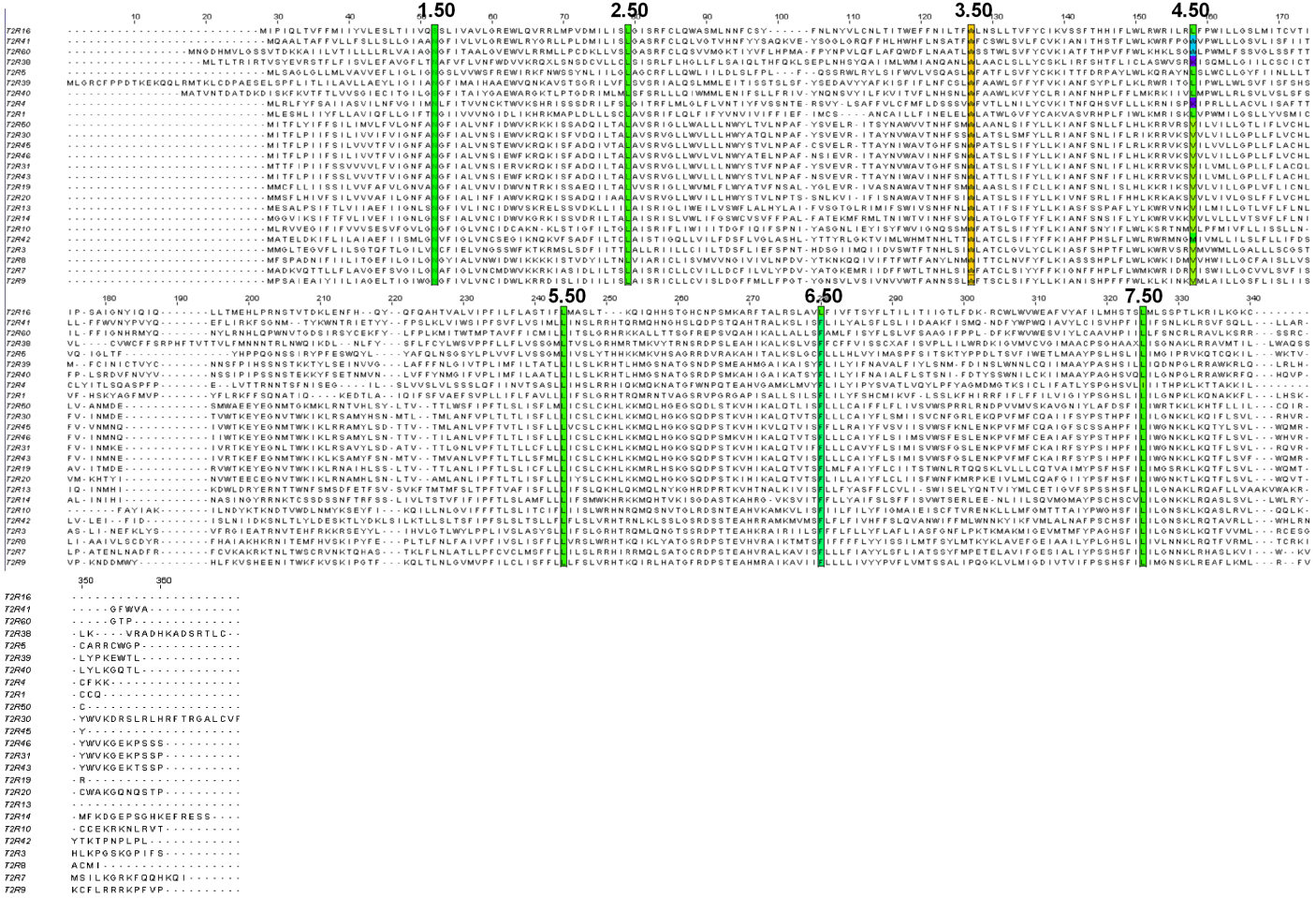

Figure 1.4.1. Prediction of generic numbers for conserved residues in T2Rs. Multiple alignment of 25 human T2Rs was performed using Clustal Omega algorithm. The highly conserved residues were highlighted in each predicted transmembrane region and designated as X.50. With X corresponding to transmembrane helix and .50 for the most conserved residue (Jaggupilli et al., 2016).

Table 1.4.1. Identification of highly conserved residues in T2Rs and alignment of class-specific generic residue numbers with other GPCR classes. Generic residue number (X.50) indicates X for the helix number and .50 for the highly conserved residue across the GPCR subfamily. The residues for the representative receptor from class A (rhodopsin), B (glucagon receptor), C (glutamate receptor 1), F (frizzled receptor 1) from GPCRdB. Residues from T2R1 (given in bold) represents the T2R family of subtypes obtained by multiple sequence alignment (Jaggupilli et al., 2016)**.**

Transmembrane helix	Generic residue number	Class A (Rho)	Class B (GCGR)	Class C (GRM1)	Class F (FZD1)	**T2Rs (T2R1)**
I	1.50	N55	S152	G603	T337	**N24**
II	2.50	D83/L	H177	Y642	Y362	**L51**
III	3.50	R135	E245	K678	W247	**W94**
IV	4.50	W161	W272	L724	W452	**L125***
V	5.50	P215	N318	L763	P494	**L197**
VI	6.50	P267	G359	W798	C554	**F233**
VII	7.50	P303	G393	P833	I615	**L277**

* 4.50 is least conserved in T2Rs

Leu (5.50), Phe (6.50) and Leu (7.50), in T2Rs (**Figure 1.4.1**). It should be noted that $X^{4.50}$ is variable across the T2Rs in humans and other species analyzed. Interestingly, most of these conserved residues are distinct from those in other classes of GPCRs (**Table 1.4.1**), further emphasizing the uniqueness of T2Rs. Mutational analysis of these residues elucidated their vital role in structure and function of T2Rs as discussed below (Singh et al., 2011a).

1.4.2 Structure-function relationship

Although there are several crystallographic studies that have been reported for GPCRs, there is no crystal structure available for any T2R till date. Extensive studies have been performed using computer-aided modeling and mutational studies to elucidate the structure-function relationship and to understand activation mechanisms of T2Rs. With this cumulative evidence, others and our lab studies demonstrated certain structural elements of T2Rs and proposed their role in T2R signaling (Singh et al., 2011a, Sakurai et al., 2010a, Brockhoff et al., 2010, Pydi et al., 2012a). These advances were broadly reviewed elsewhere (Pydi et al., 2012b, Behrens and Meyerhof, 2013).

1.4.3 Extracellular region

The extracellular region in GPCRs plays a major role in ligand binding and selectivity (Pydi et al., 2014c, Behrens and Meyerhof, 2013). Agonist interactions with residues in ECLs and TM regions enable a vast tuning breadth of receptor binding from a single ligand to a broad spectrum of ligands. Furthermore, the interactions between the residues in ECLs and TM regions are vital in receptor activation. In T2Rs, the extracellular region consists of non-conserved amino acid

residues. This composition defines the ability of T2Rs to recognize single or multiple ligands. In other GPCRs like metabotropic receptors and the T1Rs, a lengthy N-terminal domain called venus flytrap (VFT) exists which forms a primary binding pocket for ligands (Lagerstrom and Schioth, 2008). However, in T2Rs the N-terminus is short and allows the ligand to interact deep within the TM domains (Chandrashekar et al., 2000, Pydi et al., 2014b, Behrens and Meyerhof, 2013).

Studies on chimeric T2R31 and T2R43 showed that ECL1 was important for agonist selectivity (Behrens and Meyerhof, 2013). ECL2 was predicted to point away from the binding site in T2R38 (Marchiori et al., 2013). Molecular modeling guided site-directed mutagenesis studies on T2R1 and T2R4 showed that residues in ECL2 and ECL3 along with those in extracellular TM regions are required for ligand interactions (Dai et al., 2011, Pydi et al., 2014c). It is believed that T2Rs possess a single binding pocket for agonists whereas antagonists can bind in allosteric sites as well (Behrens and Meyerhof, 2013, Slack et al., 2010). N172, N173, T174 in ECL2, Y258, K270 in ECL3, A90, F91, F92 in TM3 and Y155 in TM4 shape the common binding pocket for both agonists and antagonists in T2R4 (Pydi et al., 2014c, Pydi et al., 2015). This indicates that the type of interactions with selected residues in the ligand-binding site determine the agonistic or antagonistic nature of a ligand.

It was suggested that few members of class A GPCRs (muscarinic, β_2AR and opioid receptors) possess a vestibular binding site, which directs the ligand to the orthosteric site. Very recently a combination of *in silico* molecular dynamics and *in vitro* mutational studies suggested that T2Rs might also have an access control that directs a ligand to the orthosteric site (Sandal et al., 2015). This study proposed that T2R46 possesses a vestibular site close to the extracellular region with more than 12 water molecules that solvate the agonist, strychnine, and allow interactions with a

variety of amino acids. These interactions form an access channel to the orthosteric site at deeper location with lower solvation. Residues in ECLs of T2R46 such as L71 and E70 in ECL1, N148, N150 and W154 in ECL2, and E253 in ECL3 are important for molecular recognition and receptor activation. W66 in TM2, W88 in TM3, E265 in TM6 and F269 in TM7 shape the binding site for strychnine. W88 is conserved across T2Rs and is also known to be involved in receptor activation. 50% of the functional positions in T2R46 are conserved in most of the T2Rs. This suggests a possibility that T2Rs might have two binding sites (Sandal et al., 2015).

1.4.4 Transmembrane region

The TM region in GPCRs is composed mainly of hydrophobic amino acids accommodated in the plasma membrane. The extracellular portion of TM helices participates in ligand selectivity and binding. The TM core restrains the receptor structure and undergoes helical movement upon receptor activation. The intracellular portion is involved in G protein-coupling and activation of signal transduction (Venkatakrishnan et al., 2013). Class A GPCRs possess conserved structural motifs such as LxxxD in TM2, (D/E)RY in TM3, CWxP in TM6 and NPxxY in TM7 that induce structural constraints (Arakawa et al., 2011). However, given the diversity from other classes of GPCRs, T2Rs have unique conserved TM motifs such as LxxxR in TM2 and LxxSL in TM5 (Singh et al., 2011a). LxxxR is required to restrain the receptor while LxxSL plays a structural role by stabilizing the helical conformation of TM5 at the cytoplasmic end and a functional role by interacting with residues in ICL3 (Singh et al., 2011a). Based on the sequence alignment with Class A GPCRs, a more recent study proposed that T2Rs consists of a highly conserved FYxxK motif in TM3 and HSxxL in TM7 as the counterparts of D[E]RY and NPxxY motifs respectively

(Di Pizio et al., 2016). Molecular modeling studies in T2R1 predicted the involvement of TM3-TM5-TM6-TM7 in combination with ECL2 to form the ligand binding pocket (Dai et al., 2011). In T2R38, it was previously predicted that interactions between TM3 and TM6 or TM5 and TM6 might play a role in receptor activation and signaling (Tan et al., 2012). T2R38 contains natural variants P49A in ICL1, A262V in TM6, V296I in TM7 whose interactions are crucial for the function of receptor. However, whether the interactions of A262 and V296 in TM region are involved in ligand binding or only in transduction mechanisms remains controversial (Tan et al., 2012, Marchiori et al., 2013). Residues in TM7 were shown to be important for ligand selectivity and receptor activation of T2R10 and T2R46 (Born et al., 2013). This suggests that interaction of residues of three different regions from the extracellular to intracellular side of TM helices plays a vital role in ligand binding, receptor structure and signal transduction.

1.4.5 Intracellular region

The intracellular part is relatively conserved in most of the GPCRs and play a major role in activation mechanisms by their interactions with G proteins (Pydi et al., 2014b). In T2Rs, the role of ICL regions is not completely elucidated. ICL1 is short and poorly studied (Pydi et al., 2012b). Mutation of W25 in ICL1 of T2R43 showed a functional loss of taste with low concentrations of aloin and aristolochic acid. The presence of natural variant P49A in T2R38-ICL1 contributes to the non-taster phenotype (Tan et al., 2012, Marchiori et al., 2013). Since it is believed that non-taster phenotype of T2R38 fails to bind G protein, it appears that ICL1 might be involved in G-protein coupling and receptor activation (Pydi et al., 2012b).

In class A GPCRs, ICL2 is known to be involved in different functions. The

presence of (D/E)RY motif at TM3-ICL2 interface implicates this region in receptor activation. ICL2 is also involved in physical coupling to G-protein (Itoh et al., 2001). The crystal structures of β_1-AR, β_2-AR and muscarinic receptors showed a small helix at the centre of ICL2, which probably acts as a switch for G-protein coupling and its activation (Rasmussen et al., 2011, Warne et al., 2008, Burstein et al., 1998, Hu et al., 2010). It was also further shown to be involved in determining G-protein specificity (Rasmussen et al., 2011). However, the role of ICL2 in T2Rs remains to be elucidated. In T2R1, it was shown that three amino acids H112, P113, L114 in ICL2 form a helix as a component of the active form involved in hydrophobic interactions with G-protein (Dai et al., 2011). Molecular modeling studies on T2R4 have illustrated a short helical region in ICL2, which might be involved in determining G-protein specificity and bitter taste signaling (unpublished data). ICL2 in T2R4 contains two triads of leucine residues, which is similar to that observed in T2R1 (Dai et al., 2011). Functional characterization of the ICL2 residues suggested their role in T2R signaling (unpublished data).

ICL3 has been reported to perform different functions in different GPCR classes (Pydi et al., 2014b). The role of ICL3 in T2R signalling is not completely known. Previously, the molecular determinants in ICL3 required for T2R signalling were examined (Pydi et al., 2014b). Alanine scan mutagenesis of 23 amino acid residues in ICL3 of T2R4 revealed that ICL3 has crucial role in T2R4 activation. The H214A, Q216A, V234A and M237A mutants showed constitutive activity, among which, H214A exhibited a 10-fold higher basal activity than wild type T2R4. This suggests that theses residues are important in stabilizing T2R4 in an inactive conformation. Based on these studies, it was proposed that a dynamic network of interactions between the residues in TM5-ICL3-TM6 restrain the movement of

helices. H214 position is very near to the conserved LxxSL motif in TM5 and is involved in hydrogen bond interactions with LxxSL (Pydi et al., 2014b). As suggested above, the interactions between TM5 and TM6 along with ICL3 seems to play a role in T2R structural and functional mechanisms.

The cytoplasmic C-terminus of GPCRs is known to play a vital role in receptor trafficking, intracellular signalling and receptor internalization (Pankevych et al., 2003, Upadhyaya et al., 2015). Recent report on the C-terminus of T2R4 suggests its role in receptor trafficking and function (Upadhyaya et al., 2015). The C-terminus of T2R4, which consists of 17 amino acids, is polybasic with six lysines and one histidine. Site-directed mutagenesis of 16 residues in the C-terminus region led to the identification of a KL(K/R) motif, which is conserved in 18 of the 25 human T2Rs and across 9 other species analyzed. Mutations in most of these residues have reduced the cell surface expression and function of T2R4, indicating their importance in receptor trafficking and signalling. Mutation of the distal lysine (K296) in KL(K/R) motif resulted in constitutive activity with 5-fold higher basal activity than that of wild type T2R4 (Upadhyaya et al., 2015).

1.5 Novel Insights into T2R Structure and Function

1.5.1 Role of water molecules in T2R structure and function

Internal water molecules have been proposed to play an important role in the structural conformation and activation of GPCRs (Venkatakrishnan et al., 2013). Recent crystal structures of several class A GPCRs suggested that these water molecules are co-localized at the helical bundle around the highly conserved motifs as additional conserved structural elements (Pardo et al., 2007, Sun et al., 2014). In rhodopsin and other GPCRs it was suggested that structurally conserved water

molecules mediate the activation of receptor by disruption of a continuous internal water channel present in an inactive state (Liu et al., 2012, Sun et al., 2014). In contrast, another theory suggests that a gate of hydrophobic amino acids interrupt the internal water channel in the inactive state (Yuan et al., 2014). They propose that upon activation of the receptor, the subsequent conformational changes open a continuous internal water channel in the active state receptor (Yuan et al., 2014).

In this study, I analyzed a few selected inactive state crystal structures of GPCRs from different classes with a resolution less than 3Å (**Table 1.5.1**). Structures with no internal water molecules were excluded. All the structures were superimposed on recent high-resolution crystal structures PDB: 4EIY and PDB:4N6H. Waters present outside the TM region and those with less frequency inside TM bundle were excluded from the analysis. Water molecules from at least two receptors within 2.5Å proximity were selected as same group. I observed 13 water molecules localized within the helical bundles of the analyzed four Class A and one Class F GPCRs (**Figure 1.5.1**). Only two waters (W1 and W3) were observed in smoothened receptor, conserved with 2 other Class A GPCRs (1U19 and 4EIY) towards extracellular region. W4 and W5 are located close to the ligand-binding pocket. Four waters in the helical bundle (W6 -W9) are highly conserved across all the Class A GPCRs analyzed, making contacts with the residues in TM2, 6 and 7. W10, W11 and W12 are conserved in 3 receptors (Table 4) present towards intracellular region. Water-mediated hydrogen bond network around the NPxxY motif seems to play an important role in the rearrangement of receptor (Sun et al., 2014, Yuan et al., 2014). The interactions of water clusters of W6-W9 involve the residues from NPxxY motif

Figure 1.5.1. Analysis of the crystal structures of GPCRs for conserved

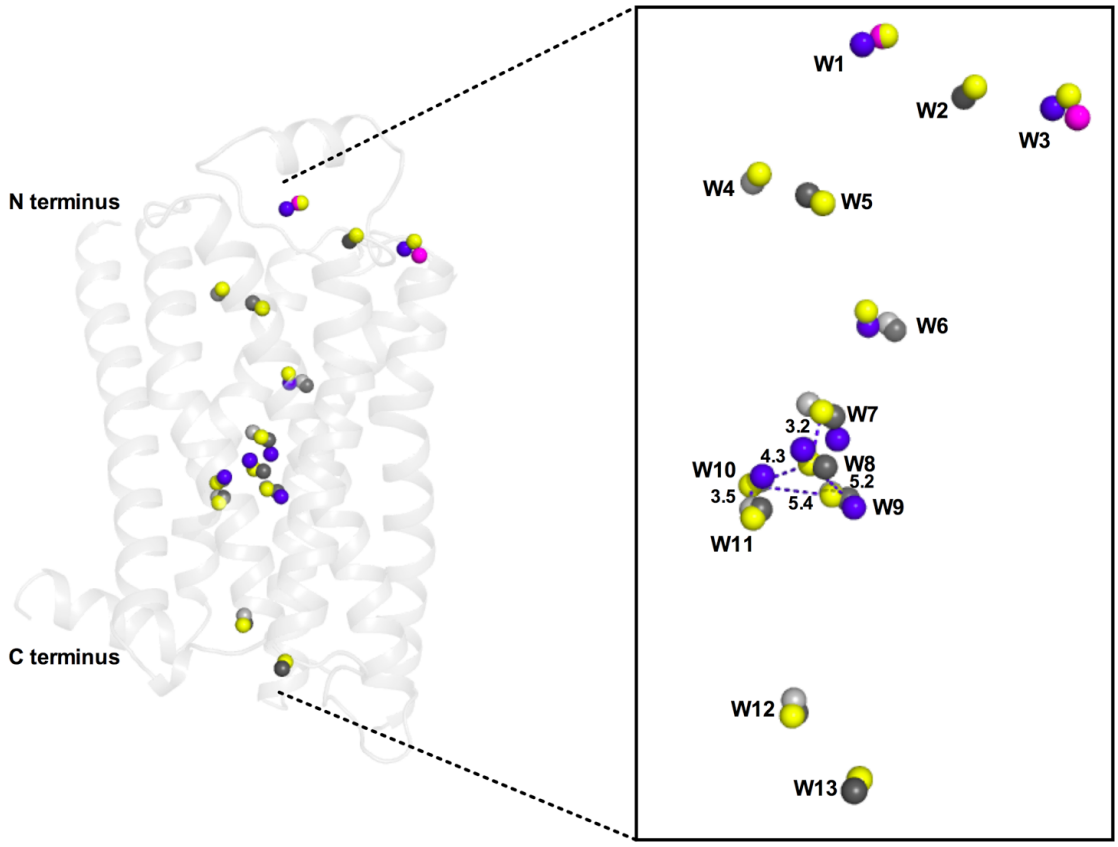

structural waters. The crystal structures of rhodopsin (PDB ID: 1U19, 2.20Å), β_2-adrenergic receptor (PDB ID: 2RH1, 2.40Å), α_2-adenosine receptor (PDB ID: 4EIY, 1.8Å), δ-opioid receptor (PDB ID: 4N6H, 1.8Å and, smoothened receptor (PDB ID: 4JKY, 2.45Å) are superimposed and the 13 most conserved waters (W) were shown in the image with respect to 4EIY structure. In the blown-up inset on the right side, the hydrogen bonded waters are shown as blue (1U19), grey (2RH1), yellow (4EIY), dark green (4N6H) and pink (4JKY) (Jaggupilli et al., 2016).

Table 1.5.1. Most conserved water molecules in Class A and F GPCR crystal structures. O, N atoms are from α helical backbone of the receptor and the underlined atoms are from side chain contacting residues of the receptors. Water molecules within 2.5Å are selected as same group (Jaggupilli et al., 2016)**.**

Water No.	β_2 Adrenergic Receptor (PDB ID:2RH1) 2.80Å	Bovine Rhodopsin (PDB ID:1U19) 2.20Å	α_2 Adenosine Receptor (PDB ID:4EIY) 1.80Å	Delta Opiod Receptor (PDB ID:4N6H) 1.80Å	Smoothened Receptor (PDB ID:4JKV) 2.45Å
1		**WAT2000** Y10 N Y10 O P180$^{4.69}$ Q184$^{4.73}$ OE1	**WAT2583** D170$^{3.18}$ OD1 WAT2541 WAT2572		**WAT736** C217 O S385 OG, N
2			**WAT2573** E169$^{3.17}$ O V172$^{3.20}$ O WAT2559 WAT2560 WAT2587	**WAT1314** K214$^{5.41}$ NZ WAT1315	
3		**WAT2057** D190 O T193 O E201$^{5.36}$ OE2 Q279 OE1	**WAT2539** M174$^{3.22}$ N N155 N WAT2540 WAT2559 WAT2586		**WAT709** R302 NH2 T311$^{3.22}$ O C314$^{3.25}$ N S315$^{3.26}$ N
4	**WAT543** W313$^{7.40}$ NE1 G90$^{2.61}$ O		**WAT2514** Y9$^{1.35}$ OH A63$^{2.61}$ O WAT2524 WAT2584		
5			**WAT2520** A81$^{3.29}$ O WAT2521 WAT2523 WAT2585	**WAT1302** D128$^{3.32}$ OD2 WAT1312 WAT1320	
6	**WAT529** L311$^{7.38}$O C285$^{6.47}$ O F289$^{6.51}$ N	**WAT964** C264$^{6.47}$ O Y268$^{6.51}$ N P291$^{7.38}$ O	**WAT2534** C245$^{6.47}$ O L249$^{6.51}$ N A273 O	**WAT1326** C273$^{6.47}$ O I277$^{6.51}$ N C303$^{7.38}$ O	
7	**WAT534** D79$^{2.49}$ OD1 S319$^{7.46}$ OG W286$^{6.48}$ NE1 G315 $^{7.42}$ O N318$^{7.45}$ ND2 WAT548	**WAT 2015** W265$^{6.48}$ NE1 Y301$^{7.48}$ OH S298$^{7.45}$ O	**WAT2529** W246$^{6.48}$ NE1 N280$^{7.45}$ OD1 WAT2528	**WAT1307** D95$^{2.50}$ OD1 W274$^{6.48}$ NE1 N310$^{7.45}$ OD1 WAT1308 WAT1337	

8	**WAT548** N318$^{7.45}$ ND2 D79 $^{2.50}$OD1 WAT534, WAT532	**WAT2030** D83$^{2.50}$ OD1 G120$^{3.35}$ O S298$^{7.45}$ O N302$^{7.49}$ OD1	**WAT2552** D52$^{2.50}$ OD1,OD2 N280$^{7.45}$ OD1 WAT2553	**WAT1308** D95$^{2.50}$ OD2 S135$^{3.39}$ OG N314$^{7.49}$ ND2 WAT1307 WAT1310	
9	**WAT528** N322 $^{7.49}$ O N318$^{7.45}$ OD1, ND2 I278$^{6.40}$ O	**WAT2020** Y301$^{7.48}$ OH N302$^{7.49}$ ND2 M257$^{6.40}$O	**WAT2532** I238$^{6.40}$ O N280$^{7.45}$ ND2 N284$^{7.49}$ OD1 WAT2553	**WAT1305** V266$^{6.40}$ O N310$^{7.45}$ ND2 N314$^{7.49}$ OD1 WAT1310	
10	**WAT532** D77$^{2.48}$ OD2 N318$^{7.45}$ O N322$^{7.49}$ N WAT506 WAT548	**WAT2017** D83$^{2.50}$ OD2 S298$^{7.45}$ O N302$^{7.49}$ N, OD1	**WAT2533** D52$^{2.50}$ OD2 N280$^{7.45}$ O N284$^{7.49}$ N, ND2 WAT2530		
11	**WAT506** N322 $^{7.49}$ND2 D79 $^{2.50}$OD2 N51$^{1.50}$ OD1 WAT532, WAT546		**WAT2530** N24$^{1.50}$ OD1 D52$^{2.50}$ OD2 N284$^{7.49}$ ND2 WAT2512 WAT2533	**WAT1306** N67$^{1.50}$ OD1 D95$^{2.50}$ OD2 Y318$^{7.53}$ OH	
12	**WAT537** N69$^{2.40}$ OD1		**WAT2641** N42$^{2.40}$ OD1 WAT2676	**WAT1329** N85$^{2.40}$ OD1 D322$^{7.57}$ OD1 WAT1328 WAT1376	
13			**WAT2511** V40$^{2.38}$ N T41$^{2.39}$ N, OG1 Y112$^{3.60}$ OH WAT2569	**WAT1340** A83$^{2.38}$ N	

highlighting its significance in the structure of Class A GPCRs. Conserved hydrogen contacts with side chains of $N^{1.50}$, $D^{2.50}$ and $N^{7.49}$ were observed in most of the clusters demonstrating their functional importance (Angel et al., 2009). However, this analysis

is limited to Class A GPCRs due to the absence of high-resolution crystal structures for other classes of GPCRs to date.

The role of water molecules in T2R structure and activation is poorly studied and understood. As discussed previously an intricate network of hydrogen bonds among the residues in TM1-TM2-TM7 plays a crucial role in the activation mechanism of T2Rs (Singh et al., 2011a). This network might either be absent or significantly modified in the inactive T2Rs and hyperactive mutant T2Rs. Based on the crystal structure of GPCRs discussed above, it is plausible that T2Rs might also have conserved water molecules that play role as both structural and functional determinants. In order to understand this phenomenon, the water molecules were introduced to the molecular model of T2R4 and those in the proximity of conserved residues Gly28$^{1.46}$, Asn32$^{1.50}$, Arg63$^{2.54}$, and Ser285$^{7.47}$ were analyzed (Pydi et al., 2012a). It was proposed that the movement of side chain of Arg63$^{2.54}$ leads to the formation of a continuous hydrogen bond network involving the highly conserved Asn32$^{1.50}$ and structural waters in T2R4 (Pydi et al., 2012a). This aids T2R4 to adopt a constitutive active conformation with structural waters performing an important role. This phenomenon is in agreement with a recent theory proposed explaining the role of internal water molecules in other GPCRs (Yuan et al., 2014). Recently the role of water molecules was studied in the agonist binding mechanism in T2R46. This interesting study proposed the formation of an access channel by water molecules for the agonist to reach its orthosteric site in T2R46 (Sandal et al., 2015). As discussed previously, agonist interacts with more than a dozen water molecules at the extracellular vestibular site. Upon agonist binding, 5-6 water molecules form an access channel with the residues in TM3, 4, 5 6 and 7 connecting the ligand with vestibular and orthosteric sites. An exchange of water molecules was predicted to be

involved in this mechanism that interacts with residues $Y85^{3.29}$, $A89^{3.33}$, $H93^{3.37}$, $T180^{5.43}$, $Y241^{6.51}$, and $Y271^{7.45}$ (generic numbering is according to the cited article) located between TM2 and ECL1 (Sandal et al., 2015). Considering low hydration at the deeper site, it is plausible that the ligand interacts with four water molecules in its orthosteric site. Collectively, the above studies on T2R4 and T2R46 have provided novel insights into the role of structural water molecules in ligand interaction and receptor activation of T2Rs.

1.5.2 Role of cholesterol in the function of T2Rs

Cholesterol is a very important component of higher eukaryotic cell membranes, required for the organization, dynamics and function. Cholesterol content plays a significant role in the membrane dynamics and seems to influence the functionality of membrane proteins. In relation to GPCRs, the role of cholesterol is an emerging area of research (Pucadyil and Chattopadhyay, 2006). It is known to regulate the function of GPCRs through direct or indirect interactions (Sengupta and Chattopadhyay, 2012). Most of the GPCRs consist of a cholesterol recognition/interaction amino acid consensus (CRAC) motif as a molecular determinant required for interaction with cholesterol (Jafurulla et al., 2011). It is characterized by the pattern –L/V-$(X)_{1-5}$-Y-$(X)_{1-5}$-R/K, in which -$(X)_{1-5}$ represents any amino acid in a stretch of one to five residues in length (Sengupta and Chattopadhyay, 2012). Depletion of membrane cholesterol using methyl-β-cyclodextrin (MβCD) negatively influenced the function of serotonin1_A (5-HT1A) receptor causing decreased ligand binding and poor G-protein coupling (Pucadyil and Chattopadhyay, 2004).

Cholesterol dependent signaling functions of T2Rs remain to be elucidated. Multiple amino acid sequence alignment of T2Rs revealed the presence of a CRAC motif (LxxYxxK/R) conserved in 22 of the 25 human T2Rs. This suggests that the CRAC motif might be an inherent characteristic feature of T2Rs as observed in serotonin receptors (Jafurulla et al., 2011). It is present at TM3-ICL2 interface of T2R4 with L110, Y114 and K117 residues possibly interacting with cholesterol. Cholesterol appears to play a role in stabilizing the structure of T2Rs in the membrane and/or modulating their function. Additional molecular details need to be deciphered to understand cholesterol mechanisms in G protein-coupling and T2R signaling.

1.5.3 Ligand bias in T2Rs

For decades, GPCR functioning was thought to be dependent on a discrete "on" and "off" state of conformation with respect to the agonism and antagonism of a ligand (Luttrell, 2014). It is well appreciated that almost every GPCR interacts with multiple intracellular proteins (G proteins, GPCR kinases (GRKs) and β-arrestins) to regulate different cellular responses (Violin et al., 2014). It was believed that a given ligand would either activate or block the entire signal repertoire of a GPCR. However, with the advancements in understanding the complexity of GPCR function, the notion of biased ligands has altered these paradigms (Violin et al., 2014). The likelihood of this concept is the "functional selectivity" of a ligand to activate or block one particular signaling pathway in the signaling repertoire of a receptor (DeWire and Violin, 2011). This infers that different agonists stabilize a unique conformation of the same receptor to create bias towards a selective pathway (Kenakin and Christopoulos, 2013, Kenakin, 2015).

The advancements in novel functional assays must be appreciated, which helped in the expansion of high-throughput screening and ligand detection (Kenakin, 2015). This has led to the emergence of biased ligand concept that further advanced the knowledge of GPCR pharmacology, opening new avenues and implications for novel therapeutics (Violin et al., 2014, DeWire and Violin, 2011). The best-studied examples of ligand bias concept are those of β-arrestin biased signaling at angiotensin II type 1 receptor (AT1R) and β-adrenergic receptors, as well as G protein biased signaling at μ-opioid receptor (Violin et al., 2014, DeWire and Violin, 2011). Early studies revealed the G protein independent signaling of AT1R and led to the discovery of Sar, Ile, Ile-AngII (SII) a synthetic derivative of AT1R's endogenous agonist angiotensin II (Ang II) (Holloway et al., 2002). SII promotes β-arrestin biased signaling to improve cardiac function without activating G protein. This further led to the discovery of TRV027, a potent β-arrestin biased ligand, that also competitively blocks AngII mediated signaling (Violin et al., 2010). TRV027's function is strikingly in contrast to other classic blockers as it is an example of a biased ligand exhibiting both agonist and antagonist features at the same receptor. Similarly, Carvedilol and alprenolol are examples of β-arrestin biased ligands at β1-adrenergic receptors (DeWire and Violin, 2011). On the other hand, TRV130 was identified as a G protein biased ligand at μ-opioid receptor that results in increased analgesia (Tan et al., 2013). In recent GPCR studies, the multiple efficacy fingerprints of ligands and qualities of efficacies are being analyzed using radar plots and clustering studies, which would help in the development of new drugs (Kenakin, 2015).

The concept of biased ligands is yet to be applied to T2Rs. As discussed above, there are indications that T2Rs also activate G proteins other than $G\alpha_{gustducin}$ (Devillier et al., 2015, Caicedo et al., 2003, Sawano et al., 2005). This emphasizes the

possibility that bitter ligands might also stimulate other signaling pathways through T2R activation. T2R studies predominantly depend on Ca^{2+} mobilization to determine the activity of bitter ligands. Focus on second-messenger signaling pathways other than Ca^{2+} mobilization would further reveal the bitter ligands with biased functions (Foster et al., 2014a). More recently it was reported that bitter ligands trigger PLC independent signaling pathways in immortalized human taste cells (HTC-8) stably expressing 13 T2Rs (Hochheimer et al., 2014). Screening alternate signaling pathways of T2Rs may allow the identification of biased bitter ligands.

It is difficult to delineate the biased action of multiple bitter agonists on multiple T2Rs based on these studies. A recent study showed the relaxation of airways at low concentration and vasoconstriction at high concentrations of dextromethorphan (DXM) (Upadhyaya et al., 2014). Knowing that DXM activates only T2R1, this study suggests a biased agonism at different concentrations of DXM at T2R1 in different tissues. At low concentrations, DXM might induce the relaxation of airways through the mechanisms proposed by other studies and at high concentration of DXM the increased Ca^{2+} leads to the activation of myosin light chain kinase subsequently causing contraction (Upadhyaya et al., 2014). When studying biased functions of a ligand, differences in the receptor density in different tissues and sensitivity towards the ligand need to be considered (Kenakin and Christopoulos, 2013). More intensive studies focused on biased functions of bitter agonists are required to understand the on-target effects of T2Rs in different organs.

1.6 T2Rs Expression and Function in Extraoral Tissues

Apart from the expression in oral tissues, T2Rs were also discovered in the gut, and were suggested to have evolved as a central warning signal to induce

aversion towards noxious or harmful substances (Wu et al., 2002). Several recent studies have demonstrated the expression of T2Rs in extraoral tissues in different model systems, reviewed in (Shaik et al., 2016). T2Rs were suggested to play distinct functions with respect to the tissue in which they are expressed. The initial evidence for extraoral expression of taste receptors came from the discovery of α-gustducin in the gut (Hofer et al., 1996). Following these studies, expression of T2Rs was shown in the gastrointestinal (GI) tract where they function in sensing luminal contents and GI hormones (Wu et al., 2002). Successive investigations have expanded the expression and function of T2Rs to detection of bacterial stimulants in upper airways, bronchodilation in lower airways, vasoconstriction in vasculature, nutrient sensing in heart, spermatogenesis in testis, regulation of thyroid stimulating hormone (TSH)-dependent functions in thyroid, anti-inflammation and detecting quorum-sensing molecules (QSMs) in immune system and keratinocyte differentiation in skin (Shah et al., 2009, Tizzano et al., 2010, Deshpande et al., 2010, Upadhyaya et al., 2014, Foster et al., 2013, Li and Zhou, 2012, Clark et al., 2015, Maurer et al., 2015, Wolfle et al., 2015). Despite the reports on the expression of functional T2Rs in brain, breast cancer and bone marrow cells, their exact role in these tissues remains to be elucidated (Singh et al., 2011b, Singh et al., 2014, Lund et al., 2013). Interestingly, in non-gustatory tissues such as the airway smooth muscle cells (ASMCs), it was proposed that T2Rs activation stimulates two opposing Ca^{2+} signaling pathways mediated by βγ subunits (Zhang et al., 2013). The *in vivo* studies on $\alpha_{gustducin}$ knockout mice demonstrated a notable sensitivity to bitter compounds indicating unknown mechanisms in bitter taste signaling other than $\alpha_{gustducin}$ pathway (Wong et al., 1996, Caicedo et al., 2003)

1.6.1 Role of T2Rs in airways

Several ground-breaking studies demonstrated the expression and function of T2Rs in extraoral tissues. The discovery of T2Rs in ASMCs and their role in ASM relaxation have opened an avenue to investigate the new mechanisms involved in asthma (Deshpande et al., 2010, Liggett, 2014). Recent studies have demonstrated that T2Rs are expressed in nasal airways and plays a vital role in transducing the signal from bacterial QSMs (Lee et al., 2012). They recognize the QSMs like acyl homoserine lactone (AHL) molecules that regulate calcium dependent NO production and direct antibacterial effects (Tizzano et al., 2010, Lee et al., 2012, Lee et al., 2014). Furthermore, in mice it was shown that T2Rs mediate the inflammatory responses triggered by AHLs in solitary chemosensory cells (SCCs) (Tizzano et al., 2010). Very recently, based on immunological studies on human neutrophils it was shown that T2R38 is the receptor for N-(3-oxododecanoyl)-l-homoserine lactone (AHL-12) (Maurer et al., 2015). This led to the notion that humans might be able to taste *Pseudomonas aeruginosa* biofilms (Maurer et al., 2015). Another study, using a heterologous system demonstrated that other T2Rs like T2R10 and T2R14 can detect these AHLs (Lossow et al., 2016). It was also speculated that the QSMs might rely on T2Rs to transduce signals in CF (Shah et al., 2009). The studies suggest that AHLs stimulate previously unrecognized receptors and increase the causes for chronic inflammation in CF. However, the existence and role of T2Rs in airway cells of CF patients or CF cell lines is not yet elucidated. T2Rs in general are poorly characterized and very little is known regarding their ligand specificity, pharmacology, and mechanism(s) of activation.

1.6.2 Cystic fibrosis

CF is a life threatening genetic disease that affects lungs, digestive tract and pancreas. It is caused due to several mutations in the ion transport channel called cystic fibrosis transmembrane conductance regulator (CFTR) (Zielenski, 2000). In 70% of the cases, CF is caused due to a 3bp deletion leading to autosomal recessive mutation of phenylalanine residue at position 508 (ΔF508) (Oglesby et al., 2013, Mickle and Cutting, 2000). This loss-of-function mutation makes CFTR dysfunctional and create ionic imbalance in the CF cells. The defective CFTR cannot transport anions, that make airway surface liquid more acidic. The acidic microenvironment may facilitate hyperactivation of ENaC and result in excessive absorption of Na^+ that cause dehydration of airway surface liquid (Garland et al., 2013). As a result, this may lead to the failure of mucus clearance and cause mucus accumulation on the airway epithelium. The subsequent reduction in pH and loss of anti-microbial activity may contribute to more adverse effects.

In such conditions, the prevalence of bacterial colonization and infection by opportunistic bacteria *P. aeruginosa* is a common phenomenon that contributes to the failure of lung function. *P. aeruginosa* produce a wide variety of secretary products that exhibit different properties in the host system. These products may prolong survival of the bacteria by inhibiting phagocytosis and impair mucociliary clearance. They are involved in cleaving immunoglobulins, cytokines and complimentary components produced by the host (Davies, 2002). Biofilm formation is one of the survival strategies of *P. aeruginosa* in the host system. Being an opportunistic pathogen, *P. aeruginosa* possess a panel of secretion systems that play an important role in the specific secretion of different effector proteins or virulence factors produced due to the induction by AHL molecules. This phenomenon facilitates the

bacteria to adapt to the environmental conditions and exhibit pathogenicity (Bleves et al., 2010). However, the signaling network in CF, which is characteristic of chronic inflammation and bacterial infection in airway epithelium is not completely elucidated.

1.6.3 Bacterial quorum sensing molecules secreted by P. aeruginosa

In Gram-negative bacteria such as *P. aeruginosa,* AHLs are the dominant QSMs. When these AHLs reach a critical threshold concentration they bind to and activate the transcriptional regulator, and consequently the quorum-sensing targeted genes are activated or repressed. The quorum sensing systems have been shown to be central to the pathogenesis of many bacterial pathogens including major CF pathogens *Pseudomonas aeruginosa* and *Staphylococcus aureus* (Pearson et al., 1994, Pearson et al., 1995). In patients with CF, *P. aeruginosa* chronic infection ultimately causes pulmonary failure resulting in premature mortality. *P. aeruginosa* produces QSMs to communicate between cells and coordinate pathogenic activity. In *P. aeruginosa*, there are three intertwined quorum-sensing systems, the AHL mediated *las* and *rhl* systems, and the 2-Alkyl-4(1*H*)-quinolone (AHQ) signal based system (Williams et al., 2007, von Bodman et al., 2008, Diggle et al., 2007, Diggle et al., 2006). The *las* and *rhl* systems consist of a transcriptional activator LasR and RhlR and a signal synthase LasI and RhlI respectively. The signals in the *las* and *rhl* systems are *N*-(3-oxododecanoyl)–AHL (3-oxo-C_{12}-AHL) and *N*-butyryl- AHL (C_4-AHL) respectively. The other cell-cell signaling system in *P. aeruginosa* functions through the AHQ signals (Diggle et al., 2006, Pesci et al., 1999). The major AHQ molecules include 2-heptyl-3-hydroxy-4-quinolone (the *Pseudomonas* Quinolone Signal, PQS) and 2-heptyl-4-hydroxyquinolone (HHQ) (Deziel et al., 2004, Diggle et al., 2006, Diggle et al., 2003, Pesci et al., 1999). Approximately 300 genes in *P. aeruginosa* genome are

controlled by QS (Wagner et al., 2003). A large array of genes, including critical virulence factors and genes involved in biofilm formation are controlled by its quorum sensing systems (Hastings, 2004).

Bacterial AHLs have been shown to interact with mammalian host cells, a process termed as inter-kingdom signaling (Shiner et al., 2005). AHLs can modulate inflammatory and immune responses (Ritchie et al., 2007). 3-oxo-C12-AHL and C4-AHL from *P. aeruginosa* are commonly detectable in the sputum from CF patients (Middleton et al., 2002), and can inhibit cytokine production in T-cells and function of antigen presenting cells (Ritchie et al., 2007). However, little is known about the molecules present outside or inside the mammalian cells that AHLs interact with. It was suggested that these AHLs act through various signaling pathways that involve cell surface receptors (Shiner et al., 2005, Shiner et al., 2006, Karlsson et al., 2012). This gives a strong rationale to consider the role of T2Rs in chemosensory mechanisms involved in CF.

1.6.4 T2Rs as host cell surface targets of antibiotics

Antibiotics play an indispensable role and are often prescribed in the treatments of several infectious diseases like CF, tuberculosis, pneumonia, chronic rhinosinusitis (CRS) and in invasive surgery (Pawlowski et al., 2016, Miravitlles and Anzueto, 2013, Sengupta et al., 2013, Perry and Wright, 2014). However, there is uncertainty about the antibiotic reaching the appropriate target and its distribution. For example in CF disease, high variability among the patient sample size, age and severity of infection commonly determines the dose of antibiotics (Geller, 2009).

In recent years, the non-antibiotic roles of these drugs that both positive and negative effects on the host have begun to be characterized. Antibiotics that belong to

macrolides can regulate inflammatory conditions, due to these properties they are gaining importance in the treatment of asthma (Culic et al., 2001, Good et al., 2012). In certain asthmatic conditions, macrolides target immune cells like leukocytes and neutrophils and decrease the production of pro-inflammatory cytokines and increase the release of anti-inflammatory cytokines by inhibiting cytochrome P450 system (Rollins et al., 2010, Gao et al., 2010). They also improve macrophage functions such as chemotactic and phagocytic capacity (Gao et al., 2010). However, in certain pathophysiological conditions, these non-antibiotic effects target immunomodulatory pathways and cause adverse effects like tendinopathy and autonomic neuropathy (Suresh Babu et al., 2013, Badal et al., 2015, Hobson-Webb et al., 2006).

Fluoroquinolones were shown to act as iron chelators causing epigenetic effects by inhibition of α-ketoglutarate-dependent dioxygenases (Badal et al., 2015). Levofloxacin a well-known fluoroquinolone, improves lung function in CF patients while reducing *P. aeruginosa* density in sputum (Suresh Babu et al., 2013). It is associated with dysglycemia observed in diabetic and non-diabetic patients (Park-Wyllie et al., 2006). In stable COPD patients, levofloxacin treatment reduced neutrophil count in the sputum (Siva et al., 2014). Levofloxacin was also shown to play an immunoregulatory function in IL-1β production by activating MAPK pathway in mouse macrophages (Kitazawa et al., 2007). Aminoglycoside antibiotics like tobramycin are widely used against gram-negative bacteria like *P. aeruginosa* in CF. However; these antibiotics often exhibit nephrotoxicity and loss of cochlear hair cell (Huth et al., 2015, Jiang et al., 2017). Based on these observations, antibiotics seem to have multiple roles in regulating or modulating physiological mechanisms in the host. As the first point of contact for these antibiotics are cell surface proteins on the host cell, it is crucial that these host receptors are identified. This would enable the

physiological responses of the host and their underlying mechanisms to be characterized.

Previously a it was proposed that any bitter tasting drug could have some unintended effects in the body through activation of T2Rs (Clark et al., 2012). With the wide spread distribution of the 25 T2Rs in human tissues, inhaled or orally administered bitter drugs could also exhibit off-target effects that are beneficial to the system (Levit et al., 2014). There are few reports of antibiotics activating T2Rs. Ofloxacin was shown to activate T2R9, and chloramphenicol, erythromycin activated multiple T2Rs (Dotson et al., 2008, Meyerhof et al., 2010). The structures of the bitter tasting compounds exhibit high diversity and include quinolones, amides, alkaloids, phenols, flavonoids, glycosides and terpenoids (Meyerhof et al., 2010). Analysis of the structural features of several classes of antibiotics that belong to fluoroquinolones, aminoglycosides and macrolides might reveal their close identity or as derivatives of the parent structures of above mentioned bitter tasting compounds.

Thus, it is necessary to investigate the expression of functional T2Rs in lower airway epithelium and elucidate the variety of ligands they recognize in CF conditions Further structure-function studies would provide insights into the binding interactions of the novel T2R ligands.

CHAPTER 2

2.0 HYPOTHESIS AND OBJECTIVES

2.1 Study Rationale

The North American Epidemiological Study of Cystic Fibrosis (ESCF) suggests >19% of CF patients (both adults and children) have asthma (Morgan et al., 1999, Kent et al., 2014). More than 88% of the asthma CF patients in the ESCF study received some form of inhaled bronchodilators. Emerging evidence indicates that the taste sensing proteins, especially T2Rs, represent a potential novel target for bronchodilators. In humans, there are 25 T2Rs, and very little is known regarding their pharmacology. Activation of T2Rs in airway smooth muscle cells leads to muscle relaxation and bronchodilation which is greater than that elicited by β_2-AR agonists. In human airway epithelia, inhaled bitter compounds activate T2Rs on motile cilia and stimulate the ciliary activity to hasten the elimination of harmful substances. The ligands that activate T2Rs have very diverse chemical structures. Recent groundbreaking studies have shown that T2Rs expressed in the human upper respiratory epithelium are activated by AHLs, the QSMs secreted by many Gram-negative bacteria. Taken together, these recent studies suggest that the chemosensory T2Rs are sentinels for detecting chemical stimuli in the airways. The major cause of mortality in CF is pulmonary infection and associated inflammation, which ultimately leads to pulmonary failure. The infecting bacteria secrete QSMs, which not only help in bacterial-bacterial communication, but are also shown to play a key role in bacteria-host interaction. However, the airway epithelial cell surface receptors that QSMs interact with in CF and cause increase in intracellular calcium responses are poorly understood. Given that T2Rs are known to be expressed in the airway epithelia and

their role in detecting chemical stimuli, they may be credible targets in the host for bacterial QSMs.

2.2 Hypothesis

Human airways show differential expression of T2Rs in pathophysiological conditions such as cystic fibrosis and mediate host-pathogen interactions by recognizing bacterial quorum sensing molecules and bitter compounds in airways.

2.3 Objectives

To test the hypotheses, I pursued the four objectives described below using a combination of sensory analysis, molecular, biochemical and pharmacological approaches.

2.3.1 To characterize the functional expression of T2Rs in normal and cystic fibrosis airway cells

The focus of this objective is, first to analyze the expression patterns of T2Rs at both transcript and protein levels in normal and cystic fibrosis airway cells. Second, to study the functionality of the T2Rs in airway cells using bitter agonists and bacterial stimulants in presence or absence of inhibitors of downstream effectors in T2R pathway.

2.3.2 Characterize the interaction of commonly used CF antibiotics with T2Rs

Here, the focus is to obtain mechanistic insights into the binding of CF antibiotics to selected T2Rs. To identify and characterize the roles of conserved,

antibiotics specific and receptor specific amino acids in T2Rs by using site-directed mutagenesis guided by molecular modeling studies.

2.3.3 Characterize the interaction of T2Rs with the major QSMs secreted by bacteria in CF

The initial focus of the objective is to characterize the taste sensory profile or bitterness of major QSMs. Then in an approach similar to objective 2.3.2, to functionally characterize the interaction of the QSMs with selected T2Rs.

2.3.4 Discovery of novel bitter ligands and their mechanisms of action on T2R4

The focus of this objective is, to discover and characterize the novel ligands of T2R4 derived from plant and meat products using pharmacological and molecular modeling studies.

CHAPTER 3

3.0 MATERIALS AND METHODS

3.1 Materials

Dulbecco's modified Eagle's medium (DMEM), Ham's F-12, DMEM-F12, penicillin, streptomycin, 100X L-glutamine, trypsin-EDTA, Calcium sensitive dye Fluo-4NW and lipofectamine 2000 were purchased from Life Technologies (Burlington, ON, Canada). Bronchial Epithelial Growth Medium (BEGM) Bullet Kit (CC-3170) was purchased from Lonza and Cedarlane (Burlington, ON, Canada). RNA isolation kit and cDNA synthesis kit were purchased from Qiagen (Toronto, ON, Canada) and Invitrogen. The nCounter CodeSets for TAS2Rs and the tissue marker genes were purchased from NanoString Technologies (Seattle, WA, USA). The HUGO gene nomenclature is used wherever the genes are mentioned. Hygromycin, abscisic acid (ABA), Nα, Nα-Bis carboxy Methyl L-Lysine (BCML), N-Butyryl-DL-homoserine lactone (C4-AHL), N-Octanoyl-DL-homoserine lactone (C8-AHL), N-3-Oxododecanoyl-L-homoserine lactone (3-oxo-C12-AHL), 2-Heptyl-3-hydroxy-4(1H)-quinolone (HHQ), phospholipase C inhibitor (U-73122), human placental collagen type IV, and Fetal bovine serum (FBS) were purchased from Sigma-Aldrich Canada Co (Oakville, ON, Canada). 2-nonyl-3-hydroxy-4-quinolone (NHQ) was purchased from Cayman chemical (Ann Arbor, MI, USA). The two advanced glycation end-products, Glyoxal-derived lysine dimer (GOLD) and Epsilon-N-carboxy methyl-L-lysine (CML) were purchased from PolyPeptide Laboratories (Strasbourg, France). Gβγ subunit inhibitor (Gallein) was purchased from Tocris and Cedarlane (Burlignton, ON, Canada). Other common chemicals and bitter compounds including antibiotics tested in this study were purchased either from Fisher Scientific (Toronto, ON, Canada) or Sigma-Aldrich (Toronto, ON, Canada). For the e-tounge

experiment most of the bitter compounds used were from Sigma Chemical Co. Acetaminophen, caffeine monohydrate, quinine hydrochloride (QHCl), leporamide hydrochloride and femotidine were purchased from MP Biomedicals (Solon, OH, USA). HCl (0.1 and 1M), sodium chloride (1M) and monosodium glutamate (MSG 0.1M) solutions were provided by Alpha M.O.S. All chemicals were of analytical grade and used without further purification. The Gα16/44 chimera plasmid was a kind gift from Dr. Takashi Ueda, Nagoya City University, Japan.

***Cells**:* Human bronchial epithelial cells from normal lung with immortalized E6/E7 and hTERT expression (NuLi-1, CRL-4011), and Human airway epithelial cells from a CF patient homozygous for ΔF508/Δ F508 and immortalized with E6/E7 and hTERT expression (CuFi-1, CRL-4013) were purchased from ATCC. Human bronchial epithelial primary cells (CF donors: BCF00710, BSCR080909, BSCR310111 and non-CF donors: BD150412, BSCD080909, BSCD310111) were obtained or purchased from the primary airway biobank of the CF Canada funded core facility, the Cystic Fibrosis Translational Research Center (CFTRc), McGill University, Canada.

***Antibodies**:* The polyclonal antibodies for flow cytometry analysis are rabbit anti-T2R3 (OAAF05229) and rabbit anti-T2R5 (OASG06985) purchased from Aviva Systems Biology (San Diego, CA, USA), rabbit anti-T2R4 (OSR00153W, whole serum) from Thermo Scientific (Burlington, ON, Canada), rabbit anti-T2R10 (sc-169473), goat anti-T2R20 (T2R49) (sc-34531), goat anti-T2R38 (sc-34294) were purchased from Santa Cruz Biotechnology (Dallas, TX, USA) and mouse anti-β_2AR monoclonal antibody (MCA2784) was purchased from Bio-Rad (Mississauga, ON, Canada). Isotype control normal rabbit serum (sc-2338), normal rabbit IgG (sc-3888),

normal mouse IgG (12-371), normal goat IgG (sc-3887) were purchased from Santa Cruz Biotechnology.

3.1.1 Media for bacterial culture

Luria-Bertain (LB) media: 10g of tryptone, 5g of yeast extract and 10g of sodium chloride were dissolved in 1 L of deionised water and autoclaved for 45 min.

LB Agar-ampicillin: 15g of agar was added to the LB media prepared as described above and dissolved. The media was autoclaved for 45 min and allowed to cool to 55°C. At this temperature, 1ml of 100 mg/ml ampicillin stock solution was added to 1000 ml and mixed well without forming bubbles. 10 ml of this media was poured into petri dishes and solidified at room temperature for 2-3 hrs. After solidification, the plates were stored at 4°C until use.

SOB medium: 20g Bacto-tryptone (2%), 5g Bacto-yeast extract (0.5%), 0.5g NaCl (10 mM) and 0.19g KCl (2.5 mM) were dissolved in 1L of deionized water and adjusted to pH 7 using 10N NaOH followed by autoclaving to sterilize. 10 ml of 1M $MgCl_2$ was added before use.

3.1.2 Media for mammalian cell culture

DMEM/F12: Ham's F-12/DMEM with High Glucose (1:1, Gibco, Invitrogen) was supplemented with 10% FBS (heat inactivated at 56°C for 45 min), 100 mg/ml pencillin, 100 mg/ml streptomycin. This media was used for culturing Human Embryonic Kidney cells (HEK cells).

Bronchial epithelial growth medium (BEGM): Bronchial epithelial basal medium (BEBM) basal medium was supplemented with 9 supplements obtained with the bullet kit. This media was used for culturing human bronchial epithelial primary

cells and cell lines.

3.1.3 Buffers

***Phosphate Buffer Solution** (PBS)*: 137 mM NaCl, 2.7 mM KCl, 1.8 mM KH_2PO_4, 10 mM Na_2HPO_4. The pH was at 6.8 for 10X and 7.4 for 1X PBS.

4% Paraformaldehyde / 1X PBS: 4 g paraformaldehyde was dissolved in 100 ml 1xPBS by heating slowly at 60°C. After cooling pH was adjusted to 7.2-7.4.

TAE (Tris Acetate-EDTA): 4.84 g Tris, 2 ml 0.5 M Na_2EDTA (pH 8.0), 1.1 ml glacial acetic acid, and water to make 1 litre.

FACS buffer: 0.5% BSA dissolved in 1xPBS

***Transformation buffer (TB)**:* 1.18g Hepes, 9.3g KCl and 1.1g $CaCl_2$ was dissolved in 500 ml deionized water and adjusted to pH 6.7 using KOH. Then 5.4g $MnCl_2$ was added, filter sterilized using 0.2 μm filter and stored at 4°C.

3.2 Molecular Biology and Cell Culture

3.2.1 TAS2R1, TAS2R4, TAS2R14 and TAS2R20

The molecular biology of N-terminal FLAG epitope tagged human TAS2R1, TAS2R4, TAS2R14 and TAS2R20 genes were codon-optimized for expression in mammalian cells and cloned into the KpnI-NotI site of pcDNA 3.1/Hygro (+) expression vector. The synthetic FLAG-TAS2R genes were designed by introducing a Kpn1 restriction site at 5' end followed by a Kozak consensus (GCCACCATGG) 5' to the ATG start codon. An octa-peptide FLAG tag (DYKDDDDK) was included after the start codon and followed by the gene sequence. NotI restriction site was introduced at the 3' end of the gene and introduced into pcDNA 3.1/hygro vector. The restriction sites were included to facilitate cloning. The sequence encoding the human TAS2R1**,** TAS2R4, TAS2R14 and TAS2R20 **(Figure 3.2.1 - 3.2.4)** genes were

optimized for mammalian cell codon usage, and each gene was synthesized commercially (Genescript, NJ, USA). The synthetic TAS2Rs gene were then inserted into the KpnI and NotI sites of the mammalian expression vector pcDNA3.1/Hygro (Invitrogen). DNA sequence for each gene was verified by automated DNA sequencing (MICB DNA Sequencing Facility, Winnipeg). The wild type TAS2R genes in pcDNA 3.1 were used for transfection.

3.2.2 Preparation of competent E. coli cells

Competent *E. coli* cells were prepared by following Inoue method (Inoue et al., 1990). DH5α cells from frozen stock in LB/50% glycerol were grown overnight in 5 ml of LB media at 37°C. From this, a 100 µl of the saturated *E.coli* DH5α culture was inoculated in 100 ml SOB media in a 1L flask and incubated at 22°C for 18 h with vigorous shaking at 200-250 rpm or until an A_{600} of 0.6 was obtained. The flask was placed on ice for 10 min to chill the cells. Subsequently, the cells were centrifuged in a 50 ml falcon tube at 2500 × g (4100 rpm) for 10 min at 4°C using SLA 1500 rotor in Sorvall RC- 6 Centrifuge. The cell pellet was resuspended gently in 32 ml of ice-cold transformation buffer and again chilled on ice for 10 min followed by centrifugation as above. The cell pellet was resuspended gently in 8 ml of ice-cold transformation buffer and DMSO was added with gentle swirling to a final concentration of 7% (0.6 ml for 8 ml transformation buffer). The cells were again chilled on ice for10 min and the cell suspension was aliquoted into 100 µl per eppendorf tube and stored at -80° C until use.

Kpn1 kozak flag tag

GGTACCGCCACCATGGACTACAAGGACGACGATGACAAACTAGAGTCTCACCTCATTATCTATTTTCTT
CTTGCAGTGATACAATTTCTTCTTGGGATTTTCACAAATGGCATCATTGTGGTGGTGAATGGCATTGAC
TTGATCAAGCACAGAAAAATGGCTCCGCTGGATCTCCTTCTTTCTTGTCTGGCAGTTTCTAGAATTTTT
CTGCAGTTGTTCATCTTCTACGTTAATGTGATTGTTATCTTCTTCATAGAATTCATCATGTGTTCTGCG
AATTGTGCAATTCTCTTATTTATAAATGAATTGGAACTTTGGCTTGCCACATGGCTCGGCGTTTTCTAT
TGTGCCAAGGTTGCCAGCGTCCGTCACCCACTCTTCATCTGGTTGAAGATGAGGATATCCAAGCTGGTC
CCATGGATGATCCTGGGGTCTCTGCTATATGTATCTATGATTTGTGTTTTCCATAGCAAATATGCAGGG
TTTATGGTCCCATACTTCCTAAGGAAATTTTTCTCCCAAAATGCCACAATTCAAAAAGAAGATACACTG
GCTATACAGATTTTCTCTTTTGTTGCTGAGTTCTCAGTGCCATTGCTTATCTTCCTTTTTGCTGTTTTG
CTCTTGATTTTCTCTCTGGGGAGGCACACCCGGCAAATGAGAAACACAGTGGCCGGCAGCAGGGTTCCT
GGCAGGGGTGCACCCATCAGCGCGTTGCTGTCTATCCTGTCCTTCCTGATCCTCTACTTCTCCCACTGC
ATGATAAAAGTTTTTCTCTCTTCTCTAAAGTTTCACATCAGAAGGTTCATCTTTCTGTTCTTCATCCTT
GTGATTGGTATATACCCTTCTGGACACTCTCTCATCTTAATTTTAGGAAATCCTAAATTGAAACAAAAT
GCAAAAAAGTTCCTCCTCCACAGTAAGTGCTGTCAG**TGA**GCGGCCGC

Stop Not1

```
ATGCTAGAGTCTCAC CTCATTATCTATTTT CTTCTTGCAGTGATA CAATTTCTTCTTGGG ATTTTCACAAATGGC
 M  L  E  S  H   L  I  I  Y  F   L  L  A  V  I   Q  F  L  L  G   I  F  T  N  G
ATCATTGTGGTGGTG AATGGCATTGACTTG ATCAAGCACAGAAAA ATGGCTCCGCTGGAT CTCCTTCTTTCTTGT
 I  I  V  V  V   N  G  I  D  L   I  K  H  R  K   M  A  P  L  D   L  L  L  S  C
CTGGCAGTTTCTAGA ATTTTTCTGCAGTTG TTCATCTTCTACGTT AATGTGATTGTTATC TTCTTCATAGAATTC
 L  A  V  S  R   I  F  L  Q  L   F  I  F  Y  V   N  V  I  V  I   F  F  I  E  F
ATCATGTGTTCTGCG AATTGTGCAATTCTC TTATTTATAAATGAA TTGGAACTTTGGCTT GCCACATGGCTCGGC
 I  M  C  S  A   N  C  A  I  L   L  F  I  N  E   L  E  L  W  L   A  T  W  L  G
GTTTTCTATTGTGCC AAGGTTGCCAGCGTC CGTCACCCACTCTTC ATCTGGTTGAAGATG AGGATATCCAAGCTG
 V  F  Y  C  A   K  V  A  S  V   R  H  P  L  F   I  W  L  K  M   R  I  S  K  L
GTCCCATGGATGATC CTGGGGTCTCTGCTA TATGTATCTATGATT TGTGTTTTCCATAGC AAATATGCAGGGTTT
 V  P  W  M  I   L  G  S  L  L   Y  V  S  M  I   C  V  F  H  S   K  Y  A  G  F
ATGGTCCCATACTTC CTAAGGAAATTTTTC TCCCAAAATGCCACA ATTCAAAAAGAAGAT ACACTGGCTATACAG
 M  V  P  Y  F   L  R  K  F  F   S  Q  N  A  T   I  Q  K  E  D   T  L  A  I  Q
ATTTTCTCTTTTGTT GCTGAGTTCTCAGTG CCATTGCTTATCTTC CTTTTTGCTGTTTTG CTCTTGATTTTCTCT
 I  F  S  F  V   A  E  F  S  V   P  L  L  I  F   L  F  A  V  L   L  L  I  F  S
CTGGGGAGGCACACC CGGCAAATGAGAAAC ACAGTGGCCGGCAGC AGGGTTCCTGGCAGG GGTGCACCCATCAGC
 L  G  R  H  T   R  Q  M  R  N   T  V  A  G  S   R  V  P  G  R   G  A  P  I  S
GCGTTGCTGTCTATC CTGTCCTTCCTGATC CTCTACTTCTCCCAC TGCATGATAAAAGTT TTTCTCTCTTCTCTA
 A  L  L  S  I   L  S  F  L  I   L  Y  F  S  H   C  M  I  K  V   F  L  S  S  L
AAGTTTCACATCAGA AGGTTCATCTTTCTG TTCTTCATCCTTGTG ATTGGTATATACCCT TCTGGACACTCTCTC
 K  F  H  I  R   R  F  I  F  L   F  F  I  L  V   I  G  I  Y  P   S  G  H  S  L
ATCTTAATTTTAGGA AATCCTAAATTGAAA CAAAATGCAAAAAAG TTCCTCCTCCACAGT AAGTGCTGTCAGTGA
 I  L  I  L  G   N  P  K  L  K   Q  N  A  K  K   F  L  L  H  S   K  C  C  Q  *
```

Figure 3.2.1. Nucleotide and amino acid sequence of codon-optimized T2R1. *EcoR1* and *Not1* restriction sites were included at the 5' and 3' end of the gene (light blue). *Kozak* sequence (brown) was introduced before the start codon (blue) followed by the FLAG sequence (red).

Kpn1 kozak flag tag

GGTACCGCCACCATGGACTACAAGGACGACGATGACAAACTTCGGTTATTCTATTTCTCTGCTATTATT
GCCTCAGTTATTTTAAATTTTGTAGGAATCATTATGAATCTGTTTATTACAGTGGTCAATTGCAAAACT
TGGGTCAAAAGCCATAGAATCTCCTCTTCTGATAGGATTCTGTTCAGCCTGGGCATCACCAGGTTTCTT
ATGCTGGGACTATTTCTGGTGAACACCATCTACTTCGTCTCTTCAAATACGGAAAGGTCAGTCTACCTG
TCTGCTTTTTTTGTGTTGTGTTTCATGTTTTTGGACTCGAGCAGTGTCTGGTTTGTGACCTTGCTCAAT
ATCTTGTACTGTGTGAAGATTACTAACTTCCAACACTCAGTGTTTCTCCTGCTGAAGCGGAATATCTCC
CCAAAGATCCCCAGGCTGCTGCTGGCCTGTGTGCTGATTTCTGCTTTCACCACTTGCCTGTACATCACG
CTTAGCCAGGCATCACCTTTTCCTGAACTTGTGACTACGAGAAATAACACATCATTTAATATCAGTGAG
GGCATCTTGTCTTTAGTGGTTTCTTTGGTCTTGAGCTCATCTCTCCAGTTCATCATTAATGTGACTTCT
GCTTCCTTGCTAATACACTCCTTGAGGAGACATATACAGAAGATGCAGAAAAATGCCACTGGTTTCTGG
AATCCCCAGACGGAAGCTCATGTAGGTGCTATGAAGCTGATGGTCTATTTCCTCATCCTCTACATTCCA
TATTCAGTTGCTACCCTGGTCCAGTATCTCCCCTTTTATGCAGGGATGGATATGGGGACCAAATCCATT
TGTCTGATTTTTGCCACCCTTTACTCTCCAGGACATTCTGTTCTCATTATTATCACACATCCTAAACTG
AAAACAACAGCAAAGAAGATTCTTTGTTTCAAAAAA**TAG**GCGGCCGC
Stop Not1

```
ATGCTTCGGTTATTC TATTTCTCTGCTATT ATTGCCTCAGTTATT TTAAATTTTGTAGGA ATCATTATGAATCTG
 M  L  R  L  F   Y  F  S  A  I   I  A  S  V  I   L  N  F  V  G   I  I  M  N  L
TTTATTACAGTGGTC AATTGCAAAACTTGG GTCAAAAGCCATAGA ATCTCCTCTTCTGAT AGGATTCTGTTCAGC
 F  I  T  V  V   N  C  K  T  W   V  K  S  H  R   I  S  S  S  D   R  I  L  F  S
CTGGGCATCACCAGG TTTCTTATGCTGGGA CTATTTCTGGTGAAC ACCATCTACTTCGTC TCTTCAAATACGGAA
 L  G  I  T  R   F  L  M  L  G   L  F  L  V  N   T  I  Y  F  V   S  S  N  T  E
AGGTCAGTCTACCTG TCTGCTTTTTTTGTG TTGTGTTTCATGTTT TTGGACTCGAGCAGT GTCTGGTTTGTGACC
 R  S  V  Y  L   S  A  F  F  V   L  C  F  M  F   L  D  S  S  S   V  W  F  V  T
TTGCTCAATATCTTG TACTGTGTGAAGATT ACTAACTTCCAACAC TCAGTGTTTCTCCTG CTGAAGCGGAATATC
 L  L  N  I  L   Y  C  V  K  I   T  N  F  Q  H   S  V  F  L  L   L  K  R  N  I
TCCCCAAAGATCCCC AGGCTGCTGCTGGCC TGTGTGCTGATTTCT GCTTTCACCACTTGC CTGTACATCACGCTT
 S  P  K  I  P   R  L  L  L  A   C  V  L  I  S   A  F  T  T  C   L  Y  I  T  L
AGCCAGGCATCACCT TTTCCTGAACTTGTG ACTACGAGAAATAAC ACATCATTTAATATC AGTGAGGGCATCTTG
 S  Q  A  S  P   F  P  E  L  V   T  T  R  N  N   T  S  F  N  I   S  E  G  I  L
TCTTTAGTGGTTTCT TTGGTCTTGAGCTCA TCTCTCCAGTTCATC ATTAATGTGACTTCT GCTTCCTTGCTAATA
 S  L  V  V  S   L  V  L  S  S   S  L  Q  F  I   I  N  V  T  S   A  S  L  L  I
CACTCCTTGAGGAGA CATATACAGAAGATG CAGAAAAATGCCACT GGTTTCTGGAATCCC CAGACGGAAGCTCAT
 H  S  L  R  R   H  I  Q  K  M   Q  K  N  A  T   G  F  W  N  P   Q  T  E  A  H
GTAGGTGCTATGAAG CTGATGGTCTATTTC CTCATCCTCTACATT CCATATTCAGTTGCT ACCCTGGTCCAGTAT
 V  G  A  M  K   L  M  V  Y  F   L  I  L  Y  I   P  Y  S  V  A   T  L  V  Q  Y
CTCCCCTTTTATGCA GGGATGGATATGGGG ACCAAATCCATTTGT CTGATTTTTGCCACC CTTTACTCTCCAGGA
 L  P  F  Y  A   G  M  D  M  G   T  K  S  I  C   L  I  F  A  T   L  Y  S  P  G
CATTCTGTTCTCATT ATTATCACACATCCT AAACTGAAAACAACA GCAAAGAAGATTCTT TGTTTCAAAAAATAG
 H  S  V  L  I   I  I  T  H  P   K  L  K  T  T   A  K  K  I  L   C  F  K  K  *
```

Figure 3.2.2. Nucleotide and amino acid sequence of codon-optimized T2R4. *Kpn1* and *Not1* restriction sites were included at the 5' and 3' end of the gene (light blue). *Kozak* sequence (brown) was introduced before the start codon (blue) followed by the FLAG sequence (red).

Kpn1 kozak flag tag

GGTACCGCCACCATGGACTACAAGGACGACGATGACAAAGGTGGTGTCATAAAGAGCATATTTACATTC
GTTTTAATTGTGGAATTTATAATTGGAAATTTAGGAAATAGTTTCATAGCACTGGTGAACTGTATTGAC
TGGGTCAAGGGAAGAAAGATCTCTTCGGTTGATCGGATCCTCACTGCTTTGGCAATCTCTCGAATTAGC
CTGGTTTGGTTAATATTCGGAAGCTGGTGTGTGTCTGTGTTTTTCCCAGCTTTATTTGCCACTGAAAAA
ATGTTCAGAATGCTTACTAATATCTGGACAGTGATCAATCATTTTAGTGTCTGGTTAGCTACAGGCCTC
GGTACTTTTTATTTTCTCAAGATAGCCAATTTTTCTAACTCTATTTTTCTCTACCTAAAGTGGAGGGTT
AAAAAGGTGGTTTTGGTGCTGCTTCTTGTGACTTCGGTCTTC
TTGTTTTTAAATATTGCACTGATAAACATCCATATAAATGCCAGTATCAATGGATACAGAAGAAACAAG
ACTTGCAGTTCTGATTCAAGTAACTTTACACGATTTTCCAGTCTTATTGTATTAACCAGCACTGTGTTC
ATTTTCATACCCTTTACTTTGTCCCTGGCAATGTTTCTTCTCCTCATCTTCTCCATGTGGAAACATCGC
AAGAAGATGCAGCACACTGTCAAAATATCCGGAGACGCCAGCACCAAAGCCCACAGAGGAGTTAAAAGT
GTGATCACTTTCTTCCTACTCTATGCCATTTTCTCTCTGTCTTTTTTCATATCAGTTTGGACCTCTGAA
AGGTTGGAGGAAAATCTAATTATTCTTTCCCAGGTGATGGGAATGGCTTATCCTTCATGTCACTCATGT
GTTCTGATTCTTGGAAACAAGAAGCTGAGACAGGCCTCTCTGTCAGTGCTACTGTGGCTGAGGTACATG
TTCAAAGATGGGGAGCCCTCAGGTCACAAAGAATTTAGAGAATCATCT**TGA**GCGGCCGC
Stop Not1

```
ATGGGTGGTGTCATA AAGAGCATATTTACA TTCGTTTTAATTGTG GAATTTATAATTGGA AATTTAGGAAATAGT
 M  G  G  V  I   K  S  I  F  T   F  V  L  I  V   E  F  I  I  G   N  L  G  N  S
TTCATAGCACTGGTG AACTGTATTGACTGG GTCAAGGGAAGAAAG ATCTCTTCGGTTGAT CGGATCCTCACTGCT
 F  I  A  L  V   N  C  I  D  W   V  K  G  R  K   I  S  S  V  D   R  I  L  T  A
TTGGCAATCTCTCGA ATTAGCCTGGTTTGG TTAATATTCGGAAGC TGGTGTGTGTCTGTG TTTTTCCCAGCTTTA
 L  A  I  S  R   I  S  L  V  W   L  I  F  G  S   W  C  V  S  V   F  F  P  A  L
TTTGCCACTGAAAAA ATGTTCAGAATGCTT ACTAATATCTGGACA GTGATCAATCATTTT AGTGTCTGGTTAGCT
 F  A  T  E  K   M  F  R  M  L   T  N  I  W  T   V  I  N  H  F   S  V  W  L  A
ACAGGCCTCGGTACT TTTTATTTTCTCAAG ATAGCCAATTTTTCT AACTCTATTTTTCTC TACCTAAAGTGGAGG
 T  G  L  G  T   F  Y  F  L  K   I  A  N  F  S   N  S  I  F  L   Y  L  K  W  R
GTTAAAAAGGTGGTT TTGGTGCTGCTTCTT GTGACTTCGGTCTTC TTGTTTTTAAATATT GCACTGATAAACATC
 V  K  K  V  V   L  V  L  L  L   V  T  S  V  F   L  F  L  N  I   A  L  I  N  I
CATATAAATGCCAGT ATCAATGGATACAGA AGAAACAAGACTTGC AGTTCTGATTCAAGT AACTTTACACGATTT
 H  I  N  A  S   I  N  G  Y  R   R  N  K  T  C   S  S  D  S  S   N  F  T  R  F
TCCAGTCTTATTGTA TTAACCAGCACTGTG TTCATTTTCATACCC TTTACTTTGTCCCTG GCAATGTTTCTTCTC
 S  S  L  I  V   L  T  S  T  V   F  I  F  I  P   F  T  L  S  L   A  M  F  L  L
CTCATCTTCTCCATG TGGAAACATCGCAAG AAGATGCAGCACACT GTCAAAATATCCGGA GACGCCAGCACCAAA
 L  I  F  S  M   W  K  H  R  K   K  M  Q  H  T   V  K  I  S  G   D  A  S  T  K
GCCCACAGAGGAGTT AAAAGTGTGATCACT TTCTTCCTACTCTAT GCCATTTTCTCTCTG TCTTTTTTCATATCA
 A  H  R  G  V   K  S  V  I  T   F  F  L  L  Y   A  I  F  S  L   S  F  F  I  S
GTTTGGACCTCTGAA AGGTTGGAGGAAAAT CTAATTATTCTTTCC CAGGTGATGGGAATG GCTTATCCTTCATGT
 V  W  T  S  E   R  L  E  E  N   L  I  I  L  S   Q  V  M  G  M   A  Y  P  S  C
CACTCATGTGTTCTG ATTCTTGGAAACAAG AAGCTGAGACAGGCC TCTCTGTCAGTGCTA CTGTGGCTGAGGTAC
 H  S  C  V  L   I  L  G  N  K   K  L  R  Q  A   S  L  S  V  L   L  W  L  R  Y
ATGTTCAAAGATGGG GAGCCCTCAGGTCAC AAAGAATTTAGAGAA TCATCTTGA
 M  F  K  D  G   E  P  S  G  H   K  E  F  R  E   S  S  *
```

Figure 3.2.3. Nucleotide and amino acid sequence of codon-optimized T2R14. *Kpn1* and *Not1* restriction sites were included at the 5' and 3' end of the gene (light blue). *Kozak* sequence (brown) was introduced before the start codon (blue) followed by the FLAG sequence (red).

Kpn1 kozak flag tag

GGTACCGCCACCATGGACTACAAGGACGACGATGACAAAATGAGTTTTCTACACATTGTTTTTTCCATT
CTAGTAGTGGTTGCATTTATTCTTGGAAATTTTGCCAATGGCTTTATAGCACTGATAAATTTCATTGCC
TGGGTCAAGAGACAAAAGATCTCCTCAGCTGATCAAATTATTGCTGCTCTGGCAGTCTCCAGAGTTGGT
TTGCTCTGGGTAATATTATTACATTGGTATTCAACTGTGTTGAATCCAACTTCATCTAATTTAAAAGTA
ATAATTTTTATTTCTAATGCCTGGGCAGTAACCAATCATTTCAGCATCTGGCTTGCTACTAGCCTCAGC
ATATTTTATTTGCTCAAGATCGTCAATTTCTCCAGACTTATTTTTCATCACTTAAAAAGGAAGGCTAAG
AGTGTAGTTCTGGTGATAGTGTTGGGGTCTTTGTTCTTTTTGGTTTGTCACCTTGTGATGAAACACACG
TATATAAATGTGTGGACAGAAGAATGTGAAGGAAACGTAACTTGGAAGATCAAACTGAGGAATGCAATG
CACCTTTCCAACTTGACTGTAGCCATGCTAGCAAACTTGATACCATTCACTCTGACCCTGATATCTTTT
CTGCTGTTAATCTACTCTCTGTGTAAACATCTGAAGAAGATGCAGCTCCATGGCAAAGGATCTCAAGAT
CCCAGCACCAAGATCCACATAAAAGCTCTGCAAACTGTGACCTCCTTCCTCATATTACTTGCCATTTAC
TTTCTGTGTCTAATCATATCGTTTTGGAATTTTAAGATGCGACCAAAAGAAATTGTCTTAATGCTTTGC
CAAGCTTTTGGAATCATATATCCATCATTCCACTCATTCATTCTGATTTGGGGGAACAAGACGCTAAAG
CAGACCTTTCTTTCAGTTTTGTGGCAGGTGACTTGCTGGGCAAAAGGACAGAACCAGTCAACTCCA**TAG**
GCGGCCGC Stop
Not1

```
ATGATGAGTTTTCTACAC ATTGTTTTTTCCATT CTAGTAGTGGTTGCA TTTATTCTTGGAAAT TTTGCCAATGGC
 M  M  S  F  L  H   I  V  F  S  I   L  V  V  V  A   F  I  L  G  N   F  A  N  G
TTTATAGCACTGATAAAT TTCATTGCCTGGGTC AAGAGACAAAAGATC TCCTCAGCTGATCAA ATTATTGCTGCT
 F  I  A  L  I  N   F  I  A  W  V   K  R  Q  K  I   S  S  A  D  Q   I  I  A  A
CTGGCAGTCTCCAGAGTT GGTTTGCTCTGGGTA ATATTATTACATTGG TATTCAACTGTGTTG AATCCAACTTCA
 L  A  V  S  R  V   G  L  L  W  V   I  L  L  H  W   Y  S  T  V  L   N  P  T  S
TCTAATTTAAAAGTAATA ATTTTTATTTCTAAT GCCTGGGCAGTAACC AATCATTTCAGCATC TGGCTTGCTACT
 S  N  L  K  V  I   I  F  I  S  N   A  W  A  V  T   N  H  F  S  I   W  L  A  T
AGCCTCAGCATATTTTAT TTGCTCAAGATCGTC AATTTCTCCAGACTT ATTTTTCATCACTTA AAAAGGAAGGCT
 S  L  S  I  F  Y   L  L  K  I  V   N  F  S  R  L   I  F  H  H  L   K  R  K  A
AAGAGTGTAGTTCTGGTG ATAGTGTTGGGGTCT TTGTTCTTTTTGGTT TGTCACCTTGTGATG AAACACACGTAT
 K  S  V  V  L  V   I  V  L  G  S   L  F  F  L  V   C  H  L  V  M   K  H  T  Y
ATAAATGTGTGGACAGAA GAATGTGAAGGAAAC GTAACTTGGAAGATC AAACTGAGGAATGCA ATGCACCTTTCC
 I  N  V  W  T  E   E  C  E  G  N   V  T  W  K  I   K  L  R  N  A   M  H  L  S
AACTTGACTGTAGCCATG CTAGCAAACTTGATA CCATTCACTCTGACC CTGATATCTTTTCTG CTGTTAATCTAC
 N  L  T  V  A  M   L  A  N  L  I   P  F  T  L  T   L  I  S  F  L   L  L  I  Y
TCTCTGTGTAAACATCTG AAGAAGATGCAGCTC CATGGCAAAGGATCT CAAGATCCCAGCACC AAGATCCACATA
 S  L  C  K  H  L   K  K  M  Q  L   H  G  K  G  S   Q  D  P  S  T   K  I  H  I
AAAGCTCTGCAAACTGTG ACCTCCTTCCTCATA TTACTTGCCATTTAC TTTCTGTGTCTAATC ATATCGTTTTGG
 K  A  L  Q  T  V   T  S  F  L  I   L  L  A  I  Y   F  L  C  L  I   I  S  F  W
AATTTTAAGATGCGACCA AAAGAAATTGTCTTA ATGCTTTGCCAAGCT TTTGGAATCATATAT CCATCATTCCAC
 N  F  K  M  R  P   K  E  I  V  L   M  L  C  Q  A   F  G  I  I  Y   P  S  F  H
TCATTCATTCTGATTTGG GGGAACAAGACGCTA AAGCAGACCTTTCTT TCAGTTTTGTGGCAG GTGACTTGCTGG
 S  F  I  L  I  W   G  N  K  T  L   K  Q  T  F  L   S  V  L  W  Q   V  T  C  W
GCAAAAGGACAGAACCAG TCAACTCCATAG
 A  K  G  Q  N  Q   S  T  P  *
```

Figure 3.2.4. Nucleotide and amino acid sequence of codon-optimized T2R20. *Kpn1* and *Not1* restriction sites were included at the 5' and 3' end of the gene (light blue). *Kozak* sequence (brown) was introduced before the start codon (blue) followed by the FLAG sequence (red).

3.2.3 Plasmid DNA transformation of competent *E. coli* cells

TAS2R wild-type and mutant genes in mammalian expression vector pcDNA 3.1, were transformed into high copy number *E. coli.* strain DH5α. 0.3 µg (2 µl) of plasmid DNA was added to 50 µl DH5α and tapped gently to mix well. Then the cells were incubated on ice for 35 min with gentle tapping every 10-minute interval. After this, the cells were incubated in a water bath at 42°C for 45 seconds and immediately placed on ice for 2 min. After this step, 400 µl LB media (without ampicillin) was added to the tube near the flame to keep it sterile and further incubated at 37°C for 1 hr in a shaker. After incubation, 100 µl of the transformed cells were plated on LB-ampicillin agar plate by spreading with a L-shaped glass spreader (sterilized in 100 % absolute ethanol). The plate was allowed to dry and incubated (flipped upside down) at 37°C overnight for 16 hrs. Bacterial colonies carrying the plasmid were selected using ampicillin and the plates were stored at 4°C.

3.2.4 Plasmid DNA purification and restriction digestion

The isolated colonies were picked and grown in 5 ml LB containing 5 µg/ml ampicillin media for 16 hrs at 37°C. The plasmid DNA was isolated using Qiagen miniprep kit following manufacturer's instructions. 2 µg of plasmid DNA was digested by preparing the following reaction mixture containing 1 µg DNA, 1 µl BSA (10X), 1 µl EcoRI buffer or buffer 2 (NEB), 1 µl *EcoRI* (20,000U/ml) or *KpnI*, 1 µl *NotI*, and water added to make up to 10 µl. The reaction mixture was incubated for 2-3 hrs at 37°C. The samples were analyzed by gel electrophoresis using 1% agarose gel. The isolates showing the correct banding pattern were again confirmed by automated DNA sequencing (MICB DNA Sequencing Facility, Winnipeg). For large scale DNA preparation, the cultures containing the appropriate sequence were grown

in 100 ml LB-Amp media and plasmid DNA was isolated using the Qiagen Midiprep or Maxiprep kit. The A260/280 ratio of plasmid DNA is between 1.6-1.8 and this DNA was used for further molecular and cell biology experiments.

3.2.5 Gene cloning

T2R4 present in pcDNA 3.1/Neo was cloned into pcDNA4-HisMaxB/Zeo plasmid. Both plasmids were subjected to restriction digestion with the same restriction enzymes (EcoR1 and Not1). The digests were separated by agarose gel electrophoresis. Then the fragments of T2R4 (gene) and pcDNA4 (vector) were collected by cutting the gel under UV light using a sterile razor blade. A 1.7 ml tube was weighed for each fragment and collected into the tubes and again weighed to take the appropriate volume of reagent. The fragments were extracted and eluted using Qiagen Gel Extraction kit. These were used for ligation using Takara ligation kit. For this process, 2 µl vector was taken in two labeled tubes and a control tube. The insert gene was added at 1:1 and 1:2 ratio in the two tubes while excluding the control tube. Then equal volumes of Takara ligation solution 1 was added to each tube (i.e 4 µl, 6 µl and 2 µl) and incubated at 16°C for 30 min for the ligation process. The ligated plasmids were used for bacterial transformation and plasmid isolation as described in section 3.2.3.

3.2.6 Mammalian cell culture

Human bronchial epithelial primary cells and cell lines (NuLi-1 and CuFi-1) were grown in cell culture plates coated with human placental collagen type IV as recommended by ATCC and maintained in serum free BEGM. HEK293T cells were

maintained in DMEM/F12 complete medium. All cells were maintained in cell culture incubator at 37°C supplied with 5% CO_2.

3.2.7 Stable cell generation

To generate stable cells expressing T2R1, T2R4, T2R14 or T2R20, HEK293T cells were transfected with TAS2Rs in pcDNA3.1/Hygro vector (each 3 μg/well) in a 6 well plate. For T2R4- Gα16/44 stable cells, TAS2R4 in pcDNA4/HisMaxB/Zeo and Gα16/44 chimera in pcDNA3.1/Hygro vectors were co-transfected. After 24 hrs, the cells were plated in growth medium at different dilutions (1:100, 1:200 and 1:500). After 48 hrs, the growth medium was replaced with selection medium containing hygromycin alone or zeocin and hygromycin at 300 μg/mL. Selection medium was changed every 2-3 days until clear isolated clones were observed. The isolated colonies were selected as individual clones and characterized for the high expression of extracellular T2R and intracellular Gα16/44 using flow cytometry analysis. The cells were stained with APC conjugated anti-FLAG antibody at 1:300 dilution for $1x10^5$ cells. The best clone was further characterized for its functionality in response to quinine using calcium mobilization assay.

3.3 Calcium Mobilization Assay

3.3.1 HEK293T cells

All the T2R studies were performed in HEK293T cells either using stable cells or transiently transfected cells. However, the protocol for functional assays are same for both methods. In experiments using transient transfection, HEK293T cells were cultured in six-well tissue culture dishes at 37°C in DMEM-F12 and 10% FBS. Once the cells reached 70–80% confluency, the cells were transfected with plasmids of WT-

TAS2R or respective mutant receptor constructs (3 μg/well). After 6–8 hrs of transfection 10^5 cells per well were plated in 96-well tissue culture treated BD-falcon biolux microplates along with DMEM-F12 and 5% FBS. In the case of stable cells, they were plated directly in 96-well plate. A pcDNA mock transfected or HEK293T cells (for stable cells) were also used in the experiments as negative control. After 14–16 hrs of incubation at 37°C, the media was removed from wells and 100 μl of 1X concentration Fluo-4 NW dye containing 2.5 mM probenecid was added to each well. The cells were incubated at 37°C for 35 min followed by 35 min at room temperature (22°C). Receptor activation was determined by measuring changes in intracellular calcium (Relative Fluorescence Units) after application of different concentrations of putative agonist for the receptor or buffer alone (for measuring basal activity) using Flexstation-3 fluorescence plate reader (Molecular Devices, CA, USA) at 525 nm following excitation at 494 nm. For T2R signaling knockdown experiments the cells were treated with the PLC inhibitor, U-73122 or Gβγ inhibitor, gallein (5μM for 30 min treatment prior to quinine addition). Calcium mobilized was expressed as ΔRFU after subtracting the responses of cells transfected with pcDNA mock transfected cells or HEK293T cells. The data from 2–5 independent experiments performed in duplicate or triplicate was analyzed. Dose-response curves were generated, and EC_{50} values were calculated by nonlinear regression analysis using Graph Pad PRISM software version 6.0 (GraphPad Software Inc., San Diego, CA) after subtracting the responses of mock-transfected cells. Statistical analysis is pursued as described in section 3.8.

3.3.2 Human bronchial epithelial cell lines or primary cells

Primary cells or NuLi-1 and CuFi-1 cells (0.5×10^5) were plated in a collagen

coated 96-well black walled BD-optilux plate and incubated in 5% CO_2 incubator for 24 hr in the same conditions as described above. Concentration-dependent changes in intracellular calcium induced by the bitter compound quinine in epithelial cells were measured. For T2R signaling knockdown experiments, the cells were treated with the PLC inhibitor, U-73122 or Gβγ inhibitor, gallein (5μM for 30 min treatment prior to quinine addition). Changes in intracellular calcium mobilized as detected by calcium sensitive dye Fluo 4NW (Invitrogen) were measured in RFUs. Data from 3-4 independent experiments with each data point in triplicate were measured and analysis done as described in section 3.8.

3.4 Competition Binding Assay

3.4.1 Agonist blocking

T2R4 is well studied and its potential blockers were previously characterized in the lab. Therefore, T2R4 was used to pursue the discovery of novel blockers. HEK293T cells stably expressing T2R4 were plated in 96-well plate and incubated overnight. Fluo–4NW dye was added to the cells as described in the previous section (section 3.3.1). To study the blocking effect, the half maximal inhibitory concentration (IC_{50}) of T2R4 blockers were used. BCML and GABA are the potential bitter blockers known to inhibit quinine response at T2R4 (Pydi et al., 2014c). BCML was used to study its blocking effect on AHLs response at T2R4. The effects of ABA isomers were studied by treating T2R4 cells with maximum concentration of each compound alone or in the presence of putative agonist quinine at 1 mM (its EC_{50} value). BCML and GABA were used as controls. When characterizing AGEs as novel ligands for T2R4, the logarithmic concentrations of 1 μM, 10 μM and 100 μM were used to treat the cells in presence or absence of quinine. The results were analyzed as

described in previous section.

3.4.2 Schild regression analysis

For Schild analysis, HEK293T cells stably expressing T2R4 and Gα16/44 chimera were used. $1x10^5$ viable cells per well were plated in a 96-well tissue culture treated BD-falcon biolux microplates in DMEM-F12 medium containing 10% FBS for 24 hrs followed by calcium assay. The cells were treated with T2R4 agonist quinine alone at different concentrations (0.07-4 mM) or in the presence of ABA (concentration kept constant at 3 μM, 30 μM, 100 μM and 300 μM). The experiments were repeated for five times in triplicates and the calcium readout was measured as relative fluorescence units (ΔRFU). The standard error mean (SEM) values of the dose-response data were fit to a sigmoid curve using Gaddum/Schild EC_{50} shift non-linear regression in Graphpad Prism v5.0. The calculation is based upon the equation for simple antagonism derived by Gaddum where [A] and [B] represents molar concentration of agonist and antagonist respectively with their equilibrium dissociation constants K_A and K_B for the receptor. y represents the percentage of receptors occupied by agonist (Kenakin, 1982).

$[A]/K_A = (1+([B]/K_B))\ .\ y/100-y$

EC_{50} values from these fits were used in calculating Schild analysis linear regression plot. The antagonist concentration and dose ratio minus one (DR-1) were plotted on X-axis and Y-axis respectively in log scale.

3.5 Gene and Protein Expression Analysis

3.5.1 mRNA extraction and cDNA synthesis

Total RNA from the cells were isolated according to manufacturer's

instructions using the RNeasy Mini kit (Qiagen, Canada). The concentration and purity of the RNA was determined using Nanodrop 2000 (ThermoFisher Scientific, Canada). Genomic DNA was removed by treating 10 µg of the extracted RNA with 8 units of DNase I (New England Biolabs) for 75 min at 37°C. For cDNA synthesis, about 1 µg of purified RNA was reverse transcribed using SSIII RT (superscript III reverse transcriptase, Invitrogen) initially with 1 µl dNTPs, 1 µl Oligo-dT primer, 9 µl sterile water and mixture was heated at 65°C on the PCR machine for 5 min followed by 1 minute incubation on ice. The mixture was centrifuged to collect contents to which 4 µl 5x first strand buffer, 1 µl 0.1 M DTT and 1 µl SSIII RT (200 units/µl) was added. The contents were mixed gently by pipetting two times and incubated at 50°C for 60 min. The reaction was inactivated by heating at 70°C for 15 min. The synthesized cDNA was used as template for amplification by PCR.

3.5.2 nCounter gene expression analysis

nCounter sequencing was performed at the Farncombe Metagenomics Facility, McMaster University, Canada. All the procedures were performed according to the recommendations from NanoString technologies. The quality of extracted mRNA was analyzed by a BioAnalyzer and based on the RNA integrity number and the 28S/18S ratios only intact RNA of good quality was used in nCounter sequencing and data analysis. From each sample, 100 ng of RNA was hybridized to the custom designed CodeSets sequences. The details of the CodeSets are shown in **Table 3.5.2.** Six synthetic positive control templates and corresponding probes are built into the CodeSet by NanoString technologies. The positive controls are used to confirm that the hybridization worked and to normalize for technical variation. Eight negative control probes were also built into the CodeSet by NanoString technologies, but there was no matching template sequence added for them to bind to and these are used to

monitor background-level hybridization. Data analysis was performed using the nSolver™ 2.0 analysis software (NanoString technologies). The geometric mean of negative controls was used for the background subtraction. This was followed by the positive control normalization where the raw counts were normalized using the geometric mean of the 6 positive control probes provided in the probe set. The data is represented as nCounter values. One count of the nCounter value can be interpreted as one mRNA transcript in 100 ng of RNA.

3.5.3 Reverse transcriptase (RT)-PCR

The primer sequences used for PCR analysis and their expected amplicon sizes are listed in **Table 3.1.1**. PCR was performed by preparing a total volume of 20 µl reaction mixture containing 1 µl reverse transcribed cDNA, 0.5 pM of each, 10 µl of 1x SYBR Green master mix containing dNTP mix and Taq polymerase and 7 µl sterile water. An initial denaturation step at 94°C for 10 min was followed by 55 cycles of denaturation at 94°C for 30 sec, annealing at 58-62°C, extension at 72°C for 30 sec and finished with a final extension at 72°C for 5 min on a thermocycler (MJ mini cycler, Bio Rad). The housekeeping gene GAPDH was used as a positive control in the PCR reactions. No RT reaction was used as an internal control and a no template control (water only) was used as a negative control. All PCR products were separated on 2% agarose gel stained with ethidium bromide. Gel images were recorded and photographed under UV light. PCR reaction was performed at least three times.

3.5.4 Flow cytometry (FACS)

FACS analysis of selected T2Rs was performed on NuLi-1, CuFi-1 and primary bronchial epithelial non-CF and CF cells by using BD FACS Canto machine as described previously (Singh et al., 2014). 1 $X10^5$ viable cells were collected for the experiment and washed 2-3 times with FACS buffer containing 0.5% BSA in PBS and stained with primary anti-T2R polyclonal antibodies 1:200 for T2R3 and T2R5, 1:300 for T2R1, T2R4, T2R10, T2R20 (T2R49) and T2R38, and monoclonal antibody at 1:25 dilution for β_2AR (positive control). Appropriate rabbit serum or rabbit IgG or goat IgG were kept as isotype controls and only cells were kept as negative controls and incubated on ice for 1 h. Subsequently the cells were washed with FACS buffer and incubated with respective secondary antibody conjugated with Alexa Fluor-488 (1:1000) in dark on ice for 1 h. In the case of HEK293T stable cells or transiently transfected cells expressing T2Rs or mutants (1 $X10^5$ viable cells) were taken into flow cytometry tube. The cells were washed twice with FACS buffer and collected by centrifugation for 4 min at 1,500 rpm. The cells were then incubated with APC-conjugated anti-FLAG monoclonal antibody (1:500) for 1 h on ice in the dark. After incubation, the cells were washed twice and resuspended in 300 µl FACS buffer. 10,000 events were collected and the results were analyzed using FACS Diva or FlowJo softwares. The mean fluorescence intensity (MFI) values of isotype controls were subtracted to analyze the protein expression.

3.6 Taste Sensory Analysis by Electronic-Tongue (E-Tongue)

The taste sensory analysis of antibiotics and QSMs used in this study was performed using the analytical instrument E-Tongue from Alpha M.O.S. (Toulouse, France) as described previously (Singh et al., 2011a). To predict the bitterness scores

of test and reference compounds, 0.5 mM solutions of the reference compounds, 0.5 mM of antibiotics, 0.1 mM of AHLs and 0.05 mM of hydroxyquinolones were prepared in water. These concentrations were chosen on the basis of Emax values for T2Rs from the calcium mobilization assays. The bitterness score was analysed by the E-Tongue against known reference solutions of caffeine, dextromethorphan and quinine.

3.7 Molecular Modeling and Ligand Docking Analysis

3.7.1 Multiple sequence alignment

The amino acid sequences of T2Rs were retrieved from the NCBI database, and multiple sequence alignment was performed using Clustal Omega multiple sequence program (https://www.ebi.ac.uk/Tools/msa/clustalo/).

3.7.2 Molecular modeling, ligand docking and simulations

The modeling and docking protocols were as described previously (Liu et al., 2018). The T2R14 and T2R20 3D models without the FLAG sequence were built using I-TASSER server. The best model generated was selected for each T2R based on the C-score and minimized using PRIME module in Schrodinger software (v11.0). The quality of the model was checked using PROCHECK and Ramachandran plot showed >98% of resides are in favored and allowed regions. For T2R4 a previous 3D model which was experimentally validated for quinine binding was used (Pydi et al., 2014c). This model also serves as a control for the docking analysis in this study, and quinine was also included in the ligand dataset. The above models were prepared for ligand docking using the Protein Preparation Wizard. A grid area was generated

Table 3.5.2. **CodeSet design of TAS2Rs for the nCounter gene expression analysis** (Jaggupilli et al., 2017)**.**

Gene	Nanostring ID	Pubmed Accession	Targeted Region	Target Sequence
TAS2R1	NM_019599.2:1228	NM_019599.2	1229-1328	TGGATCAGTTCAAAGAACCCATGATTCAATGATTTACCCATGCCTGCCACACTTCCCTCAGCCAGACAAAGCAGCCTGTTCATAAATATACAACATGTCC
TAS2R3	NM_016943.2:458	NM_016943.2	459-558	ATGCTGTTGGGTGCACTGCTCTTATCCTGTGGTAGTACCGCATCTCTGATCAATGAGTTTAAGCTCTATTCTGTCTTTAGGGGAATTGAGGCCACCAGGA
TAS2R4	NM_016944.1:272	NM_016944.1	273-372	GGACTCGAGCAGTGTCTGGTTTGTGACCTTGCTCAATATCTTGTACTGTGTGAAGATTACTAACTTCCAACACTCAGTGTTTCTCCTGCTGAAGCGGAAT
TAS2R5	NM_018980.2:248	NM_018980.2	249-348	GGATCAGAAAATTCAACTGGTCCTCATATAACCTCATTATCCTGGGCCTGGCTGGCTGCCGATTTCTCCTGCAGTGGCTGATCATTTTGGACTTAAGCTT
TAS2R7	NM_023919.2:450	NM_023919.2	451-550	TGGATTCTACTGGGGTGCGTGGTTCTCTCTGTGTTTATTAGCCTTCCAGCCACTGAGAATTTGAACGCTGATTTCAGGTTTTGTGTGAAGGCAAAGAGGA
TAS2R8	NM_023918.1:350	NM_023918.1	351-450	ACTTTTTCTCTGGCTGAAGTGGAAAATTGATATGGTGGTGCACTGGATCCTGCTGGGATGCTTTGCCATTTCCTTGTTGGTCAGCCTTATAGCAGCAATA
TAS2R9	NM_023917.2:772	NM_023917.2	773-872	ACATGAGGGCCATAAAGGCAGTGATCATCTTTCTGCTCCTCCTCATCGTGTACTACCCAGTCTTTCTTGTTATGACCTCTAGCGCTCTGATTCCTCAGGG
TAS2R10	NM_023921.1:586	NM_023921.1	587-686	TAATCATTTCCCTTTGGAGACACAACAGGCAGATGCAATCGAATGTGACAGGATTGAGAGACTCCAACACAGAAGCTCATGTGAAGGCAATGAAAGTTTT
TAS2R13	NM_023920.2:1036	NM_023920.2	1037-1136	AGAACACAGTGATCTACATGCTTTGTGAGACGATTGGAGTCTTCTCTCCTTCAAGCCACTCCTTTCTTCTGATTCTAGGAAACGCTAAGTTAAGACAGGC
TAS2R14	NM_023922.1:818	NM_023922.1	819-918	TTCATGTCACTCATGTGTTCTGATTCTTGGAAACAAGAAGCTGAGACAGGCCTCTCTGTCAGTGCTACTGTGGCTGAGGTACATGTTCAAAGATGGGGAG
TAS2R16	NM_016945.2:370	NM_016945.2	371-470	TCTACTGCATCAAGGTCTCTTCTTTCACCCATCACATCTTTCTCTGGCTGAGGTGGAGAATTTTGAGGTTGTTTCCCTGGATATTACTGGGTTCTCTGAT
TAS2R19 (TAS2R48)	NM_176888.1:768	NM_176888.1	769-868	AGCAAACTTGTACTCCTGCTTTGCCAAACTGTTGCAATCATGTATCCTTCATTCCACTCATTCATCCTGATTATGGGAAGTAGGAAGCTAAAACAGACCT
TAS2R20 (TAS2R49)	NM_176889.2:443	NM_176889.2	444-543	CACGTATATAAATGTGTGGACAGAAGAATGTGAAGGAAACGTAACTTGGAAGATCAAACTGAGGAATGCAATGCACCTTTCCAACTTGACTGTAGCCATG

TAS2R38	NM_176817.4:446	NM_176817.4	447-546	CATCCGTTTCTCTCACACCTTCCTGATCTGCTTGGCAAGCTGGGTCTCCAGGAAGATCTCCCAGATGCTCCTGGGTATTATTCTTTGCTCCTGCATCTGC
TAS2R39	NM_176881.2:564	NM_176881.2	565-664	CCTATCCACTCCTCCAACTCCACTAAGAAAACATACTTGTCTGAGATCAATGTGGTCGGTCTGGCTTTTTTCTTTAACCTGGGGATTGTGACTCCTCTGA
TAS2R40	NM_176882.1:50	NM_176882.1	51-150	GGTCACCTTCACTTTGGTGGTCTCCGGAATAGAGTGCATCACTGGCATCCTTGGGAGTGGCTTCATCACGGCCATCTATGGGGCTGAGTGGGCCAGGGGC
TAS2R41	NM_176883.2:759	NM_176883.2	760-859	GCCGCAAAATTTATCTCCATGCAGAACGACTTTTACTGGCCATGGCAAATTGCAGTCTACCTGTGCATATCTGTCCATCCCTTCATCCTCATCTTCAGCA
TAS2R42	NM_181429.1:202	NM_181429.1	203-302	TAGTGGGACTTGCTTCACATTTATATACCACATATAGACTAGGAAAAACTGTTATTATGCTTTGGCACATGACTAATCACTTGACAACCTGGCTTGCCAC
TAS2R30/31/43/45/46	NM_176884.2:820	NM_176884.2	821-920	TGATATCAGTTTGGAGTTTTGGAAGTCTGGAAAACAAACCTGTCTTCATGTTCTGCAAAGCTATTAGATTCAGCTATCCTTCAATCCACCCATTCATCCT
TAS2R50	NM_176890.2:479	NM_176890.2	480-579	ATCTTCTTGTGGCAAACATGGATGAGAGTATGTGGGCAGAAGAATATGAAGGAAACATGACTGGGAAGATGAAATTGAGGAATACAGTACATCTTTCATA
TAS2R60	NM_177437.1:76	NM_177437.1	77-176	TTTTACGCCTGGTAGCAATAGCAGGCAATGGCTTCATCACTGCTGCTCTGGGCGTGGAGTGGGTGCTACGGAGAATGTTGTTGCCTTGTGATAAGTTATT
GJA1	NM_000165.3:705	NM_000165.3	706-805	GCGAACCTACATCATCAGTATCCTCTTCAAGTCTATCTTTGAGGTGGCCTTCTTGCTGATCCAGTGGTACATCTATGGATTCAGCTTGAGTGCTGTTTAC
CDH1	NM_004360.2:1230	NM_004360.2	1231-1330	CGATAATCCTCCGATCTTCAATCCCACCACGTACAAGGGTCAGGTGCCTGAGAACGAGGCTAACGTCGTAATCACCACACTGAAAGTGACTGATGCTGAT
ACTB	NM_001101.2:1685	NM_001101.2	1686-1785	CCAACTTGAGATGTATGAAGGCTTTTGGTCTCCCTGGGAGTGGGTGGAGGCAGCCAGGGCTTACCTGTACACTGACTTGAGACCAGTTGAATAAAAGTGC
GAPDH	NM_002046.3:104	NM_002046.3	105-204	GGGGAAGGTGAAGGTCGGAGTCAACGGATTTGGTCGTATTGGGCGCCTGGTCACCAGGGCTGCTTTTAACTCTGGTAAAGTGGATATTGTTGCCATCAAT
GNAI1	NM_002069.4:670	NM_002069.4	671-770	GGAGCTGCTGAAGAAGGCTTTATGACTGCAGAACTTGCTGGAGTTATAAAGAGATTGTGGAAAGATAGTGGTGTACAAGCCTGTTTCAACAGATCCCGAG
GNAQ	NM_002072.2:1100	NM_002072.2	1101-1200	AAGGAGTACAATCTGGTCTAATTGTGCCTCCTAGACACCCGCCCTGCCCTTCCCTGGTGGGCTATTGAAGATACACAAGAGGGACTGTATTTCTGTGGAA
GNAS	NM_001077489.1:545	NM_001077489.1	546-645	GCATGTTAATGGGTTTAATGGAGATGAGAAGGCAACCAAAGTGCAGGACATCAAAAACAACCTGAAAGAGGCGATTGAAACCATTGTGGCCGCCATGAGC

GNAT3	NM_001102386.1:252	NM_001102386.1	253-352	GTGAAAGCCATGACTACCCTTGGAATTGATTATGTAAATCCCAGAAGTGCAGAGGACCAACGACAACTTTATGCAATGGCAAATACCCTGGAAGATGGTG
GNA12	NM_007353.2:4180	NM_007353.2	4181-4280	AATTTAGGGGTTCTGGGCACAGACATCTAACCTGGTATTGTAAGGCAGAGGCTCCCATTGGAATGGTAGTGGTCCGGGTCAGTTGTTCATGGTGTAAGCT
IL10	NM_000572.2:230	NM_000572.2	231-330	AAGGATCAGCTGGACAACTTGTTGTTAAAGGAGTCCTTGCTGGAGGACTTTAAGGGTTACCTGGGTTGCCAAGCCTTGTCTGAGATGATCCAGTTTTACC
IL8	NM_000584.2:25	NM_000584.2	26-125	ACAGCAGAGCACACAAGCTTCTAGGACAAGAGCCAGGAAGAAACCACCGGAAGGAACCATCTCACTGTGTGTAAACATGACTTCCAAGCTGGCCGTGGCT
CFTR	NM_000492.3:720	NM_000492.3	721-820	TTGGCACATTTCGTGTGGATCGCTCCTTTGCAAGTGGCACTCCTCATGGGGCTAATCTGGGAGTTGTTACAGGCGTCTGCCTTCTGTGGACTTGGTTTCC
AQP5	NM_001651.2:1695	NM_001651	1696-1795	TCCCCAGAGCTCCTTAGGAAGAAGACAGACTGGTTCATTGAATGCCGCCTTATTTATTTCTGGTGAGGATGCATGCGTGGGGCTGCTGGTGTTTAGAGTG

Table 3.5.3 Sequences of DNA primers (long) of human bitter taste receptors (TAS2Rs)

Bitter receptor (TAS2R)	Gene accession ID	Gene size (bp)	Primer sequence (5'-3')	Expected amplicon size (bp)
TAS2R1	NM_019599	1355	Forward-TGTGGTGGTGAATGGCATTG, Reverse-CAGCACTTACTGTGGAGGAGGAAC	813
TAS2R3	NM_016943	1101	Forward-ACACATGATTCAGGGATAATAATGCAAA, Reverse-TTAGCCATCTTGGTTTTTGGTAGGAAATT	575
TAS2R4	NM_016944	900	Forward-TACAGTGGTCAATTGCAAAACTTGG, Reverse-AATGTCCTGGAGAGTAAAGGGTGG	749
TAS2R5	NM_018980	1150	Forward-TGGTCCTCATATAACCTCATTATCCTGG, Reverse-CTGCCATGAGTGTCTCCCA	667
TAS2R7	NM_023919	1096	Forward-TGTTTTATATTGGTGCTATATCCAGATGTCTATGC, Reverse-GGATAAATGAATGACTTGAGGGGTAGATTAGAG	658
TAS2R8	NM_023918	930	Forward-TTGATATGGTGGTGCACTGG, Reverse-GTGAGTGACCCAAGGGGTAG	471
TAS2R9	NM_023917	1075	Forward-TGAATTGACCATAGGGATTTGGG, Reverse-ATAATTAGAATGAATGAATGGCTTGATGG	807
TAS2R10	NM_023921	924	Forward-GACTTGTAAACTGCATTGACTGTGCC, Reverse-AAAGAGGCTTGCTTTAGCTTGCTG	784
TAS2R13	NM_023920	1637	Forward-GGGTCAGTAAAAGAGAGCTGTCCTC, Reverse-ATCAGAAGAAAGGAGTGGCTTGAAG	742
TAS2R14	NM_023922	954	Forward-GCTTTGGCAATCTCTCGAATTAGC, Reverse-CTCTAAATTCTTTGTGACCTGAGGGC	796
TAS2R16	NM_016945	996	Forward-CCTGGGAATTTTTTAATATCCTTACATTCTGGT, Reverse-GAAGCGCGCTTTCATGCTT	419
TAS2R20	NM_176889	1914	Forward-GCACTGATAAATTTCATTGCCTGG, Reverse-TTGTTCCCCCAAATCAGAATGAAT	770
TAS2R38	NM_176817	1143	Forward-ACAGTGATTGTGTGCTGCTG, Reverse-GCTCTCCTCAACTTGGCATT	766
TAS2R39	NM_176881	1017	Forward-TGTCGCCATTTCTCATCACCTTA, Reverse-ATTGAGTGGCTGGCAGGGTAG	841
TAS2R40	NM_176882	972	Forward-AGAGTGCATCACTGGCATCCTT, Reverse-GAGGATGAGAAAGTAGCTGGTGGC	685
TAS2R41	NM_176883	924	Forward-GGTTGCTGCCCTTGGATATGA, Reverse-TGAAGATGAGGATGAAGGGATGG	738
TAS2R42	NM_181429	945	Forward-ATGGCCACCGAATTGGACA, Reverse-GCTTGCTGTTTCCCAGAATGAG	871
TAS2R43	NM_176884	1027	Forward-GGTCTCCAGAGTTGGTTTGC, Reverse-TCTTGTTTCCCCAAATCAGG	698
TAS2R44	NM_176885	1021	Forward-CATTGGTAAATTCCATTGAGC, Reverse-GATATCATTATGGACAGAAAGTAAAC	661
TAS2R45	NM_176886	900	Forward-CTCCTTTGCTGACCAAATTGTC, Reverse-GAACGGGTGGGCTGAAGAAC	709
TAS2R46	NM_176887	930	Forward-GAGTTGAATCCAGCTTTTAAC, Reverse-ATAGCTGAATGCAATAGCTTC	606
TAS2R47	NM_001097643	960	Forward-GGTGTTATTACTACATTGGTATGCAACTC, Reverse-AAGACAGGTTGCTTTTCCAGC	603
TAS2R48	NM_176888	900	Forward-GGTTTACTCTGGGTCATGTTATTC, Reverse-TTTGCTCTGCTGTGTCCTAAG	606
TAS2R50	NM_176890	1000	Forward-ATGTGGCTTGCTGCTAACCT, Reverse- CAGCCTTGCTAACCATGACA	514
TAS2R60	NM_177437	957	Forward-CAGGCAATGGCTTCATCACTG, Reverse- TCCCACACCCAGAATTTAAAGTCC	748

GNAT3	NM_001102386	1065	Forward-GTGGCATGACACCTCAACTG, Reverse-GGCCCAGTGTATTCTGGAAA	529
GAPDH	NM_002046	1310	Forward-TGTGAGGAGGGGAGATTCAG, Reverse- ACCCAGAAGACTGTGGATGG	572

around the extracellular site of the receptor (x = 75 Å, y = 53 Å, z = 70 Å) for ligand docking. The 2D chemical structures of quinine, FFA, DPH, cromolyn, levofloxacin, tobramycin, C8-AHL and 3-oxo-C12-AHL were obtained from PubChem database, and their 3D structures were optimized using Ligprep module in Schrödinger. The optimized ligands were docked into T2R protein structure using Glide (SP and XP) module. Based on the Glide score, best poses were selected and the complex was further minimized. Molecular dynamic simulations on the minimized ligand-receptor complexes were performed using standard dynamics cascade available in BIOVIA Discovery Studio (v.4.0) suite. As an initial step, the whole structure solvation was performed with periodic boundary. This complex was simulated for 10 ps using the default parameters in the standard dynamics cascade. The simulated complex of ligand and T2R was analyzed to study the interactions. Mutations were introduced into the simulated models in Schrödinger and these structures were further minimized as described above. The structural interactions between ligand and respective T2R (wild type and mutants) receptors were analyzed in both Schrödinger and Discovery Studio. PyMol visualizer was used to generate the publication quality images.

3.8 Statistics

To check the significance levels, all the statistical analyses were performed using GraphPad Prism version 6.0 software. For dose curve analysis, non-linear regression analysis was performed and EC_{50} was calculated. Statistical analysis was performed using t-test or one-way analysis of variance (ANOVA) with *Tukey's or Dunnette's* post hoc test, from a minimum of 3 independent experiments to determine the statistical significance wherever applicable. * $p<0.05$, ** $p<0.01$, *** $p<0.001$.

CHAPTER 4

4.0 RESULTS

4.1 Expression Analysis of Functional T2Rs in Human Airway Cells

(Analysis of the Expression of Human Bitter Taste Receptors in Extraoral Tissues)

Appalaraju Jaggupilli, Nisha Singh, Jasbir Upadhyaya, Anurag Sikarwar, Makoto Arakawa, Shyamala Dakshinamurti, Rajinder P. Bhullar, Kangmin Duan, Prashen Chelikani.

Mol Cell Biochem. 426(1-2):137-147.

4.1.1 Design and analysis of nCounter nanostring CodeSet

T2Rs like most other GPCRs are endogenously expressed at very low levels. The expression and distribution (or number) of T2Rs varies considerably among different tissues. The T2R subfamily with 25 TAS2Rs are next only to olfactory and adhesion receptors in numerical strength among the ~700 GPCRs in humans. Most of the previous studies employed RT-PCR, qPCR and microarray techniques to analyze the gene expression of TAS2Rs (Foster et al., 2014b). These techniques which require library preparation and/or pre-amplification can introduce bias to the results (Kulkarni, 2011). In general, the expression levels of genes and the proteins they code might vary in different tissues, depending on a number of physiological conditions.

In this work, I used state-of-the-art gene sequencing technique, the nCounter platform to analyze expression of the 25 TAS2Rs in airway cells. This technique is based on the hybridization of complementary probe sequences spanning 100 nucleotide bases for each gene. Thus, it made difficult to design specific probes or CodeSets for TAS2Rs 30, 31, 43, 45 and 46 which share a high degree of sequence similarity of >92% (**Figure 4.1.1**). The designed CodeSet could not differentiate between these five TAS2Rs (**Table 3.5.2**). Therefore, wherever listed, the nCounter value represents the total expression of those five TAS2Rs. Nevertheless, the nCounter sequencing technique has many advantages. It allows multiplexed measurement of mRNA transcripts in a single reaction without the requirement for reverse transcription and pre-amplification for analysis of 100 ng or more of nucleic acid target. nCounter sequencing utilizes molecular barcodes that enables direct digital detection of individual mRNA transcripts (Geiss et al., 2008).

Figure 4.1.1. Multiple sequence alignment of human TAS2R30, 31, 43, 45 and 46. The gene sequences were retrieved from NCBI in the FASTA format and the multiple sequence alignment was carried out using Clustal Omega.

4.1.2 Expression of T2Rs in human airway cells

NuLi-1 and CuFi-1 cells are immortalized human bronchial epithelial cell lines derived from a normal and cystic fibrosis patient, respectively. Airway smooth muscle cells (ASMCs) represent a subset of cells from the same organ (lung). Expression of T2Rs in human ASMCs was previously shown by microarray technique. Thus, including ASMCs in the nCounter analysis will act as a good control. The total RNA was extracted from the cells and subjected to the nCounter gene expression analysis which showed no statistically significant differences in TAS2R expression between these two bronchial epithelial cell types representing normal and diseased conditions (**Figure 4.1.2**). However, ASMCs showed different TAS2R levels compared to bronchial epithelial cells. Although there is a difference in the level of expression between different subset of cells from the lung, the pattern of TAS2R expression remained same. Based on the nCounter values, TAS2R14 and 20 (or 49) showed higher expression levels, followed by TAS2R3, 4, 5, 50 and then TAS2R10, 13 and 19 in all the cells analyzed. The other TAS2Rs showed very low or barely detectable expression. Hereafter, I focused only on the bronchial epithelial cells to understand the expression and function of T2Rs. In the nCounter analysis the CodeSets for reference genes of epithelium E-cadherin (CDH1), connexin 43 (GJA1), aquaporin 5 (AQP5), house-keeping genes β-actin (ACTB) and glyceraldehyde 3-phosphate dehydrogenase (GAPDH), CF markers IL-8, IL-10 and CFTR and Gα subunits Gαi1, Gα3, Gαq, $G\alpha_{gustducin}$ and Gαs were also included and analyzed for their expression (**Figure 4.1.3**). Similar to TAS2Rs, there is no difference in the expression of these genes between NuLi-1 and CuFi-1 cells. Furthermore, as a complimentary technique I pursued reverse-transcriptase (RT)-PCR analysis on the expression of 25 TAS2Rs in

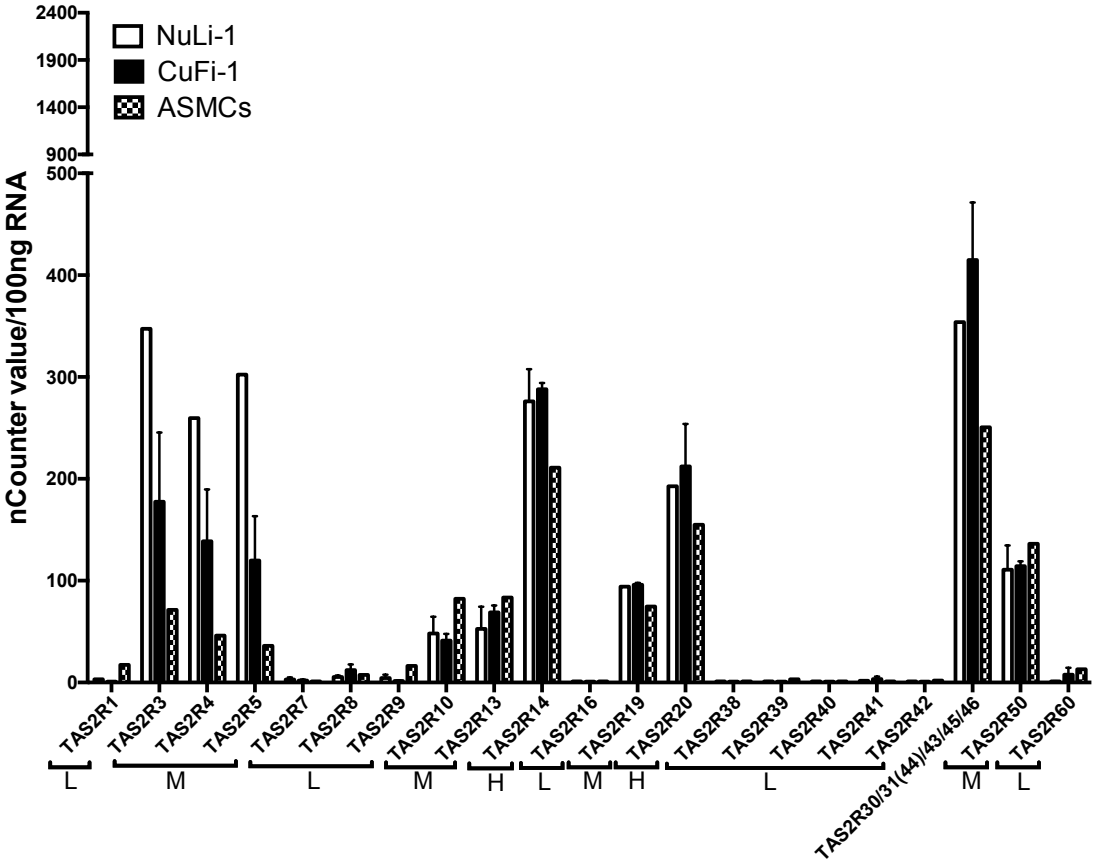

Figure 4.1.2 The mRNA expression levels of TAS2Rs in airway cells NuLi-1, CuFi- 1 and airway smooth muscle cells (ASMCs). nCounter values were represented on the Y axis and the genes analyzed on the X axis. One count of the nCounter value can be interpreted as one mRNA transcript in 100 ng of total RNA. Results presented are from two independent preparations and all values shown represent the average value. No significant difference in the expression of TAS2Rs was observed between the two cell lines. Based on the nCounter values, the TAS2Rs expressed at Low (L)-Moderate (M)-High (H) are indicated (Jaggupilli et al., 2017).

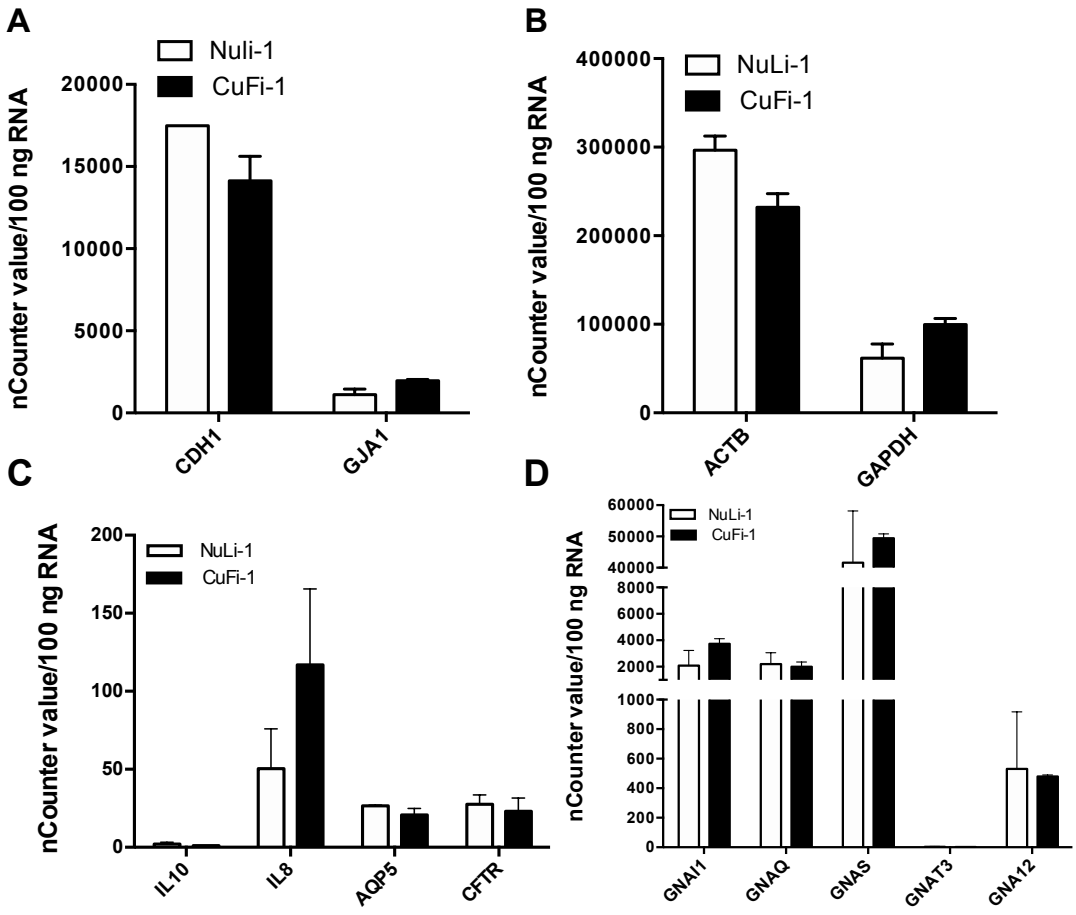

Figure 4.1.3 The mRNA expression levels of reference genes, house-keeping genes and CF epithelial markers in airway cells NuLi-1 and CuFi- 1. nCounter values were represented on the Y axis and the genes analyzed on the X axis. One count of the nCounter value can be interpreted as one mRNA transcript in 100 ng of total RNA. Results presented are from two independent preparations and all values shown represent the average value. No significant difference in the expression of the analyzed genes was observed between the two cell lines.

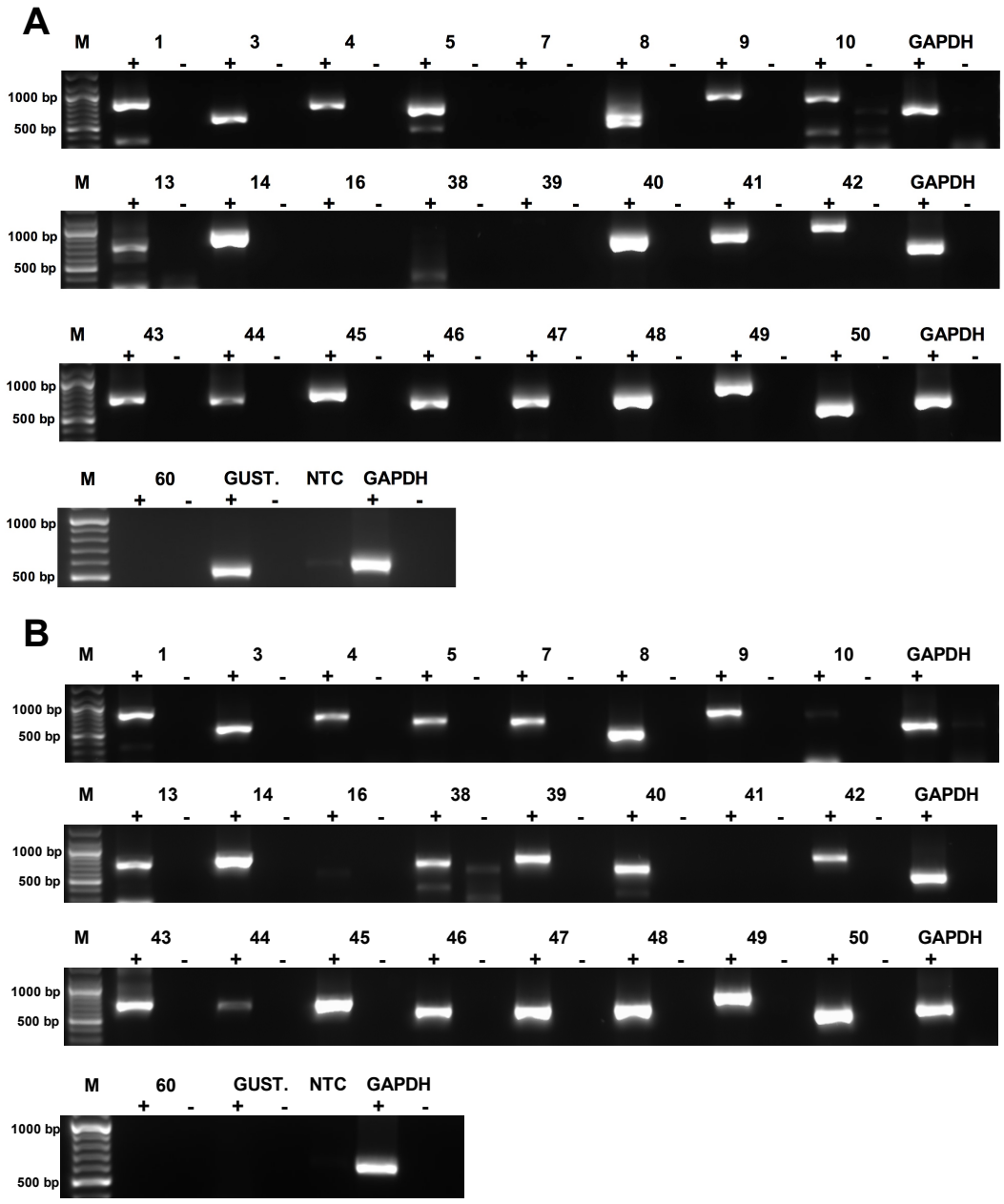

Figure 4.1.4 Reverse transcriptase (RT)-PCR analysis of the expression of bitter taste receptors genes (TAS2Rs) in CuFi-1 and NuLi-1 cells. Agarose gel electrophoresis (1%) analysis of the RT-PCR products showed that transcripts for 20 TAS2Rs were expressed in CuFi-1 (**A**), 21 TAS2Rs were expressed in NuLi-1 cells (**B**). The cognate T2R G-protein, gustducin, is not expressed in NuLi-1 cells. GAPDH was used as an internal control for the PCR reactions. + and – represent the addition and omittance of reverse transcriptase in the reaction respectively. A no template control in which the cDNA template was omitted was also included (not shown). M represents 100 bp molecular weight standard (NEB). All transcripts were observed at the expected amplicon size. Each agarose gel electrophoresis is representative of 2 independent experiments.

both NuLi-1 and CuFi-1 cells. The results show a majority (>20 of the 25 human TAS2Rs) are expressed in both CuFi-1 and NuLi-1 cells (**Figure 4.1.4**).

In order to validate the nCounter gene expression data, I analyzed the mRNA and protein levels of select TAS2Rs in CuFi-1 and NuLi-1 airway cells by quantitative (q)-RT PCR and FACS analysis for T2R3, T2R4, T2R5, T2R10, T2R20 and T2R38 along with β_2AR as a reference for airway cells. The rationale for selecting these few T2Rs is based on the different levels of expression, and commercial availability of antibodies targeting the extracellular side of these T2Rs. The specificity of the antibody for the extracellular side is important, as it would allow the detection of T2Rs expressed on the cell surface, hence eliminating the need to permeabilize the cells. FACS analysis showed similar protein expression trend as observed with the nCounter gene analysis, except for T2R3 and T2R38 (**Figure 4.1.5**).

4.1.3 Functional analysis of T2Rs in bronchial epithelial cell lines

In order to analyze whether the endogenous T2Rs expressed in bronchial epithelium are functional, I pursued calcium mobilization assays on NuLi-1 and CuFi-1 cells. I used the bitter compound quinine, which is known to activate multiple T2Rs (Upadhyaya et al., 2016). These include T2R4, T2R7, T2R14, T2R39, T2R40, T2R43, T2R44 and T2R46. Treatment of CuFi-1 and NuLi-1 cells with quinine caused a dose-dependent increase in intracellular calcium mobilization with EC_{50} values of 758 ± 77 μM and 925 ± 207 μM, respectively (**Figure 4.1.6**). Strikingly, no statistically significant change in the EC_{50} values were observed for quinine treatment between the two cell lines, indicating that the disease-causing mutations may not influence the

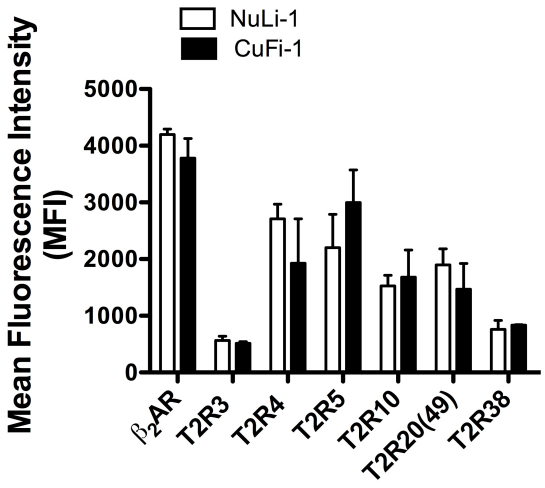

Figure 4.1.5. Analysis of cell surface expression of selected T2Rs NuLi-1 and CuFi-1 cells by FACS. Flow cytometry analysis was performed to confirm the expression of selected T2Rs at protein level, the cells were surface stained with polyclonal anti-T2R antibodies (1:200 or 1:300), monoclonal anti-β_2AR antibody (positive control), and the corresponding secondary antibody conjugated with Alexa Fluor-488 (1:1000). The data represent at least two independent experiments and the expression was presented as mean fluorescence intensity (MFI). To analyze the T2R-specific protein expression, the MFI values of isotype controls were subtracted. Two-way ANOVA with Bonferroni post hoc test was performed and no statistical significance was observed between non-CF and CF (Jaggupilli et al., 2017).

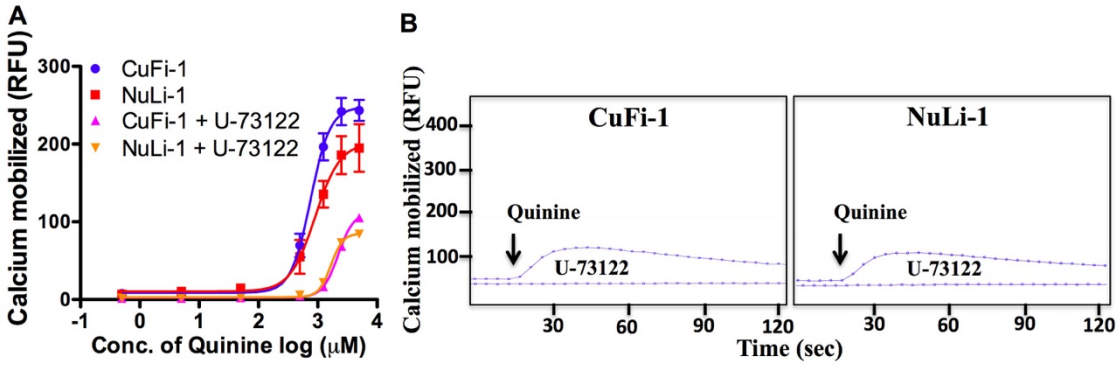

Figure 4.1.6. Functional response of CuFi-1 and NuLi-1 cells to the bitter agonist quinine. A. Concentration-dependent changes in intracellular calcium induced by the bitter compound quinine (70–5000 μM) in CuFi-1 and NuLi-1 cells and the same cells treated with the PLC inhibitor, U-73122 (5 μM for 30 min prior to quinine addition). Changes in intracellular calcium mobilized as detected by calcium-sensitive dye Fluo 4NW (Invitrogen) were measured in RFUs. Data represent four independent experiments with each data point in triplicate. For the measurement of dose–response curve, signals of 10–15 wells receiving the same concentrations of quinine were averaged. The EC_{50} values for quinine in CuFi-1 and NuLi-1 cells are 758 ± 77 μM and 925 ± 207 μM, respectively. Treatment with PLC inhibitor, U-73122, caused a dramatic inhibition of quinine-mediated calcium response. EC_{50} values and regression analysis were calculated using GraphPad Prism 5.0 software. **B.** Representative calcium traces of untreated CuFi-1 and NuLi-1 cells, and cells treated with U-73122 (5 μM for 30 min prior to quinine addition) and stimulated with quinine (625 μM). Arrows indicate the time point (20 s) at which the bitter agonist quinine was added. with EC_{50} values of 2206 ± 23 μM and 1664 ± 59 μM observed for CuFi-1 and NuLi-1 cells, respectively (Jaggupilli et al., 2017).

function of T2Rs in bronchial epithelium. To further confirm that the above observed functional response against quinine treatment is through T2R signaling pathway, I treated NuLi-1 and CuLi-1 cells with U-73122 (5 μM) for 30 min and measured their activation by quinine. Treatment with U-73122 caused a dramatic inhibition of quinine mediated calcium response resulting in a right shift of the curves with EC_{50} values of 2206 ± 23 μM and 1664 ± 59 μM observed for CuFi-1 and NuLi-1 cells, respectively (**Figure 4.1.6**). This suggest that majority of the intracellular calcium mobilization observed in these cells is due to activation of T2Rs through PLC mediated pathway.

4.1.4 Expression and functional analysis of T2Rs in bronchial epithelial primary cells

Based on the nCounter analysis on NuLi-1 and CuFi-1 cells, I selected T2R1 representing low expression, T2R4 with moderate expression and, T2R20 with high expression for further analysis in physiologically relevant bronchial epithelial primary cells from a non-CF and two CF donors. The expression of the above selected T2Rs were analyzed at protein level using FACS. Since the extracellular staining antibody for T2R14 is unavailable, it was not analyzed. Compared to β_2AR expression, T2R1 showed significantly lower expression while T2R4 and T2R20 showed moderate expression (**Figure 4.1.7**). Thus, the protein expression data corroborates with the nCounter gene expression of these T2Rs.

Following the T2R expression analysis, I performed functional assays to characterize the endogenous response of T2Rs when treated with AHLs and QSMs. In order to mimic the physiological conditions, I treated the primary cells with a cocktail of AHLs consisting of, C4-AHL, C8-AHL and 3-oxo-C12-AHL at 100 μM each, and

other QSMs consisting of 2-heptyl-3-hydroxy-4-quinolone (HHQ) and 2-nanoyl-3-hydroxy-4-quinolone (NHQ) at 50 μM each. PLC inhibitor (U-73122, 5 μM) and Gβγ inhibitor (Gallein, 5 μM) were used to elucidate the T2R signaling (**Figure 4.1.8 A**). Quinine was used as a positive control for the activation of multiple T2Rs. Both CF and non-CF cells showed calcium mobilization in response to AHLs and QSMs treatment while this was inhibited by U-73122 and gallein, confirming the Gβγ and PLC mediated signaling pathway in bronchial epithelial cells. In a similar manner, these cells were also tested with commonly used antibiotics in CF treatment. The selected antibiotics that belong to three different classes such as levofloxacin from fluorquinolones, tobramycin from aminoglycosides and azithromycin from macrolides. Although the calcium responses of these antibiotics is not as robust as compared to quinine, the statistically significant knock down of the calcium response in presence of U-73122 or gallein confirms that antibiotics can also activate the T2R signaling pathway through Gβγ and PLC (**Figure 4.1.8 B**).

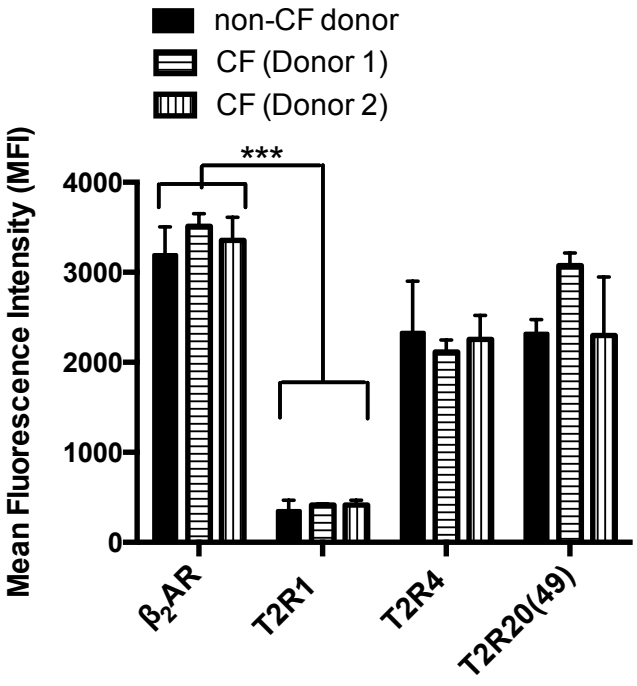

Figure 4.1.7. Analysis of cell surface expression of endogenous T2Rs expressed in non-CF and CF primary cells by FACS. Flow cytometry analysis was performed to confirm the expression of selected T2Rs at protein level, the cells were surface stained with polyclonal anti-T2R antibodies (1:200 or 1:300), monoclonal anti-β_2AR antibody (positive control), and the corresponding secondary antibody conjugated with Alexa Fluor-488 (1:1000). The data represent at least two independent experiments and the expression was presented as mean fluorescence intensity (MFI). To analyze the T2R-specific protein expression, the MFI values of isotype controls were subtracted. Two-way ANOVA with Bonferroni post hoc test was performed and no statistical significance was observed between non-CF and CF cells

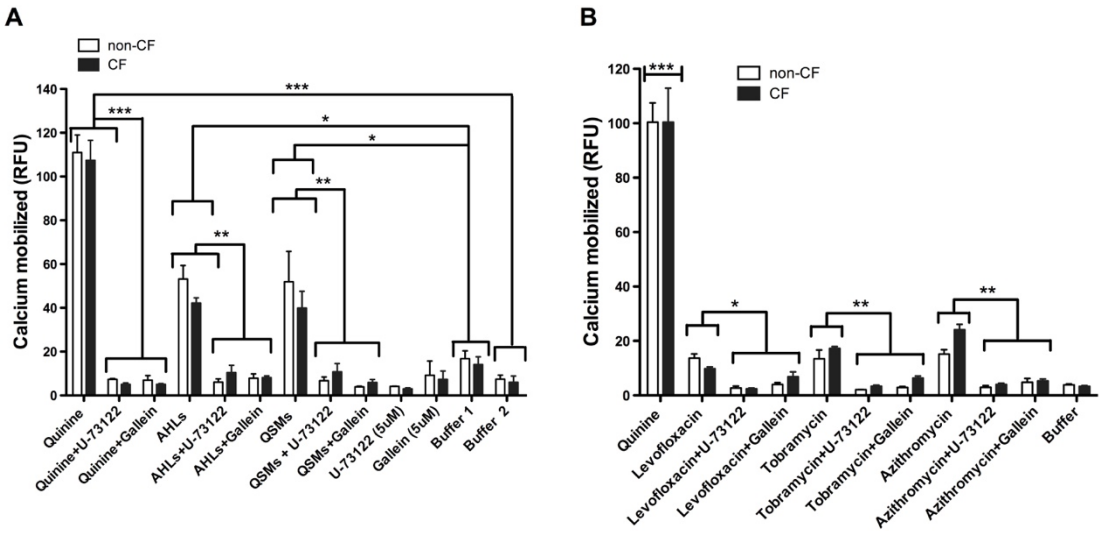

Figure 4.1.8. Functional response of non-CF and CF bronchial epithelial cells to quinine, AHLs and QSMs. (A) Primary cells from non-CF and CF donors were treated with quinine (500 μM), acyl homoserine lactones (AHLs) mixture consisting **C_4**-AHL, 3-oxo-**C_8**-AHL, 3-oxo-**C_{12}**-AHL each at 100 μM and a mixture of other quorum sensing molecules (QSMs) such as HHQ and NHQ each at 50 μM. **(B)** Primary cells treated with levofloxacin, tobramycin and azithromycin each at 200 μM. PLC inhibitor (U-73122 at 5 μM) and Gβγ inhibitor (Gallein at 5 μM) was used to elucidate the T2R signaling. DMSO (0.3) vehicle (buffer 1) and assay buffer (buffer 2) were taken as negative controls. Bar plot showing intracellular calcium mobilization from 4-5 independent experiments performed in triplicate. Two-way ANOVA with Bonferroni's multiple comparison test was performed and the significant response was calculated (*$p<0.05$; **$p<0.01$; ***$p<0.001$).

4.2 Characterize the Interaction of Commonly Used CF Antibiotics with T2Rs

(Chemosensory Bitter Taste Receptors (T2Rs) Are Activated by Multiple Antibiotics)

Appalaraju Jaggupilli, Nisha Singh, Vivianne Cruz De Jesus, Mohamed Soussi Gounni, Premnath Dhanaraj and Prashen Chelikani

FASEB Journal, 2018

4.2.1 Taste sensory analysis of antibiotics

Substantial evidence from the past decade suggests extraoral expression of T2Rs, and their physiological roles in health and disease was recently reviewed (Shaik et al., 2016, Lu et al., 2017). These studies strongly suggest that apart from taste sensing, T2Rs play important role in a variety of mechanisms depending on their tissue of origin. Advances in sequencing technologies allowed quantification of these T2Rs in several tissues from respiratory to gastrointestinal systems, where diverse microbiome harbours (Avau and Depoortere, 2016, Jaggupilli et al., 2017, Lee and Cohen, 2015). T2Rs expressed in the lung are believed to show relaxation effect in asthma patients opening an avenue for the development of new therapeutics (Deshpande et al., 2010, Liggett, 2014). In this objective, I tested the hypothesis that different antibiotics activate multiple T2Rs with different efficacies. I selected broad-spectrum antibiotics, tobramycin (aminoglycoside), levofloxacin (quinolone) and azithromycin (macrolide) that are frequently used in the treatment of CF, a disease characterized by bacterial infection of the lung leading to chronic inflammation and ultimately failure of the lung.

Electronic taste sensor analysis or E-tongue is commonly used to predict the taste of drugs including antibiotics which might be harmful, and as such, ethics approval is difficult to obtain for human taste panel analysis (Uchida et al., 2003) (Singh et al., 2011a). Here the bitterness of the antibiotics that belong to three different classes: aminoglycosides, fluoroquinolones and macrolides were predicted using an E-tongue (Alpha MOS). Known reference solutions of bitter compounds, caffeine and quinine, along with T2R1, T2R14 and T2R20 agonists' dextromethorphan (DXM), diphenhydramine (DPH) and cromolyn respectively, were used as controls (**Table 4.2.1**). The bitterness score was measured against the

reference compounds, and using a standard curve as described before (Singh et al., 2011a). The data for the tested antibiotics presented different ranges of predicted bitterness score, with a high predicted bitterness for the macrolide- azithromycin (15.8), and lower bitterness scores for levofloxacin (4.5) and tobramycin (3.5) (**Table 4.2.1**).

4.2.2 Pharmacological characterization of the activity of bitter antibiotics on T2Rs

Based on the data from E-tongue analysis, I selected the antibiotics with low (levofloxacin and tobramycin) and high (azithromycin) bitterness scores. I tested the ability of these three antibiotics to activate the T2Rs in cell based assays. I used HEK293T cells stably expressing T2R1, T2R4, T2R14 and T2R20 for the functional calcium mobilization assays. The stable cells were validated for T2R expression by flow cytometry, and functionality by calcium imaging using their respective agonists (**Figure 4.2.1**). The antibiotics were tested on the T2R stable cells at a concentration range of 7- 500 μM in calcium mobilization assays (**Figure 4.2.2**). Interestingly, the antibiotic with the highest bitterness score, azithromycin activated only T2R4 (EC_{50} = 74.45±12.3 μM), while antibiotics with lower bitter scores, levofloxacin activated T2R4 (EC_{50} = 97.83±13.1 μM), T2R14 (EC_{50} = 74.69±20.5 μM) and T2R20 (EC_{50} = 120.70±16.31 μM), and tobramycin activated T2R14 (EC_{50} = 135.40±20.2 μM) and T2R20 (EC_{50} = 50.97±19.37 μM) (**Figure 4.2.2**). No saturation in calcium mobilization was observed for T2R4 upon treating with tobramycin, and T2R14 and T2R20 with azithromycin. None of the antibiotics activated T2R1 significantly in the assays. Levofloxacin belongs to quinolone group of compounds, like quinine, that is known to activate multiple T2Rs (Upadhyaya et al., 2016, Meyerhof et al., 2010) (**Figure 4.2.3**).

Table 4.2.1. Taste sensory analysis of bitter compounds and antibiotics using E-tongue.

Bitter compound	Concentration (mM)	Bitterness score (in vivo) *	Bitterness predicated score (Alpha MOS)[$]
Caffeine	2.36	8.5	9.2
Quinine	0.03	9.0	8.5
Dextromethorphan	0.5	-	7.4
Diphenhydramine (DPH)	0.5	-	5.8
Cromolyn	0.5	-	4.8
Azithromycin	0.5	-	15.8
Erythromycin	0.5	-	12.6
Levofloxacin	0.5	-	4.5
Tobramycin	0.5	-	3.5
Ciprofloxacin	0.5	-	10.3

* *In vivo* score values from Alpha MOS. Astree electrochemical sensor technology technical note: T-SAS-04.2004.

[$] Bitterness scores predicted by E-tongue (Alpha MOS), experimental procedures are described
in methods.

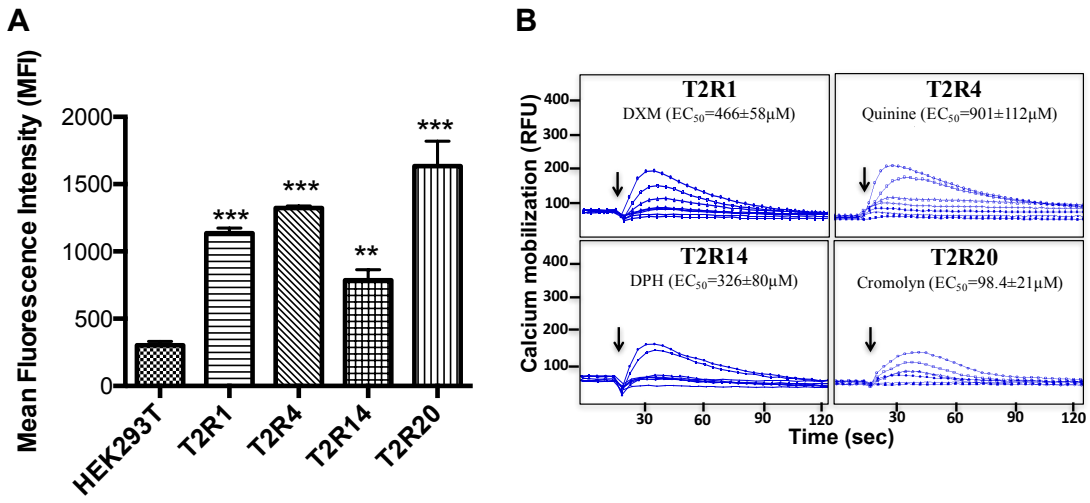

Figure 4.2.1. Characterization of T2R stable cells. (A). Cell surface expression analysis using flow cytometry. HEK293T cells stably expressing FLAG-tagged T2Rs were stained with FLAG-antibody (1:500 dilution) for 1 hr on ice in the dark, and subsequently washed 3 times. Flow cytometry analysis was performed using BD FACS-Canto analyser and the MFI values from control HEK293T cells was subtracted to obtained the expression of T2Rs. **(B)**. Functional characterization of stable cells by calcium mobilization assays. A dose response analysis of each T2R with its agonist was performed and represented as raw traces along with the EC_{50} values.

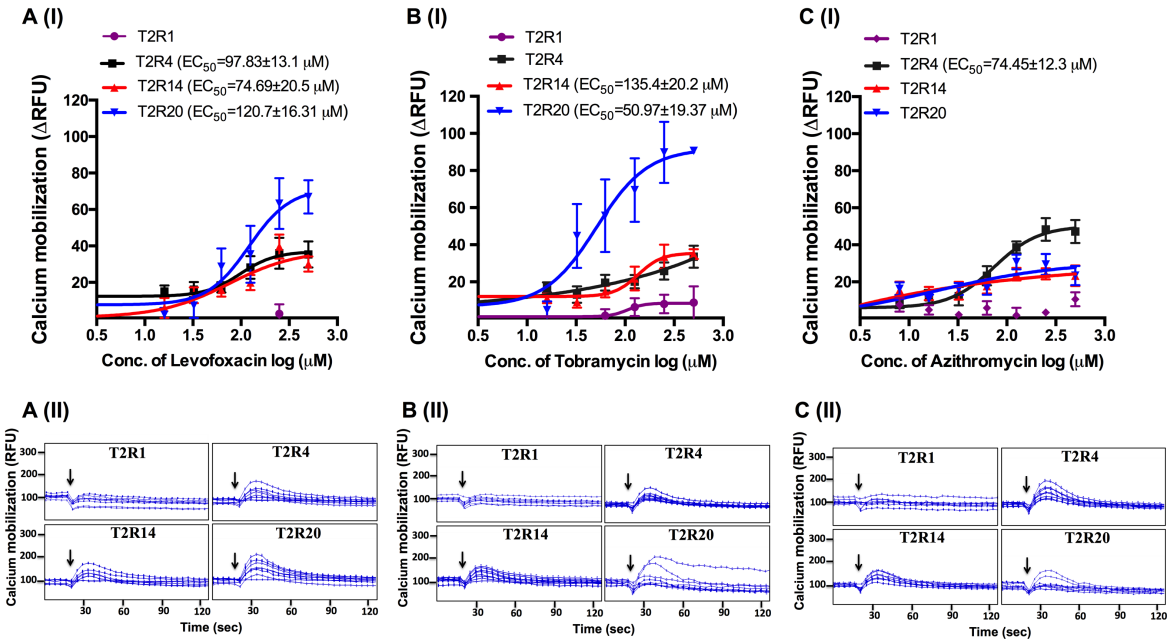

Figure 4.2.2. Dose response analysis of T2R stable cell lines in response to antibiotics. HEK293T cells stably expressing T2R1, T2R4, T2R14 and T2R49 were treated with levofloxacin, tobramycin and azithromycin at concentration range from 0.007 – 0.5 mM. Calcium mobilization was calculated by baseline subtraction of HEK293T cells from the stable cells and plotted as ΔRFU. The data in the top panel (A I, B I and C I) represents SEM of at least three independent experiments performed in triplicate. Representative calcium traces of each selected T2R in response to the antibiotics were presented in the bottom panel (A II, B II and C II).

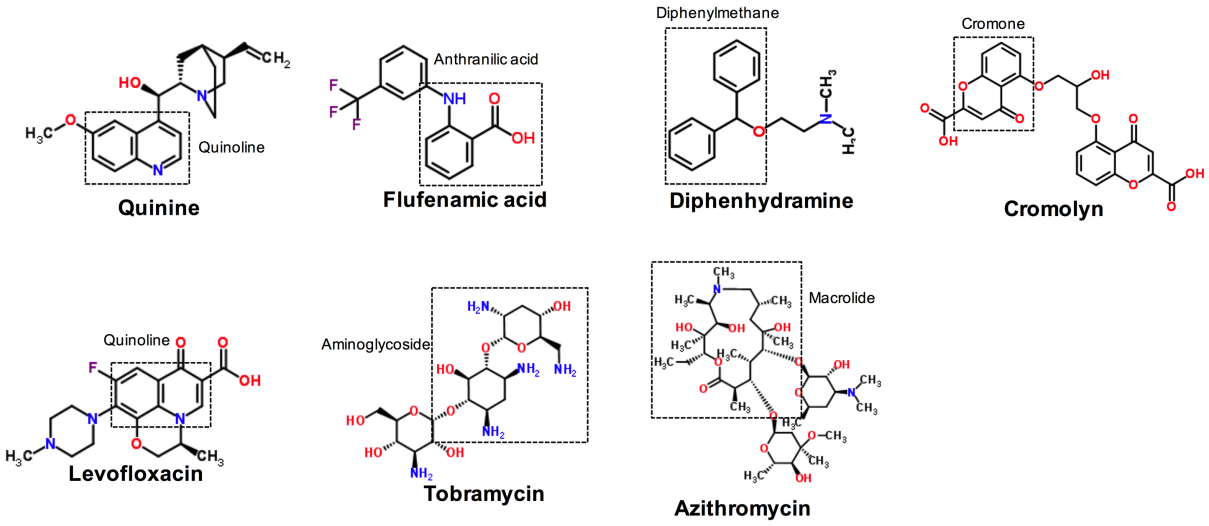

Figure 4.2.3. 2D representation of bitter compounds. The compounds shown include known T2R agonists and bitter tasting antibiotics. The parent structural group in each compound is identified and shown by the dotted box.

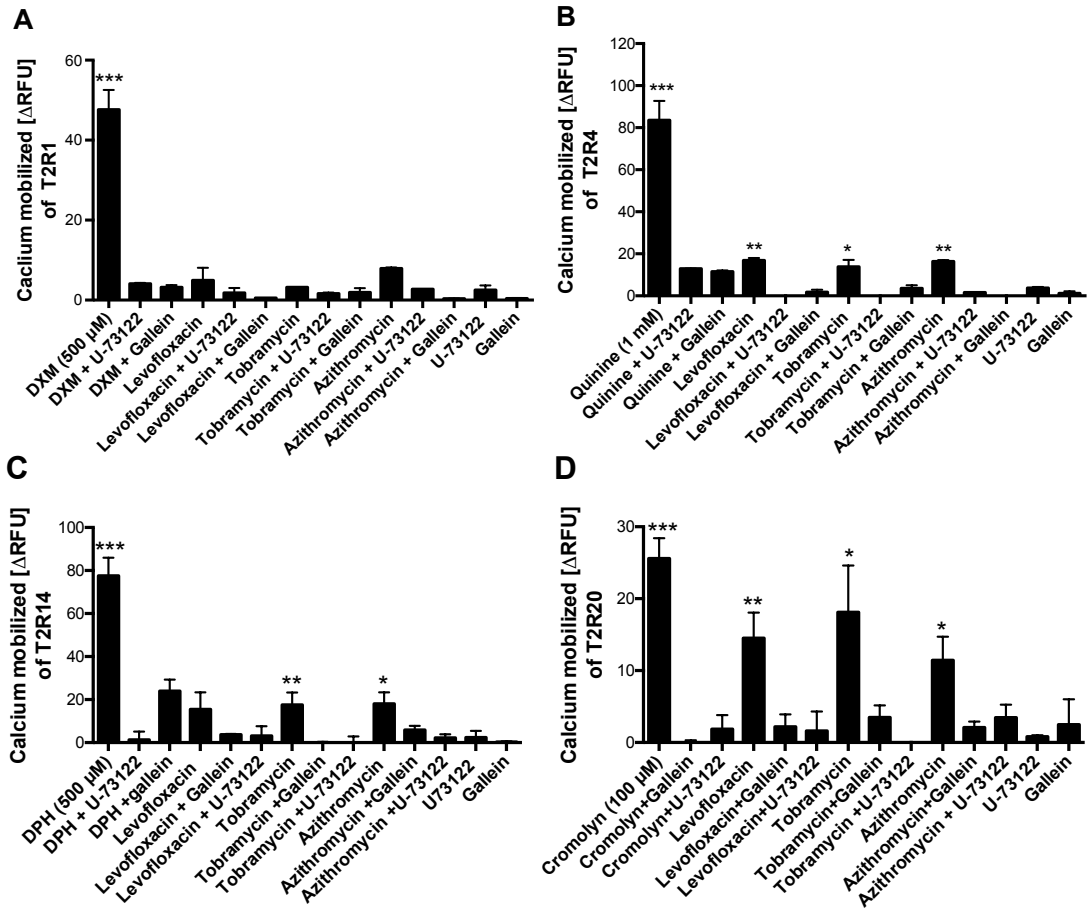

Figure 4.2.4. T2R mediated calcium mobilization in response to treatment with antibiotics. HEK293T cells stably expressing T2R1 (**A**), T2R4 (**B**), T2R14 (**C**) and T2R20 (**D**) were treated with levofloxacin, tobramycin and azithromycin each at 200 μM. PLC inhibitor (U-73122, 5 μM) and Gβγ inhibitor (Gallein, 5 μM) was used to elucidate the T2R signaling. DMSO (0.3) (buffer 1) and assay buffer (buffer 2) were taken as negative controls. Bar plot showing intracellular calcium mobilization from 4-5 independent experiments performed in triplicate Calcium mobilization after baseline subtraction with the HEK293T control cells and represented as ΔRFU. One-way ANOVA with Tukey's multiple comparison test was performed to identify the significant responses (*$p<0.05$; **$p<0.01$; ***$p<0.001$).

To confirm that the observed calcium responses were through "antibiotic-T2R-Gβγ-PLC" pathway, inhibitors for $G_{\beta\gamma}$ (gallein) and PLC (U-73122) at 5 μM each were used (**Figure 4.2.4**). Considering the non-robust activation of T2Rs in response to antibiotics, the stable cells were treated with a single concentration (200 μM) based on the dose-range of each antibiotic (**Figure 4.2.2**), in the presence or absence of PLC and $G_{\beta\gamma}$ inhibitors. This antibiotic concentration is well below the daily dosage of 250 – 750 mg for CF patients on an antibiotic regimen, which corresponds to 500 – 1000 μM of the antibiotic (Chmiel et al., 2014, Geller, 2009, Stockmann et al., 2013). The agonists for each T2R were also included as controls (**Figure 4.2.4**). Inhibition of calcium response was observed for all the three T2Rs. However, no difference for T2R1 was observed. These results suggest that antibiotics induce intracellular calcium response through activation of T2Rs.

Next, I focused on the structural features on these T2Rs that might be responsible for binding to the antibiotics. Based on the experiments above, I selected levofloxacin and tobramycin as these activated multiple T2Rs with strong potency. I pursued site-directed mutagenesis on T2R4, T2R14 and T2R20 to characterize the binding site for levofloxacin and tobramycin on these receptors. The wildtype and mutants of each receptor were transiently transfected in to HEK293T cells. Although the transfection approach has a possibility to show a variation in the expression of receptor in each repeated experiment, steps were taken to minimize the effects. The concentrations of DNA transfected and the lipofectamine were used same in all transfections and the ratio between the DNA and lipofectamine was 1:2 (w/v).

4.2.3 Prediction of levofloxacin binding site in T2R4 and site-directed mutagenesis

T2R4 is one of the moderately expressed T2Rs in most of the tissues and has been suggested to play a role in endogenous functions such as nitric oxide production in sinonasal cavity (Yan et al., 2017, Deshpande et al., 2010, Jaggupilli et al., 2017). In a previous report, the binding pocket of T2R4 for quinine was characterized (Pydi et al., 2014c). It was reported that Asn-165 and Thr-166 present in ECL2 are essential for quinine binding (For clarity, I used the actual residue numbers in the current study omitting the octapeptide FLAG. Thus, a difference of 8 in the residue number can be noticed between these studies). Since different molecular modeling suites were used in both the studies, I re-docked quinine along with levofloxacin in this study. In corroboration with the previous report, here I found quinine to bind within the same pocket and to be involved in similar interactions with previously reported amino acids, thus confirming the accuracy of the current model. Analysis of quinine and levofloxacin docked into this T2R4 model suggest that they bind in the same binding pocket in different binding poses. Amino acids within 4Å region making direct or indirect contacts in the binding pocket with these ligands were selected for mutagenesis. These amino acids are S81, Q152, S154, R163, N165, T166, Q249 and K262 (**Figure 4.2.5**). Each selected amino acid was mutated into two types of residues, replaced with a simple amino acid alanine and with a conservative substitution. Alanine replacements were expected to have minimum effect on receptor structure and conservative substitutions were expected to have similar function as the wild type receptor. The following 16 mutations were made: S81A, S81T, Q152A, Q152N, S154A, S154T, R163A, R163K, N165A, N165Q, T166A, T166S, Q249A, Q249N, K262A and K262R.

4.2.4 Functional characterization of T2R4 residues involved in quinine and levofloxacin binding

FLAG-tagged wild-type (WT) T2R4 and mutants were transiently transfected in HEK293T cells, and pcDNA (vector alone) mock transfected cells were used as control. To investigate whether the introduced mutations influence T2R4 folding and membrane trafficking, cell surface expression analysis was performed using flow-cytometry. Transfected cells were stained with anti-FLAG antibody and the expression of proteins determined by MFI after the values of mock transfected cells were deducted (**Table 4.2.2**). The percentage of the cells showing the fluorescence was calculated from the frequency of total cells from the selected population. Except N165 both mutants and K262A, no statistically significant difference in protein expression was observed between WT-T2R4 and other mutants (**Figure 4.2.6. A**). N165 is highly conserved in others T2Rs, and in T2R16 was shown to be N-glycosylated with glycosylation important for receptor expression but not for its function (Reichling et al., 2008). Thus, the low expression of N165 mutants is expected.

Pharmacological characterization of these mutants provides crucial insights on quinine and levofloxacin binding in T2R4 (**Figure 4.2.7**). WT-T2R4 and mutants were treated with different concentrations of quinine (0.07- 4 mM) and levofloxacin (0.015- 1 mM). The alanine replacement of R163 caused the loss of their native interactions with quinine and levofloxacin resulting in the loss of function. When a conservative substitution with lysine was done at this position, the quinine response was rescued while levofloxacin showed a rightward shift although the response (Emax) was rescued. This suggests the R163 in T2R4 is essential for interaction and activation by both the compounds. Based on EC_{50} values, mutations of residues Q152

and S154 affected binding to levofloxacin and not quinine, while T166A mutant showed significant loss of activity for quinine only (**Table 4.2.2**). In the case of N165, mutation at this position showed complete loss-of-function when treated with quinine but not with levofloxacin. This suggests that N165 in T2R4 might play a role in receptor expression.

Levofloxacin, a fluoroquinolone compound which belongs to the same parent structural group as quinine also docked in the same binding pocket. No polar interactions of N165 or T166 with levofloxacin besides a hydrophobic bond between N165 and quinoline ring were observed. However, R163 is involved in a polar bond with the F1 group on the quinoline and a hydrophobic bond with piperzinyl ring (**Figure 4.2.8**). Residues Q249 (TM6), Q152 and S154 (TM4-ECL2 interface) are involved in polar and ionic interactions with levofloxacin. The mutations at T166 showed different interactions with quinine and levofloxacin. Quinine is involved in interacting with only R163 and K262 in both T166A and T166S models causing weak binding as suggested by the functional data. On the other hand, mutations at T166 resulted in multiple polar interactions between neighbouring residues and levofloxacin (**Figure 4.2.9. B panels I-VI**). These increased interactions within the binding pocket might explain the gain-of-function phenotype of the T166 mutants as indicated by a reduced EC_{50} mutant/WT ratio (**Table 4.2.2**).

4.2.5 Prediction of levofloxacin and tobramycin binding sites in T2R14 and site-directed mutagenesis

T2R14 is a broadly tuned and high expressing T2R, in most of the extraoral tissues (Jaggupilli et al., 2017, Levit et al., 2014, Liggett, 2014). Using the same methodology as for T2R4 (above), a homology model of T2R14 was built and

levofloxacin, tobramycin, and known T2R14 agonists FFA and DPH were docked. As expected, they dock into the same binding pocket but present different secondary interactions based on their orientation. FFA and DPH predominantly make contacts with residues in TM helices; in contrast, levofloxacin and tobramycin make significant contacts with residues in ECLs. Similar to T2R4, amino acids within 4Å region T86, I148, R160, R161, K163, I179, T182 and V251 were selected for mutagenesis, with a total of 16 mutants characterized (**Figure 4.2.10**).

Table 4.2.2. Pharmacological characterization of the T2R4 mutants. Functional characterization of the mutants was pursued by measuring intracellular calcium mobilization in response to different concentrations of T2R4 putative agonist quinine and antibiotics (levofloxacin and azithromycin). Cell surface expression was determined by flow cytometry analysis. **ND** – not determined.

Mutant	Quinine			Levofloxacin			Cell surface expression	
	EC_{50} (μM)	EC_{50} mutant/ EC_{50} WT	E_{max} (ΔRFU)	EC_{50} (μM)	EC_{50} mutant/ EC_{50} WT	E_{max} (ΔRFU)	MFI	% of cells
T2R4	838.37±24	1.0	174.46±22	129.97±44	1.0	43.26±5	2150±523.5	61.7
S81A	922.54±35	1.17	91.52±31	203.81±82	1.56	34.73±5	2075±450.6	59.3
S81T	875.11±29	1.04	150.43±15	226.17±31	1.73	42.23±8	2172±429.3	62.5
Q152A	998.17±37	1.2	78.28±31	ND		14.05±4	1987±348.9	57.5
Q152N	757.49±78	0.9	37.17±17	ND		4.2±2	1911±392.5	51.8
S154A	765.95±21	0.91	57.66±26	ND		12.7±3	1562±212.8	44.9
S154T	834.51±15	1.0	120.56±24	ND		14.4±4	1620±175.3	47.3
R163A	ND		23.65±23	ND		16.1±6	1626±184.0	47.8
R163K	932.6±58	1.1	135.56±34	235.12±57	1.8	32.08±5	1603±181.9	50.2
N165A	ND		24.10±25	NS		30.67±7	868±161.6	23.3
N165Q	ND		45.09±26	NS		36.86±4	830±346.9	21.9
T166A	ND		24.5±32	88.12±54	0.67	34.62±2	1688±299.7	49.8
T166S	ND		112.47±36	100.1±48	0.76	33.6±6	1730±59.01	53.3
Q249A	784.47±18	0.93	68.99±20	ND		18.8±4	1893±352.9	54.6
Q249N	721.46±88	0.86	143.44±48	228.9±41	1.76	38.3±7	1608±227.1	51.9
K262A	688.26±18	0.82	220.15±13	NS		48.25±8	971±225.4	25.5
K262R	829.27±29	0.99	152.54±33	NS		36.25±3	1824±349.6	54.9

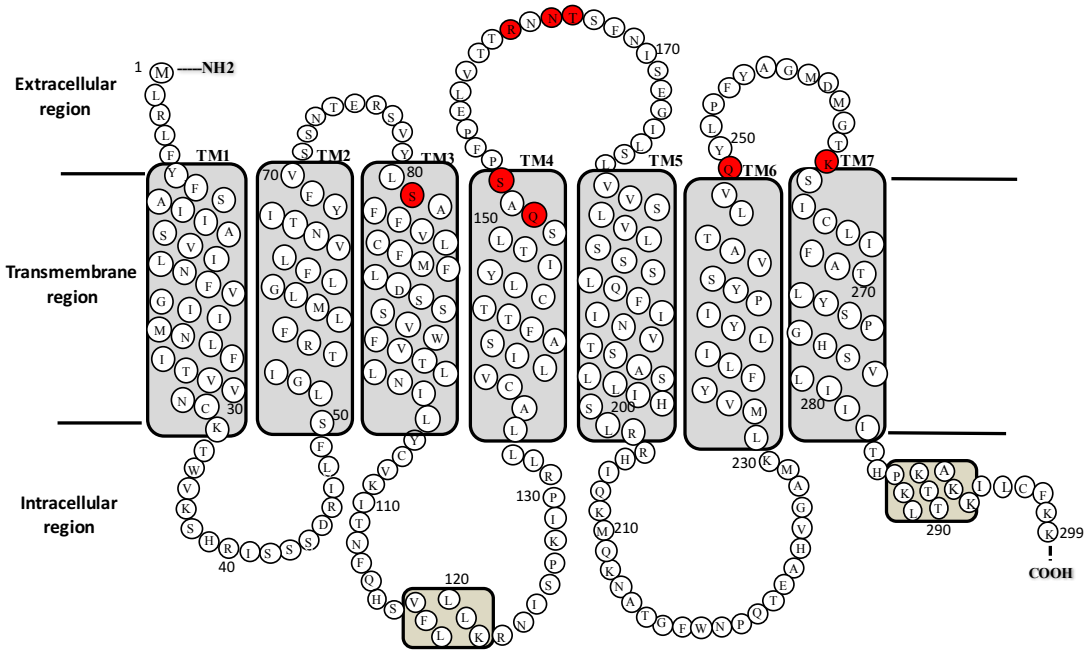

Figure 4.2.5. Two-dimensional representation of the T2R4 amino acid sequence. The N-terminus FLAG sequence is not shown in the 2D structure for simplicity. Amino acid sequence of T2R4 contains 299 residues with a very short N-terminus, seven transmembrane (TM) helices, three extracellular loops (ECLs), three intracellular loops (ICLs), and an intracellular C-terminus. The 2D structure was predicted using TMpred, TMHMM and HMMTOP servers. The amino acids predicted to be involved in ligand binding, and mutated in this study are highlighted in red for each T2R. Three of these residues are present in ECL2, and the rest on the extracellular side of the TM helices 3 and 4 or at the interface between TM6 and 7 of ECL3.

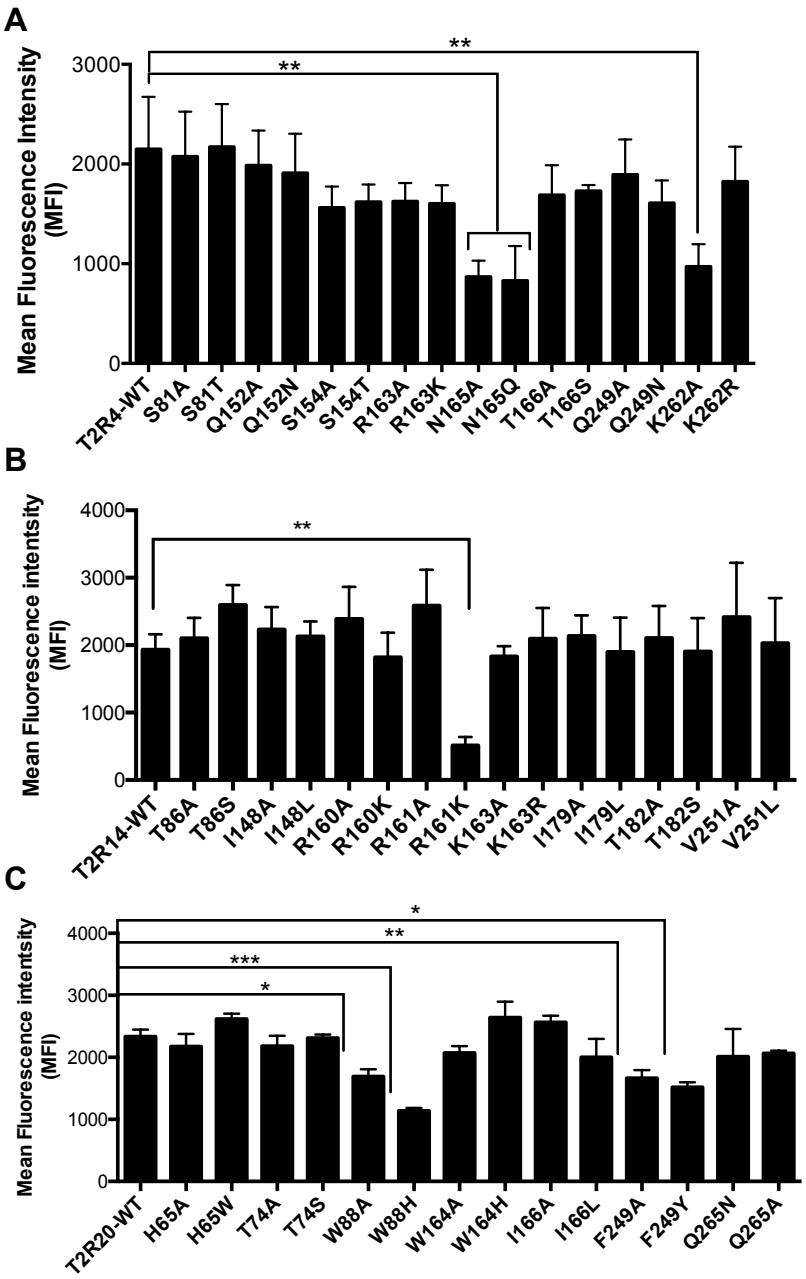

Figure 4.2.6. Expression analysis of T2R4, T2R14 and T2R20 wild type and mutants by flow cytometry. HEK293T cells transiently transfected with (**A**) T2R4, (**B**) T2R14 and (**C**) T2R20 wild type or mutants were analyzed for cell surface expression using flow cytometry analysis. Cells were stained with APC-conjugated anti-FLAG antibody (1:500) and incubated on ice for 1h in the dark. The analysis was carried using BD FACS Canto analyzer and the MFI values obtained for pcDNA mock transfected control cells (~300 MFI) were subtracted from the samples to obtain expression value of WT or mutants of T2Rs. The bar plot represents the data obtained from 2-3 independent experiments performed in duplicated. One-way ANOVA with Tukey's multiple comparison test was performed was performed to identify the significant responses (*$p<0.05$; **$p<0.01$; ***$p<0.001$).

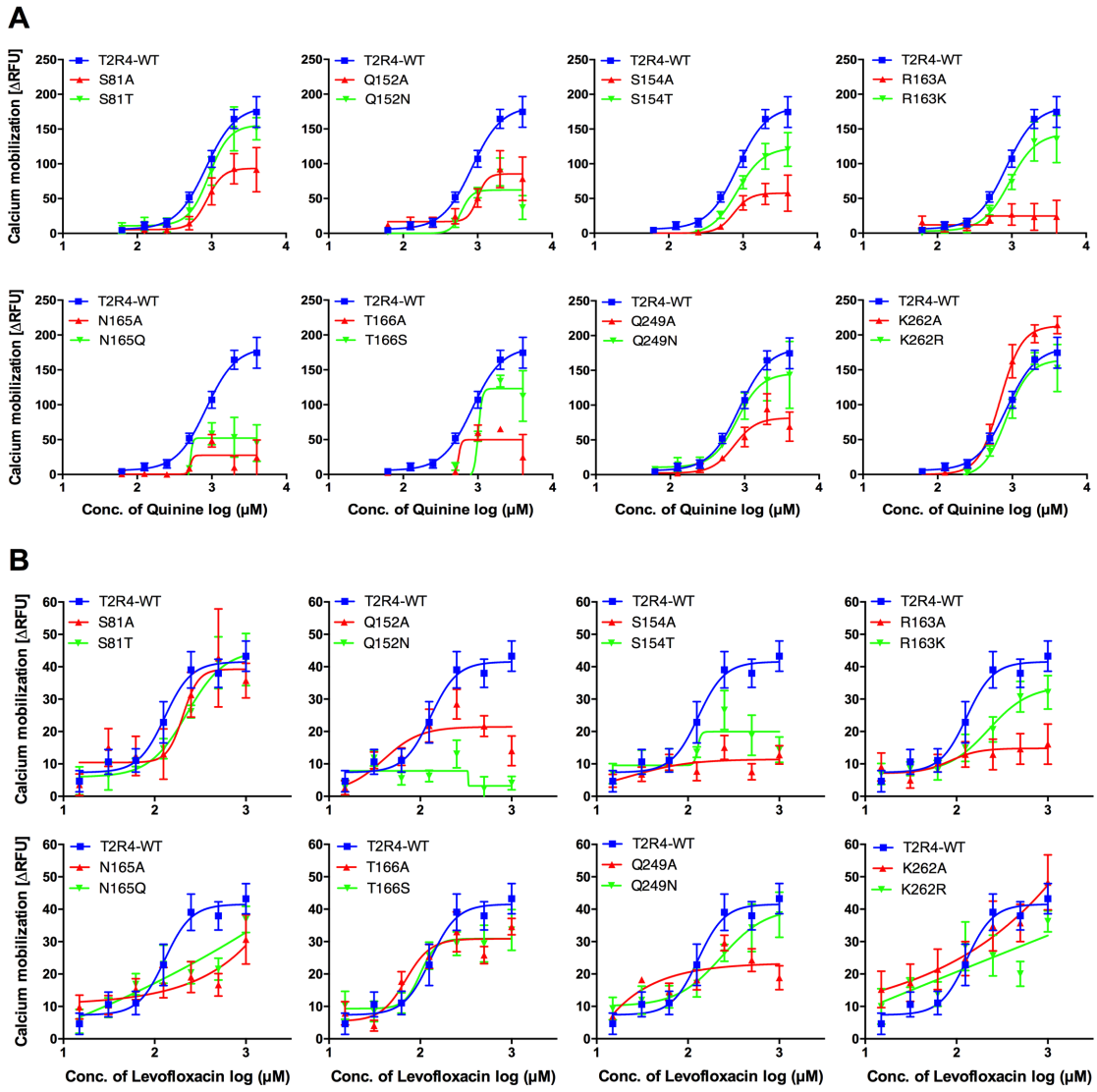

Figure 4.2.7. Concentration dependent calcium response of T2R4 wild type and mutants treated with quinine and levofloxacin. T2R4 WT and mutants for the following residues S81, Q152, S154, R163, N165, T166, Q249 and K262 were transiently transfected in HEK293T cells and (**A**) treated with quinine at concentration range from 0.07 - 4 mM and (**B**) treated with levofloxacin at concentration range from 0.015 - 1 mM. Calcium mobilization was calculated by baseline subtraction of pcDNA mock transfected cells from the WT or mutants and plotted as ΔRFU. The data represents SEM of four independent experiment performed in triplicate.

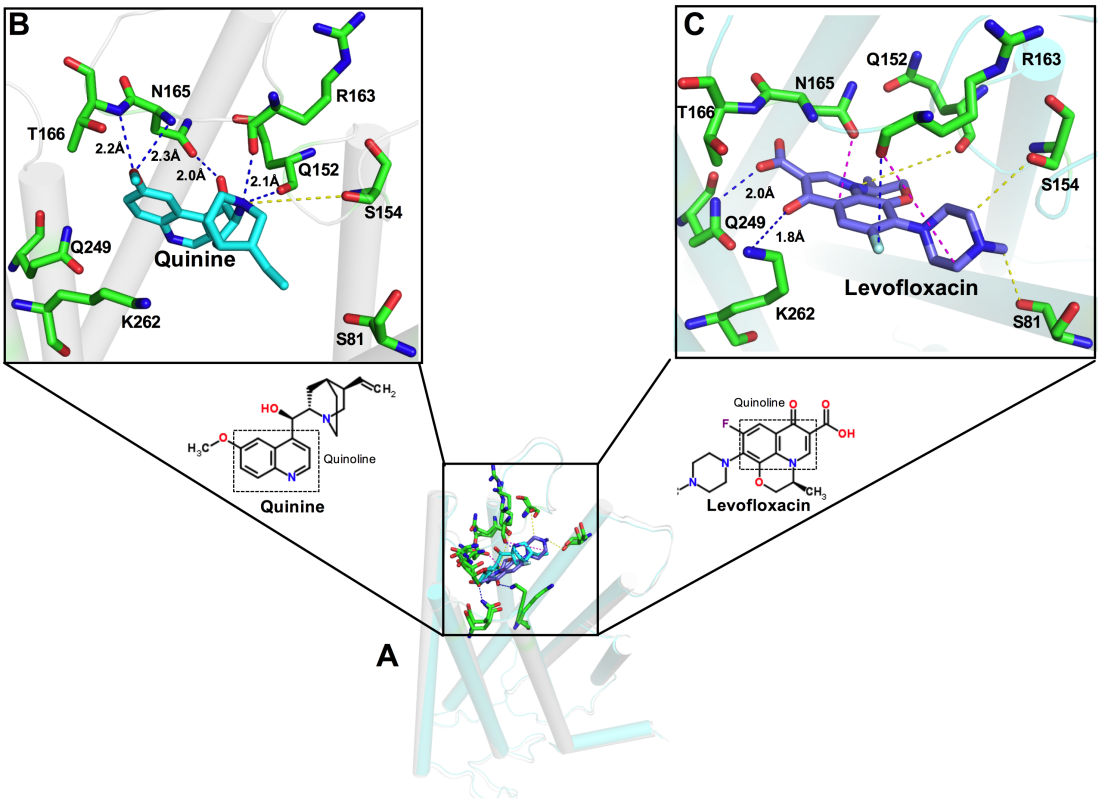

Figure 4.2.8. Model of T2R4 bound to quinine and levofloxacin. The 3D model of T2R4 docked with quinine (Inset B, cyan) and levofloxacin (Inset C, Magenta) as described in methods. The residues (sticks) interacting with the agonists and their bonds (dashes) were highlighted. The interactions were represented in different colors (Polar bond: Blue; Salt bridge: Yellow; Pi-cation: Pink). A 2D representation of each compound is presented highlighting (dotted box) the parent structure.

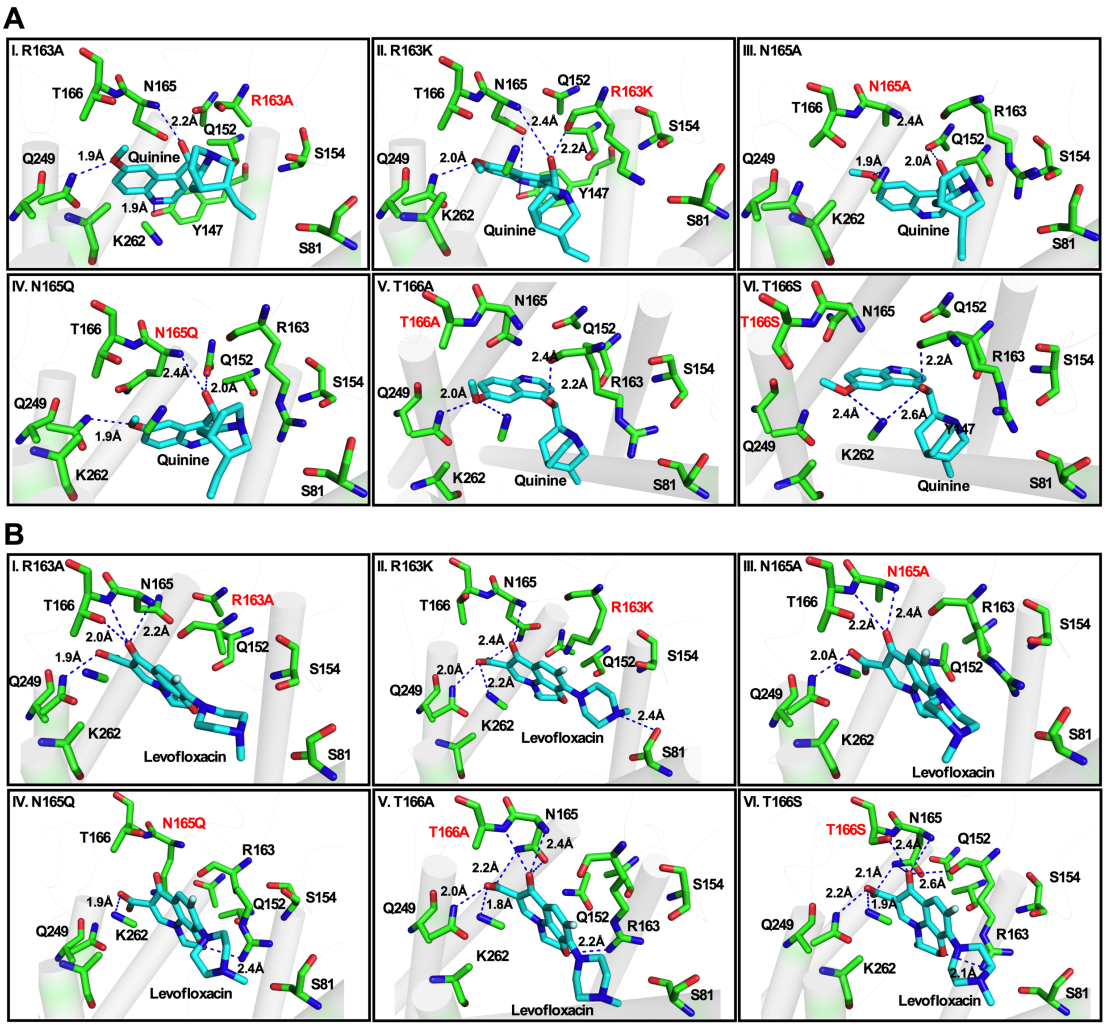

Figure 4.2.9. Molecular models showing quinine and levofloxacin interactions within T2R4. Analysis of the interactions of quinine (**A I-VI**) and levofloxacin (**B I-VI**) docked to T2R4 mutants. Quinine or levofloxacin (cyan) and amino acid residues (green) were represented as sticks showing nitrogen (blue) and oxygen (red). Corresponding mutants in each panel were labelled in red. The interactions were represented in different colors (Polar bond: Blue; Salt bridge: Yellow; Pi-cation: Pink).

4.2.6 Functional characterization of T2R14 residues involved in agonist and antibiotic binding

As described above, the FLAG-tagged WT-T2R14 and mutants were transiently transfected in HEK293T cells and examined for the cell surface expression (**Table 4.2.3**). Except for R161K, no significant difference in the expression levels was observed (**Figure 4.2.6. B**). WT-T2R14 and mutants were treated with different concentrations of FFA (0.004 – 0.3 mM), DPH (0.03 – 2 mM), levofloxacin and tobramycin (0.015- 1 mM) (**Figure 4.2.11 & Figure 4.2.12**). Previously, FFA was suggested as one of the potent agonists for T2R14 with an EC_{50} value of 137 μM (Meyerhof et al., 2010). No pharmacological characterization of DPH was reported. In this study, I obtained an EC_{50} of 77.42±15 μM for FFA and report an EC_{50} value of 424.37 ± 15 μM for DPH, at T2R14. Most of the mutants caused a rightward shift in response to FFA treatment, in contrast, DPH response was less affected by the mutations in T2R14 exhibiting loss or rightward shift only for mutations at positions I148, R161, K163 and I179 (**Figure 4.2.11 & Figure 4.2.12**). This indicates although they have a similar binding mode, they have both common and unique residues, which determine their potencies.

Mutation of R161 in T2R14 disrupted native interactions with all the compounds resulting in significant loss of function (**Figure 4.2.11 & Figure 4.2.12**). Tobramycin treatment showed a significant rightward shift in both the mutants (**Figure 4.2.12. A**). The alanine mutations at R160 and K163 showed a loss of function response to the tested compounds, while the conservative substituents had rescued the response with all compounds except FFA. This suggests that the ECL2 region comprising residues R160, R161 and K163 in T2R14 is essential for ligand binding and activation. This is in agreement, with a recent study that suggested R160 to be important for interaction with another known T2R14 agonist, aristolochic acid

(Zhang et al., 2017). In addition, there are other residues such as T86 and I179 whose mutations showed significant variation in the EC_{50} ratio with WT (**Table 4.2.3 & Table 4.2.4**).

In T2R14, T86A (rs16925868) is a missense mutation or a non-synonymous single nucleotide polymorphism (nsSNPs). However, the role of this nsSNP in human health or disease is yet to be elucidated. Interestingly, in these functional assays T86A showed a significant reduction in the E_{max} values, and the conservative substitution T86S partially rescued signaling (**Table 4.2.3**). This indicates that T86 present on ECL1 in T2R14 is important for ligand recognition and receptor activation. A similar phenomenon was observed previously for the nsSNP, A189V in T2R9 which showed a significant effect on the interaction with some of the tested ligands (Dotson et al., 2008). Molecular modeling analyses provide insights into the different interactions involved in recognizing diverse compounds by T2R14 (**Figure 4.2.13**). The docking analysis suggest FFA and DPH bound slightly deeper in the TM core while levofloxacin and tobramycin bound towards the extracellular side interacting more with ECL residues (**Figure 4.2.13. A**). This might be due to the variation in their size and complexity. Interestingly, all the tested compounds make contacts with some common residues like T86, R160, T182 and V251. There are also unique contacts, for example I148 in TM4 for FFA and DPH (**Figure 4.2.13. B-C**), I179 and R161 in ECL2 for levofloxacin and tobramycin (**Figure 4.2.13. D-E**). K163 showed no strong interactions with any of the compounds although it is in the proximity with crucial residues R160 and R161 suggesting that it might have an indirect influence on ligand binding and receptor activation (**Figure 4.2.14 & Figure 4.2.15**).

Table 4.2.3. Pharmacological characterization of the T2R14 mutants. Functional characterization of the mutants was pursued by measuring intracellular calcium mobilization in response to different concentrations of T2R14 putative agonist FFA and antibiotics (levofloxacin and tobramycin). Cell surface expression was determined by flow cytometry analysis. **ND** – not determined (no significant calcium mobilization detected), **NS** – no saturation (agonist concentration dependent increase in calcium mobilization not observed).

Mutant	FFA			Levofloxacin			Tobramycin			Cell surface expression	
	EC_{50} (μM)	EC_{50} mutant/ EC_{50} WT	E_{max} (ΔRFU)	EC_{50} (μM)	EC_{50} mutant/ EC_{50} WT	E_{max} (ΔRFU)	EC_{50} (μM)	EC_{50} mutant/ EC_{50} WT	E_{max} (ΔRFU)	MFI	% of cells
T2R14	77.42±15	1.0	43.55±11	121.9 ± 31	1.0	32.92±3	246.41±19	1.0	45.33±3	1930±66	59.6
T86A	94.59±33	1.22	10.9±8	ND		7.1±3	114.1±76	0.46	21.88±2	2103±122	62.3
T86S	NS		26.8±10	162.4±58	1.34	14.1±3	166.4±47	0.67	34.74±3	2596±120	65.9
I148A	ND		-	ND		-	344.1±32	1.4	32.76±4	2232±136	57.4
I148L	159.3±57	2.06	23.8±12	NS		5.4±9	329.9±44	1.33	27.73±4	2128±91	52.8
R160A	165.7±82	2.14	28.9±12	159.5±44	1.29	11±4	ND		10.19±3	2390±193	51.0
R160K	ND		13±8	92.7±37	0.76	19.2±4	265.53±35	1.1	24.24±2	1819±148	47.3
R161A	ND		13.12±7	ND		13.7±3	NS		36.47±5	2585±217	61.5
R161K	ND		17.03±9	176.9±35	1.46	11.6±3	NS		35.39±6	513±51	19.1
K163A	130.5±61	1.68	31.91±9	NS		15.3±4	NS		37.39±2	1832±62	49.8
K163R	76.21±43	0.99	24.70±10	69.4±42	0.57	9.8±3	377.2±38	1.53	36.25±2	2095±186	51.7
I179A	98.67±25	1.28	30.89±11	201.1±13	1.64	44.3±7	417.6±17	1.70	29.49±4	2136±124	59.8
I179L	66.80±33	0.87	20.16±7	258.12±22	2.11	37.8±8	370.8±41	1.50	32.85±3	1899±208	46.6
T182A	113.7±31	1.48	19.04±7	321.2±45	2.63	18.8±7	404.2±93	1.64	31.3±4	2106±238	54.7
T182S	97.14±42	1.25	31.16±10	209.9±41	1.71	28.4±4	238.7±32	0.97	25.60±2	1906±247	54.3
V251A	76.19±19	0.98	43.40±18	ND		15.4±9	280.2±48	1.13	29.49±6	2415±403	62.7
V251L	62.64±25	0.81	18.32±15	314.2±47	2.57	33.4±4	223.8±65	0.90	27.68±4	2030±334	53.1

Table 4.2.4. Pharmacological characterization of the T2R14 mutants with DPH. Functional characterization of the mutants was pursued by measuring intracellular calcium mobilization in response to different concentrations of T2R14 agonist DPH. Cell surface expression was determined by flow cytometry analysis. **ND** – not determined (no significant calcium mobilization detected), **NS** – no saturation (agonist concentration dependent increase in calcium mobilization not observed)

Mutant	Diphenhydramine		
	EC_{50} (μM)	EC_{50} MT/ EC_{50} WT	E_{max} (ΔRFU)
T2R14	424.37±15	1.0	179.67±12
T86A	451.13±13	1.06	194.14±18
T86S	433.52±19	1.02	182.47±19
I148A	842.11±66	1.98	96.34±25
I148L	NS		163.42±22
R160A	463.41±12	1.09	200.67±12
R160K	423.65±9	0.99	201±25
R161A	ND		112.26±13
R161K	NS		124.67±12
K163A	ND		5±24
K163R	ND		20.77±22
I179A	486.4±23	1.14	110.23±13
I179L	373.51±11	0.87	62.32±22
T182A	ND		82.21±25
T182S	436.74±14	1.02	179.53±22
V251A	417.36±19	0.98	162.85±16
V251L	412.62±15	0.97	190.42±21

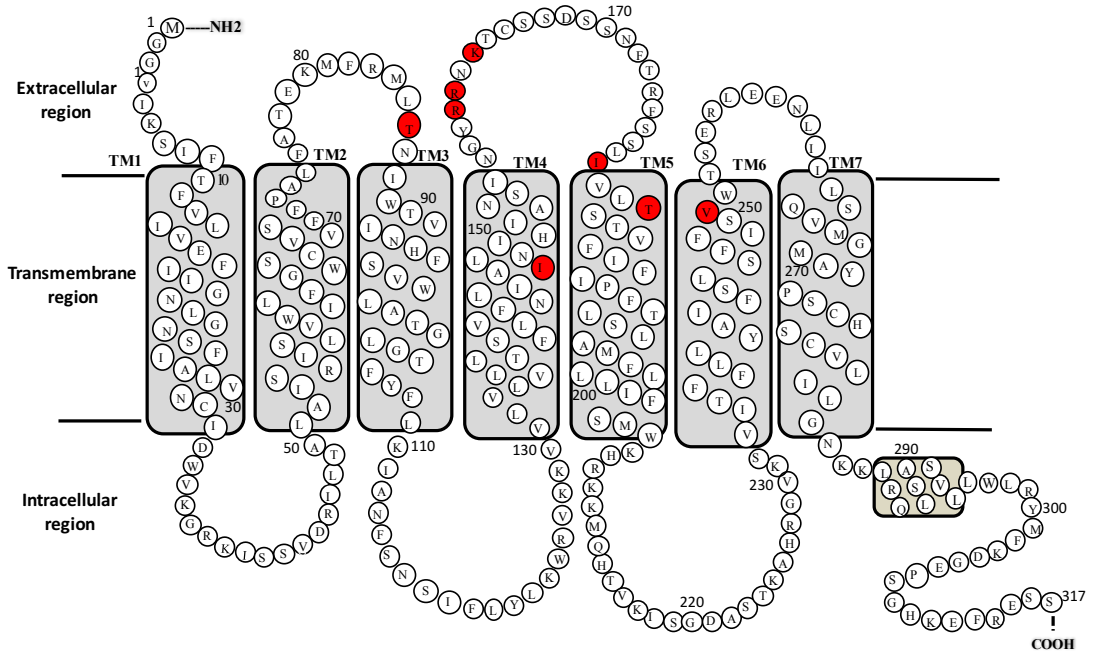

Figure 4.2.10. Two-dimensional representation of the T2R14 amino acid sequence. The N-terminus FLAG sequence is not shown in the 2D structure for simplicity. Amino acid sequence of T2R4 contains 317 residues with a very short N-terminus, seven transmembrane (TM) helices, three extracellular loops (ECLs), three intracellular loops (ICLs), and an intracellular C-terminus. The 2D structure was predicted using TMpred, TMHMM and HMMTOP servers. The amino acids predicted to be involved in ligand binding, and mutated in this study are highlighted in red for each T2R. One of these residues is present in ECL1, three of them are present in ECL2, and the rest on the extracellular side of the TM helices 4, 5 and 6 or at the interface between TM3 and ECL3.

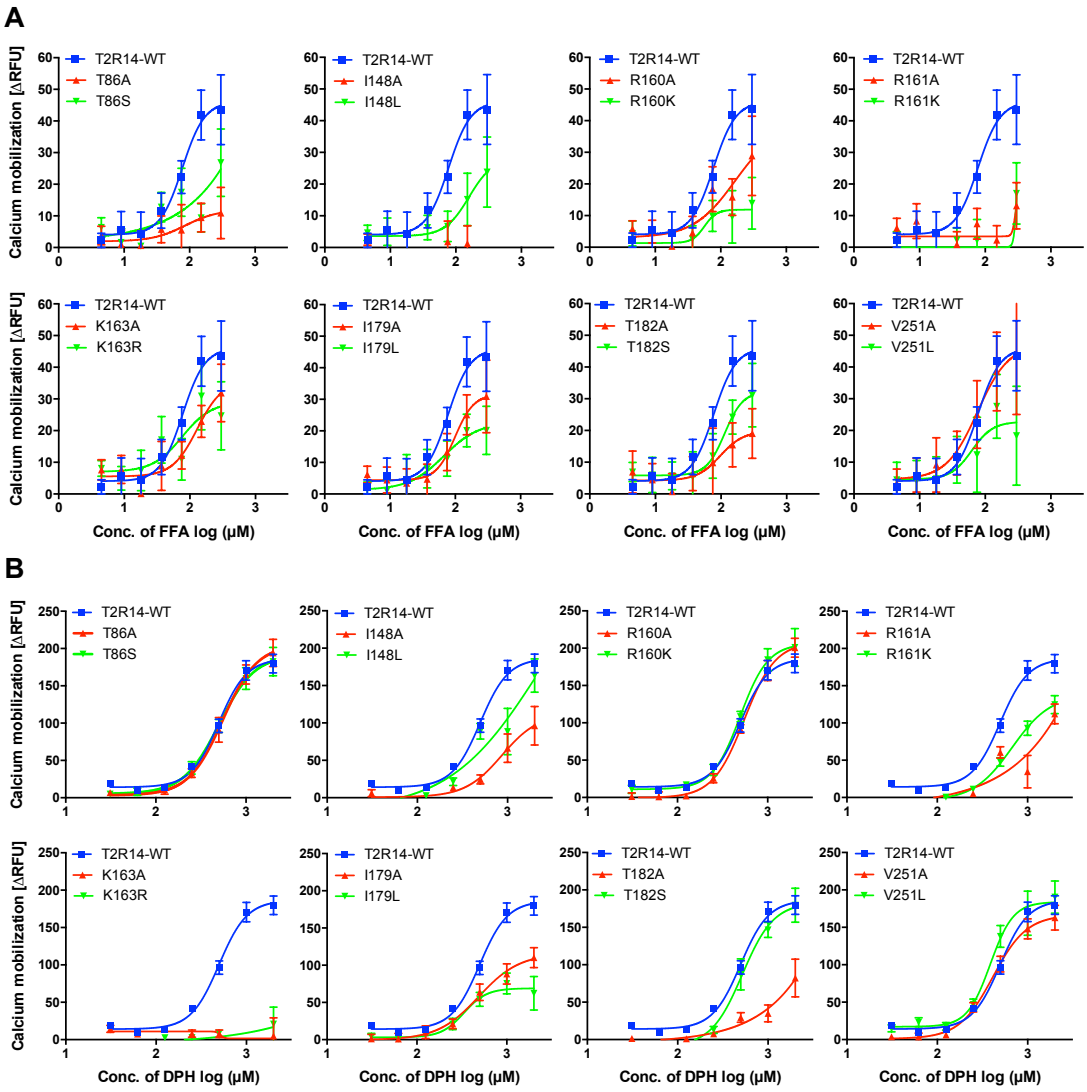

Figure 4.2.11. Dose response analysis of T2R14 wild type and mutants in response to the putative agonists FFA and DPH. T2R14 WT and mutants for following residues T86, I148, R160, R161, K163, I179, T182 and V251 were transiently transfected in HEK293T cells and, treated with (**A**) FFA at concentration range from 0.004 – 0.3 mM, (**B**) DPH at concentration range from 0.03 - 2 mM. Calcium mobilization was calculated by baseline subtraction of pcDNA mock transfected cells from the WT or mutants and plotted as ΔRFU. The data represents SEM of at three independent experiments performed in triplicate.

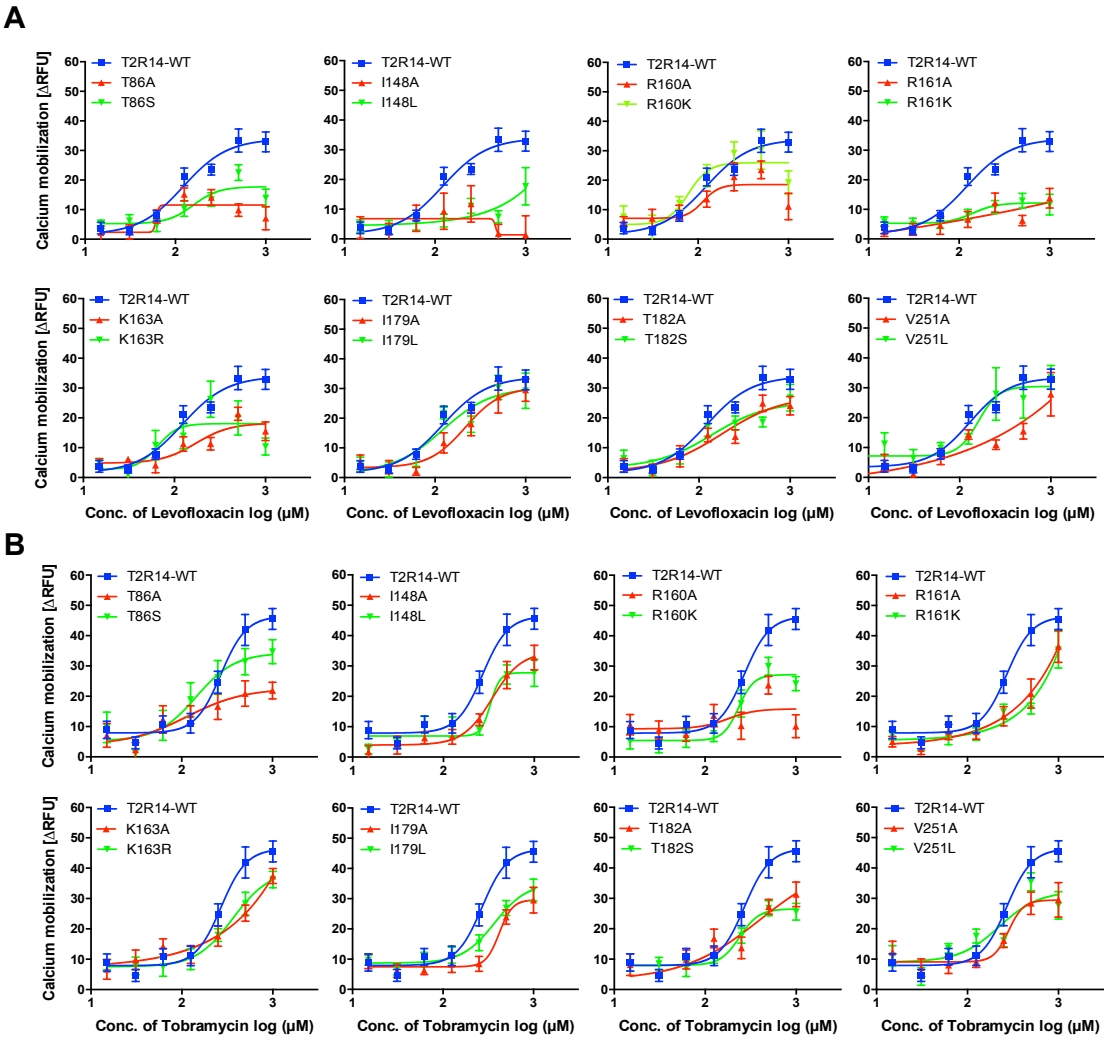

Figure 4.2.12. Dose response analysis of T2R14 wild type and mutants in response to the antibiotics levofloxacin and tobramycin. T2R14 WT and mutants for following residues T86, I148, R160, R161, K163, I179, T182 and V251 were transiently transfected in HEK293T cells and, treated with (**A**) levofloxacin at concentration range from 0.015 - 1 mM and (**B**) tobramycin at concentration range from 0.015 - 1 mM. Calcium mobilization was calculated by baseline subtraction of pcDNA mock transfected cells from the WT or mutants and plotted as ΔRFU. The data represents SEM of at three independent experiments performed in triplicate.

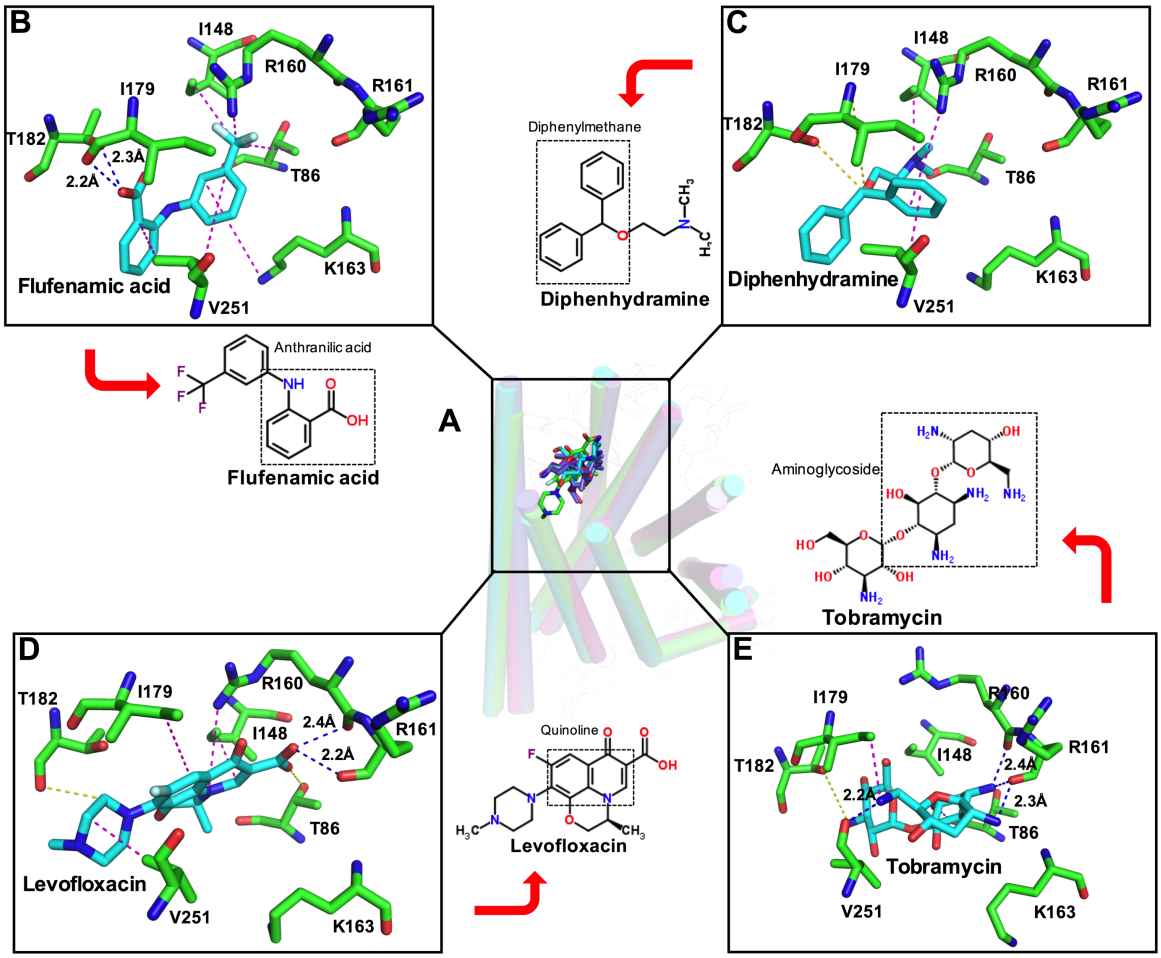

Figure 4.2.13. Model of T2R14 bound to FFA, DPH, levofloxacin and tobramycin. The 3D model of T2R14 docked with FFA (inset B), DPH (inset C), levofloxacin (inset D) and tobramycin (inset E) as described in methods. The residues (sticks) interacting with the agonists and their bonds (dashes) were highlighted. The interactions were represented in different colors (Polar bond: Blue; Salt bridge: Yellow; Pi-cation: Pink). A 2D representation of each compound is presented highlighting (dotted box) the parent structure.

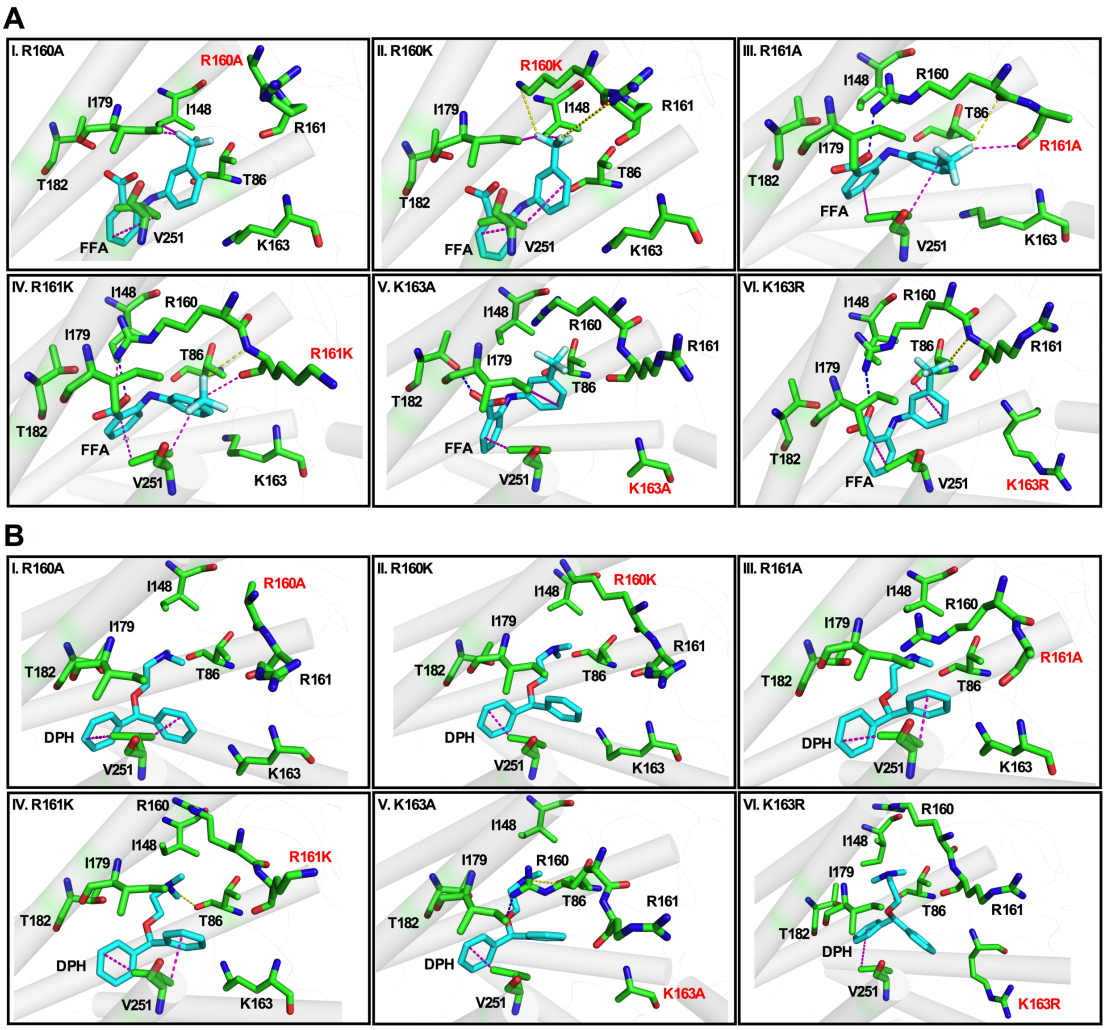

Figure 4.2.14. Molecular models showing FFA and DPH interactions within T2R14. Analysis of the interactions of FFA (**A I-VI**) and DPH (**B I-VI**) docked to T2R14 mutants and amino acid residues (green) were represented as sticks showing nitrogen (blue) and oxygen (red). Corresponding mutants in each panel were labelled in red. The interactions were represented in different colors (Polar bond: Blue; Salt bridge: Yellow; Pi-cation: Pink)

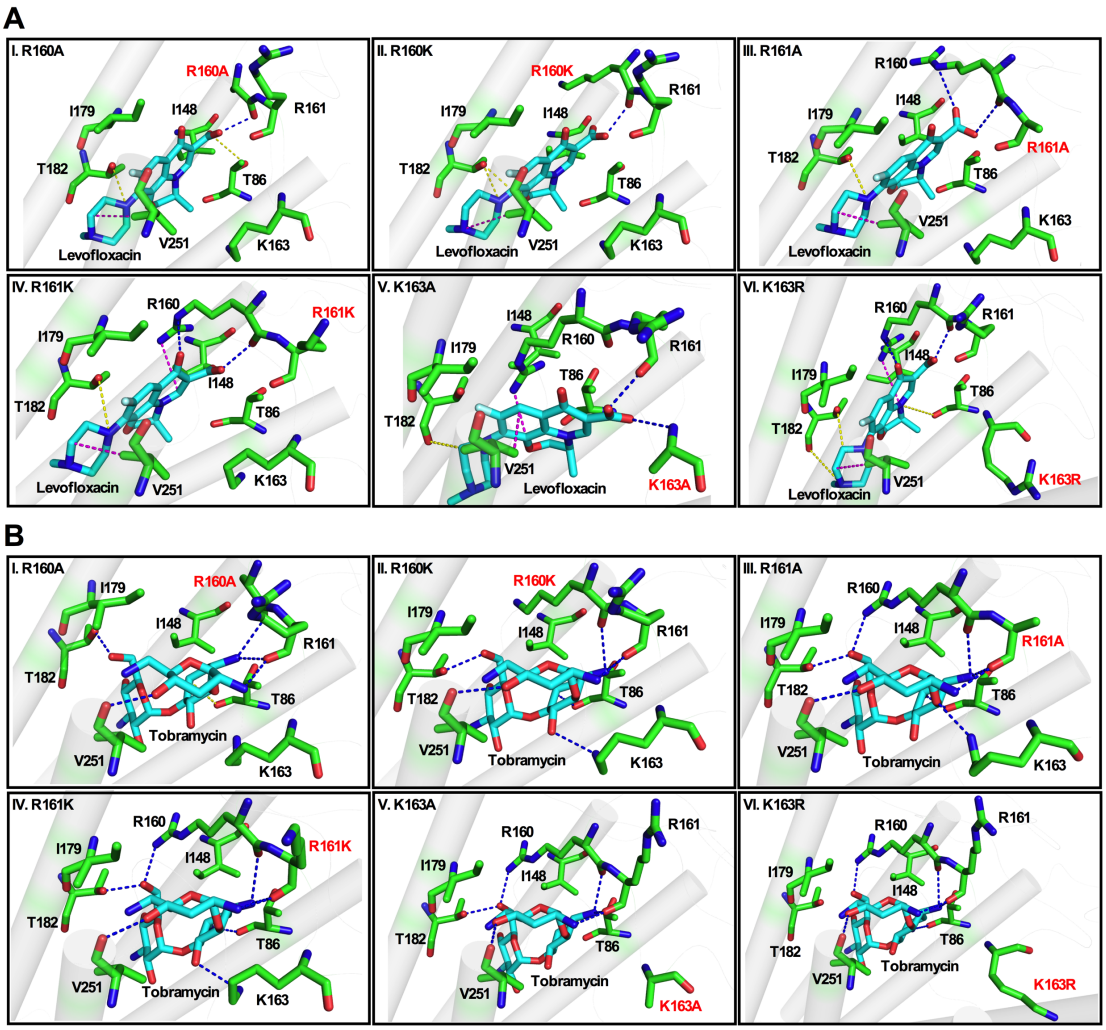

Figure 4.2.15. Molecular models showing levofloxacin and tobramycin interactions within T2R14. Analysis of the interactions of levofloxacin (**A I-VI**) and tobramycin (**B I-VI**) docked to T2R14 mutants and amino acid residues (green) were represented as sticks showing nitrogen (blue) and oxygen (red). Corresponding mutants in each panel were labelled in red. The interactions were represented in different colors (Polar bond: Blue; Salt bridge: Yellow; Pi-cation: Pink).

4.2.7 Prediction of levofloxacin and tobramycin binding sites in T2R20 and site-directed mutagenesis

T2R20 is a poorly studied T2R and only two agonists, cromolyn (EC_{50} = 45±25 μM) and diphenidol, were reported for this receptor (Meyerhof et al., 2010). Next to T2R14, T2R20 is expressed at high levels in most human tissues (Jaggupilli et al., 2017). As described for T2R4 and T2R14, levofloxacin and tobramycin along with cromolyn were docked to T2R20. In my models, cromolyn and tobramycin docked in the binding pocket spanning from TM bundle to extracellular region while levofloxacin was docked into the TM core making subtle interactions with extracellular residues. The amino acids within 4Å region H65, T74, W88, W164, I166, F249 and Q265 were selected for mutagenesis (**Figure 4.2.16**). Each residue was mutated to alanine or a conserved substitution and the following 14 mutations were made: H65A, H65W, T74A, T74S, W88A, W88H, W164A, W164H, I166A, I166L, F249A, F249Y, Q265A and Q265N.

4.2.8 Functional characterization of T2R20 residues involved in agonist and antibiotic binding

The cell surface expression analysis in HEK293T cells transiently transfected with FLAG-tagged WT-T2R20 and mutants showed no significant difference in their expression levels except for W88 and F249 mutants (**Table 4.2.5**). The transfected cells were tested with an agonist of T2R20, cromolyn and the antibiotics (levofloxacin and tobramycin) at concentrations ranging from 0.007-0.5 mM and 0.015- 1 mM, respectively. I obtained an EC_{50} value of 64 ±13 μM for cromolyn for T2R20, in similar range to previously reported value (Meyerhof et al., 2010).

Based on the EC_{50} values, it is evident that W164 plays a crucial role in T2R20 ligand interaction (**Table 4.2.5**). W164 mutants showed a loss-of-function effect with cromolyn and tobramycin while only W164H showed a rescued response with levofloxacin (**Figure 4.2.17**). In addition, an adjacent residue I166 showed a compound selective effect in T2R20 activation. Data showed that it has no involvement in recognizing the putative agonist of T2R20 while a rightward shift in the mutants can be observed with levofloxacin and tobramycin (**Figure 4.2.17 B & C**). This data suggests that the region of ECL2 containing residues W164 and I166 is involved in ligand recognition and activation of T2R20. Other residues in TM helices and ECL1 and 3 also play a compound specific role. For example, H65 (TM2) along with ECL1 residue T74 showed loss-of-function phenomenon in response to cromolyn (**Figure 4.2.17 A**). On the other hand, with no significant effect on tobramycin response, mutations in these residues showed no saturation or minimal effect when treated with levofloxacin. This suggests that the functional groups on the compounds might determine the selective interactions. W88 mutants showed a lower cell surface expression whose failure to properly fold or traffic might be the reason for its minimal effect. Similarly, the mutant F249 present at the TM6-ECL3 interface showed a low surface expression with no significant effect on the function. Moreover, Q265 (TM7) mutants showed subtle or no effect indicating minimal role of these residues in ligand interactions.

Molecular models suggest cromolyn and tobramycin docked in the upper part closer to the extracellular region, while levofloxacin was buried in the TM core (**Figure 4.2.16 & Figure 4.2.18**). There are some common residues, such as H65, W88 and W164 for the three ligands. Due to its binding location and the structural features of the quinoline ring, levofloxacin showed hydrophobic interactions with H65

and W88 present in TM2 and TM3 respectively, with the functional group making a salt bridge with W164 in ECL2. In addition, cromolyn and tobramycin make polar contacts with W164 and Q265 suggesting the importance of W164 in the ligand interaction, while Q265 may have a minimal role in ligand recognition as suggested from the functional data. T74 present in ECL1 is involved in a polar interaction specifically with cromolyn.

Table 4.2.5. Pharmacological characterization of the T2R20 mutants. Functional characterization of the mutants was pursued by measuring intracellular calcium mobilization in response to different concentrations of T2R20 putative agonist cromolyn and antibiotics (levofloxacin and tobramycin). Cell surface expression was determined by flow cytometry analysis. **ND** – not determined (no significant calcium mobilization detected), **NS** – no saturation (agonist concentration dependent increase in calcium mobilization not observed)

Mutant	Cromolyn			Levofloxacin			Tobramycin			Cell surface expression	
	EC_{50} (μM)	EC_{50} mutant/ EC_{50} WT	E_{max} (ΔRFU)	EC_{50} (μM)	EC_{50} mutant/ EC_{50} WT	E_{max} (ΔRFU)	EC_{50} (μM)	EC_{50} mutant/ EC_{50} WT	E_{max} (ΔRFU)	MFI	% of cells
T2R20	64.37±13	1.0	23.77±3	251.7 ± 29	1.0	25.55±3	143.31±39	1.0	24.61±1	2336±112	66.4
H65A	ND		23.36±3	NS		26.65±3	101.96±68	0.71	16.52±4	2176±203	54.3
H65W	79.27±19	1.23	20.83±2	NS		28.85±3	137.37±22	0.95	22.71±3	2619±85	65.3
T74A	120.9±26	1.88	16.23±3	229.54±41	0.91	31.09±4	191.81±42	1.34	28.08±2	2182±166	60.1
T74S	NS		15.98±2	NS		29.26±3	201.49±21	1.40	29.39±1	2311±57	59.0
W88A	ND		11.15±2	322.82±32	1.28	25.15±4	207.31±59	1.44	25.62±2	1691±118	51.0
W88H	200.2±31	3.11	21.81±4	377.5±34	1.49	26.86±5	167.93±45	1.17	21.52±2	1139±44	39.6
W164A	ND		5.3±2	451.37±39	1.79	30.07±3	295.39±44	2.06	17.11±3	2070±112	52.9
W164H	ND		6.3±3	195.59±23	0.78	21.44±4	ND		22.39±2	2640±258	64.7
I166A	56.58±18	0.88	19.23±3	ND		18.28±3	ND		18.28±2	2566±105	63.5
I166L	61.33±19	0.95	16.11±3	223.43±38	0.88	23.13±4	ND		15.93±3	2003±295	51.7
F249A	76.13±22	1.18	30.75±2	136.05±32	0.54	16.07±4	175.6±19	1.22	27.83±4	1666±128	49.2
F249Y	79.87±26	1.24	21.98±5	238.12±34	0.94	18.16±4	ND		24.28±1	1516±79	42.6
Q265A	55.38±17	0.86	18.06±2	ND		16.33±3	114.75±23	0.80	20.62±2	2064±44	56.7
Q265N	64.21±15	1.0	17.11±4	259.41±33	0.97	20.47±5	136.34±38	0.95	21.55±1	2013±446	48.8

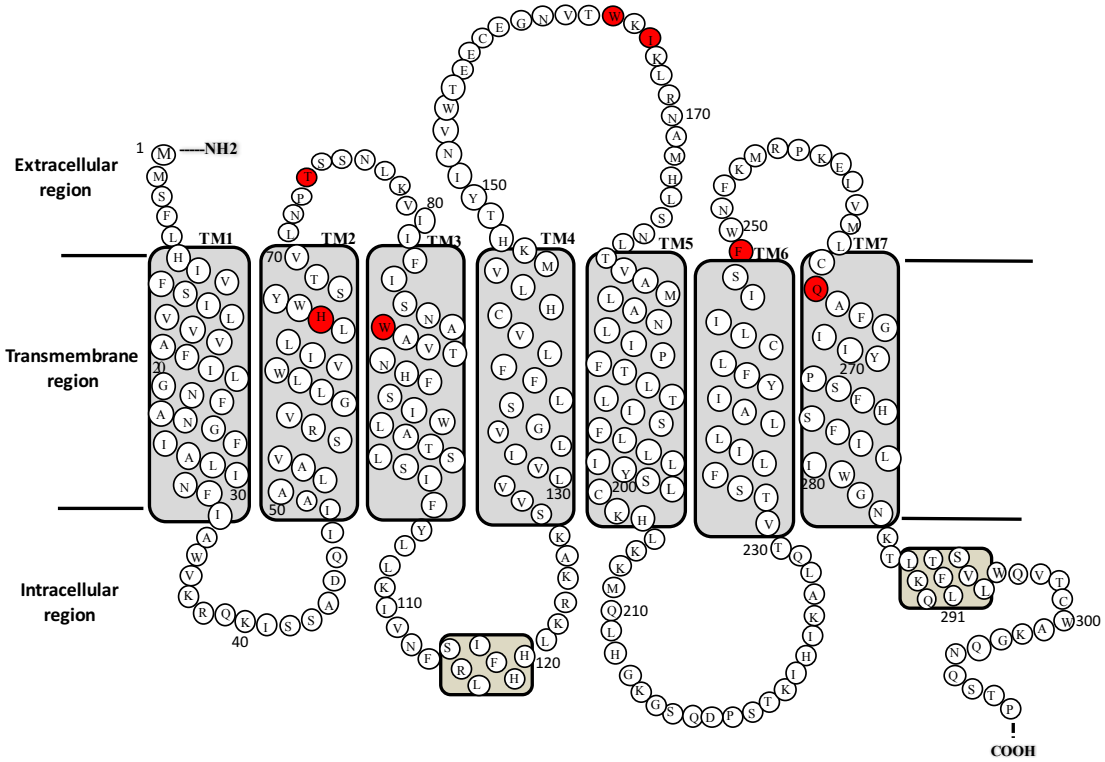

Figure 4.2.16. Two-dimensional representation of the T2R20 amino acid sequence. The N-terminus FLAG sequence is not shown in the 2D structure for simplicity. Amino acid sequence of T2R4 contains 309 residues with a very short N-terminus, seven transmembrane (TM) helices, three extracellular loops (ECLs), three intracellular loops (ICLs), and an intracellular C-terminus. The 2D structure was predicted using TMpred, TMHMM and HMMTOP servers. The amino acids predicted to be involved in ligand binding, and mutated in this study are highlighted in red for each T2R. One of these residues is present in ECL1, two of them are present in ECL2, and the rest on the extracellular side of the TM helices 2, 3 and 7 or at the interface between TM6 and ECL3.

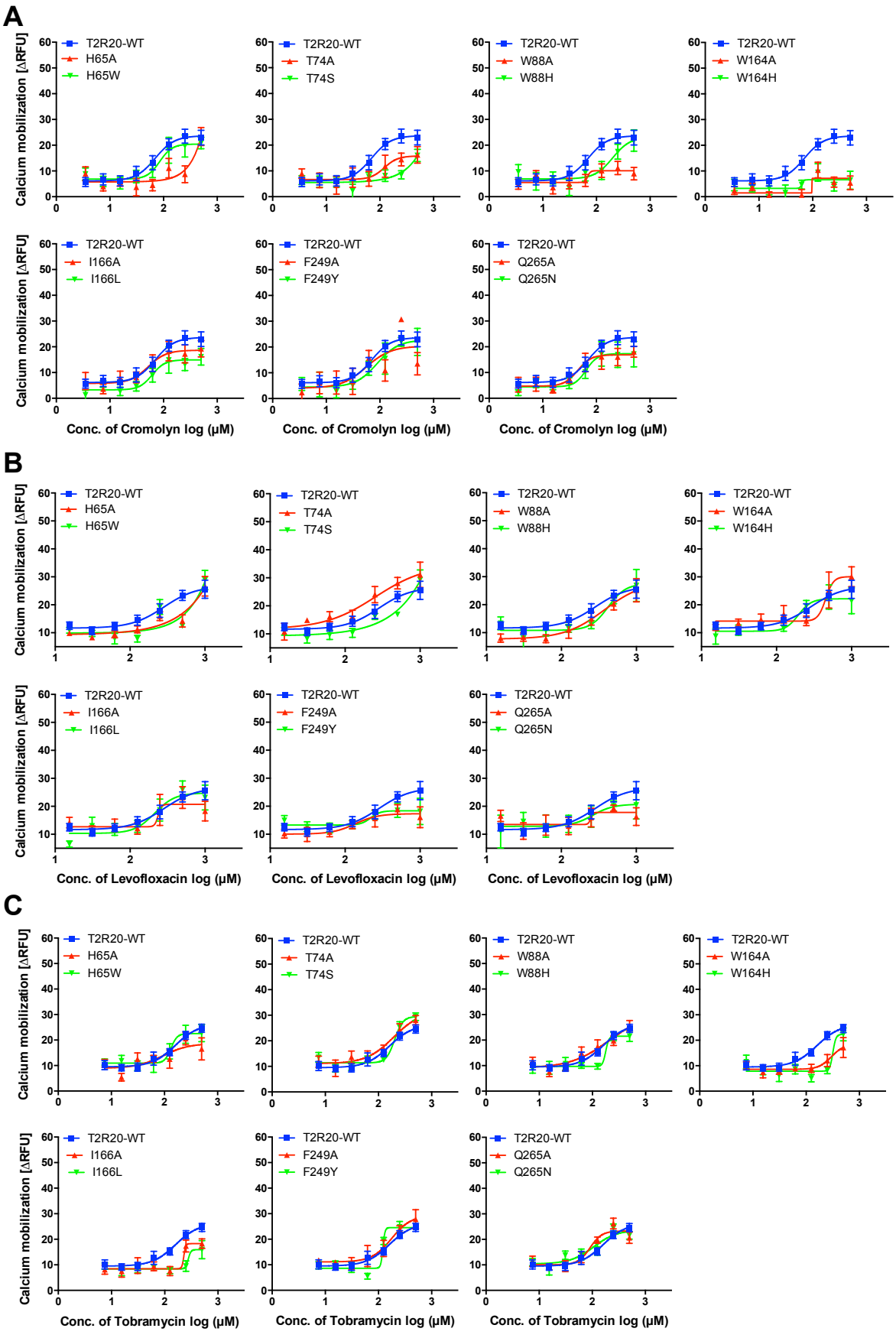
A
Calcium mobilization [ΔRFU]
T2R20-WT
H65A
H65W
T74A
T74S
W88A
W88H
W164A
W164H
I166A
I166L
F249A
F249Y
Q265A
Q265N
Conc. of Cromolyn log (μM)
B
Conc. of Levofloxacin log (μM)
C
Conc. of Tobramycin log (μM)

Figure 4.2.17. Dose response analysis of T2R20 wild type and mutants in response to cromolyn, levofloxacin and tobramycin. T2R20 WT and mutants for the following residues H65, T74, W88, W164, I166, F249 and Q265 were transiently transfected in HEK293T cells and, treated with (**A**) cromolyn at concentration range from 0.003 – 0.5 mM, (**B**) levofloxacin at concentration range from 0.015 - 1 mM and (**C**) tobramycin at concentration range from 0.015 - 1 mM. Calcium mobilization was calculated by baseline subtraction of pcDNA mock transfected cells from the WT or mutants and plotted as ΔRFU. The data represents SEM of at least three independent experiments performed in triplicate

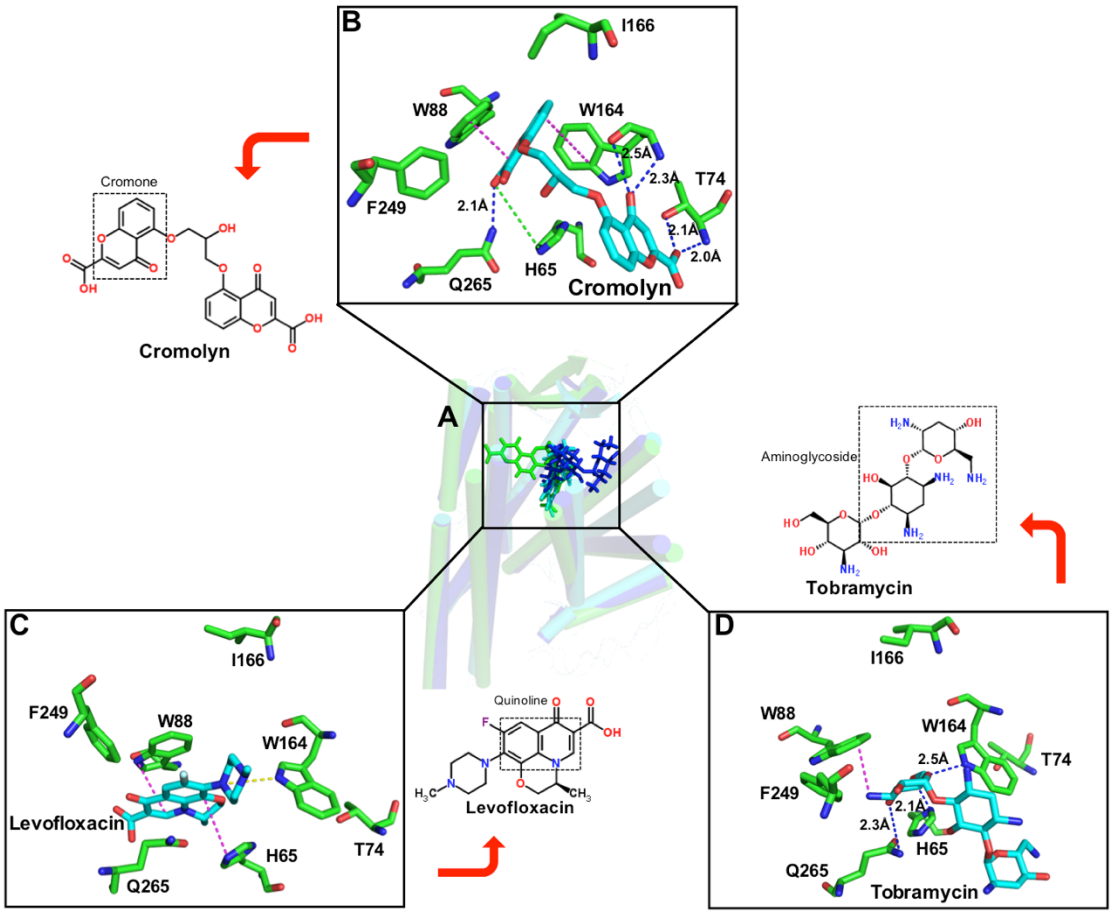

Figure 4.2.18. Model of T2R20 bound to cromolyn, levofloxacin and tobramycin. The 3D model of T2R20 docked with cromolyn (inset B), levofloxacin (inset C) and tobramycin (inset D) as described in methods. The residues (sticks) interacting with the agonists and their bonds (dashes) were highlighted. The interactions were represented in different colors (Polar bond: Blue; Salt bridge: Yellow; Pi-cation: Pink). A 2D representation of each compound is presented highlighting (dotted box) the parent structure.

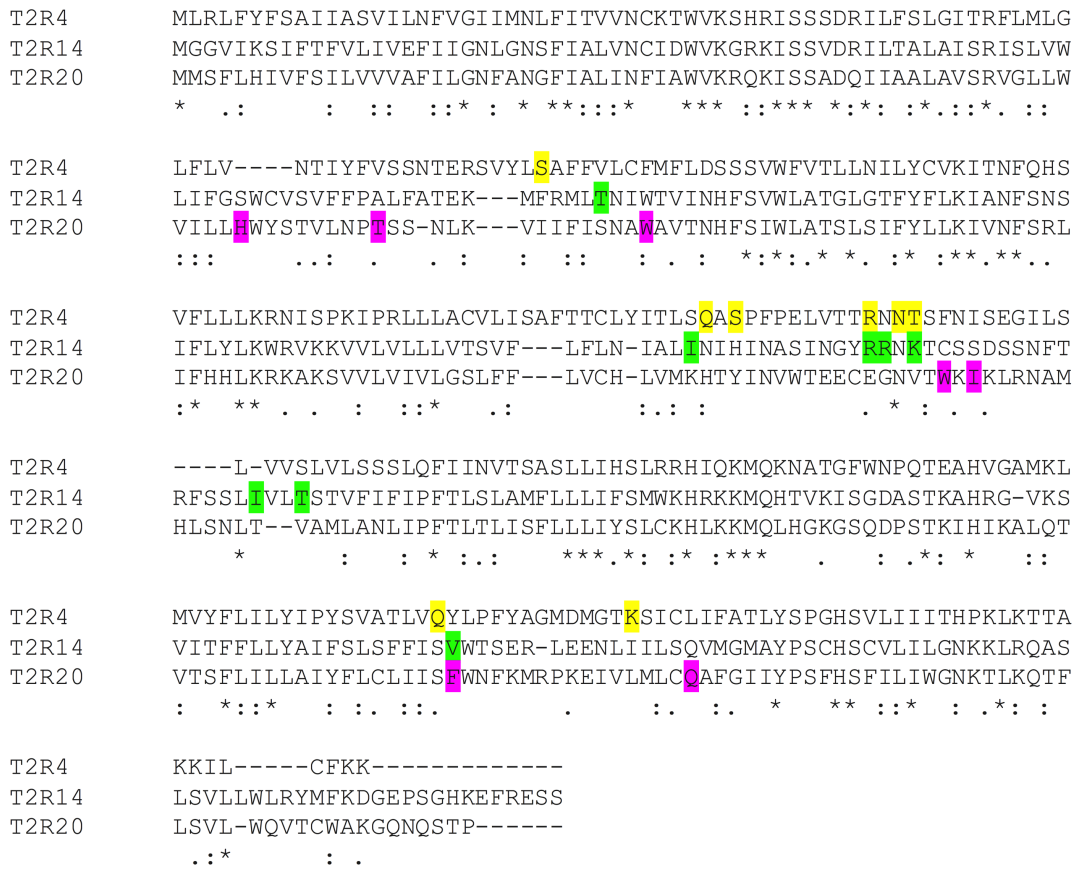

Figure 4.2.19. Multiple amino acid sequence alignment of T2R4, T2R14 and T2R20. The amino acids mutated and characterized in this study were highlighted for each receptor in a different color.

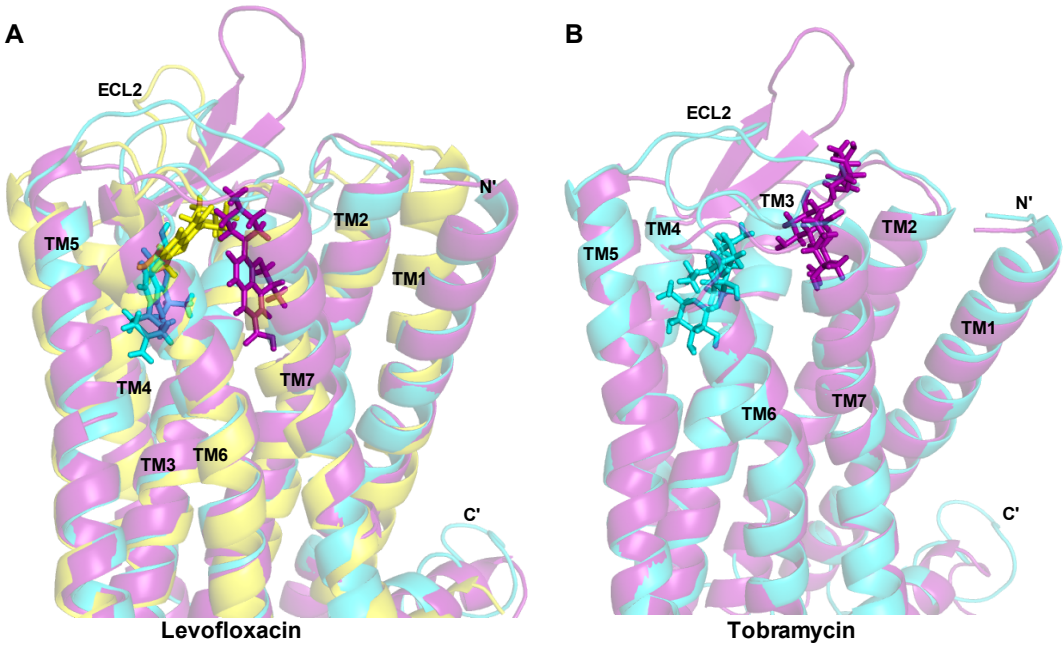

Figure 4.2.20. Comparison of binding modes of levofloxacin and tobramycin docked into the respective T2Rs. A. The superimposed homology models of T2R4 (yellow), T2R14 (cyan) and T2R20 (purple) docked with levofloxacin. **B.** T2R14 (cyan) and T2R20 (purple) docked with tobramycin. The extracellular loop 2 (ECL2) of each receptor is in the close proximity to the docked compounds. TM: transmembrane helix.

4.3 Characterize the Interaction of Acyl Homoserine Lactone (AHLs) From CF Bacteria with T2Rs

(Characterization of the Binding Sites for Bacterial Acyl Homoserine Lactones (AHLs) on Human Bitter Taste Receptors (T2Rs))

Appalaraju Jaggupilli, Nisha Singh, Vivianne Cruz De Jesus, Kangmin Duan and Prashen Chelikani

ACS Infectious Diseases, 2018; 4(7):1041-1157. (**DOI:** 10.1021/acsinfecdis.8b00094)

4.3.1 Taste sensory analysis of QSMs using E-tongue

Commensal bacteria in the human microbiome are believed to play an important role in the host physiological mechanisms such as mucosal immune system, atherosclerosis and lung homeostasis (Cohen et al., 2017, Pluznick, 2014, O'Dwyer et al., 2016). These bacteria rely on their secretory stimulants such as quorum sensing molecules (QSMs) to interact with their microenvironment as well as with the human host (Singh et al., 2000, Fuqua et al., 1994). However, the mechanism(s) by which the microbiome interacts with the host or host receptors is poorly understood. Previous studies identified few candidate T2Rs for some bacterial AHLs (Maurer et al., 2015) (Lossow et al., 2016) (Tizzano et al., 2010, Lee et al., 2012, Lee et al., 2014). However, none characterized the QSM-T2R interactions in any sensory and biochemical detail, to warrant conclusions as to their role in bacteria-host interactions.

E-tongue sensory analysis is the most commonly used method to predict the taste of unknown compounds (Uchida et al., 2003) (Singh et al., 2011a). I selected the AHLs (C4-AHL, C8-AHL and 3-oxo-C12-AHL), and other QSMs including hydroxyquinolones (HHQ and NHQ) predominantly secreted by Gram-negative bacteria, and predicted their bitterness using E-tongue as described previously in section 4.2.1 (**Table 4.3.1**). To represent a physiological microenvironment of biofilm with different QSMs present, I made a cocktail of the three AHLs (C4-AHL, C8-AHL and 3-oxo-C12-AHL), and hydroxyquinolones (HHQ and NHQ), which I refer to as the AHL load and HQ load, respectively. The predicted bitterness score was calculated against the reference compounds using standard curve as previously described (Singh et al., 2011a). From the data, I observed that individual QSMs and their cocktails (AHL and HQ loads) at 0.1 or 0.05 mM showed

Table 4.3.1. Taste sensory analysis of AHL compounds using E-tongue.

Bitter compound	Concentration (mM)	Bitterness score (in vivo) *	Bitterness predicated score (Alpha MOS)[$]
Caffeine	2.36	8.5	9.24
Quinine	0.03	9.0	8.45
Dextromethorphan	0.5	-	7.41
Diphenhydramine (DPH)	0.5	-	5.8
Cromolyn	0.5	-	4.8
AHL load	0.1	-	9.91
HQ load	0.05	-	12.48
3-oxo-C12-AHL	0.1	-	9.85
C8-AHL	0.1	-	10.06
C4-AHL	0.1	-	10.87
HHQ	0.05	-	10.62
NHQ	0.05	-	10.29

* *In vivo* score values from Alpha MOS. Astree electrochemical sensor technology technical note: T-SAS-04.2004.

[$] Bitterness scores predicted by E-tongue (Alpha MOS), experimental procedures are described
in methods.

significantly higher bitterness score (>9) than caffeine and closer to quinine. Interestingly, HHQ and NHQ showed more bitterness (>10) than the AHLs analyzed (**Table 4.3.1**).

4.3.2 Functional characterization of the treatment effects of QSMs on selected T2Rs

Further to test the ability of the QSM compounds to activate bitter taste signaling and characterize the T2R subtypes, I used HEK293T cells that stably express T2R1, T2R4, T2R14 and T2R20. The selection criteria for these T2Rs is based on my previous study that showed low, moderate and high expression in different human tissues of T2R1, T2R4 and, T2R14 and T2R20 respectively. T2R expressing stable cell lines were treated with each AHL compound at 50 μM or 100 μM or 200 μM until a significant intracellular calcium response was observed. For hydroxyquinolones, 50 μM of each compound was used to test their activity. Due to solubility limitations, the compounds could not be used beyond these concentrations in my assays. As an external control for these T2R mediated calcium mobilization assays, each T2R cell line was treated with a single concentration (EC_{50} value) of a well-characterized agonist (**Figure 4.3.1**). These agonists are DXM for T2R1, quinine for T2R4, DPH for T2R14 and cromolyn for T2R20. Statistical significance of the responses was calculated against the buffer controls. T2R1, a receptor with high (or narrow) ligand specificity and one of the least expressed T2Rs in several tissues did not show any intracellular calcium response with all the tested QSMs. T2R4 showed significant calcium mobilization upon treatment with 50 μM of C8-AHL and 100 μM of 3-oxo-C12-AHL. No significant response was measured with C4-AHL tested up to 200 μM. On the other hand, T2R14 was activated with all the three AHL compounds at 50 μM. T2R20 was activated by C8-AHL and 3-oxo-C12-AHL at higher

concentration of 200 μM and with no response to C4-AHL. Apart from AHLs, none of the hydroxyquinolones tested showed a significant response with any of the T2Rs (**Figure 4.3.1**).

4.3.3 Pharmacological characterization of the activity of AHLs at T2Rs

Although hydroxyquinolones, HHQ and NHQ showed higher bitter taste sensory profile in E-tongue analysis, they were unable to activate any of the four T2Rs significantly. Among AHLs, C4-AHL showed no activation of the tested T2Rs except for T2R14. Furthermore, in the case of T2Rs, T2R1 showed no activation with any of the tested compounds. Therefore, I focused only on T2R4, T2R14, T2R20 and C8-AHL and 3-oxo-C12-AHL in subsequent experiments. The T2Rs were treated with C8-AHL or 3-oxo-C12-AHL in a dose-dependent manner from a concentration range of 3.15 – 200 μM (**Figure 4.3.2**). An EC_{50} of 30 ±12 μM and 20 ±10 μM was obtained for C8-AHL for T2R4 and T2R14 respectively (**Figure 4.3.2 A**). C8-AHL did not activate T2R20 in a concentration dependent manner and activated it only at the highest concentration of 200 μM, which corroborates with the response obtained in the sensitization assay (**Figure 4.3.1**). Therefore, C8-AHL was excluded in the structure-function analysis with T2R20. In contrast, 3-oxo-C12-AHL activated the three tested T2Rs with EC_{50} of 41 ±13 μM, 70 ±40 μM and 58 ±13 μM for T2R4, T2R14 and T2R20 respectively (**Figure 4.3.2 B**). It is interesting to observe 3-oxo-C12-AHL, which is the predominant AHL secreted by *P. aeruginosa* in condition like CF activating many T2Rs.

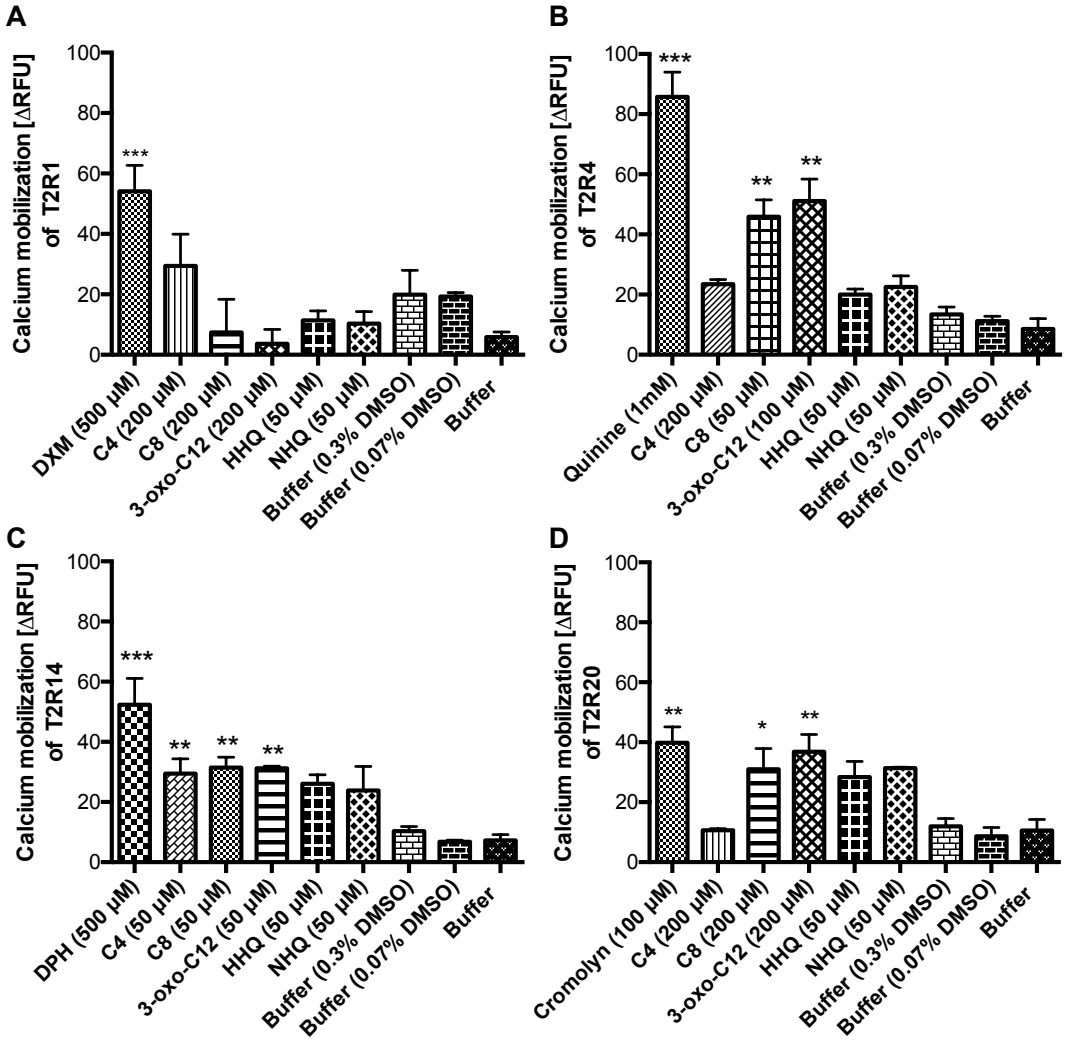

Figure 4.3.1. T2R mediated calcium mobilization in response to treatment with AHLs and QSMs. HEK293T cells stably expressing T2R1 (**A**), T2R4 (**B**), T2R14 (**C**) and T2R20 (**D**) were treated with acyl homoserine lactones (AHLs), C4-AHL, C_8-AHL and 3-oxo-C12-AHL at 50 μM, 100 μM or 200 μM and hydroxyquinolones (HHQ and NHQ) at 50 μM. Each T2R was also treated with their cognate agonist as a positive control. Buffer 1 and 2 (0.3% or 0.07% DMSO in assay buffer corresponding to 200 μM or 50 μM of the compound), and buffer 3 (assay buffer) were taken as negative controls. Calcium mobilization assay performed using Fluo-4NW dye and baseline subtraction was done with the HEK293T control cells that were represented as ΔRFU. One-way ANOVA with Tukey's multiple comparison test was performed and the significant response was calculated (*$p<0.05$; **$p<0.01$; ***$p<0.001$).

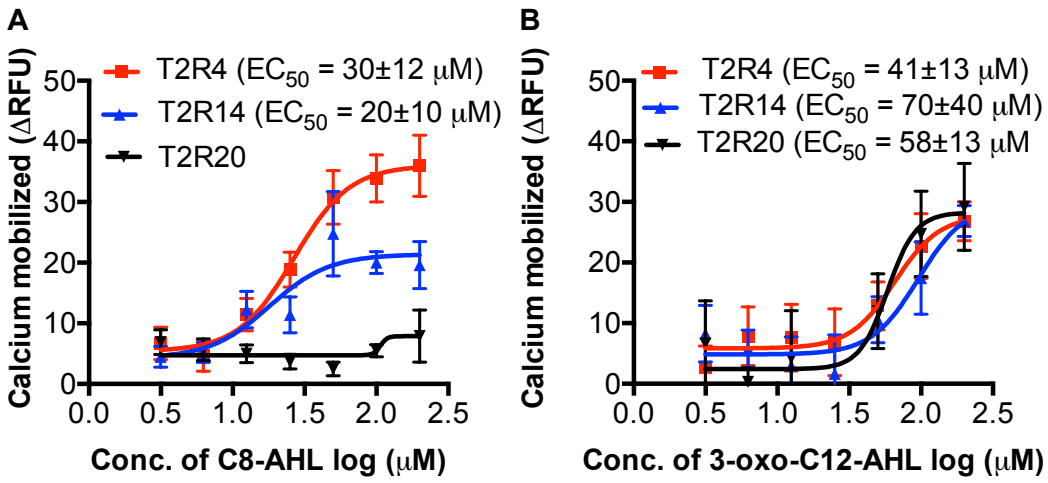

Figure 4.3.2. Dose response analysis of T2R4, T2R14 and T2R20 wild type in response to C8-AHL and 3-oxo-C12-AHL. The plasmid DNA of each T2R was transiently transfected in HEK293T cells and treated with C8-AHL and 3-oxo-C12-AHL at concentration range from 3.15 – 200 μM. Calcium mobilization assay performed using Fluo-4NW dye and baseline subtraction of pcDNA mock transfected cells from the WT or mutants and plotted as ΔRFU. The data represents SEM of at least three independent experiments performed in triplicate.

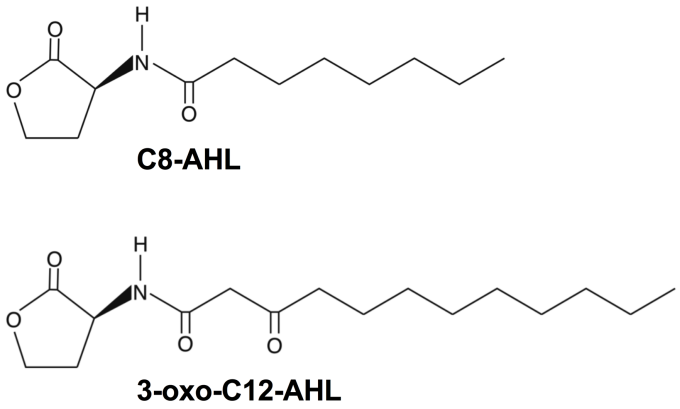

Figure 4.3.3. 2D representation of acyl homoserine lactones (AHLs). The compounds shown are the quorum sensing molecules C8-AHL and 3-oxo-C12-AHL secreted by Gram-negative bacteria.

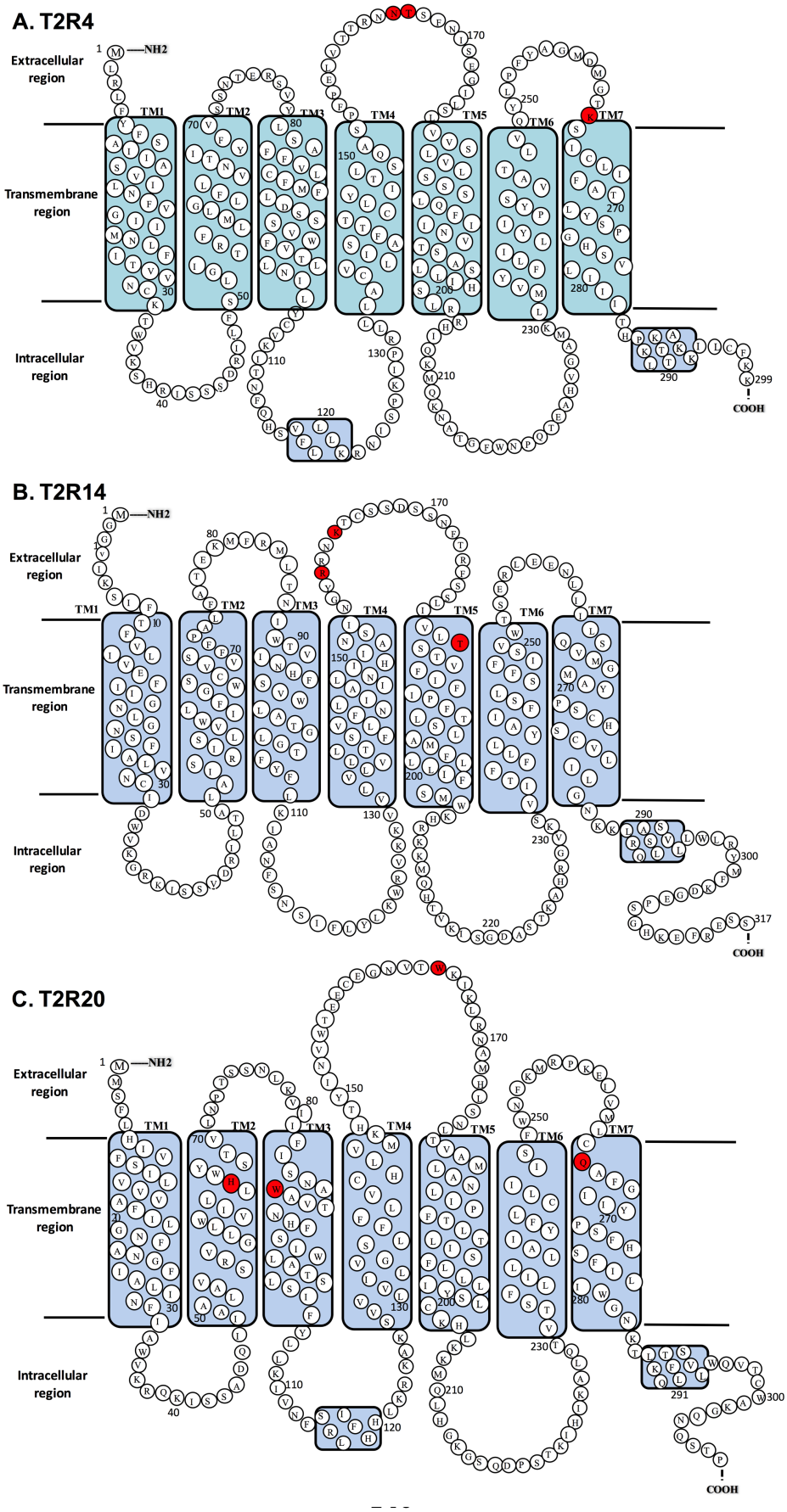
A. T2R4
Extracellular region
Transmembrane region
Intracellular region
TM1
TM2
TM3
TM4
TM5
TM6
TM7
NH2
COOH
B. T2R14
Extracellular region
Transmembrane region
Intracellular region
TM1
TM2
TM3
TM4
TM5
TM6
TM7
NH2
COOH
C. T2R20
Extracellular region
Transmembrane region
Intracellular region
TM1
TM2
TM3
TM4
TM5
TM6
TM7
NH2
COOH

Figure 4.3.4. Two-dimensional representation of the T2R4, T2R14 and T2R20 amino acid sequence. The N-terminus FLAG sequence is not shown in the 2D structure for simplicity. Amino acid sequence of (**A**) T2R4 contains 299 residues, (**B**) T2R14 contains 317 residues and (**C**) T2R20 contains 309 residues. T2Rs form a very short N-terminus, seven transmembrane (TM) helices, three extracellular loops (ECLs), three intracellular loops (ICLs), and an intracellular C-terminus. The 2D structure was predicted using TMpred, TMHMM and HMMTOP servers. The amino acids predicted to be involved in AHL binding, and mutated in this study are highlighted in red for each T2R.

4.3.4 Prediction of AHLs binding site in T2R4, T2R14 and T2R20

The AHLs, C8-AHL and 3-oxo-C12-AHL (**Figure 4.3.3**) along with the known T2R agonists were docked to previously validated molecular models of T2R4, T2R14 and T2R20 using Libdock algorithm in Discovery Studio modeling suite. Using the analyzed docked poses tool, the most favourable residues within 4Å region interacting with the docked compounds were identified in each receptor. Each selected amino acid was replaced with two types of residues, an alanine, which is expected to have minimal effect on the receptor folding but predicts the function of the mutated residue and a conservative substitution, such as lysine with arginine, with the expectation that the phenotype will be similar to wild type T2R. The amino acids N165 and T166 on extracellular loop 2 (ECL2) and K262 on the interface of ECL3-TM7 were selected in T2R4 (**Figure 4.3.4 A**). The following 6 mutations were made N165A, N165Q, T166A, T166S, K262A and K262R. For T2R14, R160, K163 on ECL2 and T182 in TM5 were selected (**Figure 4.3.4 B**) and the following 6 mutations R160A, R160K, K163A, K163R, T182A and T182S were made. Similarly, for T2R20: H65 (TM2), W88 (TM3), W164 (ECL2) and Q265 (TM7) were selected (**Figure 4.3.4 C**) and following mutations H65A, H65W, W88A, W88H, W164A, W164H, Q265A and Q265N were made.

4.3.5 Functional characterization of C8-AHL binding sites in T2Rs

C8-AHL is one of the QSMs produced by Gram-negative bacteria such as *Burkholderia* species (Chen et al., 2013). C8-AHL showed a dose-dependent activation of T2R4 and T2R14, so I focused on these two T2Rs to characterize their binding site for C8-AHL. Based on the docking analysis FLAG-tagged wild-type (WT) T2Rs and the selected mutants were transiently transfected into the HEK293T

cells along with control pcDNA (mock transfection). The WT and mutants were treated with C8-AHL at a concentration range from 3.15 – 200 μM in the cell based calcium mobilization assay (**Table 4.3.2 A**). The EC_{50} value obtained for WT-T2R4 was 30.13±12 μM. The mutations in N165 and T166 failed to show any significant dose-response while both the mutants of K262 caused an increase in EC_{50} or loss of potency for C8-AHL. All the mutants showed reduced E_{max} value suggesting loss of signaling efficacy (**Figure 4.3.5 A**). The interactions using the T2R4 agonist quinine also showed a similar pattern with N165 and T166 (**Figure 4.3.7 A**). In the case of WT-T2R14, the EC_{50} value obtained was 19.65±10 μM and this potency was lost substantially with the mutants R160, K163 and T182 (**Table 4.3.2 B, Figure 4.3.5 B**). Interestingly, mutation of R160 had no effect on agonist DPH induced signaling on T2R14 (**Figure 4.3.7 B**). This suggests that R160 in T2R14 might be important for recognizing C8-AHL. There is a minor loss of signaling efficacy for C8-AHL for the T182 mutants, with the T182S complementary mutation rescuing the E_{max} value similar to T2R14-WT levels (**Figure 4.3.5 B**). T182 mutants exhibit similar responses to the T2R14 agonist DPH (**Figure 4.3.7 B**), suggesting that hydrophilic or H-bonding is important for the amino acid at position 182 in the ligand interaction in T2R14.

The molecular modeling analysis of the C8-AHL bound T2Rs provide more insight into the binding interactions (**Figure 4.3.8**, right panel). The models predict that the functional homoserine lactone group plays critical role in interacting with the T2R residues. While the acyl side chain is buried in the TM core, the polar head group interacts with the residues in ECL2. The T2R4 residues N165 and T166 are involved in a backbone polar interactions with the lactone ring in C8-AHL. The side chain of K262 is involved in a polar bond of the ketone group at the bond between lactone and acyl chain (**Figure 4.3.8**, right panel). As suggested by the functional data, both N165

and T166 are important for the interactions with C8-AHL and activate the receptor. In T2R14, both the ECL2 residues R160 and K163 are involved in polar interactions with the lactone ring and the ketone group respectively. However, in the case of DPH, R160 is involved in a weak pi-electron interaction (data not shown), which could be the reason for the mutants showing no effect. Although the functional data indicate the importance of hydrophilic group at position 182, my molecular model did not show any polar interaction with C8-AHL since the acyl chain is in the proximity of T182. As T182 is present at the interface of the TM6 and highly flexible ECL2, it is difficult to predict its orientation and function from my model. It is also feasible that the hydroxyl group at this position might be important for inter-helical interaction and rearrangement of T2R14 structure upon AHL binding rather than having a direct contact.

4.3.6 Functional characterization of 3-oxo-C12-AHL binding sites in T2Rs

3-oxo-C12-AHL is a commonly secreted QSM by Gram-negative bacteria especially *P. aeruginosa*. It plays a crucial role in the regulation of virulence associated genes in *P. aeruginosa* and influences the host innate immune responses. It is the only QSM in my assay system that was able to activate all the major T2Rs tested. The site-directed mutagenesis and docking analysis were performed in a similar pattern as with C8-AHL. The WT-T2Rs and mutants were treated with 3-oxo-C12-AHL at a concentration range from 3.15 – 200 μM in the cell based calcium mobilization assay (**Table 4.3.2**). In T2R4, the mutations of N165 and T166 to alanine or a complementary residue caused a loss of potency for 3-oxo-C12-AHL as illustrated by an increase in EC_{50} (**Table 4.3.2**). N165A mutant showed a significant rightward shift, while the conserved

Table 4.3.2. Pharmacological characterization of the T2R mutants. Functional characterization of the mutants was pursued by measuring intracellular calcium mobilization in response to different concentrations of C8-AHL and 3-oxo-C12-AHL for T2R4 (**A**) and T2R14 (**B**), and 3-oxo-C12-AHL for T2R20 (**C**). **ND** – not determined. * indicates reduced cell surface expression of the mutant(s) up to 30 – 50 % of their respective wild type T2R, and as determined by flow cytometry analysis using anti-FLAG antibody described previously in the methods section.

A	**C8-AHL**		**3-oxo-C12-AHL**	
	EC_{50} (μM)	**E_{max} (ΔRFU)**	**EC_{50} (μM)**	**E_{max} (ΔRFU)**
T2R4	30.13±12	37.81±5.0	40.9±13	26.89±3.2
N165A*	ND	15.32±4.1	156.9±41	20.33±2.6
N165Q*	ND	22.43±3.3	53.13±21	19.9±2.2
T166A	ND	12.28±2.9	44.48±35	15.3±4.8
T166S	ND	9.68±1.5	62.23±29	16.0±6.4
K262A	37.53±22	14.41±1.7	ND	7.3±3.5
K262R	43.56±18	13.40±1.7	ND	5.4±3.9

B	**C8-AHL**		**3-oxo-C12-AHL**	
	EC_{50} (μM)	**E_{max} (ΔRFU)**	**EC_{50} (μM)**	**E_{max} (ΔRFU)**
T2R14	19.65±10	20.33±3.8	69.54±40	29.59±5.1
R160A	ND	8.18±3.1	ND	11.33±3.3
R160K	ND	13.17±5.8	ND	2.39±3.6
K163A	ND	5.75±1.3	ND	2.27±4.4
K163R	ND	8.11±2.4	62.12±33	12.51±4.6
T182A	31.98±13	11.16±1.2	ND	6.6±2.9
T182S	ND	14.25±1.3	74.37±29	24.82±4.3

C	**3-oxo-C12-AHL**	
	EC_{50} (μM)	**E_{max} (ΔRFU)**
T2R20	58.31±12	24.31±4.1
H65A	ND	8.06±3.6
H65W	34.83±22	11.98±2.9
W88A*	ND	4.04±3.2
W88H*	ND	8.11±2.8
W164A	90.76±37	21.10±3.2
W164H	NS	23.03±4.6
Q265A	ND	6.15±2.9
Q265N	ND	7.2±3.7

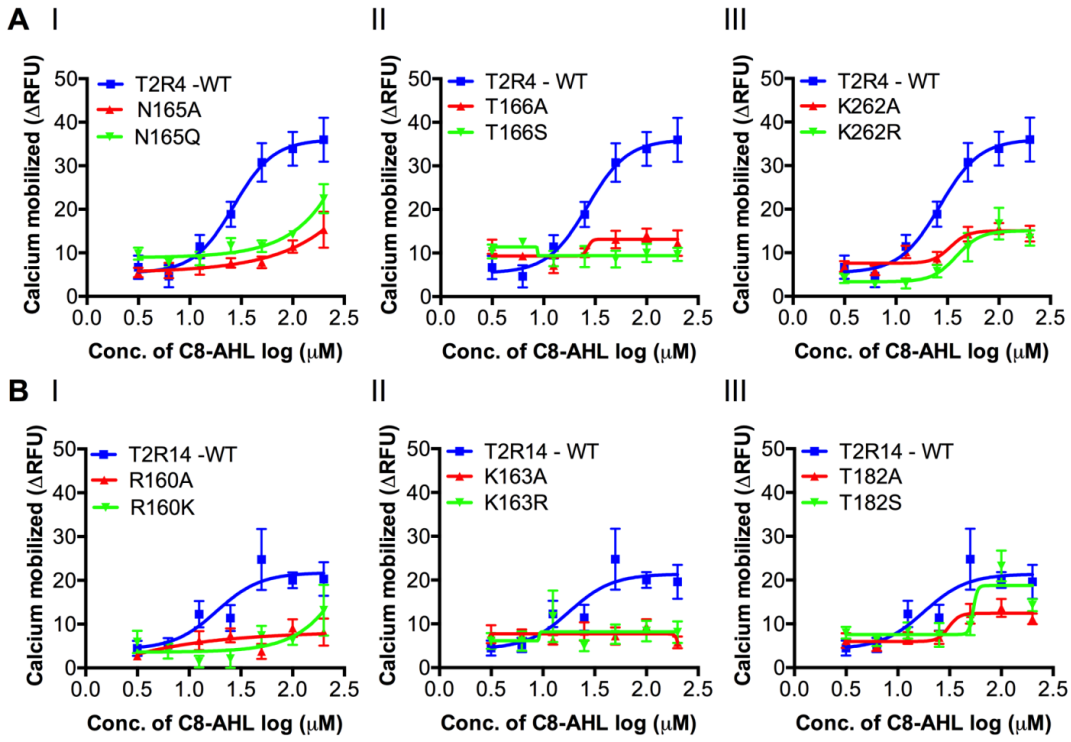

Figure 4.3.5. Dose response analysis of T2R4 and T2R14 wild type and mutants in response to C8-AHL. A. T2R4 and **B.** T2R14 WT and mutants were transiently transfected in HEK293T cells and treated with C8-AHL at concentration range from 3.15 – 200 μM. Calcium mobilization assay performed using Fluo-4NW dye and baseline subtraction of pcDNA mock transfected cells from the WT or mutants and plotted as ΔRFU. The data represents SEM of at least three independent experiments performed in triplicate.

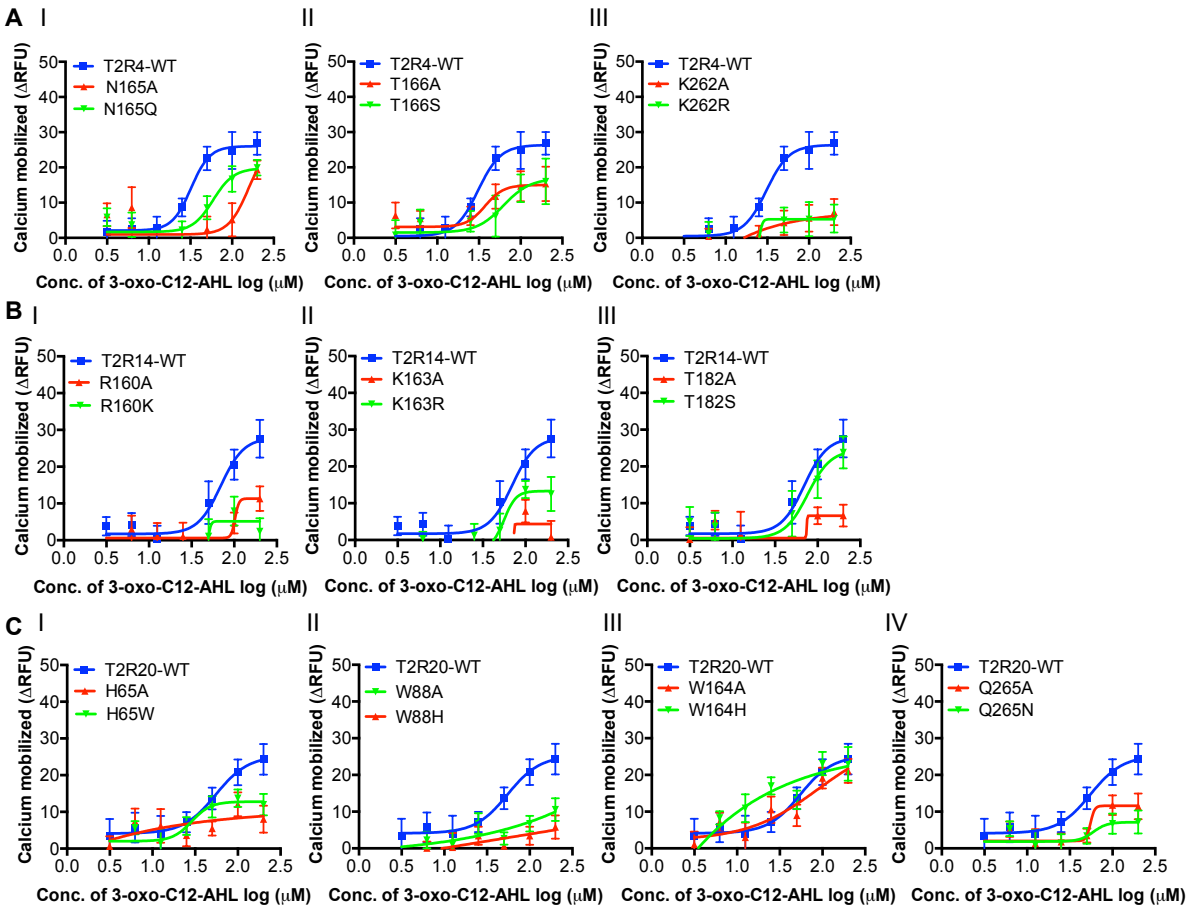

Figure 4.3.6. Dose response analysis of T2R4, T2R14 and T2R20 wild type and mutants in response to 3-oxo-C12-AHL. A. T2R4 and **B.** T2R14 WT and mutants were transiently transfected in HEK293T cells and treated with 3-oxo-C12-AHL at concentration range from 3.15 – 200 μM. Calcium mobilization assay performed using Fluo-4NW dye and baseline subtraction of pcDNA mock transfected cells from the WT or mutants and plotted as ΔRFU. The data represents SEM of at least three independent experiments performed in triplicate.

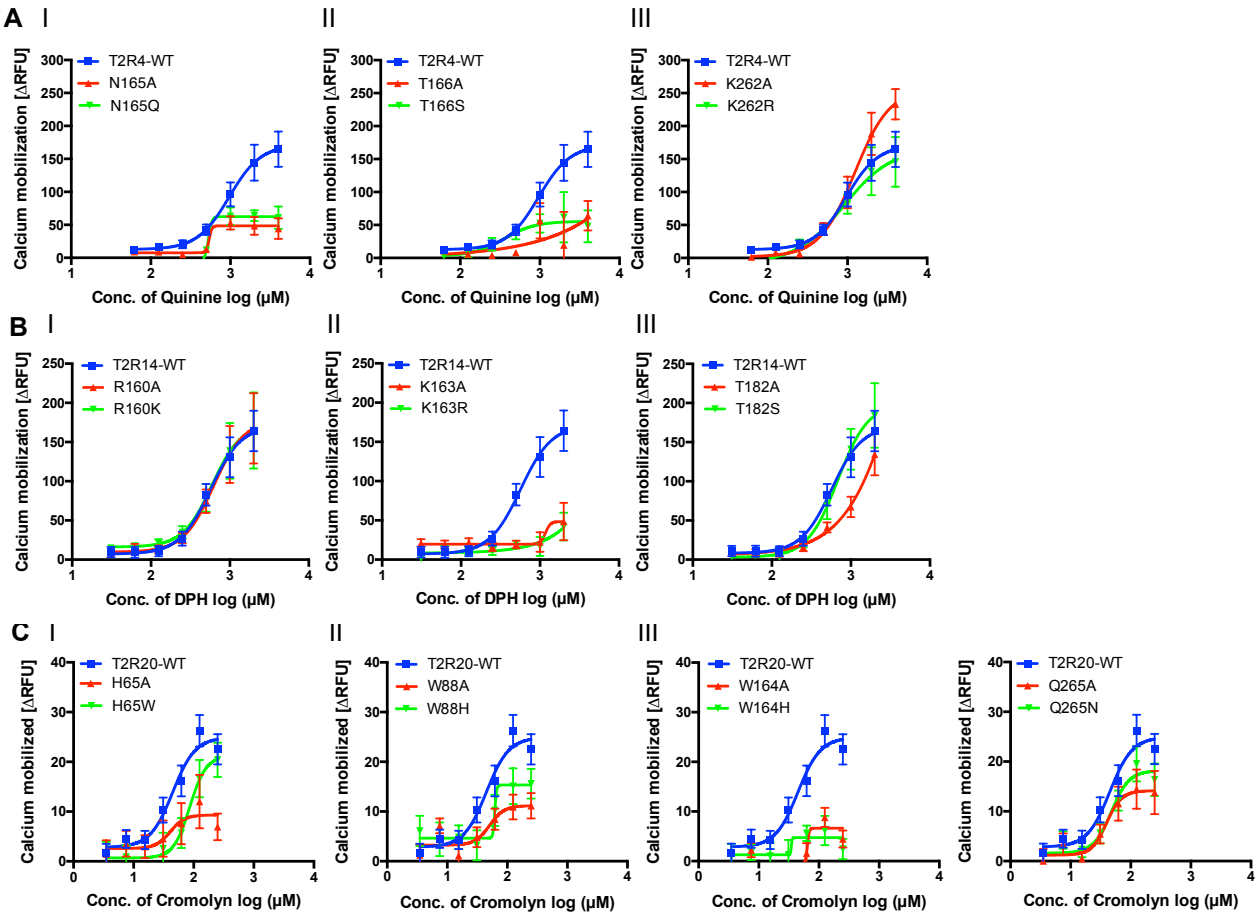

Figure 4.3.7. Functional analysis of T2R4, T2R14 and T2R20 wild type and mutants with putative agonists. T2Rs WT and mutants were transiently transfected in HEK293T cells and treated with known specific agonist. (**A**) T2R4 WT and mutants treated with quinine at concentration range from 0.07 - 4 mM (**B**) T2R14 WT and mutants treated with diphenhydramine (DPH) at concentration range from 0.03 - 2 mM. (**C**) T2R20 WT and mutants treated with cromolyn at concentration range from 0.003 – 0.5 mM. Calcium mobilization was calculated by baseline subtraction of pcDNA mock transfected cells from the WT or mutants and plotted as ΔRFU. The data represents SEM of at least two independent experiments performed in triplicate. The EC_{50} values were calculated for wild type T2R4 with quinine showing 960 ± 45 μM, T2R14 with DPH showing 566 ± 72 μM and T2R20 with cromolyn showing 45 ± 12 μM.

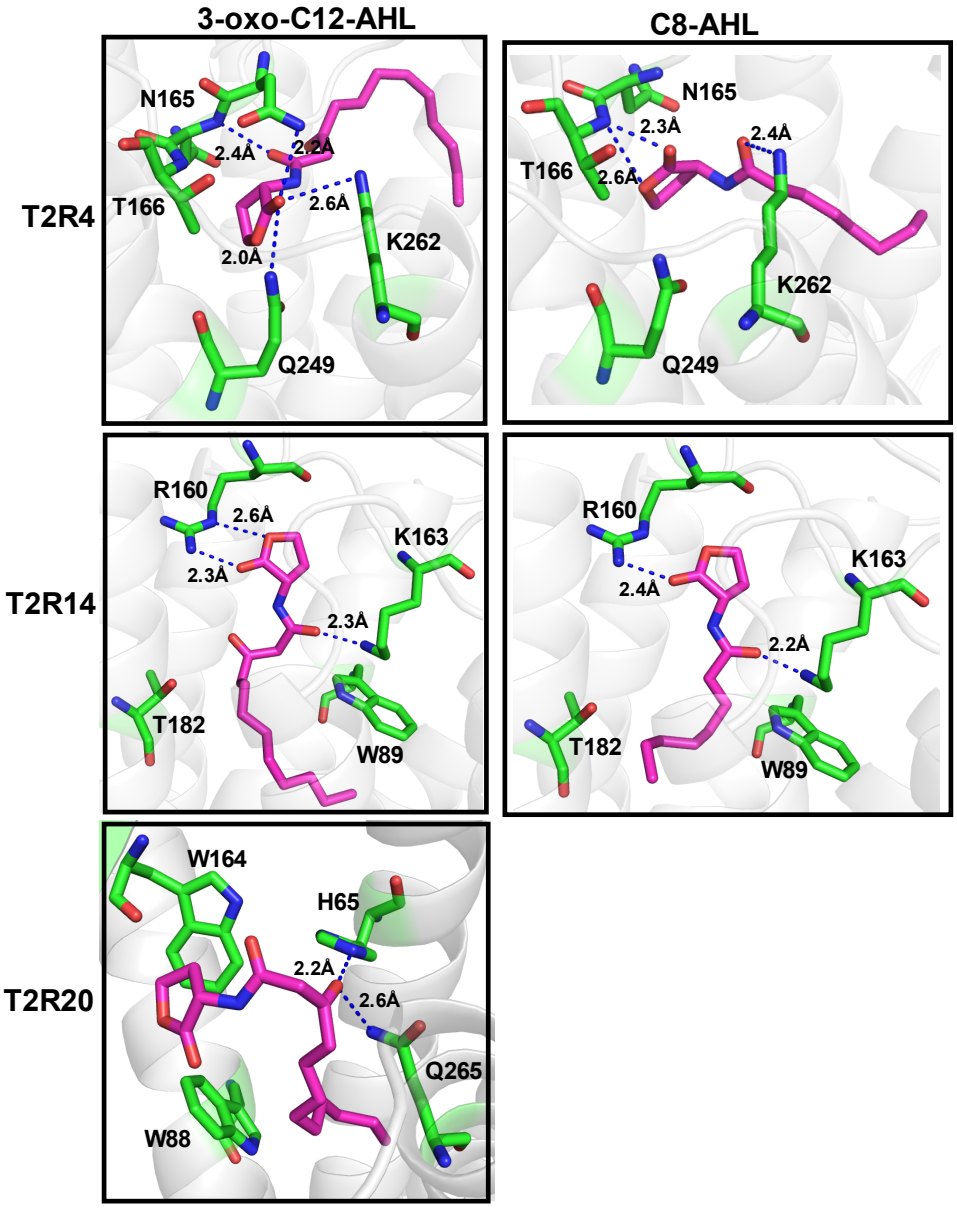

Figure 4.3.8. Amino acid interactions of T2R4, T2R14 and T2R20 docked with AHLs. The 3D model of T2R4 (top panel) and T2R14 (middle panel) docked with 3-oxo-C12-AHL and C8-AHL, and T2R20 (bottom panel) docked with 3-oxo-C12-AHL as described in methods. The residues (sticks) interacting with AHLs and polar bonds (blue dashes) were highlighted.

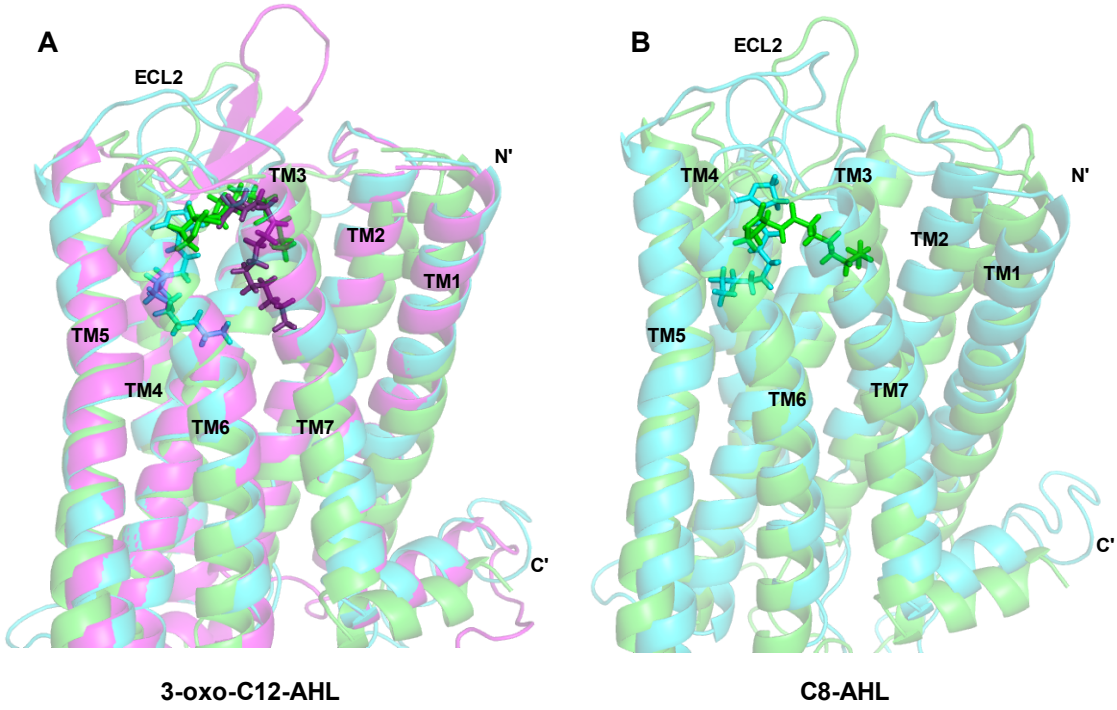

Figure 4.3.9. Comparison of binding modes of 3-oxo-C12-AHL and C8-AHL docked into the respective T2Rs. A. The superimposed homology models of T2R4 (green), T2R14 (cyan) and T2R20 (magenta) docked with 3-oxo-C12-AHL. **B.** T2R4 (green) and T2R14 (cyan) docked with C8-AHL. The extracellular loop 2 (ECL2) of each receptor and transmembrane helices (TM) were labeled accordingly.

mutant N165Q slightly rescued the function (**Figure 4.3.6 A**). Both mutations of K262 fail to show any significant dose-response (**Figure 4.3.6 A**). In comparison to C8-AHL responses, N165 showed a universal loss of function while T166 and K262 showed compound specific interactions (**Table 4.3.2 A**). In T2R14, the R160 mutants did not show a dose-dependent response to 3-oxo-C12-AHL (**Figure 4.3.6 B**). Strikingly, for K163 and T182 residues the alanine substitutions at these positions showed significant loss of potency which was rescued by the conservative substitutions K163R and T182S to WT-T2R14 levels (**Table 4.3.2 B**). This rescue in function of T2R14 was not observed for C8-AHL suggesting AHL specificity of the amino acids K163 and T182. Interestingly, the R160 mutants showed significant loss of potency to both AHLs, while they showed no loss for DPH binding suggesting that R160 might be important for AHL binding.

The WT-T2R20 showed an EC_{50} value of 58.31±12 μM for 3-oxo-C12-AHL (**Table 4.3.2 C**). The W88 and Q265 mutants failed to show a significant dose-response, while the H65A showed loss of function with the compensatory H65W mutation rescuing the functional response. The W164 mutants showed small loss of potency (EC_{50}) but had signaling efficacy (E_{max}) similar to WT-T2R20 (**Table 4.3.2 C** and **Figure 4.3.6 C**). In contrast, mutation of W164 resulted in significant loss of function for the T2R20 agonist, cromolyn (**Figure 4.3.7 C**). The results suggest the ECL2 residue W164 as a crucial amino acid while H65, W88 and Q265 are important for 3-oxo-C12-AHL binding in T2R20.

The docking analysis of 3-oxo-C12-AHL in T2R4, T2R14 and T2R20 provided insights into the mode of interactions with this compound (**Figure 4.3.8**, left panel). 3-oxo-C12-AHL is different from C8-AHL in having an extra keto group and longer acyl chain (**Figure 4.3.3**). Although the pose orientation is different in the

binding sites of T2Rs, the polar homoserine lactone directs these interactions (**Figure 4.3.9 A**). In T2R4, N165 and T166 in ECL2 are involved in the polar interactions with keto group whereas K262 is involved with the lactone ring which is opposite in the case of C8-AHL. Considering the functional data, this indicates the essential role of N165 and T166 in binding ligands. K262 presents a compound specific interaction towards 3-oxo-C12-AHL when compared to C8-AHL. R160 and K163 in T2R14 showed similar interactions with both the compounds tested and seems to be important in ligand binding. R160 is involved in stronger interactions with 3-oxo-C12-AHL while with DPH it forms a weak hydrophobic interaction (data not shown). In T2R20, the ECL2 residue W164 might be involved in hydrophobic interactions and the TM residues are crucial in polar interactions with 3-oxo-C12-AHL. H65 and Q265 are involved in the polar interactions with the extra keto group in this AHL. The importance of these residues for 3-oxo-C12-AHL is also evident from the functional data where the mutants showed no response.

4.3.7 Competitive inhibition of AHLs response with T2R4

As it is known that BCML is an inverse agonist and a potent blocker of T2R4, I studied the BCML antagonistic effect on C8-AHL and 3-oxo-C12-AHL responses at T2R4. The IC_{50} value of BCML against quinine is 60 nM at T2R4 (Pydi et al., 2014c). I treated the T2R4 stable cells with quinine (1mM) as a positive control, C8-AHL (50 µl) and 3-oxo-C12-AHL (100 µl) in presence or absence of BCML (60 nM). The concentrations of AHLs used here was based on the results obtained in section 4.3.2 (**Figure 4.3.1).** BCML exhibited a significant inhibition of both C8-AHL and 3-oxo-C12-AHL responses at T2R4 (**Figure 4.3.10**). The results indicate the potentiality of BCML in inhibiting the T2R4 agonists.

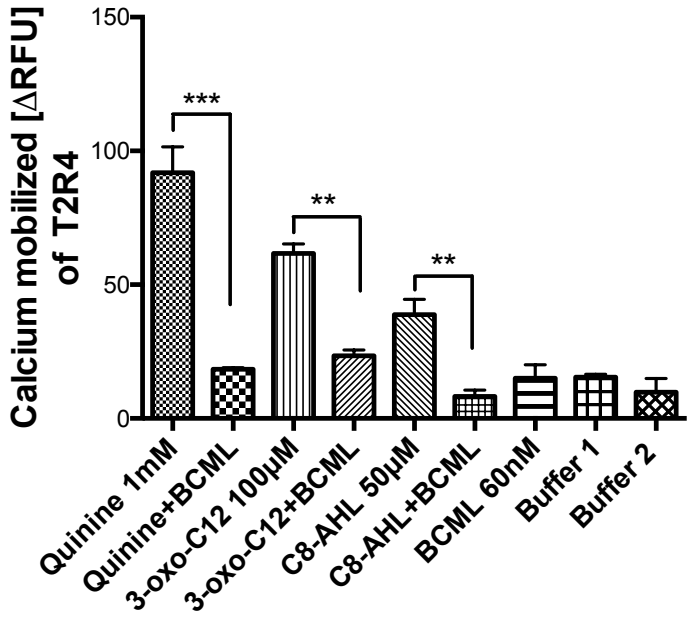

Figure 4.3.10. Competition binding assay between selected bitter agonists and BCML with T2R4. HEK293T cells stably expressing T2R4 were treated with quinine (1mM), 3-oxo-C_{12}-AHL (100 μM) and 3-oxo-C8-AHL (50 μM), in presence or absence of BCML (60 nM). Due to the precipitation issues at higher concentrations in competitive binding assay, the maximum concentration of AHLs used was 100 μM. Calcium mobilized was calculated as relative fluorescence unit (ΔRFU) after subtracting the baseline values from HEK293T cells. Buffer 1 (0.3% DMSO in assay buffer) and buffer 2 (assay buffer) were used as negative controls. The data represents two independent experiments performed in triplicates. One-way ANOVA with Tukey's post hoc test was done to calculate the significant inhibition (**$p<0.01$; (***$p<0.001$).

4.4 Discovery of Novel Bitter Ligands and Their Mechanism of Action on T2R4

(**Abscisic Acid Acts as a Blocker of the Bitter Taste G Protein-Coupled Receptor T2R4**)

Sai Prasd Pydi, **Appalaraju Jaggupilli**, Ken M, Nelson, Suzanne R. Abrams, Rajinder P. Bhullar, Michele C. Loewen, Prashen Chelikani.

Biochemistry. 54(16):2622-31

4.4.1 Nature of antagonism of abscisic acid (ABA)

Given that there are thousands of T2R agonists available and very few properly characterized antagonists are known, it is necessary to identify novel bitter blockers. Although few plant derived compounds are known to block T2R subtypes, no studies are available on the activity of phytohormones on T2Rs. In the process of screening for the compounds that are similar to quinine, a plant hormone abscisic acid (ABA) was identified as candidate T2R4 ligand. Subsequent experiments in our lab characterized ABA as an antagonist with IC_{50} value of 34.4±1.1 μM against quinine at T2R4 (Pydi et al., 2015). Therefore, to determine the nature of ABA antagonism in T2R4 against quinine, I performed Schild regression analysis which is a gold standard method in pharmacology. T2R4/Gα16/44 stable cells were used to understand the nature of antagonism of ABA. When the cells were treated with increasing concentration of quinine (0.07-5 mM), this increased the intracellular calcium mobilization. While in the presence of constant concentrations of ABA (3, 30, 100 and 300 μM) the concentration response curves were shifted towards right without affecting the maximum response (**Figure 4.4.1**). The effects of ABA are surmountable at high concentrations of quinine. However, this alone would not conclude the nature of ABA antagonism. When these data were analyzed, the Schild regression generated a slope of 0.46 ±0.02 with 95% CI (0.33-0.59). The determined pA_2 value is 1.99 based on the intercept on the abscissa (**Figure 4.4.1,** inset).

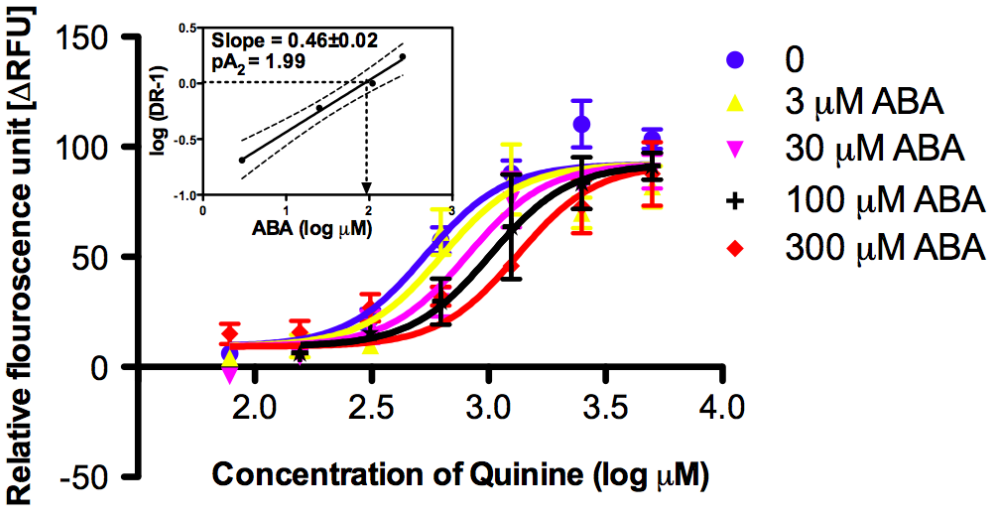

Figure 4.4.1. Schild regression analysis of ABA antagonism to quinine in T2R4. The concentration dependence of the increase in intracellular calcium mobilization in response to quinine at different concentrations (0.07-5 mM) was compared in the absence (blue) and presence of 3 μM (yellow), 30 μM (magenta), 100 μM (black) 300 μM (red) of ABA. The concentration response curves were shifted towards right with increasing concentrations of ABA. In the inset, the dose ratio minus one (DR-1) was obtained from the EC_{50} value of each curve and plotted against antagonist concentration in a log scale to calculate Schild linear regression. The Schild plot generated a slope of 0.46 ±0.02 with 95% CI (0.33-0.59) indicated in broken lines. The pA_2 value was determined as 1.99 indicated as intercept with abscissa in dotted line. Data were collected from at least five independent experiments with each data point in triplicate. EC_{50} values and regression analysis was calculated using Graphpad Prism 5.0 software (Pydi et al., 2015).

4.4.2 Activity of (+) ABA isomer on T2R4

A racemic mixture of (±) ABA was used in determining the antagonism in section 4.4.1. As the isomers of chemical compounds are known to exhibit different activities, it is important to study the activity of ABA isomers (Chhabra et al., 2013). Since (-) ABA is not commercially available, only the biologically active isomer (+) ABA was considered (**Figure 4.4.2)**. I tested (+) ABA on T2R4/Gα16/44 stable cells in a dose dependent manner (0.12-4 mM). (±) ABA and quinine were used as experimental controls. Quinine activated the T2R4 in a dose dependent manner with an EC50 value of 731±122 μM, while both (+) ABA and (±) ABA did not activate T2R4. (**Figure 4.4.3 A**). Further the cells were treated with highest concentration (4 mM) of different T2R4 ligands in different combinations to analyze the sensitization. (+) ABA did not show any response on calcium mobilization through T2R4 (**Figure 4.4.3 B**). The result indicates that isomers of ABA do not induce T2R4 activity. The sensitization assay showed that ABA isomers inhibit the quinine activity. The known T2R4 blocker γ-amino butyric acid (GABA) and Nα, Nα, Biscarboxymethyl lysine (BCML) were used as controls.

4.4.3. Advanced glycation end-products as novel T2R4 blockers

Previous studies on amino acid derivatives from our lab reported that Nα, Nα, Biscarboxymethyl lysine (BCML) is a potent antagonist of T2R4 with IC_{50} value 60 nM against quinine (Pydi et al., 2014c). BCML is a synthetic derivative of advanced glycation endproduct (AGE), Nε-carboxymethyl lysine (CML). Thus, 23 AGE compounds were selected from different groups along with quinine and BCML as

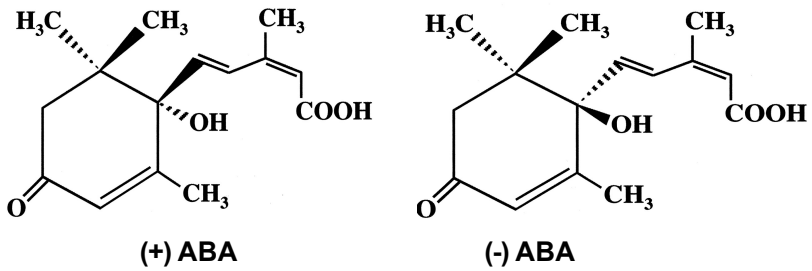

Figure 4.4.2. 2D structures of Cis (+) and trans (-) isomers of abscisic acid

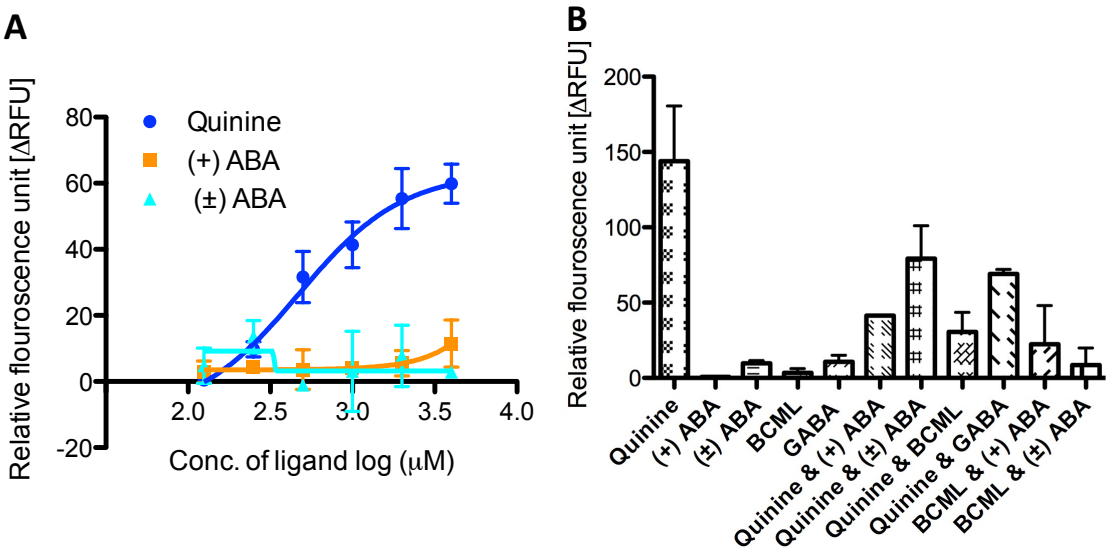

Figure 4.4.3. T2R4 response to different ligands. A. Dose dependent calcium mobilization of T2R4 in response to Quinine, (+) ABA and (±) ABA. **B.** Sensitization assay of T2R4 calcium mobilization in response to different ligands at high concentration (4 mM).

control compounds and docked into T2R4 using CDOCKER algorithm available in Discovery Studio. Scoring functions were used to calculate the binding affinities to rank the docked poses (**Table 4.4.1**). Subsequently, based on the ranking of predicted binding affinity and commercial availability of the compounds, I selected Glyoxal-derived lysine dimer (GOLD) and CML for further testing their effect on T2R4. The predicted binding affinities are 0.1096 μM for GOLD and 0.0457 μM for CML, and these were tested in a sensitization assay on T2R4 (**Table 4.4.1**). Each compound was tested in logarithmic range of 1 μM, 10 μM and 100 μM in presence or absence of quinine (**Figure 4.4.4**). GOLD and CML alone did not show any calcium mobilization indicating that they do not activate T2R4. Further to assess their blocking ability, a competitive binding assay was performed in presence of quinine at 1 mM (EC_{50}). GOLD showed a subtle inhibition of quinine response at 1 μM and a significant reduction at higher concentrations of 10 μM and 100 μM suggesting that GOLD can act as antagonist of T2R4. In the case of CML, no effect on quinine response was observed at 1 μM and 10 μM while it showed a subtle reduction at high concentration of 100 μM (**Figure 4.4.4**). Together, the results suggest that GOLD is a potent antagonist while CML a weak antagonist at T2R4 against quinine response. The docking analysis of CML and GOLD along with quinine as control showed that they are docked into the same binding pocket (**Figure 4.4.5**). However, depending on the complexity of structure the compounds were docked at different regions in the binding pocket. Quinine occupied the central region, while CML docked slightly deeper near to TM5 and TM6, and GOLD is predicted to bind towards the extracellular side.

Table 4.4.1. Predicted binding affinities of advance glycation end-products (AGEs)

AGE compound	Predicted binding affinity –log(Kd)	Predicted Kd (μM)	Structure
Pentosidine	7.71	0.0195	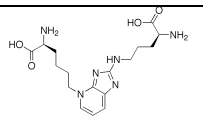
Nε-Carboxymethyl-lysine (CML)	7.34	0.0457	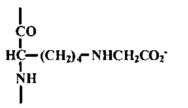
Tetrahydropyrimidine (THP)	7.3	0.0501	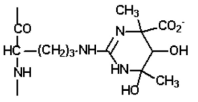
3-deoxyglucosone-derived lysine dimer (DOLD)	7.13	0.0741	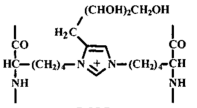
Nε-Carboxyethyl Lysine (CEL)	7.04	0.0912	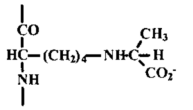
Glyoxal-derived lysine dimer (GOLD)	6.96	0.1096	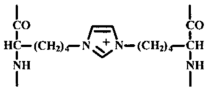
Argpyrimidine	6.81	0.1549	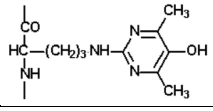
Methyl glyoxal hydroimidazolone 1(MG-H1)	6.77	0.1698	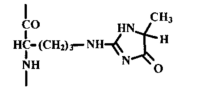
Methyl glyoxal-derived lysine dimer (MOLD)	6.6	0.2512	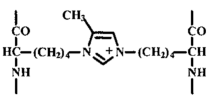
3-deoxyglucosone hydroimidazolone 3 (3DG-H3)	6.51	0.309	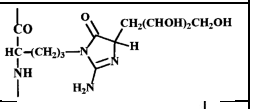
Fructosyl Lysine	6.47	0.3388	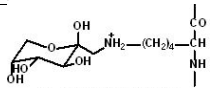
Pyrraline	6.22	0.6026	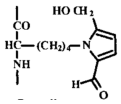

Nε-carboxymethyl-hydroxylysine (CMhL)	6.21	0.6166	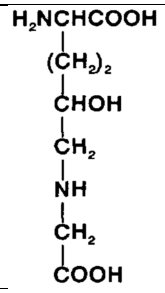
Nα,Nα-bis(carboxymethyl)-L-lysine (bis-CML)	6.05	0.8913	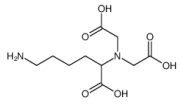
Glucosepane	5.92	1.2023	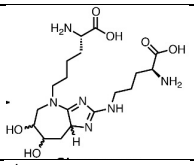
3-deoxyglucosone hydroimidazolone 2 (3DG-H2)	5.78	1.6596	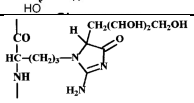
ImidazoloneA	5.72	1.9055	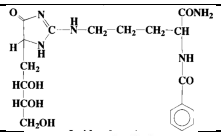
1-Alkyl-2-formyl-3,4-glycosyl-pyrrole (AFGP)	5.66	2.1878	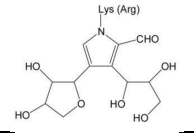
Methyl glyoxal hydroimidazolone 2 (MG-H2)	5.62	2.3988	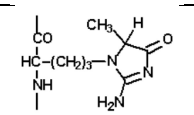
Quinine	5.56	2.7542	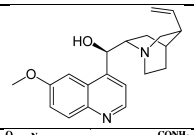
ImidazoloneB	5.29	5.1286	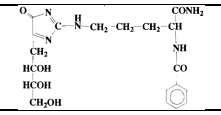
3-deoxyglucosone hydroimidazolone 1 (3DG-H1)	4.77	16.9824	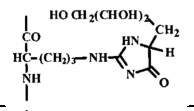
Glyoxal-derived hydroimidazolone (G-H)	4.7	19.9526	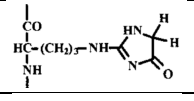
Methyl glyoxal hydroimidazolone 3 (MG-H3)	4.19	64.5654	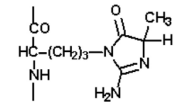

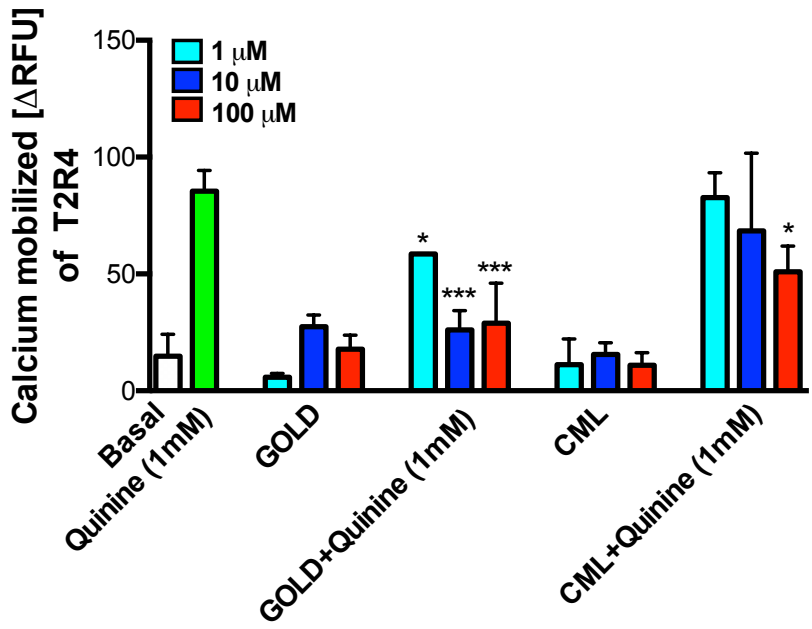

Figure 4.4.4. Sensitization assay of T2R4 calcium mobilization in response to AGE compounds. T2R4/Gα16/44 stable cells were treated with AGE compounds Glyoxal-derived lysine dimer (GOLD) and carboxy methyl lysate (CML) at logarithmic concentrations 1 μM, 10 μM and 100 μM in presence or absence of quinine at 1 mM. Assay buffer (basal) and quinine (1 mM) were included as negative and positive controls respectively.

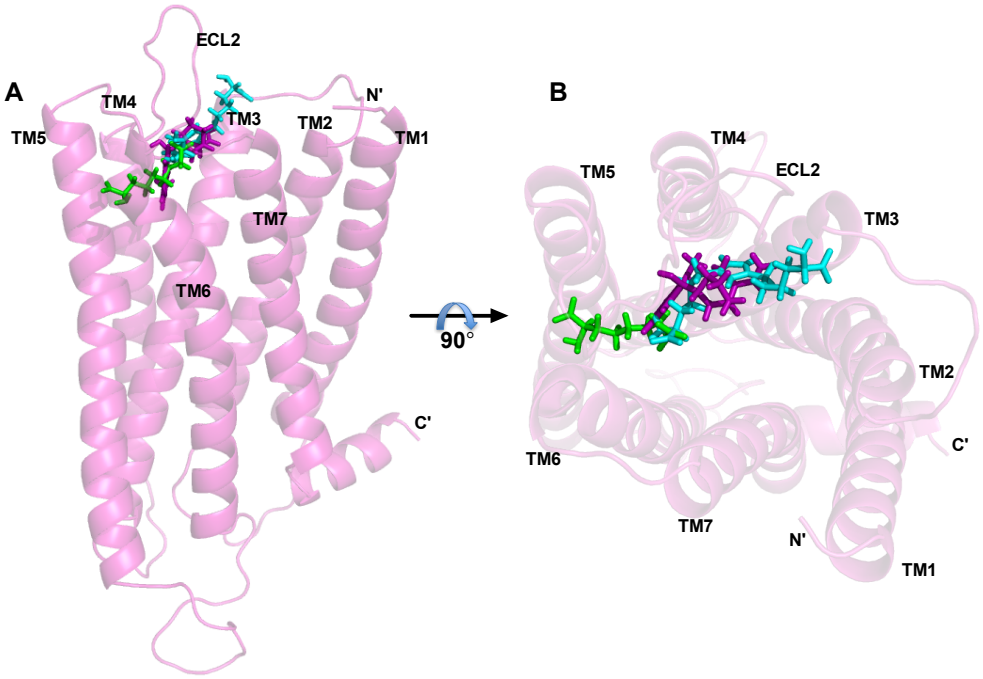

Figure 4.4.5. Comparison of binding modes of GOLD and CML docked into T2R4. A. The side view of superimposed homology models of T2R4 docked with carboxy methyl lysate (CML) (green), Glyoxal-derived lysine dimer (GOLD) (cyan) and quinine (purple) as control. **B.** The top view of the binding pocket of T2R4 showing the docked compounds. The extracellular loop 2 (ECL2) of T2R4 is in the close proximity to the docked compounds. TM: transmembrane helix.

CHAPTER 5

5.0 DISCUSSION

5.1. Expression Analysis of Functional T2Rs In Human Airway Cells

Considering the extraoral expression of T2Rs and their crucial role in regulating bacterial infections through the recognition of AHLs in the upper airways, it is reasonable to assume the presence of T2Rs in lower airway epithelium and their involvement in pathophysiological condition like CF. Thus, it is important to analyze the expression of T2Rs and their functionality in these tissues.

5.1.1 Human airway smooth muscle and bronchial epithelial cell lines

As observed in case of NuLi-1 and CuFi-1 the expression pattern of the different TAS2Rs was similar. Though TAS2R30/31/43/45/46 showed statistically significant differential expression between the cell lines, given the ambiguity with the CodeSet for these five TAS2Rs their individual transcript levels could not be confirmed. In ASMCs, similar TAS2R expression pattern was observed, which correlates with PCR and microarray data for these cells from previous studies (Upadhyaya et al., 2014, Liggett, 2013, Lund et al., 2013). These earlier analyses in ASMCs showed a similar pattern of expression for most of the TAS2Rs except TAS2R10 being more abundant than TAS2R14 followed by TAS2R31 which were termed as 'high expressors' with respect to the expression of ADRB2 (Liggett, 2013). The other TAS2Rs (TAS2R3, 4, 5, 19, 20, 45, 50, 30, 9, 13, 42, 46, 1 and 8) were considered as modest and the rest as low expressors. Moreover, the level of expression of these TAS2Rs correlates with the receptor function in response to their respective agonists.

Cell lines offer a unique and unparalleled advantage when trying to elucidate the role of novel cellular signal transduction pathways. The results in this thesis suggest a

specific pattern of TAS2R expression with TAS2R3, 4, 5, 10, 13, 19, 50 transcripts expressed at moderate levels and TAS2R14 and TAS2R20 (or 49) at high levels. The transcripts for the rest of the TAS2Rs are barely detectable or expressed at very low levels. Further, the expression analysis on selected T2Rs using PCR and FACS showed similar pattern which was slightly different from nCounter data for few T2Rs. The discrepancy in T2R4 expression at genetic and protein levels could be due to polyclonal antibody used. It should be noted that monoclonal antibodies for T2Rs are currently not available, and the approaches used to raise these different T2R polyclonal antibodies might vary.

It is unclear whether pathological conditions influence the expression or regulation of TAS2Rs. In previous studies, qPCR analysis on healthy and diseased human heart tissues showed a similar pattern of TAS2R transcript expression (Foster et al., 2013, Foster et al., 2015). *In silico* analysis also demonstrated no relative changes in both healthy and diseased hearts (Foster et al., 2015). A similar pattern of TAS2R expression was also observed between asthmatic and non-asthmatic hASMCs (Robinett et al., 2014). The data which suggest no differential expression of TAS2Rs in CF vs. non-CF airway cell lines is in agreement with these studies. The pathological environment in diseased conditions may regulate T2R functions and was recently reviewed elsewhere (Shaik et al., 2016). Furthermore, apart from studying the expression of T2Rs in different organs and tissues, it is important to study their functionality. Previous studies demonstrated that T2Rs expressed in brain, breast epithelium and vasculature are functional (Upadhyaya et al., 2014, Singh et al., 2011b, Singh et al., 2014).

The intracellular calcium response upon quinine treatment on NuLi-1 and CuFi-1 cells suggested that the T2Rs expressed in these cells are functional. However, no

statistically significant change in the EC_{50} values were observed for quinine treatment between the two cell lines. T2Rs signal predominantly through the heterotrimeric Gαβγ protein - phospholipase C (PLC) dependent pathway leading to intracellular calcium mobilization. The PLC inhibitor, U-73122 inhibits the coupling of Gαβγ protein-phospholipase C activation, making it a very useful tool to validate the T2R - Gαβγ - PLC - Ca^{2+} pathway in these cells (Deshpande et al., 2010, Zhang et al., 2013). Thus, the pre-incubation of cells with U-73122 diminished the quinine response significantly in both the cell lines. This suggest that majority of the intracellular calcium mobilization observed in these cells is due to activation of T2Rs and PLC pathway. This is the first study reporting the presence of functional T2Rs in the CF and non-CF bronchial epithelial cell lines. Interestingly, there is no significant difference in the EC_{50} values between NuLi-1 and CuFi-1 cell treated with U-73122. This indicates that the CFTR might not influence the function of T2Rs in CF bronchial epithelium.

5.1.2 Human bronchial epithelial primary cells

While immortalized cell lines like NuLi-1 and CuFi-1 are a good starting point, primary cells from patient biopsy will be more physiologically relevant. It will also rule out artifacts introduced due to the immortalization process. Analysis of mRNA and T2R protein expression of selected T2Rs showed no differential expression between healthy and CF primary cell cultures. T2R1 which is one of the low expressed T2Rs in several tissues showed low expression in the bronchial epithelium as well. T2R4 is a moderately expressed subtype and its expression was in line with the data obtained from CuFi-1 and NuLi-1 cell lines. The broadly tuned T2R14 showed highest expression as expected. However, due to the unavailability of

specific antibody for surface staining, the FACs was not performed on T2R14. T2R20 showed good expression at protein level when compared to the gene level with no difference among non-CF and CF cells. The functional characterization involved the treatment with AHLs and QSMs loads to mimic the physiological conditions of CF. A similar approach was employed with the commonly used CF antibiotics. Cells from one non-CF and one CF donor used in the functional assays showed good response with AHLs and QSMs while the response with antibiotics is not robust. These calcium responses were sensitive to inhibition of Gβγ and PLC suggesting the involvement of AHL/antibiotic-T2R-$G_{\alpha\beta\gamma}$-PLC-Ca^{2+} pathway. Here the healthy and CF cells did not show any difference in functional response. Collectively these studies suggest that the pathological conditions might not necessarily regulate the expression of T2Rs in the extraoral tissues. However, the presence of bacterial stimulants or other factors in pathological conditions might influence the functionality of the T2Rs.

5.2 Characterization of the Interaction of Commonly Used CF Antibiotics with T2Rs

Apart from the primary role of antibiotics in targeting bacteria, their role in influencing host immune responses and regulating physiological pathways remains poorly understood. Antibiotics were known to reduce mucus secretion by inhibiting TNF-α (Sadarangani et al., 2015). Macrolides like azithromycin were shown to inhibit the production of pro-inflammatory cytokines like interleukin (IL)-1, IL-6 and IL-8 (Suresh Babu et al., 2013). In CF, IL-8 acts as a potent chemoattractant of neutrophils that correlates with chronic inflammation. Immune cells such as neutrophils, monocytes and lymphocytes are known to express T2Rs and play a role in innate immune response (Maurer et al., 2015, Gaida et al., 2016). T2R agonists treatment in mouse lungs decreased the features of asthma by attenuation of chemokines and cytokines production, suggesting immune cells sense through T2Rs (Sharma et al., 2017). Thus, antibiotic treatment appears to contribute to the reduction of inflammation through activating T2Rs in some airway diseases.

The activation of the T2R9 in enteroendocrine cells elicits GLP-1 secretion, suggesting a possible mechanism that could influence the regulation of glucose and insulin in the gut (Dotson et al., 2008). Interestingly, the activation of T2R9 by ofloxacin but not with other tested fluoroquinolones indicates a compound specific link through T2Rs in glucose homeostasis (Dotson et al., 2008). Furthermore, levofloxacin is also known to associate with hypoglycemia (Park-Wyllie et al., 2006). In this objective, I show that levofloxacin activates all the tested T2Rs except T2R1, suggesting that antibiotics selectively activate T2Rs and might regulate physiological mechanisms. Interestingly, I did not observe an activation of T2R1 by any of the

tested compounds. This is in line with previous studies on T2Rs, for example, erythromycin activated only T2R10 in contrast, chloramphenicol activated T2R1, T2R8, T2R10, T2R39 and T2R43 (Meyerhof et al., 2010).

Despite the non-availability of a crystal structure for any taste receptor, the structure-function studies on different T2R subtypes from the last decade have revealed many interesting facts (Di Pizio et al., 2016, Jaggupilli et al., 2016). The 25 T2Rs in humans detect thousands of different chemical compounds, suggesting that diverse yet specific receptor determinants might be at play. For example, high ligand affinity (nanomolar to picomolar range) usually observed in the case of the Class A GPCRs is missing with T2Rs. Given their sensory nature, it does seem logical for T2Rs to have low affinities for their ligands, so as to enable detection of a broad range of compounds. To detect these diverse compounds, it is imperative that flexible regions of the receptor, such as the ECLs are involved rather than the more rigid TM helices. The current work targeting multiple T2Rs suggests that residues on ECL2 play an important role in ligand recognition and receptor activation. These are residues, R163, N165, T166 in T2R4; R160, R161 in T2R14; and W164 in T2R20. The amino acid sequence alignment of the three T2Rs showed that the important residues identified in ECL2 region are conserved among T2R4 and T2R14 (**Figure 4.2.19**). Interestingly, W164 in T2R20 is conserved in 12 of the 25 T2Rs and recent structure-function analysis of this residue (W170) in T2R7 also suggests its crucial role in ligand recognition (Liu et al., 2018). Taken together these results suggest an important role for ECL2 in T2R ligand recognition and receptor activation as observed in other classes of GPCRs (Zhang et al., 2015).

The nature of a ligand-binding pocket of a GPCR depends on the size, shape and electrostatic properties of the residues present in the pocket. Due to the huge

diversity of the amino acids in the extracellular region, the binding-pockets exhibit distinct features between GPCRs to recognize different ligands (Zhang et al., 2015). For example, the binding pocket for negative allosteric modulator of class C GPCR, mGluR5 is located deeper in the 7TM bundle while the general ligand-binding site in CRF1R and mGluR is slightly closer to the extracellular region but deeper than the binding sites in several class A GPCRs SMO receptor (Wang et al., 2014). However, the binding modes are also dependent on the type of ligands that the receptor is interacting with. In peptide receptors such as opioid receptors and chemokine receptors, the ligands bind to a more shallow and open binding pocket. By contrast, the small molecule ligands in aminergic receptors bind deeper in the TM bundle suggesting that the size of the ligand also determines the location of the binding pocket in GPCRs (Zhang et al., 2015).

My modeling studies suggest no overlap of the binding regions of the antibiotics in all the three T2Rs (**Figure 4.2.20**). In T2R14, levofloxacin and tobramycin docked in the same binding regions. In T2R20, levofloxacin docked deep in the pocket while tobramycin bound towards the extracellular part of the receptor. In all three receptors, the ECL2 is in close proximity and interacting with the docked compounds (**Figure 4.2.20**). Based on the results from this study, it is tempting to propose that T2Rs expressed in extraoral tissues and cells are crucial in responding specifically to different antibiotics and might be involved in regulating physiological mechanisms. This study sets the stage for mechanistic studies focused on elucidating the “antibiotic-T2R-immune response” nexus in innate immunity and possible development of novel therapies.

5.3 Characterization of the Binding Sites for Bacterial AHLs on T2Rs

Recent studies have demonstrated that T2Rs are expressed in nasal airways and play a vital role in transducing the signal from bacterial QSMs (Lee et al., 2012). Immunological studies on human neutrophils suggest T2R38 is the receptor for 3-oxo-C12-AHL on these immune cells (Maurer et al., 2015). This led to the notion that humans might be able to taste *P. aeruginosa* biofilms (Maurer et al., 2015). In this study, I report the predicted bitter taste of many common QSMs secreted by Gram-negative bacteria. The E-tongue analysis predicts some QSMs to be bitter than quinine, one of the most intense bitter tasting compounds isolated from plants. Structurally the quinolone QSMs have the same parent structure as with in the bitter compounds quinine and chloroquine (Freund et al., 2018). These quinolone compounds are detectable at high concentrations in sputum, plasma and urine samples from CF patients (Barr et al., 2015). Interestingly, I found that HHQ and NHQ which were predicted to taste very bitter could not significantly activate the T2R4, T2R14 and T2R20 that are highly expressed in various human tissues. Although T2R14 showed a notable response with both HHQ and NHQ, it is not significant under these assay conditions. Using a different heterologous assay system that involves co-transfection of both T2R14 and Gα16/44 chimera, another study reported activation of T2R14 by HHQ at 3.3 μM threshold concentration (Lossow et al., 2016). It is possible that the hydroxyquinolones might activate other T2Rs not analyzed in my study. A very recent study tested *Pseudomonas* quinolone signal (PQS), dihydroxyquinolone (DHQ) and HHQ on T2Rs expressed in both heterologous system and several lung epithelial cells including primary sinonasal cells (Freund et al., 2018). They reported the activation of T2R4, T2R16 and T2R38 by PQS while T2R14 was activated by HHQ. Interestingly the observation that HHQ activating only T2R14 is in agreement

with the results obtained in my study although the response is non-significant.

E-tongue predicted the three AHLs to taste bitter almost similar in intensity to quinine bitterness. Among the analyzed AHLs, C4-AHL activated only T2R14 while C8-AHL and 3-oxo-C12-AHL activated T2R4, T2R14 and T2R20. In comparison to other T2Rs, T2R14 was activated with all three AHLs at a lower concentration (50 μM). It has been proposed that T2R14 is one of the broadly tuned T2Rs in humans that can recognize a wide variety of compounds (Karaman et al., 2016). This might partly explain the observed activation of T2R14 with almost all the tested compounds. On the other hand, the agonistic potency of these compounds at T2R20 is very low (200 μM), compared to T2R4 and T2R14. Furthermore, the dose dependent analysis on T2R20 with C8-AHL showed no response suggesting its selectivity among the AHLs. The EC_{50} values obtained for 3-oxo-C12-AHL at the tested three T2Rs showed between 40 – 70 μM. The concentration range appears to be similar to the values 50-80 μM obtained in mouse SSCs treated with 3-oxo-C12-AHL and 3-oxo-C6-AHL (Tizzano et al., 2010). However, comparison with the activation of T2Rs in human primary cells would give more appropriate inference although the prevalence of bacterial population might vary. Considering the results from primary cells as discussed in section 5.1.2, collectively they suggest a role of quinolones and AHLs in T2R-mediated signaling in the lower epithelium. Previous studied on the primary cells showed quiniolones and AHLs increased the NO levels indicating their role in activating bactericidal effects in the upper airway epithelium (Lee et al., 2012, Freund et al., 2018). Thus, it is tempting to propose the role of AHLs and QSMs in immune responses in the lower airway epithelium as observed in the upper airway epithelium in the presence of bacteria.

The biochemical characterization of AHL-T2R interactions here, gives

interesting insights into their mechanism(s) of binding. It is known that N165 in T2R4 is highly conserved among the human T2Rs. In this study, mutations at N165 fail to show significant response with C8-AHL and 3-oxo-C12-AHL. This is in agreement with the previous studies, where the crucial role of N165 in T2R4 ligand binding and receptor activation was demonstrated (Pydi et al., 2014c). T166 and K262 displayed a compound specific phenomenon. The selectivity of K262 interactions in terms of both agonists and antagonists was also previously reported (Pydi et al., 2014c). In a recent report, T2R14 was suggested to be activated by HHQ, C6-AHL, C8-AHL but not 3-oxo-C12-AHL (Lossow et al., 2016). Here in this analysis, T2R14 was activated by all the 3 tested AHLs, C4-AHL, C8-AHL and 3-oxo-C12-AHL. As discussed previously, these differences might be due to the different T2R heterologous assay systems used. The mutational analysis showed the ECL2 residues R160 and K163 are important for both the AHLs, C8-AHL and 3-oxo-C12-AHL. The importance of R160 was also previously reported for the T2R14 agonist aristolochic acid (Zhang et al., 2017). In T2R20, this data suggests W88 and Q265 to be important residues for interaction with 3-oxo-C12-AHL which is the only tested AHL that activated. The important AHL binding residues in T2R4 and T2R14 are predominantly located in the ECL2, which is known to play vital role in the ligand interaction and activation of a GPCR. In contrast, the ligand binding residues in T2R20 are predominantly located in the TM helices.

Superimposing of the T2R models docked with 3-oxo-C12-AHL or C8-AHL showed these AHLs bind to a single orthosteric site situated close to the extracellular surface in all the T2Rs (**Fig. 6**). However, there are slight variations in the orientation of the pose of 3-oxo-C12-AHL or C8-AHL in each T2R. In T2R4, 3-oxo-C12-AHL was docked in the upper region with the homoserine lactone group interacting

substantially with ECL2 while extending the acyl chain towards TM3-TM7. However, in T2R14 and T2R20 the long acyl chain was buried in the TM core with the homoserine lactone group interacting with ECL2 (**Fig. 6A**). C8-AHL was docked in a similar region in both T2R4 and T2R14 where the homoserine lactone group was overlapped between the ECL2 and TM4-TM5-TM6 while the acyl chains were buried into the TM core in opposite directions (**Fig. 6B**). The composition of hydrophobic amino acids in the three T2Rs might play a role in directing the orientation of the hydrophobic acyl chains. It appears that acyl chains might anchor the molecules into the binding site with hydrophobic interactions while the polar groups present in the homoserine lactone form stronger interaction that might facilitate receptor activation.

In addition, the inhibitory effects of BCML on AHLs response with T2R4 were pursued. BCML is the only known inverse agonist for any T2R. When C8-AHL and 3-oxo-C12-AHL were added in presence of BCML, the T2R4 response with both the AHLs was significantly inhibited. BCML is involved in strong polar interactions with N164, N165 and T166 in T2R4 (Pydi et al., 2014c). The modeling studies on AHLs in T2R4 binding pocket shows N165 and T166 are required for their interaction. Thus together, the results suggest a competitive inhibition of AHLs response by BCML. Here in this thesis, only a sensitization assay was performed with single concentration, further pharmacological experiments such as a competitive dose response analysis is required. This would provide more insights into the potency of BCML with respect to the individual AHLs.

5.4 Identification of ABA and AGE Compounds as Novel T2R4 Blockers

Following the identification of ABA as an antagonist of T2R4 against quinine, the nature of antagonism was studied. In the Schild analysis, although the maximum response of quinine was not affected with increasing concentrations of ABA, a rightward shift was observed in the dose response curves for quinine, and the Schild plot generated a slope of 0.46 ±0.02 at 95% CI of 0.33-0.59 with pA_2 value 1.99 (**Figure 4.4.1**). A slope significantly less than unity indicates a number of possibilities such as; (i) non-competitive antagonism, (ii) multimolecular interactions among drugs and receptors, and (iii) non-equilibrium conditions in the experimental procedures. When the reduction of slope is antagonist related, this would cause a diminished potency of antagonist. With the increasing concentrations of antagonist greater than the K_B for its antagonism, the Schild equation would not predict a simple competitive antagonism. A possibility can be an agonist related reduction in the slope. At high concentrations (in the millimolar range), agonists might produce non-specific responses such as those mediated by other proteins or receptors, which cannot be blocked by the antagonist (Kenakin, 1982). In addition to T2Rs, at higher concentrations quinine can also activate other cellular effectors. Since I performed a simultaneous treatment with quinine and ABA on the HEK293T-T2R4-Gα16/44 stable cells, a multimolecular interaction could be another reason for the reduction in the slope obtained in Schild regression analysis. Similar conditions were reported in a previous study in which, agouti-signaling protein (ASIP) was determined as a surmountable antagonist at human melanocortin receptors exhibiting complex mechanisms with slopes significantly less than unity (Yang et al., 1997). When the slope is equal to unity, the pA_2 value gives the antagonist concentration to produce a dose ratio equal to 2 basing on the intercept with abscissa. Considering the above,

with slope less than unity I could not determine the K_B value of ABA or conclude the interaction is simple competitive inhibition (Wyllie and Chen, 2007).

I used (±) ABA, which is a racemic mixture of ABA isomers. Isomerism is an important criterion in drug development and many pharmacologically relevant events when different isomers of the same compound show different effects (Agranat et al., 2002). There are many isomers used as drugs that show different activities (Chhabra et al., 2013). In the case of taste stimulating compounds, it is known that the gentiobiose tastes bitter and isomaltose tastes sweet and these two compounds are anomers (Sakurai et al., 2010b). Since (+) ABA is the naturally occurring and biologically active compound (**Figure 4.4.2)** and it was found that xanthaxine (precursor of ABA) as a weak agonist of T2R4, it is likely that each ABA isomer can show different activity. However, only (+) ABA was commercially available and was used in the study. The dose response analysis using (+) ABA showed no calcium mobilized, and indicates that the isomer cannot activate T2R4. Further in sensitization assay, testing with high concentration blocked the quinine response on T2R4 similar to the blocking effect of racemic (±) ABA, and known antagonists BCML and GABA. This confirms that the (+) ABA acts as a blocker of T2R4 similar to the racemic mixture of (±) ABA.

AGEs are a spectrum of glycated heterogeneous compounds formed by the non-enzymatic reactions of reducing sugars such as glucose or other carbohydrate adducts (α-carbonylic compounds) with amino group containing residues (lysine and/or arginine) in proteins and also amino groups within lipids and nucleic acids (Ahmad et al., 2008, Vlassara et al., 1984, Han et al., 2013). AGEs in humans have significant pathophysiological implications causing diabetes, arthritis, retinopathy and cardiovascular diseases (Ahmad et al., 2008, Reddy et al., 1995). Excessive

generation of AGEs is very harmful and causes tissue damage (Ahmad et al., 2008). Their interaction with specific cell surface receptors such as RAGEs, induce inflammatory responses (Horvat and Jakas, 2004). Prolonged cooking or thermal processing such as grilling, broiling, roasting and frying of meat will generate new complex compounds in the form of AGEs (Han et al., 2013). Meat extracts also comprise other compounds like cyclopeptides. As BCML an inverse agonist of T2R4 is a synthetic derivative of the AGE, further analysis of other AGE compounds was performed to identify novel T2R ligands. Out of 23 compounds docked into T2R4, CML and GOLD are commercially available and were tested in this work. T2R4 was treated with both the compounds and no response was recorded. Based on the predicted binding affinity CML showed higher affinity than GOLD and it is structurally similar to BCML. However, in contrast to BCML potency as blocker (IC_{50} = 60 nM), CML showed very weak inhibition even at high concentration. Interestingly, GOLD exhibited significant blocking effect. The docking analysis provided insights into the binding orientation of these compounds in T2R4. It seems the complexity of the compounds played key role in binding and effecting the function of T2R4. When compared to the putative agonist quinine that was bound in the central region of the binding pocket covering TM helices and ECLs, CML was bound a bit deeper towards TM5 and TM6 away from ECL2. GOLD being a more complex compound, bound in the center of the cavity extending slightly towards the extracellular part and mostly interacting with ECL2. CML structure is simpler than GOLD and this could be the factor that determined the stronger antagonistic of GOLD effect on T2R4. Although CML is structurally similar to BCML which is an inverse agonist of T2R4, the complexity in the latter also supports the inference that a

complex structure with reactive functional groups might hold the receptor rigid to attain an inactive confirmation (Pydi et al., 2014c).

CHAPTER 6

6.0 CONCLUSION AND FUTURE DIRECTIONS

6.1 Conclusion

Since the discovery of the human 25 T2Rs in the oral cavity in 2000, the field has expanded exponentially driven in part by the discovery of T2Rs in extraoral tissues. The early years were dedicated to identifying the putative ligands and deorphanize the T2Rs. Since then, our knowledge of T2R structure-function and physiology has vastly improved. The key structural determinants were characterized, binding sites were explored and several comparative studies (human T2Rs vs animal models) were being performed to recognize the peculiarity of T2Rs. Due to their diversity, it has been proposed that T2Rs be placed into separate group as Class T receptors among the GPCR superfamily (Munk et al., 2016).

Recently the role of T2Rs have been explored in several extraoral tissues and known to be involved in a variety of physiological mechanisms like digestion, airway relaxation, thyroid hormone regulation and skin cell differentiation. AHLs are produced by opportunistic bacteria like *P. aeruginosa* that predominate in CF airways. Thus, expression of functional T2Rs and characterization of AHL-T2R interaction was performed using lower airway cells. The results from airway cell lines, NuLi-1, CuFi-1 and ASMCs suggest a specific pattern of TAS2R expression with TAS2R3, 4, 5, 10, 13, 19, 50 transcripts expressed at moderate levels and TAS2R14 and TAS2R20 (or 49) at high levels. The transcripts for the rest of the TAS2Rs are barely detectable in nCounter analysis. Similar expression patterns were also obtained in the primary cells from normal and CF donors. This work suggests significant expression of a number of TAS2Rs, and with no differential expression between normal and pathological conditions. The pathological environment in diseased conditions may

regulate T2R functions. The quinine treatment on NuLi-1 and CuFi-1 activated T2R-Gβγ-PLC pathway and it was confirmed by the inhibition of PLC using U-73122. Similar approach in primary cells treated with AHLs and commonly used CF antibiotics suggested these compounds can activate T2Rs signaling pathway. Taken together, this work establishes the expression of functional T2Rs in bronchial epithelium.

In order to understand the binding interactions of antibiotics with T2Rs amino acids, I characterized by sensory and structure-function analyses, how antibiotics frequently used to treat airway infections in CF, activate multiple human T2Rs. Taste sensory analysis using E-tongue was carried out on the broad-spectrum antibiotics, tobramycin, levofloxacin and azithromycin to measure their bitter tasting ability. Then, the potency of the selected antibiotics from different classes on highly expressed T2Rs in airways, T2R4, T2R14 and T2R20 was pursued. The amino acids and structural features of T2R4, T2R14 and T2R20 important for antibiotic binding were characterized by mutational analysis in heterologous cell based assays. Strikingly, extracellular loop 2 in T2Rs performs a key function in binding to antibiotics with contribution from residues in transmembrane helices. The results conclude that different antibiotics activate multiple T2Rs with different potencies. Understanding the non-antibiotic and physiological effects mediated through T2Rs on the host cells need to be elucidated.

Subsequently, the QSMs including AHLs and hydroxyquinolones were tested for their bitter taste sensation using E-tongue. Although hydroxyquinolones showed stronger bitterness than the reference compounds, they did not induce significant calcium mobilization when compared to AHLs. No response from T2R1 and C4-AHL activating only the broadly tuned T2R14 suggests the existing promiscuity and

selectivity with respect to the agonist or receptor. Amino acid and binding site interactions was carried out using mutational analysis in heterologous cell based assays and molecular modeling analysis on T2R4, T2R14 and T2R20. C8-AHL and 3-oxo-C12-AHL showed different potencies at each T2R suggesting the selective activation. The AHLs share the same binding pocket while attaining different orientations depending on the functional groups present in the compound. Testing with BCML, the inverse agonist of T2R4 inhibited the response of C8-AHL and 3-oxo-C12-AHL. Together these results suggest the presence of a single orthosteric site for AHLs in T2Rs, and reinforce the significant role of ECL2 in T2R ligand binding and activation. This study will facilitate mechanistic studies aimed at understanding the role of these T2Rs as "sensors" of bacteria and in host pathogen interactions. Future studies need to investigate the effects of activation of T2R signaling mediated by bacterial molecules and compare the responses between CF and non-CF conditions. As T2Rs are known to be expressed in other systems like immunes cells and are activated by AHLs, it is plausible that the T2Rs might have a significant role in regulating the immune responses in CF. Also, the testing of both AHLs and QSMs against the rest of the 25 T2Rs in a more extensive manner would determine their selectivity and sensitivity.

To identify potential bitter blockers and understand their antagonism, plant and meat derived compounds were screened. In this process, the nature of antagonism of plant hormone (±) ABA was studied using standard pharmacological analysis. The work from Schild regression analysis concluded the antagonism of ABA as surmountable and probably competitive. Next, to test the activity of individual ABA isomers on T2R4, the activity of (+) ABA, which is the naturally occurring isomer of ABA was tested at T2R4. The results conclude that the (+) ABA cannot activate T2R4

and it inhibits quinine response on T2R4. In addition, meat products such as AGEs were screened to identify the potential compounds with high affinity. Since these compounds are produced by both endogenous reactions and from exogenous food sources, identification of AGEs as ligands for T2Rs will have applied potential for use as bitter taste maskers in the food industry. The AGE, GOLD exhibited a blocking effect as the concentration was increased while CML acted as weak antagonist against quinine response at T2R4. In conclusion, the amino acid derivatives such as AGEs in addition to their potential use in food industry, can also be used as blockers to understand the molecular role of T2Rs in various physiological mechanisms.

6.2 Future directions

In recent years, the T2R field gained interest with the elucidation of their unique signaling mechanisms and receptor deorphanization. It has been further expanded with the discovery of T2Rs in extraoral tissues which led to their potential involvement in many diseases and in understanding the role of T2Rs in different physiological mechanisms. Nevertheless, the current information on the biochemical pharmacology, structural determinants and function of T2Rs is limited. Thus, studies are needed to understand the ligand-interaction and activation mechanisms of T2Rs. In the absence of a high-resolution structure, the role of waters, ligand binding and receptor conformational changes while exciting, needs to be interpreted with caution. The role of T2Rs in pathological conditions such as CF need more elucidations at the downstream level and how they influence the pathophysiology of CF lung. Given the almost ubiquitous presence of these chemosensory receptors in different human tissues, it does make it interesting to elucidate how bacteria acting through T2Rs influence host cell responses in these different tissues. For example, while this study tested only a few of the common QSMs, there are others such as competence stimulating peptides (CSPs) and XIP secreted by cariogenic bacteria like *S. mutans* and it would be worthwhile pursuing studies elucidating CSP-T2R interactions and how they influence oral innate immunity. Similarly, elucidating the physiological role of QSM-T2R interactions in other airway diseases such as CRS would help develop novel therapeutics targeting T2Rs in these pathophysiological conditions. The T2R mediated inflammatory responses, tissue remodeling and the proliferation effects in presence of elevated concentrations of AHLs in airways need to be elucidated to develop better therapeutics. Identification of novel bitter blockers with higher potency is required for their use in food and pharmaceutical industry. They will also aid in

deciphering T2R signal transduction in various tissues. Appropriate techniques, such as the use of CAMs facilitates the recognition of inverse agonists, and Schild regression analysis aids in studying the nature of a given bitter ligand's antagonism. The functional selectivity of bitter ligands and ligand bias need to be studied. Focus on the signaling pathways other than Ca^{2+} mobilization is necessary. Given the amount of work to be done in understanding the structure and function of these receptors, the next few years will be an interesting and exciting phase in T2R biology.

CHAPTER 7

7.0 REFERENCES

AGRANAT, I., CANER, H. & CALDWELL, J. 2002. Putting chirality to work: the strategy of chiral switches. *Nat Rev Drug Discov,* 1**,** 753-68.

AHMAD, W., LI, L. & DENG, Y. 2008. Identification of AGE-precursors and AGE formation in glycation-induced BSA peptides. *BMB Rep,* 41**,** 516-22.

ANGEL, T. E., CHANCE, M. R. & PALCZEWSKI, K. 2009. Conserved waters mediate structural and functional activation of family A (rhodopsin-like) G protein-coupled receptors. *Proc Natl Acad Sci U S A,* 106**,** 8555-60.

ARAKAWA, M., CHAKRABORTY, R., UPADHYAYA, J., EILERS, M., REEVES, P. J., SMITH, S. O. & CHELIKANI, P. 2011. Structural and functional roles of small group-conserved amino acids present on helix-H7 in the beta(2)-adrenergic receptor. *Biochim Biophys Acta,* 1808**,** 1170-8.

AVAU, B. & DEPOORTERE, I. 2016. The bitter truth about bitter taste receptors: beyond sensing bitter in the oral cavity. *Acta Physiol (Oxf),* 216**,** 407-20.

BADAL, S., HER, Y. F. & MAHER, L. J., 3RD 2015. Nonantibiotic Effects of Fluoroquinolones in Mammalian Cells. *J Biol Chem,* 290**,** 22287-97.

BAKER, J. G. & HILL, S. J. 2007. Multiple GPCR conformations and signalling pathways: implications for antagonist affinity estimates. *Trends Pharmacol Sci,* 28**,** 374-81.

BALDWIN, J. M., SCHERTLER, G. F. & UNGER, V. M. 1997. An alpha-carbon template for the transmembrane helices in the rhodopsin family of G-protein-coupled receptors. *J Mol Biol,* 272**,** 144-64.

BALLESTEROS, J. A. & WEINSTEIN, H. 1995. [19] Integrated methods for the construction of three-dimensional models and computational probing of structure-function relations in G protein-coupled receptors. *In:* STUART, C. S. (ed.) *Methods in Neurosciences.* Academic Press.

BARR, H. L., HALLIDAY, N., CAMARA, M., BARRETT, D. A., WILLIAMS, P., FORRESTER, D. L., SIMMS, R., SMYTH, A. R., HONEYBOURNE, D., WHITEHOUSE, J. L., NASH, E. F., DEWAR, J., CLAYTON, A., KNOX, A. J. & FOGARTY, A. W. 2015. Pseudomonas aeruginosa quorum sensing molecules correlate with clinical status in cystic fibrosis. *Eur Respir J,* 46**,** 1046-54.

BEHRENS, M., BROCKHOFF, A., BATRAM, C., KUHN, C., APPENDINO, G. & MEYERHOF, W. 2009. The human bitter taste receptor hTAS2R50 is activated by the two natural bitter terpenoids andrographolide and amarogentin. *J Agric Food Chem,* 57**,** 9860-6.

BEHRENS, M. & MEYERHOF, W. 2013. Bitter taste receptor research comes of age: from characterization to modulation of TAS2Rs. *Semin Cell Dev Biol,* 24**,** 215-21.

BLEVES, S., VIARRE, V., SALACHA, R., MICHEL, G. P. F., FILLOUX, A. & VOULHOUX, R. 2010. Protein secretion systems in Pseudomonas aeruginosa: A wealth of pathogenic weapons. *International Journal of Medical Microbiology,* 300**,** 534-543.

BORN, S., LEVIT, A., NIV, M. Y., MEYERHOF, W. & BEHRENS, M. 2013. The Human Bitter Taste Receptor TAS2R10 Is Tailored to Accommodate Numerous Diverse Ligands. *Journal of Neuroscience,* 33**,** 201-213.

BROCKHOFF, A., BEHRENS, M., MASSAROTTI, A., APPENDINO, G. & MEYERHOF, W. 2007. Broad tuning of the human bitter taste receptor hTAS2R46 to various sesquiterpene lactones, clerodane and labdane diterpenoids, strychnine, and denatonium. *J Agric Food Chem,* 55**,** 6236-43.

BROCKHOFF, A., BEHRENS, M., NIV, M. Y. & MEYERHOF, W. 2010. Structural requirements of bitter taste receptor activation. *Proc Natl Acad Sci U S A,* 107**,** 11110-5.

BROCKHOFF, A., BEHRENS, M., ROUDNITZKY, N., APPENDINO, G., AVONTO, C. & MEYERHOF, W. 2011. Receptor agonism and antagonism of dietary bitter compounds. *J Neurosci,* 31**,** 14775-82.

BURSTEIN, E. S., SPALDING, T. A. & BRANN, M. R. 1998. The second intracellular loop of the m5 muscarinic receptor is the switch which enables G-protein coupling. *Journal of Biological Chemistry,* 273**,** 24322-24327.

CAICEDO, A., PEREIRA, E., MARGOLSKEE, R. F. & ROPER, S. D. 2003. Role of the G-protein subunit alpha-gustducin in taste cell responses to bitter stimuli. *J Neurosci,* 23**,** 9947-52.

CASAROSA, P., KIECHLE, T., SIEGER, P., PIEPER, M. & GANTNER, F. 2010. The constitutive activity of the human muscarinic M3 receptor unmasks differences in the pharmacology of anticholinergics. *J Pharmacol Exp Ther,* 333**,** 201-9.

CERIONE, R. A., CODINA, J., BENOVIC, J. L., LEFKOWITZ, R. J., BIRNBAUMER, L. & CARON, M. G. 1984. The mammalian beta 2-adrenergic receptor: reconstitution of functional interactions between pure receptor and pure stimulatory nucleotide binding protein of the adenylate cyclase system. *Biochemistry,* 23**,** 4519-25.

CHALMERS, D. T. & BEHAN, D. P. 2002. The use of constitutively active GPCRs in drug discovery and functional genomics. *Nat Rev Drug Discov,* 1**,** 599-608.

CHANDRASHEKAR, J., HOON, M. A., RYBA, N. J. & ZUKER, C. S. 2006. The receptors and cells for mammalian taste. *Nature,* 444**,** 288-94.

CHANDRASHEKAR, J., MUELLER, K. L., HOON, M. A., ADLER, E., FENG, L., GUO, W., ZUKER, C. S. & RYBA, N. J. 2000. T2Rs function as bitter taste receptors. *Cell,* 100**,** 703-11.

CHAUDHARI, N. & ROPER, S. D. 2010. The cell biology of taste. *J Cell Biol,* 190**,** 285-96.

CHEN, J. W., KOH, C. L., SAM, C. K., YIN, W. F. & CHAN, K. G. 2013. Short chain N-acyl homoserine lactone production by soil isolate Burkholderia sp. strain A9. *Sensors (Basel),* 13**,** 13217-27.

CHHABRA, N., ASERI, M. L. & PADMANABHAN, D. 2013. A review of drug isomerism and its significance. *Int J Appl Basic Med Res,* 3**,** 16-8.

CHMIEL, J. F., AKSAMIT, T. R., CHOTIRMALL, S. H., DASENBROOK, E. C., ELBORN, J. S., LIPUMA, J. J., RANGANATHAN, S. C., WATERS, V. J. & RATJEN, F. A. 2014. Antibiotic management of lung infections in cystic fibrosis. II. Nontuberculous mycobacteria, anaerobic bacteria, and fungi. *Ann Am Thorac Soc,* 11**,** 1298-306.

CHU, A., CALDWELL, J. S. & CHEN, Y. A. 2010. Identification and characterization of a small molecule antagonist of human VPAC(2) receptor. *Mol Pharmacol,* 77**,** 95-101.

CLARK, A. A., DOTSON, C. D., ELSON, A. E., VOIGT, A., BOEHM, U., MEYERHOF, W., STEINLE, N. I. & MUNGER, S. D. 2015. TAS2R bitter taste receptors regulate thyroid function. *FASEB J,* 29**,** 164-72.

CLARK, A. A., LIGGETT, S. B. & MUNGER, S. D. 2012. Extraoral bitter taste receptors as mediators of off-target drug effects. *Faseb Journal,* 26**,** 4827-4831.

COHEN, L. J., ESTERHAZY, D., KIM, S. H., LEMETRE, C., AGUILAR, R. R., GORDON, E. A., PICKARD, A. J., CROSS, J. R., EMILIANO, A. B., HAN, S. M., CHU, J., VILA-FARRES, X., KAPLITT, J., ROGOZ, A., CALLE, P. Y., HUNTER, C., BITOK, J. K. & BRADY, S. F. 2017. Commensal bacteria make GPCR ligands that mimic human signalling molecules. *Nature,* 549**,** 48-53.

CULIC, O., ERAKOVIC, V. & PARNHAM, M. J. 2001. Anti-inflammatory effects of macrolide antibiotics. *Eur J Pharmacol,* 429**,** 209-29.

DAI, W., YOU, Z., ZHOU, H., ZHANG, J. & HU, Y. 2011. Structure-function relationships of the human bitter taste receptor hTAS2R1: insights from molecular modeling studies. *J Recept Signal Transduct Res,* 31**,** 229-40.

DAVIES, J. C. 2002. Pseudomonas aeruginosa in cystic fibrosis: pathogenesis and persistence. *Paediatr Respir Rev,* 3**,** 128-34.

DESHPANDE, D. A., WANG, W. C., MCILMOYLE, E. L., ROBINETT, K. S., SCHILLINGER, R. M., AN, S. S., SHAM, J. S. & LIGGETT, S. B. 2010. Bitter taste receptors on airway smooth muscle bronchodilate by localized calcium signaling and reverse obstruction. *Nat Med,* 16**,** 1299-304.

DEVILLIER, P., NALINE, E. & GRASSIN-DELYLE, S. 2015. The pharmacology of bitter taste receptors and their role in human airways. *Pharmacol Ther*.

DEWIRE, S. M. & VIOLIN, J. D. 2011. Biased ligands for better cardiovascular drugs: dissecting G-protein-coupled receptor pharmacology. *Circ Res,* 109**,** 205-16.

DEZIEL, E., LEPINE, F., MILOT, S., HE, J., MINDRINOS, M. N., TOMPKINS, R. G. & RAHME, L. G. 2004. Analysis of *Pseudomonas aeruginosa* 4-hydroxy-2-alkylquinolines (HAQs) reveals a role for 4-hydroxy-2-heptylquinoline in cell-to-cell communication. *Proc Natl Acad Sci U S A,* 101**,** 1339-44.

DI PIZIO, A., LEVIT, A., SLUTZKI, M., BEHRENS, M., KARAMAN, R. & NIV, M. Y. 2016. Comparing Class A GPCRs to bitter taste receptors: Structural motifs, ligand interactions and agonist-to-antagonist ratios. *Methods in Cell Biology.* Academic Press.

DI PIZIO, A. & NIV, M. Y. 2015. Promiscuity and selectivity of bitter molecules and their receptors. *Bioorg Med Chem,* 23**,** 4082-91.

DIGGLE, S. P., CRUSZ, S. A. & CAMARA, M. 2007. Quorum sensing. *Curr Biol,* 17**,** R907-10.

DIGGLE, S. P., LUMJIAKTASE, P., DIPILATO, F., WINZER, K., KUNAKORN, M., BARRETT, D. A., CHHABRA, S. R., CAMARA, M. & WILLIAMS, P. 2006. Functional genetic analysis reveals a 2-Alkyl-4-quinolone signaling system in the human pathogen Burkholderia pseudomallei and related bacteria. *Chem Biol,* 13**,** 701-10.

DIGGLE, S. P., WINZER, K., CHHABRA, S. R., WORRALL, K. E., CAMARA, M. & WILLIAMS, P. 2003. The *Pseudomonas aeruginosa* quinolone signal molecule overcomes the cell density-dependency of the quorum sensing hierarchy, regulates *rhl*-dependent genes at the onset of stationary phase and can be produced in the absence of LasR. *Mol Microbiol,* 50**,** 29-43.

DOTSON, C. D., ZHANG, L., XU, H., SHIN, Y. K., VIGUES, S., OTT, S. H., ELSON, A. E., CHOI, H. J., SHAW, H., EGAN, J. M., MITCHELL, B. D., LI, X., STEINLE, N. I. & MUNGER, S. D. 2008. Bitter taste receptors influence glucose homeostasis. *PLoS One,* 3**,** e3974.

FLETCHER, J. N., KINGHORN, A. D., SLACK, J. P., MCCLUSKEY, T. S., ODLEY, A. & JIA, Z. 2011. In vitro evaluation of flavonoids from Eriodictyon californicum for antagonist activity against the bitterness receptor hTAS2R31. *J Agric Food Chem,* 59**,** 13117-21.

FOSTER, S. R., BLANK, K., SEE HOE, L. E., BEHRENS, M., MEYERHOF, W., PEART, J. N. & THOMAS, W. G. 2014a. Bitter taste receptor agonists elicit G-protein-dependent negative inotropy in the murine heart. *FASEB J,* 28**,** 4497-508.

FOSTER, S. R., PORRELLO, E. R., PURDUE, B., CHAN, H. W., VOIGT, A., FRENZEL, S., HANNAN, R. D., MORITZ, K. M., SIMMONS, D. G., MOLENAAR, P., ROURA, E., BOEHM, U., MEYERHOF, W. & THOMAS, W. G. 2013. Expression, regulation and putative nutrient-sensing function of taste GPCRs in the heart. *PLoS One,* 8**,** e64579.

FOSTER, S. R., PORRELLO, E. R., STEFANI, M., SMITH, N. J., MOLENAAR, P., DOS REMEDIOS, C. G., THOMAS, W. G. & RAMIALISON, M. 2015. Cardiac gene expression data and in silico analysis provide novel insights into human and mouse taste receptor gene regulation. *Naunyn Schmiedebergs Arch Pharmacol,* 388**,** 1009-27.

FOSTER, S. R., ROURA, E. & THOMAS, W. G. 2014b. Extrasensory perception: odorant and taste receptors beyond the nose and mouth. *Pharmacol Ther,* 142**,** 41-61.

FREUND, J. R., MANSFIELD, C. J., DOGHRAMJI, L. J., ADAPPA, N. D., PALMER, J. N., KENNEDY, D. W., REED, D. R., JIANG, P. & LEE, R. J. 2018. Activation of airway epithelial bitter taste receptors by Pseudomonas aeruginosa quinolones modulates calcium, cyclic-AMP, and nitric oxide signaling. *J Biol Chem,* 293**,** 9824-9840.

FUQUA, W. C., WINANS, S. C. & GREENBERG, E. P. 1994. Quorum sensing in bacteria: the LuxR-LuxI family of cell density-responsive transcriptional regulators. *J Bacteriol,* 176**,** 269-75.

GAIDA, M. M., DAPUNT, U. & HANSCH, G. M. 2016. Sensing developing biofilms: the bitter receptor T2R38 on myeloid cells. *Pathog Dis,* 74.

GAO, X., RAY, R., XIAO, Y., ISHIDA, K. & RAY, P. 2010. Macrolide antibiotics improve chemotactic and phagocytic capacity as well as reduce inflammation in sulfur mustard-exposed monocytes. *Pulm Pharmacol Ther,* 23**,** 97-106.

GARLAND, A. L., WALTON, W. G., COAKLEY, R. D., TAN, C. D., GILMORE, R. C., HOBBS, C. A., TRIPATHY, A., CLUNES, L. A., BENCHARIT, S., STUTTS, M. J., BETTS, L., REDINBO, M. R. & TARRAN, R. 2013. Molecular basis for pH-dependent mucosal dehydration in cystic fibrosis airways. *Proc Natl Acad Sci U S A,* 110**,** 15973-8.

GEISS, G. K., BUMGARNER, R. E., BIRDITT, B., DAHL, T., DOWIDAR, N., DUNAWAY, D. L., FELL, H. P., FERREE, S., GEORGE, R. D., GROGAN, T., JAMES, J. J., MAYSURIA, M., MITTON, J. D., OLIVERI, P., OSBORN, J. L., PENG, T., RATCLIFFE, A. L., WEBSTER, P. J., DAVIDSON, E. H., HOOD, L. & DIMITROV, K. 2008. Direct multiplexed measurement of gene expression with color-coded probe pairs. *Nat Biotechnol,* 26**,** 317-25.

GELLER, D. E. 2009. Aerosol antibiotics in cystic fibrosis. *Respir Care,* 54**,** 658-70.
GOOD, J. T., JR., ROLLINS, D. R. & MARTIN, R. J. 2012. Macrolides in the treatment of asthma. *Curr Opin Pulm Med,* 18**,** 76-84.
GRAY, K. A., YATES, B., SEAL, R. L., WRIGHT, M. W. & BRUFORD, E. A. 2015. Genenames.org: the HGNC resources in 2015. *Nucleic Acids Res,* 43**,** D1079-85.
GREENE, T. A., ALARCON, S., THOMAS, A., BERDOUGO, E., DORANZ, B. J., BRESLIN, P. A. & RUCKER, J. B. 2011. Probenecid inhibits the human bitter taste receptor TAS2R16 and suppresses bitter perception of salicin. *PLoS One,* 6**,** e20123.
GUADAGNI, D. G., HOROWITZ, R. M., GENTILI, B. & MAIER, V. P. 1977. Method of reducing bitterness in citrus juices. Google Patents.
HAN, L., LI, L., LI, B., ZHAO, D., LI, Y., XU, Z. & LIU, G. 2013. Review of the characteristics of food-derived and endogenous ne-carboxymethyllysine. *J Food Prot,* 76**,** 912-8.
HASTINGS, J. W. 2004. Bacterial quorum-sensing signals are inactivated by mammalian cells. *Proc Natl Acad Sci U S A,* 101**,** 3993-4.
HERNESS, M. S. & GILBERTSON, T. A. 1999. Cellular mechanisms of taste transduction. *Annu Rev Physiol,* 61**,** 873-900.
HILL, S. J. 2006. G-protein-coupled receptors: past, present and future. *Br J Pharmacol,* 147 Suppl 1**,** S27-37.
HOBSON-WEBB, L. D., ROACH, E. S. & DONOFRIO, P. D. 2006. Metronidazole: newly recognized cause of autonomic neuropathy. *J Child Neurol,* 21**,** 429-31.
HOCHHEIMER, A., KROHN, M., RUDERT, K., RIEDEL, K., BECKER, S., THIRION, C. & ZINKE, H. 2014. Endogenous gustatory responses and gene expression profile of stably proliferating human taste cells isolated from fungiform papillae. *Chem Senses,* 39**,** 359-77.
HOFER, D., PUSCHEL, B. & DRENCKHAHN, D. 1996. Taste receptor-like cells in the rat gut identified by expression of alpha-gustducin. *Proc Natl Acad Sci U S A,* 93**,** 6631-4.
HOFMANN, T., CHUBANOV, V., GUDERMANN, T. & MONTELL, C. 2003. TRPM5 is a voltage-modulated and Ca(2+)-activated monovalent selective cation channel. *Curr Biol,* 13**,** 1153-8.
HOLLOWAY, A. C., QIAN, H., PIPOLO, L., ZIOGAS, J., MIURA, S., KARNIK, S., SOUTHWELL, B. R., LEW, M. J. & THOMAS, W. G. 2002. Side-chain substitutions within angiotensin II reveal different requirements for signaling, internalization, and phosphorylation of type 1A angiotensin receptors. *Mol Pharmacol,* 61**,** 768-77.
HOON, M. A., ADLER, E., LINDEMEIER, J., BATTEY, J. F., RYBA, N. J. & ZUKER, C. S. 1999. Putative mammalian taste receptors: a class of taste-specific GPCRs with distinct topographic selectivity. *Cell,* 96**,** 541-51.
HORVAT, T. & JAKAS, A. 2004. Peptide and amino acid glycation: new insights into the Maillard reaction. *Journal of Peptide Science,* 10**,** 119-137.
HU, J., WANG, Y., ZHANG, X., LLOYD, J. R., LI, J. H., KARPIAK, J., COSTANZI, S. & WESS, J. 2010. Structural basis of G protein-coupled receptor-G protein interactions. *Nat Chem Biol,* 6**,** 541-8.
HUTH, M. E., HAN, K. H., SOTOUDEH, K., HSIEH, Y. J., EFFERTZ, T., VU, A. A., VERHOEVEN, S., HSIEH, M. H., GREENHOUSE, R., CHENG, A. G. & RICCI, A. J.

2015. Designer aminoglycosides prevent cochlear hair cell loss and hearing loss. *J Clin Invest,* 125**,** 583-92.
INOUE, H., NOJIMA, H. & OKAYAMA, H. 1990. High efficiency transformation of Escherichia coli with plasmids. *Gene,* 96**,** 23-8.
ISBERG, V., DE GRAAF, C., BORTOLATO, A., CHEREZOV, V., KATRITCH, V., MARSHALL, F. H., MORDALSKI, S., PIN, J. P., STEVENS, R. C., VRIEND, G. & GLORIAM, D. E. 2015. Generic GPCR residue numbers - aligning topology maps while minding the gaps. *Trends Pharmacol Sci,* 36**,** 22-31.
ITOH, Y., CAI, K. & KHORANA, H. G. 2001. Mapping of contact sites in complex formation between light-activated rhodopsin and transducin by covalent crosslinking: use of a chemically preactivated reagent. *Proc Natl Acad Sci U S A,* 98**,** 4883-7.
JAFURULLA, M., TIWARI, S. & CHATTOPADHYAY, A. 2011. Identification of cholesterol recognition amino acid consensus (CRAC) motif in G-protein coupled receptors. *Biochem Biophys Res Commun,* 404**,** 569-73.
JAGGUPILLI, A., HOWARD, R., UPADHYAYA, J. D., BHULLAR, R. P. & CHELIKANI, P. 2016. Bitter taste receptors: Novel insights into the biochemistry and pharmacology. *Int J Biochem Cell Biol,* 77**,** 184-96.
JAGGUPILLI, A., SINGH, N., UPADHYAYA, J., SIKARWAR, A. S., ARAKAWA, M., DAKSHINAMURTI, S., BHULLAR, R. P., DUAN, K. & CHELIKANI, P. 2017. Analysis of the expression of human bitter taste receptors in extraoral tissues. *Mol Cell Biochem,* 426**,** 137-147.
JI, M. F., SU, X. B., SU, X. H., CHEN, Y. Y., HUANG, W. K., ZHANG, J., GAO, Z. B., LI, C. G. & LU, X. F. 2014. Identification of Novel Compounds for Human Bitter Taste Receptors. *Chemical Biology & Drug Design,* 84**,** 63-74.
JIANG, M., KARASAWA, T. & STEYGER, P. S. 2017. Aminoglycoside-Induced Cochleotoxicity: A Review. *Front Cell Neurosci,* 11**,** 308.
JUNEJA, L. R., CHU, D.-C., OKUBO, T., NAGATO, Y. & YOKOGOSHI, H. 1999. L-theanine—a unique amino acid of green tea and its relaxation effect in humans. *Trends in Food Science & Technology,* 10**,** 199-204.
KARA, E., LIN, H., SVENSSON, K., JOHANSSON, A. M. & STRANGE, P. G. 2010. Analysis of the actions of the novel dopamine receptor-directed compounds (S)-OSU6162 and ACR16 at the D2 dopamine receptor. *Br J Pharmacol,* 161**,** 1343-50.
KARAMAN, R., NOWAK, S., DI PIZIO, A., KITANEH, H., ABU-JAISH, A., MEYERHOF, W., NIV, M. Y. & BEHRENS, M. 2016. Probing the Binding Pocket of the Broadly Tuned Human Bitter Taste Receptor TAS2R14 by Chemical Modification of Cognate Agonists. *Chem Biol Drug Des,* 88**,** 66-75.
KARLSSON, T., TURKINA, M. V., YAKYMENKO, O., MAGNUSSON, K. E. & VIKSTROM, E. 2012. The Pseudomonas aeruginosa N-Acylhomoserine Lactone Quorum Sensing Molecules Target IQGAP1 and Modulate Epithelial Cell Migration. *Plos Pathogens,* 8.
KENAKIN, T. 2015. New Lives for Seven Transmembrane Receptors as Drug Targets. *Trends Pharmacol Sci,* 36**,** 705-6.
KENAKIN, T. & CHRISTOPOULOS, A. 2013. Signalling bias in new drug discovery: detection, quantification and therapeutic impact. *Nat Rev Drug Discov,* 12**,** 205-16.
KENAKIN, T. P. 1982. The Schild regression in the process of receptor classification. *Can J Physiol Pharmacol,* 60**,** 249-65.

KENT, B. D., LANE, S. J., VAN BEEK, E. J., DODD, J. D., COSTELLO, R. W. & TIDDENS, H. A. 2014. Asthma and cystic fibrosis: a tangled web. *Pediatr Pulmonol,* 49**,** 205-13.

KITAZAWA, T., NAKAYAMA, K., OKUGAWA, S., KOIKE, K., SHIBASAKI, Y. & OTA, Y. 2007. Biphasic regulation of levofloxacin on lipopolysaccharide-induced IL-1beta production. *Life Sci,* 80**,** 1572-7.

KOHL, S., BEHRENS, M., DUNKEL, A., HOFMANN, T. & MEYERHOF, W. 2013. Amino acids and peptides activate at least five members of the human bitter taste receptor family. *J Agric Food Chem,* 61**,** 53-60.

KOSKI, G., STREATY, R. A. & KLEE, W. A. 1982. Modulation of sodium-sensitive GTPase by partial opiate agonists. An explanation for the dual requirement for Na+ and GTP in inhibitory regulation of adenylate cyclase. *J Biol Chem,* 257**,** 14035-40.

KROHN, S. C., BONVIN, P. & PROUDFOOT, A. E. 2013. CCL18 exhibits a regulatory role through inhibition of receptor and glycosaminoglycan binding. *PLoS One,* 8**,** e72321.

KULKARNI, M. 2011. Digital multiplexed gene expression analysis using the NanoString nCounter system. *Current protocols in molecular biology/edited by Frederick M. Ausubel...[et al.]***,** Unit25B. 10.

KVIST, T., STEFFENSEN, T. B., GREENWOOD, J. R., MEHRZAD TABRIZI, F., HANSEN, K. B., GAJHEDE, M., PICKERING, D. S., TRAYNELIS, S. F., KASTRUP, J. S. & BRAUNER-OSBORNE, H. 2013. Crystal structure and pharmacological characterization of a novel N-methyl-D-aspartate (NMDA) receptor antagonist at the GluN1 glycine binding site. *J Biol Chem,* 288**,** 33124-35.

LAGERSTROM, M. C. & SCHIOTH, H. B. 2008. Structural diversity of G protein-coupled receptors and significance for drug discovery. *Nat Rev Drug Discov,* 7**,** 339-57.

LEE, R. J. & COHEN, N. A. 2015. Taste receptors in innate immunity. *Cell Mol Life Sci,* 72**,** 217-36.

LEE, R. J., KOFONOW, J. M., ROSEN, P. L., SIEBERT, A. P., CHEN, B., DOGHRAMJI, L., XIONG, G., ADAPPA, N. D., PALMER, J. N., KENNEDY, D. W., KREINDLER, J. L., MARGOLSKEE, R. F. & COHEN, N. A. 2014. Bitter and sweet taste receptors regulate human upper respiratory innate immunity. *J Clin Invest,* 124**,** 1393-405.

LEE, R. J., XIONG, G., KOFONOW, J. M., CHEN, B., LYSENKO, A., JIANG, P., ABRAHAM, V., DOGHRAMJI, L., ADAPPA, N. D., PALMER, J. N., KENNEDY, D. W., BEAUCHAMP, G. K., DOULIAS, P. T., ISCHIROPOULOS, H., KREINDLER, J. L., REED, D. R. & COHEN, N. A. 2012. T2R38 taste receptor polymorphisms underlie susceptibility to upper respiratory infection. *J Clin Invest,* 122**,** 4145-59.

LEVIT, A., NOWAK, S., PETERS, M., WIENER, A., MEYERHOF, W., BEHRENS, M. & NIV, M. Y. 2014. The bitter pill: clinical drugs that activate the human bitter taste receptor TAS2R14. *FASEB J,* 28**,** 1181-97.

LEY, J. P. 2008. Masking Bitter Taste by Molecules. *Chemosensory Perception,* 1**,** 58-77.

LEY, J. P., BLINGS, M., PAETZ, S., KRAMMER, G. E. & BERTRAM, H. J. 2006. New bitter-masking compounds: hydroxylated benzoic acid amides of aromatic

amines as structural analogues of homoeriodictyol. *J Agric Food Chem,* 54**,** 8574-9.
LEY, J. P., DESSOY, M., PAETZ, S., BLINGS, M., HOFFMANN-LUCKE, P., REICHELT, K. V., KRAMMER, G. E., PIENKNY, S., BRANDT, W. & WESSJOHANN, L. 2012. Identification of enterodiol as a masker for caffeine bitterness by using a pharmacophore model based on structural analogues of homoeriodictyol. *J Agric Food Chem,* 60**,** 6303-11.
LEY, J. P., KRAMMER, G., REINDERS, G., GATFIELD, I. L. & BERTRAM, H. J. 2005. Evaluation of bitter masking flavanones from Herba Santa (Eriodictyon californicum (H. and A.) Torr., Hydrophyllaceae). *J Agric Food Chem,* 53**,** 6061-6.
LI, F. & ZHOU, M. L. 2012. Depletion of bitter taste transduction leads to massive spermatid loss in transgenic mice. *Molecular Human Reproduction,* 18**,** 289-297.
LIGGETT, S. B. 2013. Bitter taste receptors on airway smooth muscle as targets for novel bronchodilators. *Expert Opin Ther Targets,* 17**,** 721-31.
LIGGETT, S. B. 2014. Bitter taste receptors in the wrong place: novel airway smooth muscle targets for treating asthma. *Trans Am Clin Climatol Assoc,* 125**,** 64-74; discussion 74-5.
LIU, K., JAGGUPILLI, A., PREMNATH, D. & CHELIKANI, P. 2018. Plasticity of the ligand binding pocket in the bitter taste receptor T2R7. *Biochim Biophys Acta,* 5**,** 991-999.
LIU, W., CHUN, E., THOMPSON, A. A., CHUBUKOV, P., XU, F., KATRITCH, V., HAN, G. W., ROTH, C. B., HEITMAN, L. H., AP, I. J., CHEREZOV, V. & STEVENS, R. C. 2012. Structural basis for allosteric regulation of GPCRs by sodium ions. *Science,* 337**,** 232-6.
LOSSOW, K., HUBNER, S., ROUDNITZKY, N., SLACK, J. P., POLLASTRO, F., BEHRENS, M. & MEYERHOF, W. 2016. Comprehensive Analysis of Mouse Bitter Taste Receptors Reveals Different Molecular Receptive Ranges for Orthologous Receptors in Mice and Humans. *J Biol Chem,* 291**,** 15358-77.
LU, P., ZHANG, C. H., LIFSHITZ, L. M. & ZHUGE, R. 2017. Extraoral bitter taste receptors in health and disease. *J Gen Physiol,* 149**,** 181-197.
LUND, T. C., KOBS, A. J., KRAMER, A., NYQUIST, M., KUROKI, M. T., OSBORN, J., LIDKE, D. S., LOW-NAM, S. T., BLAZAR, B. R. & TOLAR, J. 2013. Bone marrow stromal and vascular smooth muscle cells have chemosensory capacity via bitter taste receptor expression. *PLoS One,* 8**,** e58945.
LUTTRELL, L. M. 2014. Minireview: More than just a hammer: ligand "bias" and pharmaceutical discovery. *Mol Endocrinol,* 28**,** 281-94.
MARCHIORI, A., CAPECE, L., GIORGETTI, A., GASPARINI, P., BEHRENS, M., CARLONI, P. & MEYERHOF, W. 2013. Coarse-grained/molecular mechanics of the TAS2R38 bitter taste receptor: experimentally-validated detailed structural prediction of agonist binding. *PLoS One,* 8**,** e64675.
MAURER, S., WABNITZ, G. H., KAHLE, N. A., STEGMAIER, S., PRIOR, B., GIESE, T., GAIDA, M. M., SAMSTAG, Y. & HANSCH, G. M. 2015. Tasting Pseudomonas aeruginosa Biofilms: Human Neutrophils Express the Bitter Receptor T2R38 as Sensor for the Quorum Sensing Molecule N-(3-Oxododecanoyl)-l-Homoserine Lactone. *Front Immunol,* 6**,** 369.

MENNELLA, J. A., REED, D. R., ROBERTS, K. M., MATHEW, P. S. & MANSFIELD, C. J. 2014. Age-related differences in bitter taste and efficacy of bitter blockers. *PLoS One,* 9**,** e103107.

MEYERHOF, W., BATRAM, C., KUHN, C., BROCKHOFF, A., CHUDOBA, E., BUFE, B., APPENDINO, G. & BEHRENS, M. 2010. The molecular receptive ranges of human TAS2R bitter taste receptors. *Chem Senses,* 35**,** 157-70.

MICKLE, J. E. & CUTTING, G. R. 2000. Genotype-phenotype relationships in cystic fibrosis. *Med Clin North Am,* 84**,** 597-607.

MIDDLETON, B., RODGERS, H. C., CAMARA, M., KNOX, A. J., WILLIAMS, P. & HARDMAN, A. 2002. Direct detection of N-acylhomoserine lactones in cystic fibrosis sputum. *FEMS Microbiol Lett,* 207**,** 1-7.

MIRAVITLLES, M. & ANZUETO, A. 2013. Antibiotics for acute and chronic respiratory infection in patients with chronic obstructive pulmonary disease. *Am J Respir Crit Care Med,* 188**,** 1052-7.

MORGAN, W. J., BUTLER, S. M., JOHNSON, C. A., COLIN, A. A., FITZSIMMONS, S. C., GELLER, D. E., KONSTAN, M. W., LIGHT, M. J., RABIN, H. R., REGELMANN, W. E., SCHIDLOW, D. V., STOKES, D. C., WOHL, M. E., KAPLOWITZ, H., WYATT, M. M. & STRYKER, S. 1999. Epidemiologic study of cystic fibrosis: design and implementation of a prospective, multicenter, observational study of patients with cystic fibrosis in the U.S. and Canada. *Pediatr Pulmonol,* 28**,** 231-41.

MUNK, C., ISBERG, V., MORDALSKI, S., HARPSOE, K., RATAJ, K., HAUSER, A. S., KOLB, P., BOJARSKI, A. J., VRIEND, G. & GLORIAM, D. E. 2016. GPCRdb: the G protein-coupled receptor database - an introduction. *Br J Pharmacol,* 173**,** 2195-207.

NARUKAWA, M., NOGA, C., UENO, Y., SATO, T., MISAKA, T. & WATANABE, T. 2011. Evaluation of the bitterness of green tea catechins by a cell-based assay with the human bitter taste receptor hTAS2R39. *Biochem Biophys Res Commun,* 405**,** 620-5.

NEUBIG, R. R., SPEDDING, M., KENAKIN, T., CHRISTOPOULOS, A., INTERNATIONAL UNION OF PHARMACOLOGY COMMITTEE ON RECEPTOR, N. & DRUG, C. 2003. International Union of Pharmacology Committee on Receptor Nomenclature and Drug Classification. XXXVIII. Update on terms and symbols in quantitative pharmacology. *Pharmacol Rev,* 55**,** 597-606.

O'DWYER, D. N., DICKSON, R. P. & MOORE, B. B. 2016. The Lung Microbiome, Immunity, and the Pathogenesis of Chronic Lung Disease. *J Immunol,* 196**,** 4839-47.

OGLESBY, I. K., CHOTIRMALL, S. H., MCELVANEY, N. G. & GREENE, C. M. 2013. Regulation of cystic fibrosis transmembrane conductance regulator by microRNA-145, -223, and -494 is altered in DeltaF508 cystic fibrosis airway epithelium. *J Immunol,* 190**,** 3354-62.

OLIVEIRA, L., PAIVA, A. C. M. & VRIEND, G. 1993. A common motif in G-protein-coupled seven transmembrane helix receptors. *Journal of Computer-Aided Molecular Design,* 7**,** 649-658.

PANKEVYCH, H., KORKHOV, V., FREISSMUTH, M. & NANOFF, C. 2003. Truncation of the A1 adenosine receptor reveals distinct roles of the membrane-proximal carboxyl terminus in receptor folding and G protein coupling. *J Biol Chem,* 278**,** 30283-93.

PARDO, L., DEUPI, X., DOLKER, N., LOPEZ-RODRIGUEZ, M. L. & CAMPILLO, M. 2007. The role of internal water molecules in the structure and function of the rhodopsin family of G protein-coupled receptors. *Chembiochem,* 8**,** 19-24.

PARK-WYLLIE, L. Y., JUURLINK, D. N., KOPP, A., SHAH, B. R., STUKEL, T. A., STUMPO, C., DRESSER, L., LOW, D. E. & MAMDANI, M. M. 2006. Outpatient gatifloxacin therapy and dysglycemia in older adults. *N Engl J Med,* 354**,** 1352-61.

PARNOT, C., MISEREY-LENKEI, S., BARDIN, S., CORVOL, P. & CLAUSER, E. 2002. Lessons from constitutively active mutants of G protein-coupled receptors. *Trends Endocrinol Metab,* 13**,** 336-43.

PAWLOWSKI, A. C., JOHNSON, J. W. & WRIGHT, G. D. 2016. Evolving medicinal chemistry strategies in antibiotic discovery. *Curr Opin Biotechnol,* 42**,** 108-117.

PEARSON, J. P., GRAY, K. M., PASSADOR, L., TUCKER, K. D., EBERHARD, A., IGLEWSKI, B. H. & GREENBERG, E. P. 1994. Structure of the Autoinducer Required for Expression of Pseudomonas-Aeruginosa Virulence Genes. *Proceedings of the National Academy of Sciences of the United States of America,* 91**,** 197-201.

PEARSON, J. P., PASSADOR, L., IGLEWSKI, B. H. & GREENBERG, E. P. 1995. A second N-acylhomoserine lactone signal produced by Pseudomonas aeruginosa. *Proc Natl Acad Sci U S A,* 92**,** 1490-4.

PERRY, J. A. & WRIGHT, G. D. 2014. Forces shaping the antibiotic resistome. *Bioessays,* 36**,** 1179-84.

PESCI, E. C., MILBANK, J. B., PEARSON, J. P., MCKNIGHT, S., KENDE, A. S., GREENBERG, E. P. & IGLEWSKI, B. H. 1999. Quinolone signaling in the cell-to-cell communication system of Pseudomonas aeruginosa. *Proc Natl Acad Sci U S A,* 96**,** 11229-34.

PLUZNICK, J. L. 2014. Gut microbes and host physiology: what happens when you host billions of guests? *Front Endocrinol (Lausanne),* 5**,** 91.

POCH, G., BRUNNER, F. & KUHBERGER, E. 1992. Construction of antagonist dose-response curves for estimation of pA2-values by Schild-plot analysis and detection of allosteric interactions. *Br J Pharmacol,* 106**,** 710-6.

PRONIN, A. N., TANG, H., CONNOR, J. & KEUNG, W. 2004. Identification of ligands for two human bitter T2R receptors. *Chem Senses,* 29**,** 583-93.

PUCADYIL, T. J. & CHATTOPADHYAY, A. 2004. Cholesterol modulates ligand binding and G-protein coupling to serotonin(1A) receptors from bovine hippocampus. *Biochim Biophys Acta,* 1663**,** 188-200.

PUCADYIL, T. J. & CHATTOPADHYAY, A. 2006. Role of cholesterol in the function and organization of G-protein coupled receptors. *Prog Lipid Res,* 45**,** 295-333.

PYDI, S. P., BHULLAR, R. P. & CHELIKANI, P. 2012a. Constitutively active mutant gives novel insights into the mechanism of bitter taste receptor activation. *J Neurochem,* 122**,** 537-44.

PYDI, S. P., BHULLAR, R. P. & CHELIKANI, P. 2014a. Constitutive activity of bitter taste receptors (T2Rs). *Adv Pharmacol,* 70**,** 303-26.

PYDI, S. P., JAGGUPILLI, A., NELSON, K. M., ABRAMS, S. R., BHULLAR, R. P., LOEWEN, M. C. & CHELIKANI, P. 2015. Abscisic Acid Acts as a Blocker of

the Bitter Taste G Protein-Coupled Receptor T2R4. *Biochemistry,* 54**,** 2622-31.
PYDI, S. P., SINGH, N., UPADHYAYA, J., BHULLAR, R. P. & CHELIKANI, P. 2014b. The third intracellular loop plays a critical role in bitter taste receptor activation. *Biochim Biophys Acta,* 1838**,** 231-6.
PYDI, S. P., SOBOTKIEWICZ, T., BILLAKANTI, R., BHULLAR, R. P., LOEWEN, M. C. & CHELIKANI, P. 2014c. Amino acid derivatives as bitter taste receptor (T2R) blockers. *J Biol Chem,* 289**,** 25054-66.
PYDI, S. P., UPADHYAYA, J., SINGH, N., PAL BHULLAR, R. & CHELIKANI, P. 2012b. Recent advances in structure and function studies on human bitter taste receptors. *Curr Protein Pept Sci,* 13**,** 501-508.
RASMUSSEN, S. G., DEVREE, B. T., ZOU, Y., KRUSE, A. C., CHUNG, K. Y., KOBILKA, T. S., THIAN, F. S., CHAE, P. S., PARDON, E., CALINSKI, D., MATHIESEN, J. M., SHAH, S. T., LYONS, J. A., CAFFREY, M., GELLMAN, S. H., STEYAERT, J., SKINIOTIS, G., WEIS, W. I., SUNAHARA, R. K. & KOBILKA, B. K. 2011. Crystal structure of the beta2 adrenergic receptor-Gs protein complex. *Nature,* 477**,** 549-55.
REDDY, S., BICHLER, J., WELLS-KNECHT, K. J., THORPE, S. R. & BAYNES, J. W. 1995. N. epsilon.-(Carboxymethyl) lysine Is a Dominant Advanced Glycation End Product (AGE) Antigen in Tissue Proteins. *Biochemistry,* 34**,** 10872-10878.
REICHLING, C., MEYERHOF, W. & BEHRENS, M. 2008. Functions of human bitter taste receptors depend on N-glycosylation. *J Neurochem,* 106**,** 1138-48.
RITCHIE, A. J., WHITTALL, C., LAZENBY, J. J., CHHABRA, S. R., PRITCHARD, D. I. & COOLEY, M. A. 2007. The immunomodulatory Pseudomonas aeruginosa signalling molecule N-(3-oxododecanoyl)-L-homoserine lactone enters mammalian cells in an unregulated fashion. *Immunology and Cell Biology,* 85**,** 596-602.
ROBINETT, K. S., KOZIOL-WHITE, C. J., AKOLUK, A., AN, S. S., PANETTIERI, R. A., JR. & LIGGETT, S. B. 2014. Bitter taste receptor function in asthmatic and nonasthmatic human airway smooth muscle cells. *Am J Respir Cell Mol Biol,* 50**,** 678-83.
ROLAND, W. S., GOUKA, R. J., GRUPPEN, H., DRIESSE, M., VAN BUREN, L., SMIT, G. & VINCKEN, J. P. 2014. 6-methoxyflavanones as bitter taste receptor blockers for hTAS2R39. *PLoS One,* 9**,** e94451.
ROLAND, W. S., VAN BUREN, L., GRUPPEN, H., DRIESSE, M., GOUKA, R. J., SMIT, G. & VINCKEN, J. P. 2013. Bitter taste receptor activation by flavonoids and isoflavonoids: modeled structural requirements for activation of hTAS2R14 and hTAS2R39. *J Agric Food Chem,* 61**,** 10454-66.
ROLLINS, D. R., BEUTHER, D. A. & MARTIN, R. J. 2010. Update on infection and antibiotics in asthma. *Curr Allergy Asthma Rep,* 10**,** 67-73.
SADARANGANI, S. P., ESTES, L. L. & STECKELBERG, J. M. 2015. Non-anti-infective effects of antimicrobials and their clinical applications: a review. *Mayo Clin Proc,* 90**,** 109-27.
SAINZ, E., CAVENAGH, M. M., GUTIERREZ, J., BATTEY, J. F., NORTHUP, J. K. & SULLIVAN, S. L. 2007. Functional characterization of human bitter taste receptors. *Biochem J,* 403**,** 537-43.
SAKURAI, T., MISAKA, T., ISHIGURO, M., MASUDA, K., SUGAWARA, T., ITO, K., KOBAYASHI, T., MATSUO, S., ISHIMARU, Y., ASAKURA, T. & ABE, K. 2010a.

Characterization of the beta-D-glucopyranoside binding site of the human bitter taste receptor hTAS2R16. *J Biol Chem,* 285**,** 28373-8.
SAKURAI, T., MISAKA, T., UENO, Y., ISHIGURO, M., MATSUO, S., ISHIMARU, Y., ASAKURA, T. & ABE, K. 2010b. The human bitter taste receptor, hTAS2R16, discriminates slight differences in the configuration of disaccharides. *Biochem Biophys Res Commun,* 402**,** 595-601.
SANDAL, M., BEHRENS, M., BROCKHOFF, A., MUSIANI, F., GIORGETTI, A., CARLONI, P. & MEYERHOF, W. 2015. Evidence for a Transient Additional Ligand Binding Site in the TAS2R46 Bitter Taste Receptor. *J Chem Theory Comput,* 11**,** 4439-4449.
SANEMATSU, K., YOSHIDA, R., SHIGEMURA, N. & NINOMIYA, Y. 2014. Structure, function, and signaling of taste G-protein-coupled receptors. *Curr Pharm Biotechnol,* 15**,** 951-61.
SAWANO, S., SETO, E., MORI, T. & HAYASHI, Y. 2005. G-protein-dependent and -independent pathways in denatonium signal transduction. *Biosci Biotechnol Biochem,* 69**,** 1643-51.
SCHWARTZ, T. W. 1994. Locating ligand-binding sites in 7TM receptors by protein engineering. *Curr Opin Biotechnol,* 5**,** 434-44.
SEIFERT, R. & WENZEL-SEIFERT, K. 2002. Constitutive activity of G-protein-coupled receptors: cause of disease and common property of wild-type receptors. *Naunyn Schmiedebergs Arch Pharmacol,* 366**,** 381-416.
SENGUPTA, D. & CHATTOPADHYAY, A. 2012. Identification of cholesterol binding sites in the serotonin1A receptor. *J Phys Chem B,* 116**,** 12991-6.
SENGUPTA, S., CHATTOPADHYAY, M. K. & GROSSART, H. P. 2013. The multifaceted roles of antibiotics and antibiotic resistance in nature. *Front Microbiol,* 4**,** 47.
SHAH, A. S., BEN-SHAHAR, Y., MONINGER, T. O., KLINE, J. N. & WELSH, M. J. 2009. Motile cilia of human airway epithelia are chemosensory. *Science,* 325**,** 1131-4.
SHAIK, F. A., SINGH, N., ARAKAWA, M., DUAN, K., BHULLAR, R. P. & CHELIKANI, P. 2016. Bitter taste receptors: Extraoral roles in pathophysiology. *Int J Biochem Cell Biol*.
SHARAFI, M., HAYES, J. E. & DUFFY, V. B. 2013. Masking Vegetable Bitterness to Improve Palatability Depends on Vegetable Type and Taste Phenotype. *Chemosens Percept,* 6**,** 8-19.
SHARMA, P., YI, R., NAYAK, A. P., WANG, N., TANG, F., KNIGHT, M. J., PAN, S., OLIVER, B. & DESHPANDE, D. A. 2017. Bitter Taste Receptor Agonists Mitigate Features of Allergic Asthma in Mice. *Sci Rep,* 7**,** 46166.
SHARMAN, J. L., BENSON, H. E., PAWSON, A. J., LUKITO, V., MPAMHANGA, C. P., BOMBAIL, V., DAVENPORT, A. P., PETERS, J. A., SPEDDING, M., HARMAR, A. J. & NC, I. 2013. IUPHAR-DB: updated database content and new features. *Nucleic Acids Res,* 41**,** D1083-8.
SHINER, E. K., RUMBAUGH, K. P. & WILLIAMS, S. C. 2005. Interkingdom signaling: Deciphering the language of acyl homoserine lactones. *Fems Microbiology Reviews,* 29**,** 935-947.
SHINER, E. K., TERENTYEV, D., BRYAN, A., SENNOUNE, S., MARTINEZ-ZAGUILAN, R., LI, G., GYORKE, S., WILLIAMS, S. C. & RUMBAUGH, K. P. 2006. Pseudomonas aeruginosa autoinducer modulates host cell responses through calcium signalling. *Cell Microbiol,* 8**,** 1601-10.

SINGH, N., CHAKRABORTY, R., BHULLAR, R. P. & CHELIKANI, P. 2014. Differential expression of bitter taste receptors in non-cancerous breast epithelial and breast cancer cells. *Biochemical and Biophysical Research Communications,* 446**,** 499-503.

SINGH, N., PYDI, S. P., UPADHYAYA, J. & CHELIKANI, P. 2011a. Structural Basis of Activation of Bitter Taste Receptor T2R1 and Comparison with Class A G-protein-coupled Receptors (GPCRs). *J Biol Chem,* 286**,** 36032-41.

SINGH, N., VRONTAKIS, M., PARKINSON, F. & CHELIKANI, P. 2011b. Functional bitter taste receptors are expressed in brain cells. *Biochem Biophys Res Commun,* 406**,** 146-51.

SINGH, P. K., SCHAEFER, A. L., PARSEK, M. R., MONINGER, T. O., WELSH, M. J. & GREENBERG, E. P. 2000. Quorum-sensing signals indicate that cystic fibrosis lungs are infected with bacterial biofilms. *Nature,* 407**,** 762-4.

SIVA, R., BAFADHEL, M., MONTEIRO, W., BRIGHTLING, C. E. & PAVORD, I. D. 2014. Effect of levofloxacin on neutrophilic airway inflammation in stable COPD: a randomized, double-blind, placebo-controlled trial. *Int J Chron Obstruct Pulmon Dis,* 9**,** 179-86.

SLACK, J. P., BROCKHOFF, A., BATRAM, C., MENZEL, S., SONNABEND, C., BORN, S., GALINDO, M. M., KOHL, S., THALMANN, S., OSTOPOVICI-HALIP, L., SIMONS, C. T., UNGUREANU, I., DUINEVELD, K., BOLOGA, C. G., BEHRENS, M., FURRER, S., OPREA, T. I. & MEYERHOF, W. 2010. Modulation of bitter taste perception by a small molecule hTAS2R antagonist. *Curr Biol,* 20**,** 1104-9.

SOARES, S., KOHL, S., THALMANN, S., MATEUS, N., MEYERHOF, W. & DE FREITAS, V. 2013. Different phenolic compounds activate distinct human bitter taste receptors. *J Agric Food Chem,* 61**,** 1525-33.

SOLDO, T. & HOFMANN, T. 2005. Application of hydrophilic interaction liquid chromatography/comparative taste dilution analysis for identification of a bitter inhibitor by a combinatorial approach based on Maillard reaction chemistry. *J Agric Food Chem,* 53**,** 9165-71.

STAMP, L. K., O'DONNELL, J. L. & CHAPMAN, P. T. 2007. Emerging therapies in the long-term management of hyperuricaemia and gout. *Internal Medicine Journal,* 37**,** 258-266.

STOCKMANN, C., SHERWIN, C. M., ZOBELL, J. T., YOUNG, D. C., WATERS, C. D., SPIGARELLI, M. G. & AMPOFO, K. 2013. Optimization of anti-pseudomonal antibiotics for cystic fibrosis pulmonary exacerbations: III. fluoroquinolones. *Pediatr Pulmonol,* 48**,** 211-20.

SUEN, J. Y., BARRY, G. D., LOHMAN, R. J., HALILI, M. A., COTTERELL, A. J., LE, G. T. & FAIRLIE, D. P. 2012. Modulating human proteinase activated receptor 2 with a novel antagonist (GB88) and agonist (GB110). *Br J Pharmacol,* 165**,** 1413-23.

SUN, X., AGREN, H. & TU, Y. 2014. Functional water molecules in rhodopsin activation. *J Phys Chem B,* 118**,** 10863-73.

SURESH BABU, K., KASTELIK, J. & MORJARIA, J. B. 2013. Role of long term antibiotics in chronic respiratory diseases. *Respir Med,* 107**,** 800-15.

TAN, J., ABROL, R., TRZASKOWSKI, B. & GODDARD, W. A., 3RD 2012. 3D structure prediction of TAS2R38 bitter receptors bound to agonists phenylthiocarbamide (PTC) and 6-n-propylthiouracil (PROP). *J Chem Inf Model,* 52**,** 1875-85.

TAN, Q., ZHU, Y., LI, J., CHEN, Z., HAN, G. W., KUFAREVA, I., LI, T., MA, L., FENALTI, G., LI, J., ZHANG, W., XIE, X., YANG, H., JIANG, H., CHEREZOV, V., LIU, H., STEVENS, R. C., ZHAO, Q. & WU, B. 2013. Structure of the CCR5 chemokine receptor-HIV entry inhibitor maraviroc complex. *Science,* 341**,** 1387-90.

THALMANN, S., BEHRENS, M. & MEYERHOF, W. 2013. Major haplotypes of the human bitter taste receptor TAS2R41 encode functional receptors for chloramphenicol. *Biochem Biophys Res Commun,* 435**,** 267-73.

TIZZANO, M., GULBRANSEN, B. D., VANDENBEUCH, A., CLAPP, T. R., HERMAN, J. P., SIBHATU, H. M., CHURCHILL, M. E., SILVER, W. L., KINNAMON, S. C. & FINGER, T. E. 2010. Nasal chemosensory cells use bitter taste signaling to detect irritants and bacterial signals. *Proc Natl Acad Sci U S A,* 107**,** 3210-5.

UCHIDA, T., TANIGAKE, A., MIYANAGA, Y., MATSUYAMA, K., KUNITOMO, M., KOBAYASHI, Y., IKEZAKI, H. & TANIGUCHI, A. 2003. Evaluation of the bitterness of antibiotics using a taste sensor. *J Pharm Pharmacol,* 55**,** 1479-85.

UPADHYAYA, J., PYDI, S. P., SINGH, N., ALUKO, R. E. & CHELIKANI, P. 2010. Bitter taste receptor T2R1 is activated by dipeptides and tripeptides. *Biochem Biophys Res Commun,* 398**,** 331-5.

UPADHYAYA, J., SINGH, N., BHULLAR, R. P. & CHELIKANI, P. 2015. The structure-function role of C-terminus in human bitter taste receptor T2R4 signaling. *Biochim Biophys Acta,* 1848**,** 1502-8.

UPADHYAYA, J. D., CHAKRABORTY, R., SHAIK, F. A., JAGGUPILLI, A., BHULLAR, R. P. & CHELIKANI, P. 2016. The Pharmacochaperone Activity of Quinine on Bitter Taste Receptors. *PLoS One,* 11**,** e0156347.

UPADHYAYA, J. D., SINGH, N., SIKARWAR, A. S., CHAKRABORTY, R., PYDI, S. P., BHULLAR, R. P., DAKSHINAMURTI, S. & CHELIKANI, P. 2014. Dextromethorphan mediated bitter taste receptor activation in the pulmonary circuit causes vasoconstriction. *PLoS One,* 9**,** e110373.

VENKATAKRISHNAN, A. J., DEUPI, X., LEBON, G., TATE, C. G., SCHERTLER, G. F. & BABU, M. M. 2013. Molecular signatures of G-protein-coupled receptors. *Nature,* 494**,** 185-94.

VIOLIN, J. D., CROMBIE, A. L., SOERGEL, D. G. & LARK, M. W. 2014. Biased ligands at G-protein-coupled receptors: promise and progress. *Trends Pharmacol Sci,* 35**,** 308-16.

VIOLIN, J. D., DEWIRE, S. M., YAMASHITA, D., ROMINGER, D. H., NGUYEN, L., SCHILLER, K., WHALEN, E. J., GOWEN, M. & LARK, M. W. 2010. Selectively engaging beta-arrestins at the angiotensin II type 1 receptor reduces blood pressure and increases cardiac performance. *J Pharmacol Exp Ther,* 335**,** 572-9.

VLASSARA, H., BROWNLEE, M. & CERAMI, A. 1984. Accumulation of diabetic rat peripheral nerve myelin by macrophages increases with the presence of advanced glycosylation endproducts. *J Exp Med,* 160**,** 197-207.

VON BODMAN, S. B., WILLEY, J. M. & DIGGLE, S. P. 2008. Cell-cell communication in bacteria: united we stand. *J Bacteriol,* 190**,** 4377-91.

WAGNER, V. E., BUSHNELL, D., PASSADOR, L., BROOKS, A. I. & IGLEWSKI, B. H. 2003. Microarray analysis of Pseudomonas aeruginosa quorum-sensing regulons: effects of growth phase and environment. *J Bacteriol,* 185**,** 2080-95.

WANG, C., WU, H., EVRON, T., VARDY, E., HAN, G. W., HUANG, X. P., HUFEISEN, S. J., MANGANO, T. J., URBAN, D. J., KATRITCH, V., CHEREZOV, V., CARON, M. G., ROTH, B. L. & STEVENS, R. C. 2014. Structural basis for Smoothened receptor modulation and chemoresistance to anticancer drugs. *Nat Commun,* 5**,** 4355.

WARNE, T., SERRANO-VEGA, M. J., BAKER, J. G., MOUKHAMETZIANOV, R., EDWARDS, P. C., HENDERSON, R., LESLIE, A. G., TATE, C. G. & SCHERTLER, G. F. 2008. Structure of a beta1-adrenergic G-protein-coupled receptor. *Nature,* 454**,** 486-91.

WIENER, A., SHUDLER, M., LEVIT, A. & NIV, M. Y. 2012. BitterDB: a database of bitter compounds. *Nucleic Acids Research,* 40**,** D413-D419.

WILLIAMS, P., WINZER, K., CHAN, W. C. & CAMARA, M. 2007. Look who's talking: communication and quorum sensing in the bacterial world. *Philos Trans R Soc Lond B Biol Sci,* 362**,** 1119-34.

WOLFLE, U., ELSHOLZ, F. A., KERSTEN, A., HAARHAUS, B., MULLER, W. E. & SCHEMPP, C. M. 2015. Expression and functional activity of the bitter taste receptors TAS2R1 and TAS2R38 in human keratinocytes. *Skin Pharmacol Physiol,* 28**,** 137-46.

WONG, G. T., GANNON, K. S. & MARGOLSKEE, R. F. 1996. Transduction of bitter and sweet taste by gustducin. *Nature,* 381**,** 796-800.

WU, S. V., ROZENGURT, N., YANG, M., YOUNG, S. H., SINNETT-SMITH, J. & ROZENGURT, E. 2002. Expression of bitter taste receptors of the T2R family in the gastrointestinal tract and enteroendocrine STC-1 cells. *Proc Natl Acad Sci U S A,* 99**,** 2392-7.

WYLLIE, D. J. & CHEN, P. E. 2007. Taking the time to study competitive antagonism. *Br J Pharmacol,* 150**,** 541-51.

XIAO, X., ZHU, M. X. & XU, T. L. 2013. 2-Guanidine-4-methylquinazoline acts as a novel competitive antagonist of A type gamma-aminobutyric acid receptors. *Neuropharmacology,* 75**,** 126-37.

YAMAZAKI, T., NARUKAWA, M., MOCHIZUKI, M., MISAKA, T. & WATANABE, T. 2013. Activation of the hTAS2R14 human bitter-taste receptor by (-)-epigallocatechin gallate and (-)-epicatechin gallate. *Biosci Biotechnol Biochem,* 77**,** 1981-3.

YAMAZAKI, T., SAGISAKA, M., IKEDA, R., NAKAMURA, T., MATSUDA, N., ISHII, T., NAKAYAMA, T. & WATANABE, T. 2014. The human bitter taste receptor hTAS2R39 is the primary receptor for the bitterness of theaflavins. *Biosci Biotechnol Biochem,* 78**,** 1753-6.

YAN, C. H., HAHN, S., MCMAHON, D., BONISLAWSKI, D., KENNEDY, D. W., ADAPPA, N. D., PALMER, J. N., JIANG, P., LEE, R. J. & COHEN, N. A. 2017. Nitric oxide production is stimulated by bitter taste receptors ubiquitously expressed in the sinonasal cavity. *Am J Rhinol Allergy,* 31**,** 85-92.

YANG, Y. K., OLLMANN, M. M., WILSON, B. D., DICKINSON, C., YAMADA, T., BARSH, G. S. & GANTZ, I. 1997. Effects of recombinant agouti-signaling protein on melanocortin action. *Mol Endocrinol,* 11**,** 274-80.

YUAN, S., FILIPEK, S., PALCZEWSKI, K. & VOGEL, H. 2014. Activation of G-protein-coupled receptors correlates with the formation of a continuous internal water pathway. *Nat Commun,* 5**,** 4733.

ZHANG, C. H., LIFSHITZ, L. M., UY, K. F., IKEBE, M., FOGARTY, K. E. & ZHUGE, R. 2013. The cellular and molecular basis of bitter tastant-induced bronchodilation. *PLoS Biol,* 11**,** e1001501.
ZHANG, D., ZHAO, Q. & WU, B. 2015. Structural Studies of G Protein-Coupled Receptors. *Mol Cells,* 38**,** 836-42.
ZHANG, L., XIA, Y. & PETERSON, D. G. 2014. Identification of bitter modulating maillard-catechin reaction products. *J Agric Food Chem,* 62**,** 8470-7.
ZHANG, Y., WANG, X., LI, X., PENG, S., WANG, S., HUANG, C. Z., HUANG, C. Z., ZHANG, Q., LI, D., JIANG, J., OUYANG, Q., ZHANG, Y., LI, S. & QIAO, Y. 2017. Identification of a specific agonist of human TAS2R14 from Radix Bupleuri through virtual screening, functional evaluation and binding studies. *Sci Rep,* 7**,** 12174.
ZHAO, G. Q., ZHANG, Y., HOON, M. A., CHANDRASHEKAR, J., ERLENBACH, I., RYBA, N. J. & ZUKER, C. S. 2003. The receptors for mammalian sweet and umami taste. *Cell,* 115**,** 255-66.
ZIELENSKI, J. 2000. Genotype and phenotype in cystic fibrosis. *Respiration,* 67**,** 117-33.